Mechanistic studies of two phosphatase enzymes involved in inostiol metabolism

Author: Yang Wei

Boston College

The Graduate School of Arts and Sciences

Department of Chemistry

MECHANIC STUDIES OF TWO PHOSPHATASE ENZYMES INVOLVED IN INOSITOL METABOLISM

a dissertation

by YANG WEI

submitted in partial fulfillment of the requirements

for the degree of

Doctor of Philosophy

May, 2013

Mechanic studies of two phosphatase enzymes involved in inositol metabolism

by Yang Wei

Under the direction of Dr. Mary F. Roberts

Abstract

Inositol-containing molecules and inositol phosphatases have diverse roles in cells. One of the inositol phospholipids phosphatases, PTEN (Phosphatase and Tensin Homolog deleted on Chromosome Ten), is a tumor suppressor and antagonizes the PI3K signaling pathway by dephosphorylating $PI(3,4,5)P_3$ at the 3 position of the inositol ring. In testing predictions of a molecular dynamics simulation, a hydrophobic site adjacent to the active site on PTEN was identified and verified by protein kinetic studies. This hydrophobic site plays an important role in substrate and substrate analogue binding with one of residues, Arg47, critical for PTEN phosphatase activity. Mutations of Arg47 reduced enzyme activities toward both the short-chain substrate as monomers and micelles and long-chain phospholipid presented in vesicles. $PI(4,5)P_2$, the product of $PI(3,4,5)P_3$ dephosphorylation, activates PTEN. Studies by others suggested this occurred when the product was bound to the N-terminal region of the protein (not visible in the crystal structure). However, no direct proof of this existed. The effect of $PI(4,5)P_2$ on PTEN enzyme activities in different substrates systems was studied. ^{31}P NMR was used to probe the spatial location and functional role of $PI(4,5)P_2$ binding site. The fixed field ^{31}P NMR and high resolution field cycling ^{31}P NMR results indicated there are discrete sites for

both substrate and activator lipids on PTEN, and both of sites are spatially separate from the hydrophobic site. The active site, adjacent hydrophobic site, and N-terminal activator binding site worked synergistically to regulate PTEN interacting with the membrane.

Thermophilic and hyperthermophilic archaea and bacteria thrive at high temperatures. They often accumulate small organic molecules, called compatible solutes or osmolytes, to protect proteins from thermal denaturation. The thermoprotection mechanism of compatible solutes was explored using inositol monophosphatase (IMPase) from *Archaeoglobus fulgidus* as the model protein. The protective effect of unusual compatible solutes, di-inositol-1,1'-phosphate (DIP) and diglycerol phosphate (DGP), as well as common compatible solutes glutamate and other anions, on the IMPase thermostability was studied. Specific binding sites of glutamate ions on the IMPase were identified by crystallography and field cycling NMR. However, mutations at these discrete binding sites did not eliminate the thermoprotection, but reduced the thermal stability (T_m) of the protein. Our results indicate the specific binding of osmolytes to the protein exists, but they do not account for the thermoprotection.

This dissertation is dedicated to

my parents Xiaofei Wei, Lin Yuan

and my fiancé Kai Hong

Acknowledgement

First, I would like to express my deep gratitude to my advisor, Dr. Mary F. Roberts, for her continuous guidance and support throughout my graduate study. Without her enthusiastic encouragement and confidence, this work would not have been completed. I always appreciate her kindness, patience and generosity.

I would like to thank Dr. Goran Krilov and Dr. Qin Wang for doing the simulations of PTEN and discussing this project.

I wish to thank Dr. Rebecca Goldstein in the Roberts group for solving the crystal structures of IMPase and collaborations on this project.

I wish to thank Dr. Scott Miller, Dr. Yingju Xu and Dr. Christina Longo for providing synthetic deoxy-PI and DIP compounds.

I would like to thank Dr. Eranthie Weerapana and Julianne Martell for doing mass spectrometry and data analysis of PTEN spin-labeling samples. I also thank Dr. Weerapana for being my committee member and spending time to read my thesis.

I would like to thank Dr. Patrick Wintrode for letting me work in his laboratory to use hydrogen exchange mass spectrometry to study PTEN and PI-PLC.

I would like to thank Dr. John Boylan and Dr. Thusitha Jayasundera at Boston College and Dr. Alfred Redfield at Brandeis University for maintaining the NMR facility to make my extensive usage of NMR possible.

I wish to thank Dr. Jianmin Gao for letting me use some equipment in his laboratory and being my committee member to read my thesis.

I wish to thank Dr. Olga Gursky for being a committee member and reading my thesis.

I would like to thank Dr. Yanling Karen Wang in the Roberts group for her guidance in my first year.

I would like to express my thanks to present and past members of the Roberts group for discussions and help to my projects. I am happy to work and be friends with them.

Last, a special thank goes to my family, my parents Xiaofei Wei and Lin Yuan, and my fiancé, Kai Hong, for their love, care and support in my life.

Abbreviation

A. fulgidus	*Archaeaoglubus fulgidus*
AHS	adjacent hydrophobic site
C2	protein kinase C conserved region 2
CD	circular dichroism
CMC	critical micelle concentration
CSA	chemical shift anisotropy
DAG	diacylglycerol
Dansyl-PE	1,2-dioleoyl-sn-glycero-3-phosphoethanolamine-N-(5-dimethylamino-1-naphthalene-sulfonyl)
DGP	diglycerol phosphate
D-I-1-P	D-myo-inositol 1-phosphate
diC_6PI	1,2-dihexanoyl-sn-glycero-3-phospho-(1'-myo-inositol)
diC_6PI(3,4)P_2	1,2-dihexanoyl-sn-glycero-3-phospho-(1'-myo-inositol-3',4'-bisphosphate)
diC_6PI(4,5)P_2	1,2-dihexanoyl-sn-glycero-3-phospho-(1'-myo-inositol-4',5'-bisphosphate)
diC_7PC	1,2-diheptanoyl-sn-glycero-3-phosphocholine
diC_8PI	1,2-dioctanoyl-sn-glycero-3-phospho-(1'-myo-inositol)
diC_8PI(3)P	1,2-dioctanoyl-sn-glycero-3-phospho-(1'-myo-inositol-3'-phosphate)
diC_8PI(3,4)P_2	1,2-dioctanoyl-sn-glycero-3-phospho-(1'-myo-inositol-3',4'-bisphosphate)
diC_8PI(4,5)P_2	1,2-dioctanoyl-sn-glycero-3-phospho-(1'-myo-inositol-4',5'-bisphosphate)

DIP	di-myo-inositol-1,1’ phosphate
DOPI(3,4)P_2	1,2-dioleoyl-sn-glycero-3-phospho-(1’-myo-inositol-3’,4’-bisphosphate)
DOPI(4,5)P_2	1,2-dioleoyl-sn-glycero-3-phospho-(1’-myo-inositol-4’,5’-bisphosphate)
DTT	dithioreitol
FBP	fructose 1,6-bisphosphate
G6P	glucose-6-phosphate
I(1,3,4,5)P_4 or IP_4	D-myo-inositol-1,3,4,5-tetraphosphate
I(1,4,5)P_3 or IP_3	D-myo-inositol-1,4,5-triphosphate
IMPase	inositol monophosphatase
IP	inositol phosphate
IPTG	isopropyl-β-D-thiogalactopyranoside
L-3,5-dd-diC_8PI	L-3,5-dideoxy-dioctanoyl-phosphatidylinositol
L-I-1-P	L-myo-inositol 1-phosphate
LUV	large unilamellar vesicle
MTSL	S-(2,2,5,5-tetramethyl-2,5-dihydro-1H-pyrrol-3-yl)methyl methanesulfonothioate
NBP	N-terminal PI(4,5)P_2 binding patch
NMR	nuclear magnetic resonance
PA	phosphatidic acid
PAGE	polyacrylamide gel electrophoresis

PCR	polymerase chain reaction
PDZ	post synaptic density protein, drosophila disc large tumor suppressor, and zonula occludens-1 protein
PH	pleckstrin homology
PI	phosphatidylinositol
PI(3)P	phosphatidylinositol 3-phosphate
$PI(3,4)P_2$	phosphatidylinositol 3,4-bisphosphate
$PI(3,4,5)P_3$	phosphatidylinositol 3,4,5-triphosphate
$PI(3,5)P_2$	phosphatidylinositol 3,5-bisphosphate
$PI(4,5)P_2$	phosphatidylinositol 4,5-bisphosphate
PI3K	phosphatidylinositol 3-phosphate kinase
PLC	phospholipase C
POPC	1-palmitoyl-2-oleoyl-sn-glycero-phosphocholine
PS	phosphatidylserine
PTEN	phosphatase and tensin homolog deleted on chromosome ten
Pyrene-PE	1,2-dioleoyl-sn-glycero-3-phosphoethanolamine-N-(1-pyrenesulfonyl)
SDS	sodium dodecyl sulfate
SUV	small unilamellar vesicle
TX-100	triton X-100
WT	wild type

Table of Contents

Table of Figures

List of Tables

Chapter 1

Introduction

1.1 Inositol and inositol metabolism

Inositol is the name of a group of cyclohexane hexols with nine possible stereoisomers. One of them, D-*myo*-inositol (Ins), or cis-1,2,3,5-tran-4,6-cyclohexanehexol, is extensively used in biology (Michell, 2008). Perhaps the best known function of *myo*-inositol is that it is the building block of a series of second messengers, inositol phosphates and inositol-containing phospholipids (Downes & Macphee, 1990). Nowadays, about half of the 63 possible *myo*-inositol phosphomonoesters, or inositol polyphosphates (IPs), have been identified in eukaryotic cells (Agranoff, 2009).

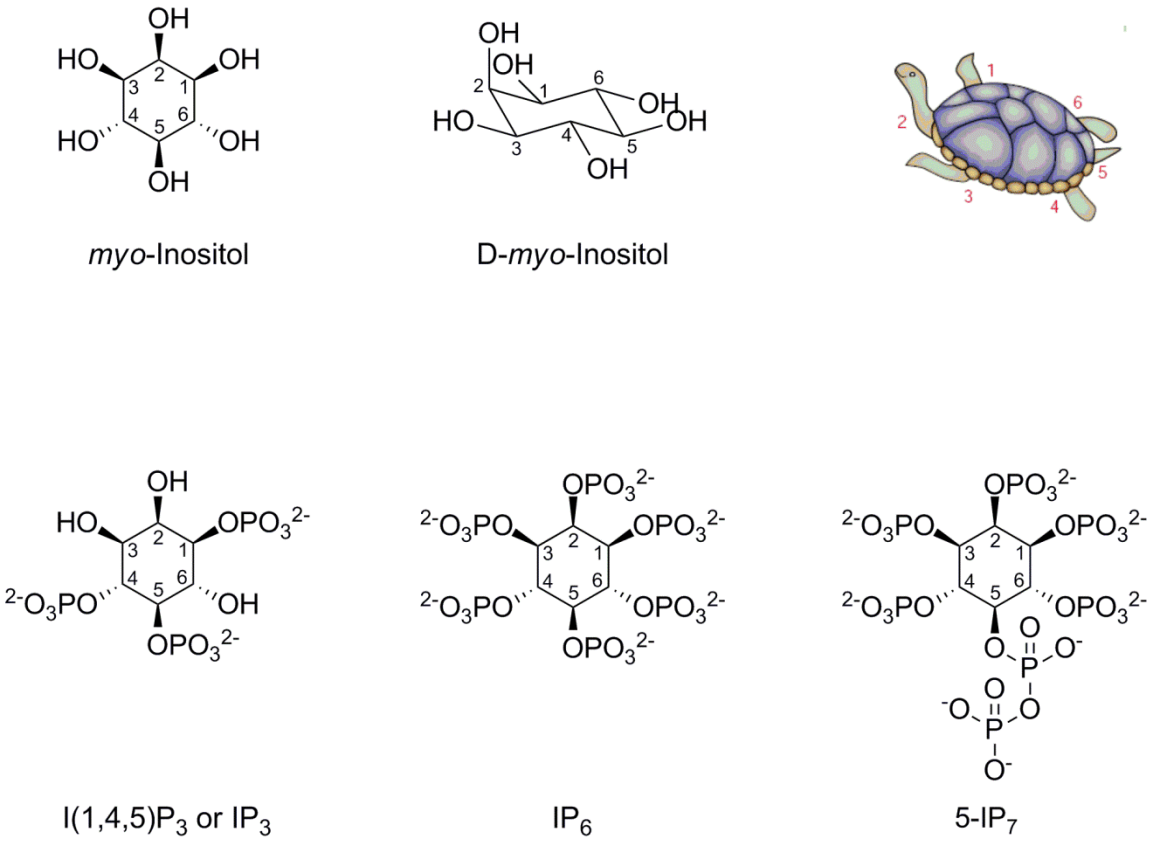

Figure 1.1 Structures of inositol and inositol phosphates (Irvine & Schell, 2001)

In order to prevent confusion in nomenclature, the 'turtle' analogy was introduced. The carbon with the axial hydroxyl group in the Haworth projection of D-*myo*-inositol is the 2 position, the turtle head. The numbering in D convention proceeds anticlockwise with the equatorial hydroxyl linked to the D1 carbon as the turtle's front right flipper (Agranoff, 1978) (Figure 1.1). The simplest form of inositol-containing phospholipid in eukaryotes is phosphatidylinositol (PtdIns or PI) in which the phosphatidic acyl portion part is esterified to the hydroxyl group of inositol D1. The hydroxyl groups at D3, D4 and D5 carbon of PI can be phosphorylated to generate a total of 7 phosphorylated PIs, termed phosphoinositides (PIPs) (Figure 1.2).

The distribution of inositol and inositol-containing compounds among the three kingdoms of life, the eukarya, bacteria, and archaea, is quite different (Michell, 2011). Inositol, inositol polyphosphate and phosphoinositides are found in nearly all eukaryotes. Archaea also have inositols and use inositol-containing lipids for their cell membrane. However the structural features of the lipids differ from what is used in eukaryotes (see discussion below). Archaea also synthesize some unusual water soluble inositol-containing molecules, such as di-*myo*-inositol-1,1'-phosphate (DIP), that have distinctive functions (see discussion below). Inositol and inositol derivatives are seldom found in bacteria and appear restricted to only a few classes. PI is found in some mycobacteria where it is extensively modified and used in cell walls (Morita et al, 2011). Previously it was thought that phosphoinositides were only found in eukaryotes. Very recently it was reported that PI(3)P is synthesized in mycobacteria (Morita et al, 2010).

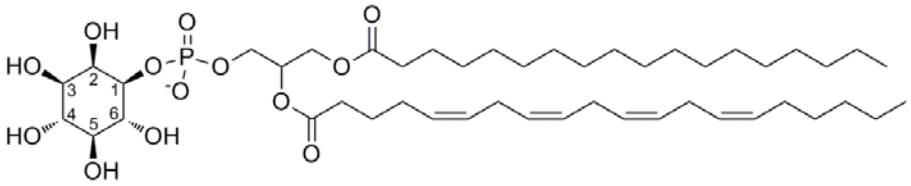

Phosphatidylinositol or PI

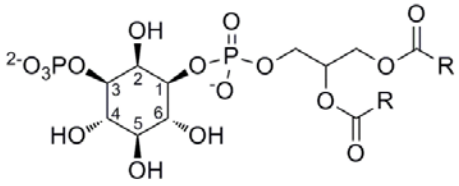

PI(3)P

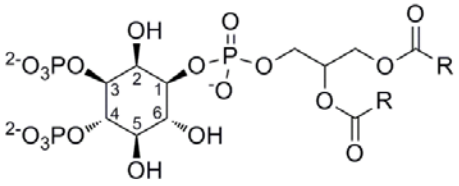

$PI(3,4)P_2$

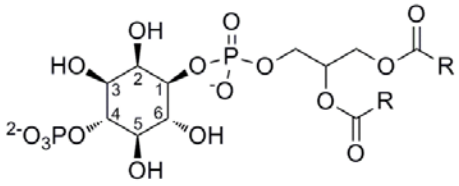

PI(4)P

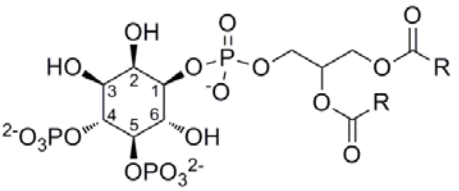

$PI(4,5)P_2$

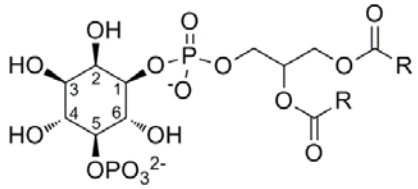

PI(5)P

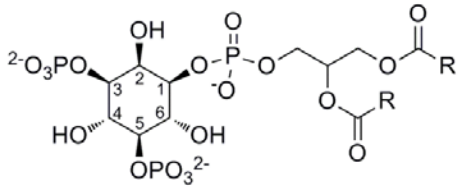

$PI(3,5)P_2$

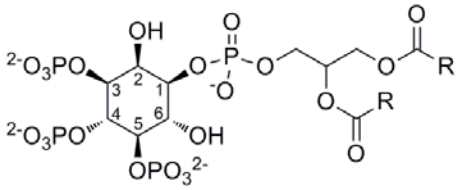

$PI(3,4,5)P_3$

Figure 1.2 Structures of phosphoinositides

Myo-inositol can be transported into cells from the environment, or synthesized *de novo* from D-glucose-6-phosphate (G6P). G6P is first cyclized to form D-*myo*-inositol-3-phosphate (Ins3P or I3P), which is the same as L-inositol-1-phosphate, (L-I-1-P) by NAD^+-dependent D-*myo*-inositol-3-phosphate synthase (MIPS). D-Ins3P is then dephosphorylated by inositol monophosphatase (IMPase) to *myo*-inositol (Michell, 2008) (Figure 1.3). The incorporation of inositol in phospholipids is catalyzed by phosphatidylinositol synthase, which condenses *myo*-inositol with CDP-diacylglycerol to produce PI (Antonsson, 1997). PI and seven phosphoinositides – phosphatidylinositol monophosphates (PI(3)P, PI(4)P, PI(5)P), phosphatidylinositol bisphosphates ($PI(3,4)P_2$, $PI(3,5)P_2$, $PI(4,5)P_2$) and phosphatidylinositol-3,4,5-trisphosphate ($PI(3,4,5)P_3$) can be interconverted by a series of kinase and phosphatase catalyzed reactions (Sasaki et al, 2009) (Figure 1.3).

The biosynthesis of inositol polyphosphates in eukaryotes is not very straight-forward. It appears that the center of inositol polyphosphate metabolism is *myo*-inositol-1,4,5-triphosphate ($I(1,4,5)P_3$ or IP_3), the degradation product of $PI(4,5)P_2$. $I(1,4,5)P_3$ can be further phosphorylated or dephosphorylated to produce other water soluble inositol phosphates (Hatch & York, 2010; Irvine & Schell, 2001). An additional one or two phosphates can be attached to the phosphate group of inositol hexakisphosphate (IP_6 or phytic acid), to form another group of water soluble inositol-containing compounds, the diphosphoryl-inositol phosphates or inositol pyrophosphates (PP-IPs) (Bennett et al, 2006; Chakraborty et al, 2011) (Figure 1.3).

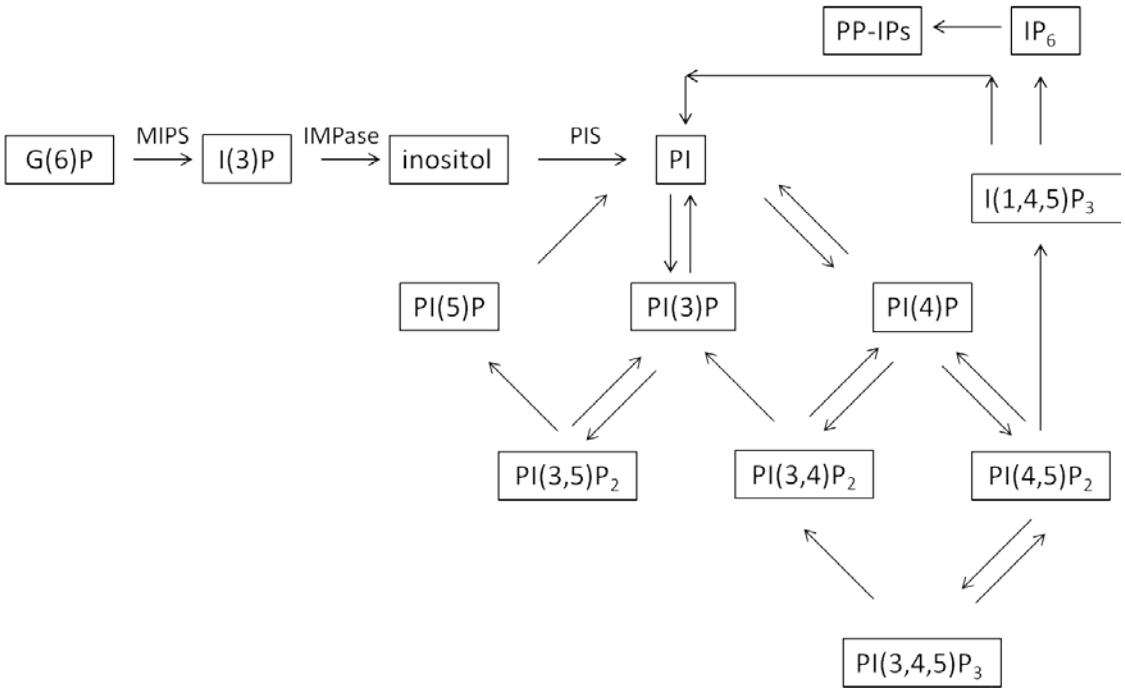

Figure 1.3 Inositol and inositol containing molecules metabolism (Michelle, 2008)

1.2 Function of inositol phosphates in eukaryotes

Inositol phosphates have many functions in eukaryotic cells. The best characterized function of IPs is the use of $I(1,4,5)P_3$ as a second messenger in calcium signaling (Berridge, 2009; Berridge et al, 2000; Streb et al, 1983). Membrane imbedded $PI(4,5)P_2$ is hydrolyzed by phospholipase C (PLC) to produce $I(1,4,5)P_3$ and diacylglycerol (DAG). While DAG, still in the membrane, serves as a lipid second messenger, water soluble IP_3 can diffuse through the cytosol and bind to the IP_3 receptor in the endoplasmic reticulum (ER) and other places where calcium is stored internally to stimulate the calcium release. In this signaling, IP_3 works as the second messenger to pass the information from the cell membrane to intracellular organelles. This IP_3/calcium signaling is involved in diverse cellular processes such as contraction, fertilization, proliferation and metabolism (Berridge, 2009).

Besides the involvement in the calcium signaling pathway, inositol phosphates have other functions in cells (Hatch & York, 2010). IP_6 and IP_5 kinase (IPK1), which accounts for IP_6 production, and various protein factors mediate mRNA export and translation (Alcazar-Roman et al, 2006; Bolger et al, 2008; Tsui & York, 2010; York et al, 1999). IP_6 and other inositol polyphosphates also regulate gene expression at different levels (Alcazar-Roman & Wente, 2008). IPs and PP-IPs also have roles in immune cell development, ion channel permeability, protein phosphorylation and other cellular processes (Barker et al, 2009; Burton et al, 2009; Mitchell et al, 2008; Sauer & Cooke, 2010).

1.3 Function of phosphoinositides in eukaryotes

Unlike water soluble inositol phosphates, PI and PIPs only exist in membrane systems in eukaryotic cells. PI is generally thought to constitute less than 15% of the total phospholipids and the content of PIPs is even an order of magnitude lower than PI (Di Paolo & De Camilli, 2006). The spatial distribution of PIPs is heterogeneous throughout the cell, and each PIPs undergone rapid turnover (Di Paolo & De Camilli, 2006). All seven PIPs are found in mammalian cells, while $PI(3,4,5)P_3$ is not found in plants and yeast lacks both $PI(3,4)P_2$ and $PI(3,4,5)P_3$ (Liu & Bankaitis, 2010).

Although PI and PIPs are minor components of membrane phospholipids, phosphoinositides play major roles in cells by serving as the specific anchors for proteins through protein-phosphoinositide headgroup interactions (Kutateladze, 2010; Lemmon, 2008). Phosphorylated inositol head groups are recognized by different protein domains (Table 1.1). By binding to PIPs these proteins are recruited to the membrane interface. There the proteins can catalyze the interconversion of the PIPs, or interact with other

proteins to regulate different cellular functions ranging from cell signaling, membrane trafficking, cytoskeleton dynamics, nuclear events, ion channel and transporter functions (Bunney & Katan, 2010; Di Paolo & De Camilli, 2006; Gamper & Shapiro, 2007; Martelli et al, 2011; Mayinger, 2012).

Table 1.1 Protein domains that bind different PIPs specifically (Kutateladze, 2010; Lemmon, 2008)

PIPs	Protein domains
PI(3)P	FYVE, PH, PX
PI(4)P	GOLPH3, PH, PTB, PX
PI(5)P	
PI(4,5)P_2	ANTH, ENTH, C2, FERM, PDZ, PH, PTB, PX, Tubby
PI(3,4)P_2	PH, PX
PI(3,5)P_2	PH, PROPPINs
PI(3,4,5)P_3	C2, PH, PX

1.3.1 Phosphatidylinositol monophosphates: PI(3)P, PI(4)P and PI(5)P

PI(3)P can be generated by phosphorylation of PI by class II and class III phosphoinositide 3-kinase (PI3K). It can also be produced by dephosphorylation of PI(3,4)P_2 by PI 4-phosphatase and of PI(3,5)P_2 by PI 5-phosphatase. It can also be dephosphorylated to PI by myotubularins (Sasaki et al, 2009). PI(3)P is found mostly in endosomes. It is generally thought that this molecule mostly exists in resting cells as a constitutive pool to regulate endosome dynamics (Di Paolo & De Camilli, 2006) and is critical for sorting endosomes (Clague et al, 2009). This molecule can be recognized by and bound to FVYE (Fab1, YOTB, Vac1 and EEA1) domain containing proteins, including the components of endosome sorting machinery (Clague et al, 2009; Kutateladze, 2006). Recent reports have revealed PI(3)P is a new dynamic second messenger (Falasca & Maffucci, 2009). The stimulated pool of PI(3)P, which is

generated by the cellular stimulation, is involved in glucose transport, cell migration and other processes (Falasca & Maffucci, 2009).

PI(4)P is one of the most abundant phosphoinositides in cells (Lemmon, 2008). It can be produced from phosphorylation of PI by PI 4-kinase, or dephosphorylation of $PI(4,5)P_2$ by PI 5-phosphatase. It can also be dephosphorylated by PI 4-phosphatase or Sac family phosphatase Sac1 (Sasaki et al, 2009). PI(4)P is found in Golgi as well as plasma membranes (Bunney & Katan, 2010). Initially it was thought that PI(4)P function is to serve as the precursor pool for $PI(4,5)P_2$, but more and more studies show this molecule itself has many functions (D'Angelo et al, 2008). With the detection of many protein effectors of PI(4)P, this molecule is important for Golgi complex morphology and function, and it can regulate membrane trafficking, control protein and lipid flux toward the cell surface and contribute to lipid metabolism (D'Angelo et al, 2008).

PI(5)P is perhaps the least characterized phosphoinositide. PI(5)P is generated *in vitro* from direct phosphorylation of PI at D5 by two kinases PIP5K (PI(4)P 5-kinase) and PIKfyve. The ability of these kinases to generate PI(5)P from PI *in vivo* is still uncertain (Grainger et al, 2012). Instead, PI(5)P can be generated from dephosphorylation of $PI(4,5)P_2$ by $PI(4,5)P_2$ 4-phosphatase and of $PI(3,5)P_2$ by myotubularins. PI(5)P is found constitutively in several cell types and the majority of PI(5)P exists in the plasma membrane as well as intracellular membrane compartments such as the ER and Golgi (Sarkes & Rameh, 2010). Nuclei also have a PI(5)P pool, and this pool is responsive to the cellular stress (Jones et al, 2006). Although few protein effectors of PI(5)P have been identified, studies showed this molecule plays roles in nuclear protein function regulation,

gene expression, glucose metabolism, and also possibly in membrane trafficking (Grainger et al, 2012).

1.3.2 Phosphatidylinositol bisphosphates: PI(3,5)P_2, PI(4,5)P_2 and PI(3,4)P_2

PI(4,5)P_2 is also one of the most abundant phosphoinositides in cells (Lemmon, 2008). It is generated by phosphorylation of PI(4)P and PI(5)P by phosphatidylinositol phosphate kinases (PIPKs). It can be dephosphorylated to PI(4)P by PI 5-phosphatase and to PI(5)P by PI 4-phosphatase (Sasaki et al, 2009). As addressed before, PI(4,5)P_2 can be degraded to IP_3 and DAG by PLC enzymes. PI(4,5)P_2 is mostly found at the plasma membrane and participates in nearly all cellular processes involving the cell surface (Di Paolo & De Camilli, 2006). First, it is considered as an intermediate of second messenger generation that propagates and amplifies the signaling (Di Paolo & De Camilli, 2006). PI(4,5)P_2 is cleaved by PLC upon stimulation to generate IP_3 and DAG. IP_3 is responsible for calcium signaling, and DAG can activate protein kinase C (PKC), which accounts for much cellular signaling by phosphorylating diverse proteins (Nishizuka, 1988). In parallel, PI(4,5)P_2 can be phosphorylated at D3 to produce PI(3,4,5)P_3, which generates a key component of another important signaling pathway (PI3K signaling pathway, see discussion below). Besides being a precursor, PI(4,5)P_2 itself also mediates plasma membrane-cytoskeleton interactions with PI(3,4,5)P_3 and small GTPases, to control cell shape, motility and other processes (Di Paolo & De Camilli, 2006). It is directly involved in exocytosis and all forms of endocytosis. Some of the proteins required for these processes have the ability to bind PI(4,5)P_2 (Mayinger, 2012). The PI(4,5)P_2 signal can be turned off through dephosphorylation of PI(4,5)P_2 by PI 5-phosphatase, and this process is important for a functional endocytic pathway (Mayinger, 2012).

$PI(3,5)P_2$ is generated by phosphorylation of PI(3)P by type III phosphatidylinositol phosphate kinase (PIPKIII) initially known as PIKfyve in mammals (Sasaki et al, 2009). It can be dephosphorylated to PI(3)P by type IV 5-phosphatase and sac family Sac3. It can also be dephosphorylated to PI(5)P by myotubularins (Sasaki et al, 2009). In higher eukaryotes, $PI(3,5)P_2$ exists in endolysosomes, and it is important for endolysosomes functions, including endolysosome morphology, acidification and trafficking (Ho et al, 2012). It also regulates membrane transport, autophagy, and other cellular processes, although the identities of some of the protein effectors involved in these processes are not very clear (Ho et al, 2012).

$PI(3,4)P_2$ can be generated from PI(4)P phosphorylation by class II PI3K, although this class of enzyme mainly accounts for generation of PI(3)P from PI. Dephosphorylation of $PI(3,4)P_2$ is accomplished by type II 4-phosphatase (INPP4) to produce PI(3)P (Sasaki et al, 2009). $PI(3,4)P_2$ appears to be part of the PI 3-kinase signaling pathway, and the specific signaling role of $PI(3,4)P_2$ remains unassigned (Leslie et al, 2008). Akt, a component of PI3K signaling pathway, binds to $PI(3,4)P_2$ by its pleckstrin homology (PH) domain (Franke et al, 1997). $PI(3,4)P_2$ also plays a distinct role in Akt phosphorylation and activity (Ma et al, 2008). There are also some proteins that contain PH domains that specifically bind to $PI(3,4)P_2$. Examples are TAPP (tandem pleckstrin-homology domain-containing protein) (Dowler et al, 2000) and lamellipodin (Krause et al, 2004). The two phosphatases that dephosphorylate $PI(3,4)P_2$ also have some functional significance. INPP4A suppresses excitotoxic cell death in neurons (Sasaki et al, 2010) and INPP4B is proposed as a potential tumor suppressor (Agoulnik et al, 2011). These observations

imply that PI(3,4)P_2 may have distinct roles in cellular function besides acting in PI3K signaling.

1.3.3 PI(3,4,5)P_3 and the PI 3-kinase (PI3K) signaling pathway

Before identification of PI(3,4,5)P_3, PI 3-kinase (PI3K) was first found to be associated with oncogene products and platelet-derived growth factor (PDGF) receptors. It was later identified as a kinase that phosphorylates phosphoinositides at the D3 position of the inositol ring to generate PI(3)P from PI (Whitman et al, 1988). The same year, PI(3,4,5)P_3 was identified as a novel phosphoinositide in activated neutrophiles (Traynorkaplan et al, 1988). In 1989, PI(3,4,5)P_3 was reported to be generated from PI(4,5)P_2 by PI3K in anti-phosphotyrosine immunoprecipitants of PDGF stimulated vascular smooth muscle cells. This novel phosphoinositide was proposed as the signaling molecule that propagates PDGF signal into the cells (Auger et al, 1989). Today, numerous studies on PIP_3 and the PI3K signaling pathway demonstrate this signaling regulates many cellular processes including cell growth, proliferation, migration, differentiation, survival, chemotaxis, and metabolism (Di Paolo & De Camilli, 2006) (Figure 1.4).

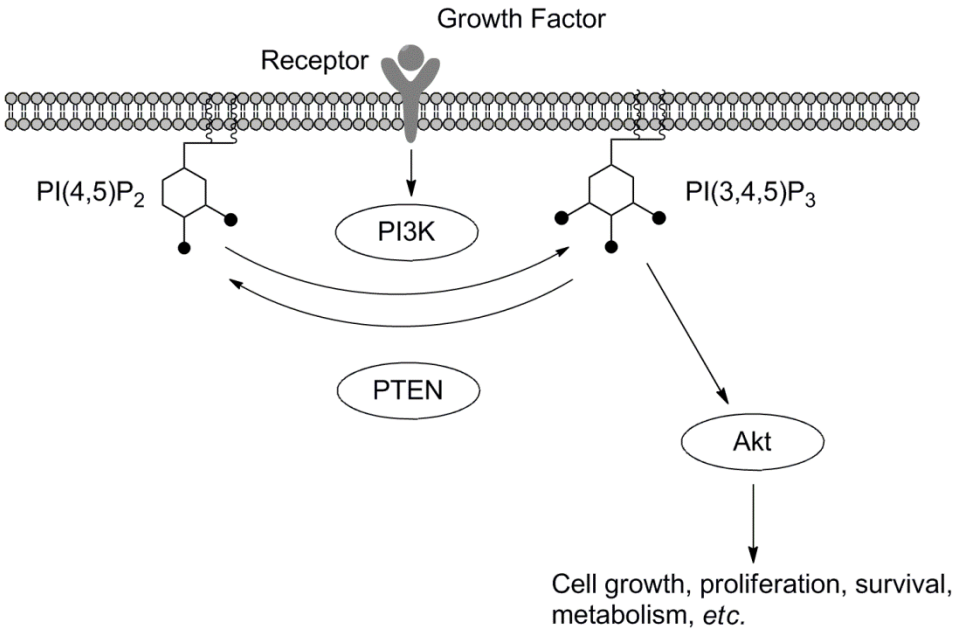

Figure 1.4 PI3K/ Akt signaling pathway

The level of $PI(3,4,5)P_3$ in resting cells is negligible, but it can be increased dramatically and transiently due to the activation of PI3K by growth factor stimulation (Di Paolo & De Camilli, 2006). There are three classes of PI 3-kinase, with Class I PI3K phosphorylating $PI(4,5)P_2$ to $PI(3,4,5)P_3$ preferentially (Hawkins et al, 2006). Once ligands, such as growth factors, bind to the cell surface receptors, for example receptor tyrosine kinase (RTK) or G-protein coupled receptor (GPCR), PI3K is recruited to the inner leaflet of plasma membrane and activated by binding to phosphorylated tyrosine on RTK or Gβγ subunits of GPCR downstream G proteins. PI3K can also be recruited to the membrane by activated GTPase, Ras family members (Hawkins et al, 2006; Vanhaesebroeck et al, 2010; Vanhaesebroeck et al, 2012). Upon translocation to the membrane and activation, PI3K phosphorylates $PI(4,5)P_2$ to generate $PI(3,4,5)P_3$. PIP_3 mediates downstream signaling by binding to proteins containing domains that bind PIP_3 specifically. One of the key downstream effectors of $PI(3,4,5)P_3$ is Akt (also known as protein kinase B or

PKB) (Bunney & Katan, 2010; Hers et al, 2011). This protein contains a pleckstrin homology (PH) domain, a common domain found in most PIP_3 binding proteins. Upon binding to PIP_3, Akt is recruited to the plasma membrane where it undergoes a conformational change. After phosphorylation on Thr308 by co-recruited PDK1 (3-phosphoinositide-dependent protein kinase 1) and on Ser473 by mTORC2 (mammalian target of rapamycin complex 2), Akt is activated and dissociates from the plasma membrane into the cytosol as well as traffics to the nucleus. In those locations, Akt phosphorylates its substrates, including but not limited to FOXO (forkhead box O), GSK3 (glycogen synthase kinase 3), Bad (B cell lymphoma 2 (BCL-2) antagonist of cell death), and the E3 ubiquitin-protein ligase MDM2. These phosphorylations affect downstream signaling molecules, leading to the regulation of many cellular process such as proliferation, cell survival, metabolism and angiogenesis (Hers et al, 2011; Manning & Cantley, 2007).

$PI(3,4,5)P_3$ can be dephosphorylated by PI 3-phosphatase or PI 5-phosphatase, but these two dephosphorylation steps lead to different fates. PTEN (phosphatase and tensin homolog deleted on chromosome ten) dephosphorylates $PI(3,4,5)P_3$ at the D3 position and turns off the signal (see discussion below), while SHIP1 and SHIP2 (SH2 domain-containing inositol 5-phosphatase 1 and 2) dephosphorylate PIP_3 to generate $PI(3,4)P_2$, another second messenger that can regulate cell signaling and lengthen the duration of PIP_3 signaling (Bunney & Katan, 2010; Di Paolo & De Camilli, 2006).

Dysregulation of the PI3K /Akt signaling pathway is linked to many diseases, including cancer, metabolic dysfunction, cardiovascular diseases and mental diseases (Franke, 2008). Due to its importance, PI3K is now considered as a drug target for disease

treatment. Many PI3K inhibitors have been generated and some of them are already in clinic trials with promising results (Vanhaesebroeck et al, 2012).

1.4 PTEN

Back in 1997, two groups reported the identification of a gene located on chromosome 10q23, the mutation of which was found in most advanced cancers. This gene was proposed as a tumor suppressor and one of the groups named it as Phosphatase and Tensin homolog deleted on chromosome Ten, *PTEN*, due to the presence of a protein tyrosine phosphatase (PTP) signature motif and protein sequence homology to tensin (Myers et al, 1997; Steck et al, 1997). From then on, numerous studies on the role of this gene and its encoded protein, PTEN, revealed the importance of this protein as the gatekeeper of the PI 3-kinase signaling pathway. In cells where PTEN function is lost, excessive $PI(3,4,5)P_3$ recruits and activates Akt and other downstream signaling molecules at higher levels, leading to abnormal cell growth and proliferation which in turn causes many diseases (Song et al, 2012).

The deletion, insertion and/or mutation of the PTEN gene are often found in a wide variety of tumor cells including endometrial cancer, glioblastoma, prostate cancer, breast cancer and lung tumor (Salmena et al, 2008). Germline mutations of the *PTEN* gene are also present in patients having PTEN hamartoma toumor syndromes (PHTs), including Bannayan–Riley–Ruvalcaba syndrome (BRRS), Cowden syndrome, Proteus syndrome (PS), and Proteus-like syndrome (PSL), with which patients may have developmental disorders, neurological deficits, and have an increased risk of developing breast and other cancers (Salmena et al, 2008; Song et al, 2012). Studies also found that overexpression of PTEN in tumor cells which have lost PTEN expression suppresses cell growth and

tumorigenicity (Leslie & Downes, 2004). Besides serving as a tumor suppressor, PTEN has many roles in other cellular processes, such as cell metabolism, cell polarity, stem cell self-renewing activity and neuronal injury (Chang et al, 2007; Song et al, 2012). Most of the functions of PTEN are linked to its ability to dephosphorylate phosphoinositides. Since PTEN has such clinical significance, there has been intense study of this enzyme in many laboratories; the function and regulation of PTEN has also been highly reviewed (Gericke et al, 2006; Leslie et al, 2008; Leslie & Downes, 2004; Maehama et al, 2001; Shi et al, 2012; Song et al, 2012).

1.4.1 Substrate specificity

PTEN was first identified as a dual-specificity phosphatase (it can dephosphorylate phosphotyrosine and phosphoserine or phosphothreonine) based on the observation that it contained the signature motif of the protein tyrosine phosphatase (PTP) superfamily of enzymes (Li et al, 1997; Myers et al, 1997). Initial enzymatic activity studies of recombinant PTEN showed it could dephosphorylate proteins and peptides commonly used as PTP substrates, but the activity toward these phosphorylated Ser/Thr/Tyr substrates was very low. PTEN also had a strong preference for extremely acidic peptide substrates (Myers et al, 1997). Later on, PTEN was found to dephosphorylate the D3 position of the inositol ring of PIPs, with highest activity observed toward PI(3,4,5)P_3 and lower activity toward PI(3,4)P_2 and PI(3)P *in vitro*. PTEN could also dephosphorylate I(1,3,4,5)P_4, the water soluble head group of PI(3,4,5)P_3, at the D3 position of the inositol ring (Maehama & Dixon, 1998). However the activity toward lipid substrates was significantly higher than that toward water soluble inositol polyphosphates (Myers et al, 1998). PTEN's function as a lipid PIP_3 phosphatase to suppress PI3K/Akt signaling *in*

vivo was also demonstrated (Myers et al, 1998; Stambolic et al, 1998). As summarized in Table 1.2 (Maehama et al, 2001), the specific activity of PTEN toward PI(3,4,5)P_3 is 50-1500 fold higher than other substrates, suggesting this lipid is the physiological substrate of PTEN. Our group also reported the apparent K_m and V_{max} value of PTEN toward short chain diC_8PI(3)P were 0.2±0.07 mM and 14±1 nmol/mg/min, consistent with the results of other groups (Wang et al, 2008).

Table 1.2 PTEN phosphatase activity toward different substrates (adapted from Meahama, et al. 2001, N.D. not determined). Unless indicated the PIP_x were obtained from natural sources so they have unsaturated acyl chains.

Substrate	K_m (μM)	Specific activity (min^{-1})
pNPP (*p*-nitrophenyl phosphate)	25600	0.77
I(1,3,4)P_3	N.D.	0.078
I(1,3,4,5)P_4	98.9	0.30
PI(3)P	N.D.	2.0
PI(3,4)P_2	N.D.	2.6
PI(3,4,5)P_3	<50	120

1.4.2 PTEN structure

The *PTEN* gene encodes a 403-amino-acid long protein that belongs to the dual-specificity protein phosphatase and PI 3-phosphatase family (EC 3.1.3.16, 3.1.3.48, 3.1.3.67). The crystal structure of PTEN was solved in 1999 by cocrystallization of tartrate with a truncated form of protein (Lee et al, 1999). The structure is composed of the N-terminal catalytic phosphatase domain and a C-terminal lipid-binding C2 domain (Figure 1.5). The phosphatase domain has a five-stranded β sheet in the center with two and four α helices packed on each side. Its structure is similar to dual-specificity phosphatase VHR (vaccinia H1-related phosphatase, also known as DUSP3, the dual specificity protein phosphatase 3) with several residues inserted in some loops. One of the insertions is an 11-residue insertion in the pβ2-α1 loop from residue 42 to 52. The

phosphatase domain of PTEN contains the PTP signature motif HCXXGXXR (residues 123-130), which comprises the "P loop" located at the bottom of the active site pocket. Cys124 in this P loop acts as the nucleophile to attack D3 phosphate. The "WPD" loop (residues 91-94) and the "TI" loop (pα5-α6) form the wall of the active site (Figure 1.6). Due to a 4-residue insertion in the "TI" loop, the active site pocket of PTEN is wider when compared to that of VHR and PTP1B (protein tyrosine phosphatase 1B) and deeper than VHR. The larger width of the active site pocket can accommodate the larger size of the phosphorylated inositol ring of the substrate, PI(3,4,5)P_3. The positive charges on two unique residues, Lys125 and Lys128, in the signature motif are consistent with interacting with the negative charges of the PI(3,4,5)P_3 substrate. A tartrate molecule was found bound in the active site pocket (Figure 1.6). I(1,3,4,5)P_4, the head group of physiological substrate PI(3,4,5)P_3, can be superimposed on the tartrate. In this *in silico* complex, the substrate D3 phosphate was superimposed on one carboxylate group of tartrate, forming hydrogen bonds with Cys124 and Arg130 on the P loop. The D4 phosphate was superimposed on the other carboxylate group, forming hydrogen bonds with residues in both the WPD and TI loops. The phosphate at the D5 position of IP_4 in this superposition structure resides next to Lys128 and His93. The interaction between the D5 phosphate and those two basic residues was demonstrated by mutation. The proteins K128M and H93A had reduced activity toward PI(3,4,5)P_3 but comparable activity toward PI(3,4)P_2 and PI(3)P (Lee et al, 1999).

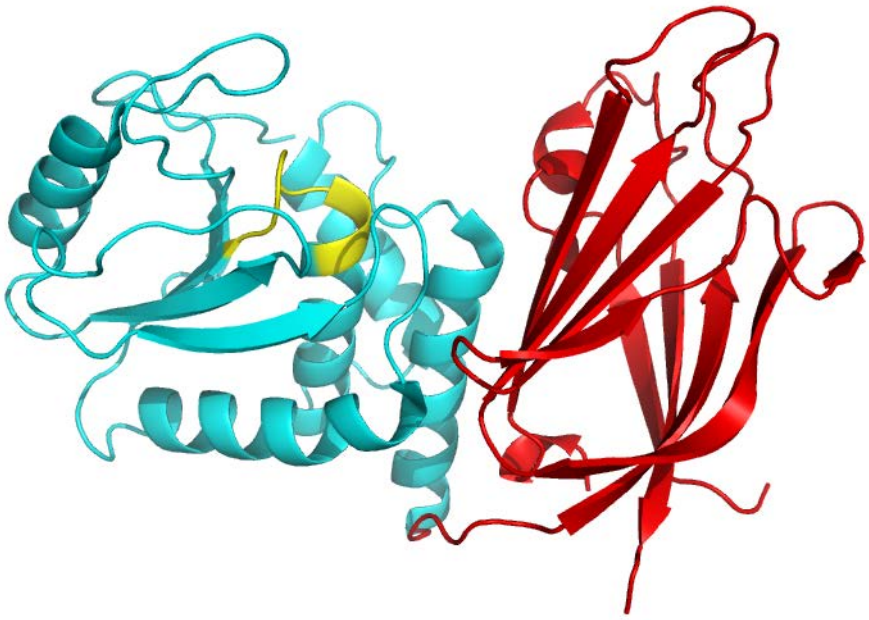

Figure 1.5 Ribbon diagram showing the crystal structure of PTEN. The phosphatase domain is colored in cyan, C2 domain in red, and P loop is colored in yellow. (PDB 1D5R)

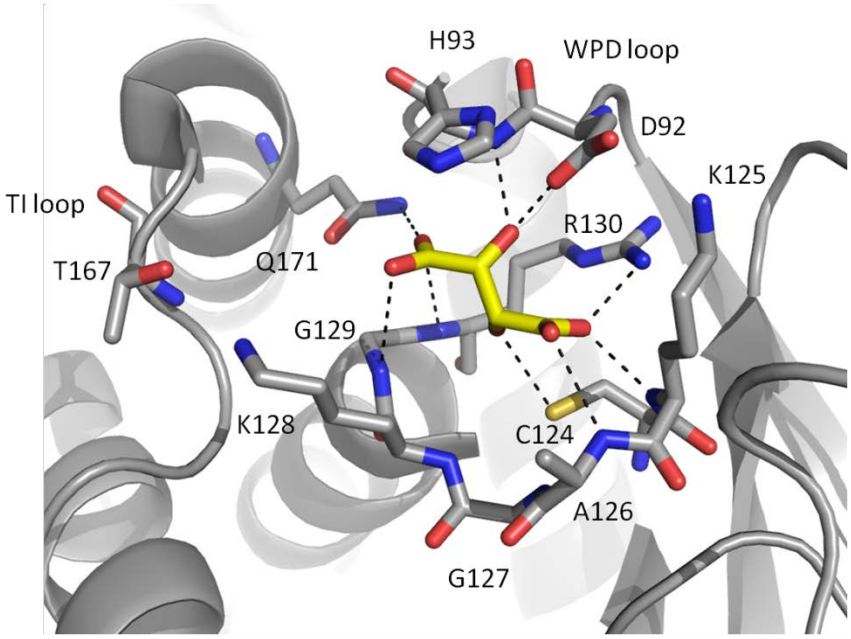

Figure 1.6 Structure of the PTEN active site. A tartrate molecule is colored in yellow with oxygen atoms in red. The hydrogen bonds formed by tartrate with protein active site are shown as dashed lines (Lee et al, 1999)

The structure of the C-terminal domain adopts a type II C2 fold topology, a β sandwich consisting of two antiparallel β sheets with two α helices intervening between. This domain is similar to the C2 domains of PKCδ, PLCδ1, and $cPLA_2$ (cytosolic phospholipase A_2). Unlike the PLCδ1 and cPLA2 C2 domains, the PTEN C2 domain does not bind Ca^{2+} and so is Ca^{2+} independent. It has only one of the three loops (termed the CBR3 loop) that are needed for calcium binding. The PTEN C2 domain has been shown to bind to phospholipid vesicles *in vitro* (Lee et al, 1999). There are two basic patches on the CBR3 and the adjacent Cα2 helix of C2 domain, proposed as the important membrane-binding elements of PTEN. Mutation at these two basic patches made the protein lose its tumor suppressor function (Lee et al, 1999).

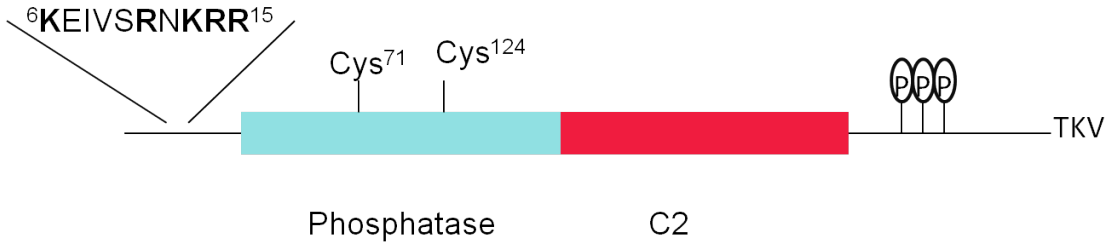

Figure 1.7 Representation of PTEN sequence showing key residues. Phosphatase and C2 domains are indicated as boxes. The sequence of the N-terminal cationic binding patch (NBP) is shown with the conserved residues in bold. Two cysteines in the phosphatase domain that can be oxidized are also shown. The C-terminal tail contains multiple phosphorylation sites; the last three residues are assigned as a PDZ binding domain.

Along with these two globular domains, the PTEN protein has an N-terminal loop containing a $PI(4,5)P_2$ binding consensus sequence (N-terminal $PI(4,5)P_2$ binding patch or NBP) (Maehama et al, 2001), a 50-amino acid C-terminal tail containing Ser and Thr residues that could be phosphorylated, and a PSD-95/Dlg/ZO-1 homology (PDZ) binding domain at the C-terminal end (Figure 1.7). All these elements are not included in the

protein crystal structure, but are shown to play important roles in PTEN function (see discussion below).

1.4.3 PTEN membrane binding and the role of the N-terminal loop

Most PTEN molecules are found in cytosol. However, the substrate of PTEN, $PI(3,4,5)P_3$, resides in the inner leaflet of plasma membrane. In order to catalyze dephosphorylation of the substrate, PTEN has to bind to the membrane. This membrane binding event is critical for PTEN function. Initial studies showed that both PTEN full length protein and GST-fused C2 domain alone had some affinity for phosphatidylcholine (PC) multilamellar vesicles. Mutations in the CBR3 and Cα2 regions to remove most of positive charges as well as hydrophobic residues reduced the binding affinity for vesicles and reduced the growth suppression effect in U87-MG glioblastoma cells (Lee et al, 1999). These results indicated the importance of the C2 domain in mediating PTEN membrane binding. Later, binding of PTEN to immobilized vesicles was explored by surface plasma resonance analysis, and the results showed that *both* phosphatase and C2 domains are important for lipid binding (Das et al, 2003). PTEN full length protein and C2 domain had low affinity for neutral PC vesicles, but the lipid binding affinity was increased by incorporating anionic lipids such as phosphatidylserine (PS) into the vesicles. For phosphatase domain contribution to vesicle binding, surface Lys and Arg clusters (R11/K13/R14/R15 and R161/K163/K164) provide nonspecific electrostatic interactions with the negatively charged lipids. Deletion of this domain increased the vesicle dissociation constant (K_d). A kinetic study of PTEN with unilamellar vesicles revealed that PTEN is an interfacial enzyme whose activity is dependent on both the mole fraction of the substrate in the vesicles and the bulk concentration of the lipid vesicles

(McConnachie et al, 2003). A single molecule study of PTEN binding to membranes in live cells showed that the binding is highly dynamic with a dwell time less than 400 ms but long enough for PIP_3 dephosphorylation (Vazquez et al, 2006).

Incorporation of the anionic lipid $PI(4,5)P_2$, the dephosphorylation product of $PI(3,4,5)P_3$, into the lipid vesicles, enhanced protein activity (McConnachie et al, 2003). When the substrate $PI(3,4,5)P_3$ was in PIP_3/PC vesicles (starting from a mole fraction of 0.0001 with a bulk concentration 10μM), adding 100-fold greater $PI(4,5)P_2$ (mole fraction 0.01 in the vesicles) enhanced protein activity 5-fold, while incorporation of 0.05 mole fraction PS enhanced activity only slightly. In contrast, with $PI(4,5)P_2$ present, PTEN activity toward water soluble $I(1,3,4,5)P_4$ substrates was inhibited. So the mechanism for how $PI(4,5)P_2$ enhanced protein activity was suggested as interfacial activation. The excess of anionic lipids in the vesicles enhanced protein proximity to substrates and thus activated the protein (McConnachie et al, 2003).

The $PI(4,5)P_2$ activation of PTEN was also reported in a phospholipid monomer system (Campbell et al, 2003). Dioctanoyl-$PI(3,4,5)P_3$ ($diC_8PI(3,4,5)P_3$) was used as the substrate at the concentration of 45 μM, below the critical micelle concentration (CMC) of diC_8PI (stated as 60μM, but it depends critically on the ionic strength and is usually about 5- to 10-fold higher). Adding half (22.5 μM) or equal (45 μM) amounts of $diC_8PI(4,5)P_2$ compared to substrate enhanced protein activity. This kinetic activation was more obvious when using $PI(3,4)P_2$ as the substrate. The results suggested a positive feedback of dephosphorylation of PIP_3 since $PI(4,5)P_2$ is the dephosphorylation product. PI(5)P also promoted PIP_3 dephosphorylation, while PI(4)P did not. $DiC_4PI(4,5)P_2$ could not activate PTEN. The $PI(4,5)P_2$ activation effect also occurred when all the substrates

and activator molecules were monomers (at least in the absence of protein), suggesting that a membrane interface is not a necessary factor for activation. The PTEN N-terminus has a $PI(4,5)P_2$ binding consensus sequence K/R-X-X-X-X-K/R-X-K/R-K/R. Mutation studies at this binding motif showed that K13A and R14A exhibited much less activity in the presence and absence of $PI(4,5)P_2$. The authors then proposed that PTEN binds to $PI(4,5)P_2$ specifically with this N-terminal motif and a critical conformational change is induced that enhances catalytic activity.

The study looking at tumor-derived point mutations in this potential N-terminal PIP_2 binding patch (NBP), and notably K13E, led to a somewhat different conclusion (Walker et al, 2004). *In vitro* studies with this mutant PTEN showed it had similar activity toward $PI(3,4,5)P_3$ and $I(1,3,4,5)P_4$, but PTEN K13E lost activation by $PI(4,5)P_2$ and PS. Furthermore, $PI(4,5)P_2$ could not inhibit PTEN-K13E activity toward $I(1,3,4,5)P_4$, while this molecule could inhibit wild type PTEN activity toward IP_4. Due to the different effects of $PI(4,5)P_2$ on PTEN activity toward PIP_3 and IP_4, and the reversed behavior of PTEN-K13E, the authors argued that the role of $PI(4,5)P_2$ is to enhance protein recruitment on lipid vesicles and orient the protein active site for interaction with substrate, rather than to act as a purely allosteric activator. The role of this N-terminal loop in PTEN function would appear to be quite important. PTEN-K13E no longer suppresses Akt phosphorylation or prevents cell proliferation in *pten*-null U87MG cells. However, the physiological binding partner of this N-terminal loop is uncertain, since PS could also activate PTEN and it is more abundant than $PI(4,5)P_2$ in the plasma membrane (Walker et al, 2004).

Another *in vitro* investigation of the N-terminal $PI(4,5)P_2$ binding patch was done using florescence spectroscopy (Redfern et al, 2008). The fluorophore was incorporated into the PC vesicles containing anionic lipids ($PI(4,5)P_2$ and/or PS). When PTEN binds to these vesicles, its intrinsic fluorescence (due to Trp residues) is quenched. This technique can be used to monitor vesicle binding. Incorporation of 5 mol% $PI(4,5)P_2$ into PC vesicles enhanced protein binding by lowering the apparent K_d from near 600 μM to 163 μM. Adding higher amount of PS (10 mol%) also enhanced binding 3-fold. $PI(4,5)P_2$ and PS were found to work synergistically so that the highest affinity binding (the lowest K_d, 42 μM) was observed when using vesicles contained both PIP_2 and PS (5 mol% $PI(4,5)P_2$ /5 mol% PS / PC). The binding affinity was even higher than with 10 mol% PIP_2 containing vesicles. Deletion of the first 15 residues or a point mutation at Lys13 (K13E) weakened the binding to PIP_2 containing vesicles. The peptide derived from PTEN residues 1-21 also showed preferential binding to vesicles with PIP_2. These results suggest that binding of PIP_2 with the N-terminal region is specific. Evidence for a protein conformational change was investigated using infrared spectroscopy (IR). The α-helix content of PTEN increased when it bound to $PI(4,5)P_2$, while binding to PS increased protein β-sheet content slightly. These authors suggested that PTEN binding to $PI(4,5)P_2$ is specific and uses the N-terminal binding motif. They also argue that there is a conformational change in the phosphatase domain upon $PI(4,5)P_2$ binding since this domain mostly consists of α-helices. However, in this study, validation of PTEN specifically binding to $PI(4,5)P_2$ via the NBP was only demonstrated indirectly by the different behavior of mutated proteins. $PTEN_{1-21}$ showed preferential binding to $PI(4,5)P_2$ but there is no way to demonstrate this peptide has the same behavior as full-length

protein. There was also no detailed information about any conformational change upon vesicle binding.

Other studies looking at this potential N-terminal PIP_2 binding patch (NBP) also showed the importance of this binding motif in PTEN function. A study of chemotaxis in *Dictyostelium discoideum* showed PTEN is important for this process of moving toward chemoattractants (Iijima & Devreotes, 2002; Iijima et al, 2004). Cells lacking PTEN activity lost polarity and directional sensing. In *D. discoideum*, PTEN is associated with the plasma membrane at the rear of the cell when the extracellular stimuli were detected, and this membrane association is important for cell chemotaxis. PTEN membrane binding is independent of its phosphatase activity, since the catalytically dead C124S and G129E both bound to membranes. However, deletion of first 15 residues of PTEN, containing the whole NBP, abrogated PTEN membrane binding and proper function, and this truncated version of PTEN had no activity toward $PI(3,4,5)P_3$ but higher activity toward $I(1,3,4,5)P_4$ (Iijima et al, 2004). This led to a model for PTEN regulation. In the cytosol, the N-terminal PIP_2 binding motif masks the PTEN catalytic domain, but when the protein is bound to a membrane this constraint is relieved and protein regains catalytic function (Iijima et al, 2004). However, this chemotaxis study only demonstrated the importance of this binding motif in membrane association; it was not related to $PI(4,5)P_2$ activation. The importance of this PIP_2 binding motif in PTEN membrane binding and proper function was also confirmed by using single-molecule total internal reflection fluorescence microscopy (TIRF) to study PTEN membrane binding dynamics in HEK293 cells. Deletion of the first 10 residues, part of the NBP, eliminated PTEN binding to the plasma membrane and prevented it from rescuing function in *pten*$^-$ cells (Vazquez et al,

2006). However, again, PI(4,5)P_2 was not involved. The first report of the necessity of PI(4,5)P_2 at the plasma membrane for PTEN binding was in 2009 (Rahdar et al, 2009). The report showed that in HeLa cells, if the PI(4,5)P_2 was depleted from the inner leaflet of the membrane, a dephosphorylated dead version of PTEN ($PTEN_{C124S,\ A4}$) fused to YFP (yellow fluorescent protein) ($PTEN_{C124S,\ A4}$-YFP) was re-localized to the cytosol, indicating the membrane binding site for PTEN disappeared. This result clearly demonstrated that PI(4,5)P_2 is required for PTEN binding to membrane, but the work did not answer whether or not deletion or mutation at the NBP eliminated this particular version of PTEN association with the membrane, although combined with the other results discussed above this is highly probable.

To date there is no definitive evidence that an individual PI(4,5)P_2 molecule binds to the N-terminal binding motif of PTEN. There is more evidence supporting a PI(4,5)P_2 activation mechanism that is due to the PI(4,5)P_2 binding to the NBP and inducing the conformational change, but the details of this mechanism are still missing.

To complicate matters, phosphorylation of the C-terminal tail and interaction with PDZ domain-containing proteins also regulate PTEN membrane binding events (see discussion below). Taken together, PTEN uses all of its different domains and motifs to regulate its binding to membranes (Figure 1.8).

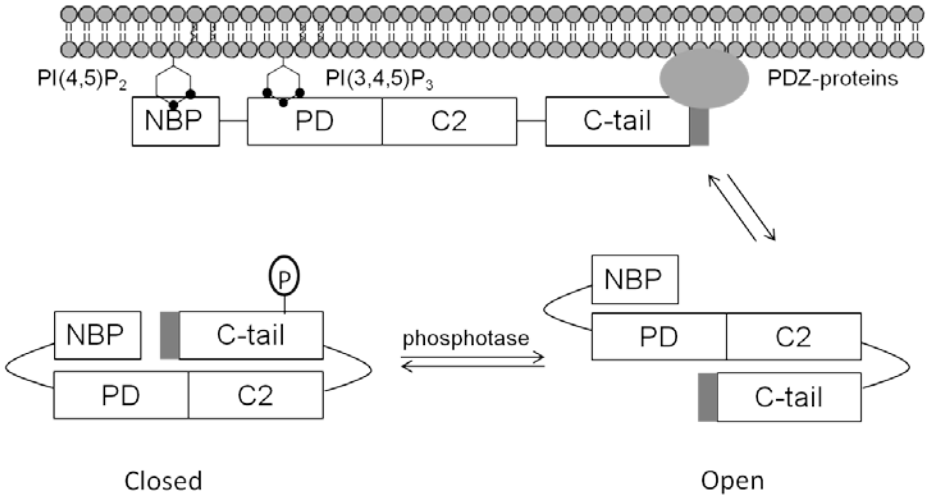

Figure 1.8 Regulation of PTEN binding to membranes. In the cytosol, phosphorylated PTEN is in a 'closed' conformation, and the N-terminal PI(4,5)P_2 binding patch masks the active site. After dephosphorylation, PTEN is in an 'open' conformation, and the NBP is released from the phosphatase domain. NBP interacts with PI(4,5)P_2 to activate protein. PDZ binding domain (shown as grey box) also interacts with PDZ domain containing proteins on the membrane. PTEN binds to membranes and dephosphorylates PI(3,4,5)P_3 (Iijima et al, 2004; Rahdar et al, 2009; Vazquez et al, 2000).

1.4.4 PTEN C-tail, regulation by phosphorylation

PTEN has a 53-amino-acid long unstructured flexible tail, from residue 351 to the C-terminus, which was not included in the crystal structure. Several Ser and Thr residues on this C-tail have been reported to be phosphorylated. To date, up to 9 residues on the C-tail, Ser361, Ser362, Thr363, Thr366, Ser370, Ser380, Thr382, Thr383 and Ser385 have been reported as phosphorylation sites (Cordier et al, 2012; Gericke et al, 2006; Leslie et al, 2008). The effect of phosphorylation of the C-tail on PTEN function was studied extensively, especially for the Ser380-Ser385 cluster. Dephosphorylation mimics, where alanine was substituted for the Ser residues in the Ser380-Ser385 cluster ($PTEN_{A4}$ or S380A/T382A/T383A/S385A), had higher phosphatase activity but decreased stability. Phosphorylation at these sites inhibited protein function and prevented PTEN binding to

protein complexes via its PDZ binding domain (Vazquez et al, 2001; Vazquez et al, 2000). A two-conformation model was proposed whereby phosphorylation at the C-tail makes the protein adopt a 'closed' conformation in which its PDZ binding domain is masked, and dephosphorylation biases the protein to adopt a more active but less stable 'open' conformation (Vazquez et al, 2001; Vazquez et al, 2000). Many studies support this closed/open model. For example, the phosphorylation mimic, substituting a glutamate at phosphorylation sites (PTEN S380E/T382E/T383E) lowers the protein affinity for PS containing vesicles (Das et al, 2003). $PTEN_{A4}$ was shown to have enhanced membrane association, and phosphorylation reduced protein membrane binding (Vazquez et al, 2006). The peptide containing part of C-tail (residues 368-390) with glutamate mutations mimicking the phosphorylation was able to inhibit the PTEN phosphatase activity toward PIP_3 (Odriozola et al, 2007). A detailed study of this closed/open model provided more evidence (Rahdar et al, 2009). Truncated PTEN which had no C-tail ($PTEN_{1-351}$) had higher membrane binding than full length protein, and co-expression of PTEN C-tail ($PTEN_{352-403}$) in U87 cells prevented $PTEN_{1-351}$ binding to membranes, while co-expression of the C-tail containing dephosphorylation mimicking alanine mutations ($PTEN_{352-403(A4)}$) did not. Coimmunoprecipitation of $PTEN_{1-351}$ with $PTEN_{352-403}$ happened regardless of whether $PTEN_{1-351}$ and $PTEN_{352-403}$ were expressed together or separately in HEK293T cells; the 'dephosphorylated' C-tail ($PTEN_{352-403(A4)}$ or phosphatase treatment) did not coimmunoprecipitate with $PTEN_{1-351}$. All these findings demonstrated phosphorylated PTEN C-tail has specific interactions with the other part of the protein, and this interaction was phosphorylation dependent. Interestingly, part of the NBP (residues 11-15), active site integrity and accessibility, a

positively charged cluster on the phosphatase domain (R161, K163, K164), and the CBR3 loop in the C2 domain were all important for the interaction with phosphorylated C-tail. This work strongly supported the closed/open model of PTEN, and provided an explanation for the fact that most PTEN was cytoplasmic although the protein is constitutively active (Ross & Gericke, 2009) (Figure 1.8).

Several kinases are found to be responsible for PTEN phosphorylation. Casein kinase 2 (CK2) phosphorylates the protein at Ser370, Ser380, Thr382, Thr383 and Ser385 (Miller et al, 2002; Torres & Pulido, 2001), and glycogen synthase kinase-3 β (GSK3β) accounts for Ser362 and Thr366 phosphorylation (Al-Khouri et al, 2005; Miller et al, 2002). A very recent study of PTEN phosphorylation was done using high-resolution NMR spectroscopy (Cordier et al, 2012). The results showed that the phosphorylation by CK2 and GSK3β were relatively independent but each phosphorylation process proceeded in a defined order. Late phosphorylation of Ser361 and Thr363 by CK2 was first reported; this occurred after phosphorylation of Ser362 by GSK3β.

Along with Ser380-Ser385 cluster, the role of phosphorylation on other sites has been studied, although some results are controversial (Song et al, 2012). For example, phosphorylation on Thr366 by GSK3β was reported to destabilize PTEN (Maccario et al, 2007), while phosphorylation by Polo-like kinase 3 (Plk3) on the same residue increased PTEN stability (Xu et al, 2010). Aside from phosphorylation on the C-tail, some residues on the C2 domain were also reported as the phosphorylation sites, and their roles are under investigation (Shi et al, 2012; Song et al, 2012).

1.4.5 Regulation of PTEN by other post-translational modification

PTEN can be oxidized and inactivated *in vitro* by H_2O_2. Upon oxidation, Cys124, the active site cysteine, forms a disulfide bond with Cys71, which is near the active site (the distance between the two Cys is 5.9 Å). This oxidation is reversible and PTEN can be reduced by thioredoxin (Lee et al, 2002). This fact suggested PTEN can be regulated by reactive oxygen species (ROS) in cells. Indeed, studies reported the inactivation of PTEN and regulation of the PI3K/Akt pathway by H_2O_2 and endogenous ROS in macrophages (Kwon et al, 2004; Leslie et al, 2003). Furthermore, the oxidation of PTEN can also be regulated. Peroxidase peroxiredoxin 1 (Prdx1) can protect PTEN from oxidation-induced inactivation by directly binding to PTEN (Cao et al, 2009), and thioredoxin-interacting protein (Txnip) keeps PTEN in a reduced form by maintaining the thioredoxin NADPH-dependent disulfide reduction activity (Hui et al, 2008).

PTEN can also be regulated by ubiquitylation. NEDD4 (neural precursor cell expressed, developmental downregulated-4), a E3 ligase, can polyubiquitylate PTEN to mediate its cellular level through proteasomal degradation (Wang et al, 2007). Besides NEDD4, two other E3 ligases were also proposed as mediators for PTEN polyubiquitylation (Maddika et al, 2011; Van Themsche et al, 2009). It has been suggested that the regulation of PTEN by polyubiqutylation occurs in a context-dependent manner to achieve specific functions (Shi et al, 2012). Interestingly, PTEN can be monoubiquitylated at Lys13 and Lys289, and this monoubiquitylation dictates the nuclear import of PTEN (Trotman et al, 2007). In the nucleus, PTEN plays important roles in controlling cell cycle progression, maintaining chromosomal stability and promoting tumor suppression (Shi et al, 2012; Song et al, 2012).

1.4.6 PDZ binding domain and regulation of PTEN by protein-protein interactions

The last three residues of PTEN are assigned to a PDZ binding domain, or PDZ domain-interaction motif, which could allow PTEN to interact with PDZ domain containing proteins (Figure 1.8). PTEN was shown to bind the MAGI-2 (membrane associated guanylate kinase inverted-2) PDZ domain 2 via its C-terminal PDZ binding domain (Wu et al, 2000). MAGI-2 exists at the membrane of epithelial cells where PTEN was colocalized by this protein-protein interaction. This interaction enhanced the tumor suppression function of PTEN (Wu et al, 2000). PTEN also binds to the PDZ domain containing protein NHERF (Na^+/H^+ exchanger regulatory factor) and this binding recruits PTEN to protein complexes on the membrane to suppress PI3K activation (Takahashi et al, 2006).

Besides interacting with other proteins through PDZ binding domain, other regions of PTEN, such as C2 domain and C-tail, also participate in protein-protein interactions. This protein-protein interaction can affect PTEN activity and stability differently. Some interactions can even have opposite effects on activity in response to different stimuli (Leslie et al, 2008; Shi et al, 2012). This calls for further investigations of the PTEN-protein interactions. Given the many processes in which PTEN participates, more protein binding partners will certainly be detected in the future.

1.4.7 Role of PTEN protein phosphatase activity and its function beyond PI3K/Akt signaling pathway

Along with acting as a lipid phosphatase, PTEN is also a dual-specific protein phosphatase. Studies of PTEN mutations have identified some mutant proteins which only have one of the phosphatase activities. Mutation of Gly129 to Glu (G129E)

abrogated lipid phosphatase activity but preserved protein phosphatase activity (Myers et al, 1998), while Y138L has intact lipid phosphatase activity but undetectable protein phosphatase activity (Davidson et al, 2010). These results provided a strategy for investigating the function of PTEN lipid and protein phosphatase activities separately. Although inactive as a lipid phosphatase, PTEN G129E had the same effect as wild type PTEN in inhibiting glioblastoma cell invasion and migration. This effect was linked to PTEN function as phosphotyrosine phosphatase that dephosphorylates focal adhesion kinase (FAK) (Tamura et al, 1999). PTEN also inhibited human glioma cell migration, and this function was dependent on its protein phosphatase activity and dephosphorylation of Thr383. This finding also suggested that one of the physiological substrates for PTEN protein phosphatase activity could be PTEN itself (Raftopoulou et al, 2004). A very recent study of PTEN function using neuronal spine density as the read-out showed the presence of PTEN or PTEN-G129E reduced neuronal spine density in cultured hippocampal slices, while catalytically dead mutant C124S and protein phosphatase-deficient mutant Y138L did not reduce neuronal spine density (Zhang et al, 2012). Furthermore, the ability to decrease spine density only required the dephosphorylation of the PTEN C-tail and the presence of PDZ binding domain, suggesting phosphorylation on the C-tail also regulated PTEN binding to PDZ domain containing proteins. The observations that the phosphorylated peptide which has the C-tail sequence could be dephosphorylated by PTEN *in vitro* and that PTEN autophosphorylation could be observed in HEK293 cells were also reported (Zhang et al, 2012). These results provided evidence that PTEN protein phosphatase is critical for autodephosphorylation to control cellular processes independent of the PI3K/Akt

signaling pathway. Although studies on the function of PTEN in the PI3K/Akt pathway have made considerable progress, less is known about the role of PTEN in PI3K/Akt-independent pathways. A thorough understanding of PTEN should provide insights for developing novel therapies for cancers and other diseases that modulate particular activities and regulation strategies of PTEN.

1.5 Inositol-containing molecules in Bacteria and Archaea

Although primarily associated with eukaryotes, inositol-containing molecules are found in many archaea but seldom found in bacteria (Michell, 2011). The one group of bacteria noted for containing inositol lipids are mycobacteria (and other actinobacteria). The majority of bacteria do not incorporate inositol lipids into their membranes. In contrast, many members of the archaeal domain synthesize inositol containing lipids in their membranes; they also synthesize and accumulate small, water-soluble molecules derived from inositol (Michell, 2011).

1.5.1 Inositol and its derivatives in bacteria

In actinobacteria, inositol can be synthesized *de novo* following the same biosynthetic pathway used in eukaryotes. The two genes encoding inositol phosphate synthase (MIPS) and inositol monophosphatase (IMPase) are found in all actinobacteria (Morita et al, 2011). *Myo*-inositol can also be transported into the cells from the environment (Newton et al, 2006). In actinobacteria, the majority of the inositol serves as the precursor for synthesizing PI and its derivatives and mycothiol, a redox-active analogue of glutathione in these organisms (Morita et al, 2011).

Similar to eukaryotes, *de novo* synthesis of PI occurs by the exchange of the CMP moiety of CDP-DAG with inositol. This reaction is catalyzed by PI synthase (Salman et al, 1999). PI was demonstrated to be an essential phospholipid for mycobacteria survival since disruption of its gene in *Mycobacterium smegmatis* caused the organism to lose cell viability (Jackson et al, 2000). PI also serves as the lipid anchor of complex glycosylated derivatives (Morita et al, 2011). PI can be mannosylated to form PI mannoside (PIM), and PIM can be further mannosylated and arabinosylated to form lipomannan (LM) and lipoarabinomannan (LAM) (Morita et al, 2011) (Figure 1.9). All these inositol containing lipids are important for mycobacteria growth and the ability to infect their targets (Fratti et al, 2003; Geijtenbeek et al, 2003).

Mycothiol (MSH or AcCys-GlcN-Ins) is synthesized from inositol (in this case D-I3P, which is the same as L-I1P). After the generation of D-I-3-P, an activated GlcNAc (N-acetyl-D-glucosamine) is linked to the hydroxyl group at D1 position of the inositol ring, then the glycosylated inositol is further linked to N-acetylated cysteine to form mycothiol (Newton et al, 2008) (Figure 1.9). Mycothiol is a substitute for glutathione in mycobacteria and plays important roles in maintaining the reducing environment in the cells; it is also important in detoxification of alkaline reagents, reactive oxygen species and antibiotics (Newton et al, 2008).

PI(3)P has recently been identified in mycobacteria, although the role of this inositol phospholipid is still under debate. One group suggested PI(3)P is the intermediate prior to the synthesis of PI. PI(3)P, produced by condensing L-I-1-P with CDP-DAG, can be dephosphorylated to produce PI (Morii et al, 2010). Others proposed that it is produced upon cell stress and can be a mediator of cellular signaling (Morita et al, 2010).

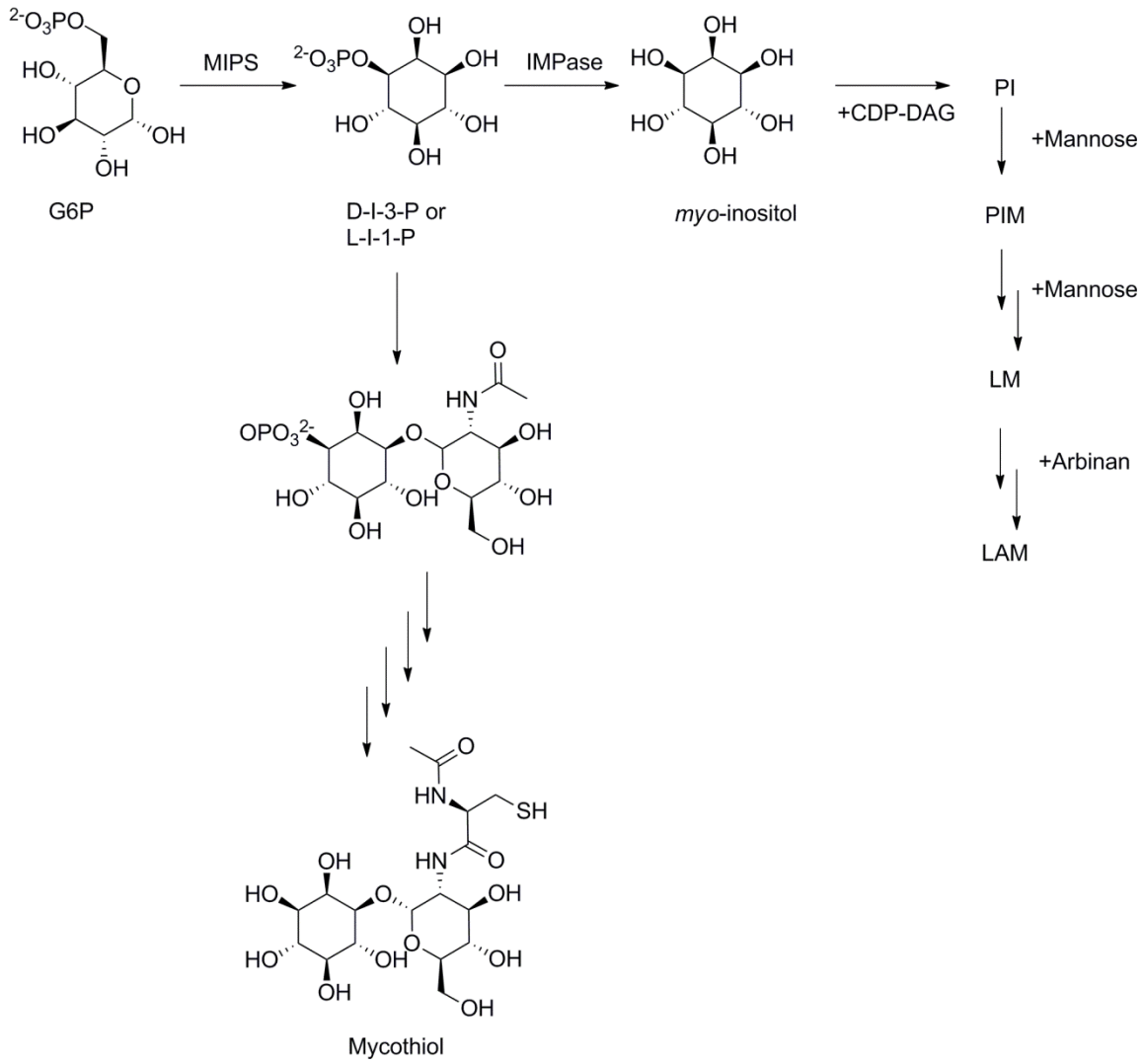

Figure 1.9 Inositol and inositol-containing molecules in actinobacteria (Morita et al, 2011; Newton et al, 2008)

1.5.2 Inositol-containing molecules in archaea

Inositols occur in at least two different kinds of molecules in archaea (Michell, 2011). The first group includes the inositol phospholipids, although most of them have different structures than inositol-containing phospholipids in eukaryotes. The second group is based on the water soluble molecule di-myo-inositol-1, 1'-phosphate (DIP). DIP and several of its derivatives are used to protect cells against harsh environments (increased salinity or temperature).

The structures of phospholipids found in archaea are different from those in eukaryotes and bacteria (Koga & Morii, 2007; Lombard et al, 2012; Michell, 2011) (Figure 1.10). The phosphate group in eukaryotic phospholipids is linked at *sn*-3 position of the glycerol backbone, while in archaea, the phosphate is attached at *sn*-1 position of the glycerol. This feature makes the glycerolphosphate backbone of lipids in archaea the enantiomer of that found in eukaryotes. Another noticeable difference is that the bonds linking the hydrophobic hydrocarbon tails to the glycerol backbone are ethers in archaea instead of esters seen in eukaryotes. The hydrocarbon tails of archaeal lipids are branched based on an isoprenoid structure instead of the straight chain fatty acid in eukaryotes and bacteria (or the bacterial lipids with a single cyclohexyl or isopropyl group at the end of the acyl chain). These striking features of archaeal phospholipids compared to lipids in eukaryotes gives archaeal lipids different physical properties and are partly responsible for the survival of archaea in extreme environments (Koga & Morii, 2007; Lombard et al, 2012; Michell, 2011). However, the head groups of lipids found in all three domains are mostly the same, including *myo*-inositol. Inositols are also linked to the phosphate group of glycerol at D1 position to form the phospholipids (Koga & Morii, 2007). The biosynthesis of *myo*-inositol in archaea is the same as that in eukaryotes and bacteria. D-I3P (L-I1P) is first generated from D-G6P by MIPS, then dephosphorylated by IMPase to form *myo*-inositol (Michell, 2011). The biosynthetic pathway for the primary inositol phospholipid in archaea, archaetidylinositol (ArcIns), has been recently reported. Instead of directly linking inositol with CDP-archaetol, these organisms link phosphorylated inositol D-I3P to CDP-archaetol to form phosphorylated ArcIns. That phosphorylated molecule is then dephosphorylated to form the archaetidylinositol (Morii et al, 2009).

Inositol can also be incorporated into a series of water-soluble small molecules, with the prominent one di-*myo*-inositol-1, 1'-phosphate or DIP. DIP is accumulated as a compatible solute in thermophiles / hyperthermophiles and aids in protecting cells against increased temperature.

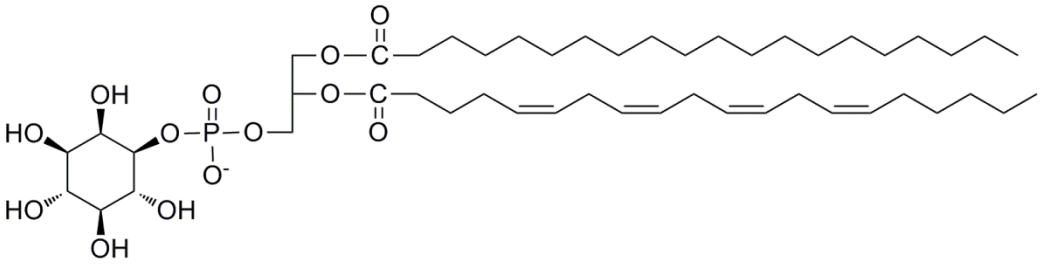

Phosphatidylinositol, PtdIns or PI

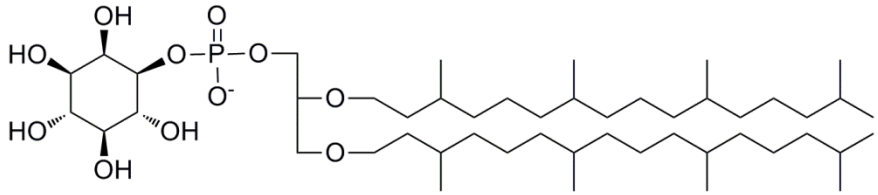

Archaetidylinositol or ArcIns

Figure 1.10 Structure of inositol phospholipid in eukaryotes (phosphatidylinositol) and in archaea (archaetidylinositol) (Michell, 2011).

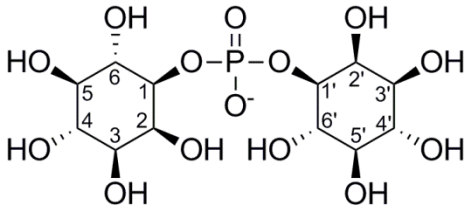

Di-myo-inositol-1,1'-phosphate
L,L-DIP

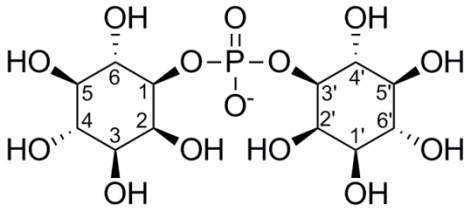

Di-myo-inositol-1,3'-phosphate
L, D-DIP

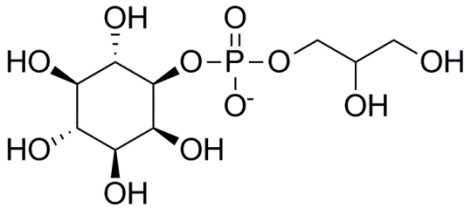

1-glyceryl-1-myo-inosityl phosphate
GIP

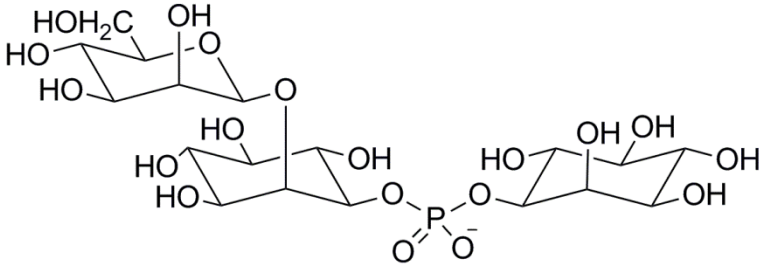

2-(O-β-D-mannosyl)-di-myo-inositol-1,3'-phosphate
MDIP

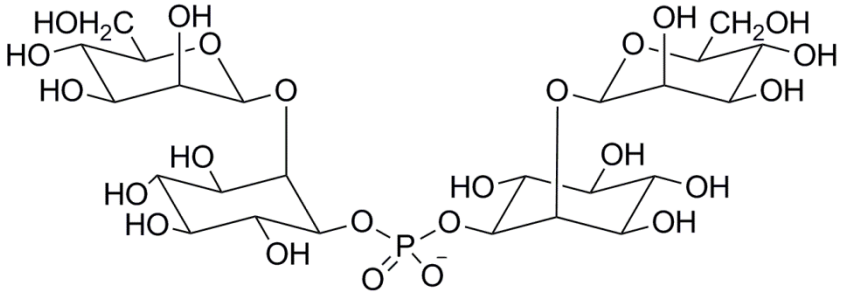

Di-2-O-β-mannosyl-di-myo-inositol-1,1'-phosphate
DMDIP

Figure 1.11 DIP and its derivatives found in (hyper)thermophilic bacteria and archaea (Lamosa et al, 2006; Martins et al, 1996; Rodrigues et al, 2009)

1.5.3 DIP and its derivatives

Thermophiles and hyperthermophiles are groups of organisms that thrive at high temperatures. The organisms with an optimal growth temperature between 65°C and 80°C are termed thermophiles; the optimal growth temperature of hyperthermophiles is above 80°C (Santos & da Costa, 2002). Although some bacteria are thermophiles/ hyperthermophiles, most hyperthermophiles are archaea (Empadinhas & da Costa, 2006; Santos & da Costa, 2002). In order to survive at high temperatures as well as adjust to altered water activity caused by fluctuations in salt concentrations, thermophiles and hyperthermophiles have had to develop some adaptive strategies. Proteins in thermophiles and hyperthermophiles have higher thermal stability than their homologues in mesophilic organisms by making subtle changes in their structures (Luke et al, 2007). However, this may not be sufficient for all proteins in thermo-/hyperthermophiles subjected to thermal stress. These organisms also accumulate small molecular weight molecules, by de novo synthesis or by uptake from the environment, to maintain the cell turgor pressure and protect enzyme activity. These small molecules are termed osmolytes or compatible solutes since they are thought to be benign (not very reactive) in the cytoplasm (Burg & Ferraris, 2008; Empadinhas & da Costa, 2006; Khan et al, 2010; Roberts, 2004; Yancey, 2005). Osmolytes almost always have a thermoprotective effect as well as contributing to osmotic balance. DIP is one of the more unusual compatible solutes identified in a variety of thermophiles and hyperthermophiles.

DIP was first identified as an intracellular counter ion of K^+ in *Pyrococcus woesei* and was shown to protect glyceraldehyde-3-phosphate dehydrogenase from heat inactivation effectively at high temperatures (Scholz et al, 1992). DIP is also accumulated by

Methanococcus igneus (later rename as *Methanotorris igneus*). In this methanogen, DIP is accumulated as a compatible solute, and its accumulation is dependent on the temperature. DIP accumulation has also been reported in hyperthermophilic archaea including *Archeaglobus fulgidus* (Goncalves et al, 2003; Martins et al, 1997), *Pyrococcus furious* (Martins & Santos, 1995), order *Thermococcus* (Lamosa et al, 1998) and *Pyrolobus fumarii* (Goncalves et al, 2008), and in hyperthermophilic bacteria including *Thermotoga maritima* (Ramakrishnan et al, 1997) and order *Thermotogales* (Martins et al, 1996). DIP also exists in the thermophilic actinobacterium *Rubrobacter xylanophilus* (Empadinhas et al, 2007). In all these organisms, there is a strong correlation between the accumulation of DIP and growth at supraoptimal temperatures. This correlation clearly indicates DIP has a role in thermoprotection.

DIP is an unusual phosphodiester. Originally it was identified as a chiral molecule, di-*myo*-inositol-1,1'-phosphate or L,L-DIP (Figure 1.11), by synthesis of the molecule and comparing the synthetic material to isolated DIP from *P. woesei* (Scholz et al, 1992). The optical rotation of DIP purified from *P. woesei* was reported as $[\alpha]_D^{20}$ = 2.39°, comparable with that of synthesized L,L-DIP. Initial studies of DIP biosynthesis in *M. igneus* proposed a pathway based on this identification (Chen et al, 1998). However, based on the HMQC NMR result, another stereoisomer of DIP was found in *Thermotoga neapolitana* cell extract, and this stereoisomer was thought to be di-myo-inositol-1,3-phosphate or L,D-DIP (Martins et al, 1996) (Figure 1.11). Currently, it is thought that all these organisms synthesize L,D-DIP as a natural product. This was based on results with a key enzyme, CTP:inositol-1-phosphate cytidylyltransferase (IPCT) (see discussion below).

The first biosynthetic pathway of DIP was proposed in 1998 based on the activities of enzymes in cell extracts of *M. igneus* (Chen et al, 1998). The pathway has four steps: (1) G6P is converted to L-I1P (equivalent to D-I3P) by myo-inositol phosphate synthase (MIPS); (2) L-I1P is dephosphorylated by inositol monophosphatase (IMPase) to produce inositol; (3) inositol is activated by attaching it to CDP through CTP:I-1-P cytidylyltransferase (IPCT) to produce CDP-inositol; (4) the CMP part in CDP-inositol was exchanged with inositol through nucleophilic attack to generate DIP by DIP synthases (DIPS) (Figure 1.12). However, direct detection of the production of CDP-inositol failed, although the enzymes in cell extract can catalyze the DIP generation reaction with synthetic CDP-inositol and inositol. Four enzymes are involved in the biosynthesis of DIP from G6P, MIPS, IMPase, IPCT and DIPS. Since MIPS and IMPase account for the generation not only DIP, but also other inositol-containing molecules, the identification of IPS and IMPase in hyperthermophiles is easier, and there has been extensive characterization of these two hyperthermophilic enzymes (Chen et al, 2000; Stieglitz et al, 2002). However, for many years there was no identification of genes encoding IPCT and DIPS.

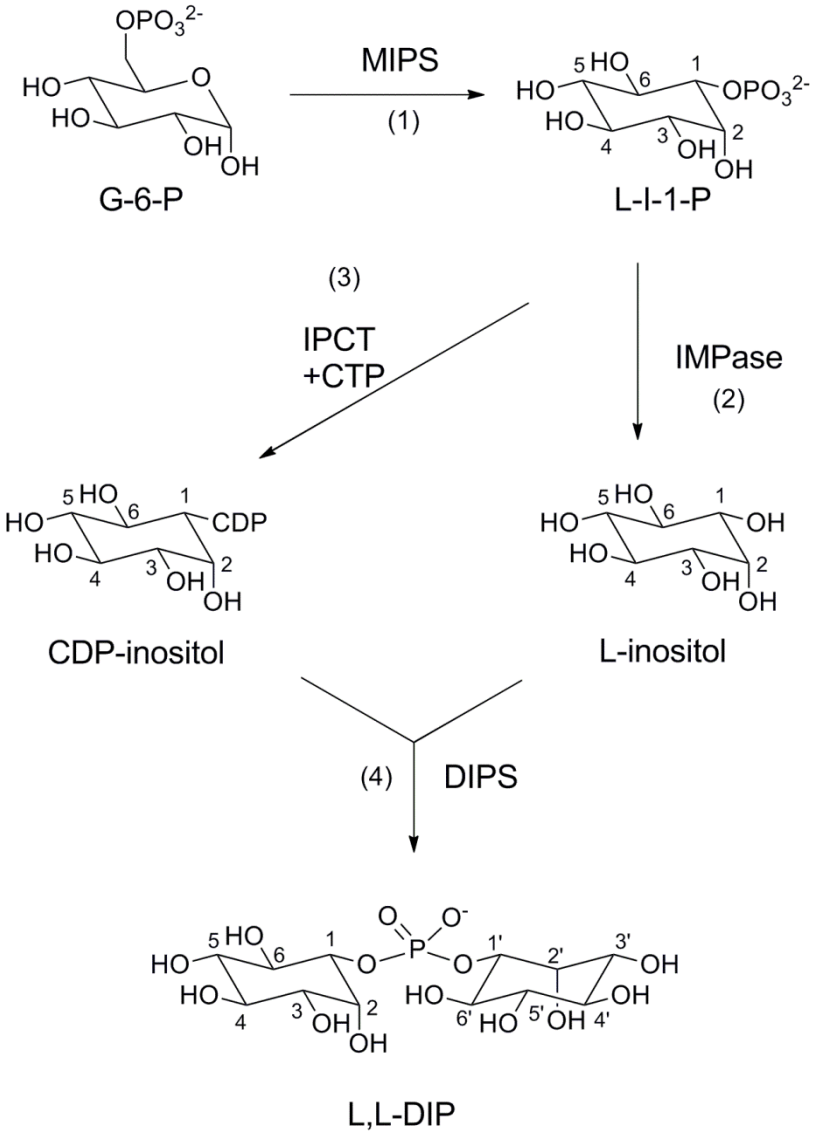

Figure 1.12 Proposed DIP synthesis pathway (Chen et al, 1998)

The DIP biosynthetic pathway was revised by the finding a phosphorylated form of DIP (P-DIP) in some organisms (Borges et al, 2006) and characterization of enzymes IPCT and DIPS (Rodionov et al, 2007). The genes encoding these two enzymes were identified by comparative genomics and were found in all the organisms that synthesized DIP. These two genes were found clustered on the chromosome with the gene encoding MIPS (Rodionov et al, 2007). The activity of IPCT from *T. maritima* was shown to

preferentially catalyze the transferase reaction with CTP and L-I1P as the substrates to produce CDP-inositol. The MIPS activity was tested using the cell lysate. In the absence of the IMPase, a novel product, phosphorylated DIP (P-DIP) was identified by NMR. These findings suggested a revised DIP biosynthesis pathway (Figure 1.13). Instead of direct condensation of CDP-inositol with free inositol to form DIP, a phosphorylated DIP (P-DIP) was first formed by condensing CDP-inositol with L-I1P catalyzed by PDIPS. After this, the P-DIP was dephosphorylated by a phosphatase to generate DIP. *In vitro* P-DIP can be dephosphorylated by adding purified IMPase enzymes. Due to the specificity of IPCT activity toward L-I1P, DIP generated by this pathway was L,D-DIP. This revised pathway was further confirmed by the study of the protein encoded by fused IPCT and DIPS genes (ipct/dipps) from *A. fulgidus* and other hyperthermophiles, which showed the same substrate specificity (Rodrigues et al, 2007). By using ^{13}C labeled L-I-1-P, it was demonstrated that only D,L-DIP was produced.

Besides DIP, other inositol containing compounds are also identified in archaea as compatible solutes. For example, 1-glyceryl-1-myo-inosityl phosphate (GIP) (Figure 1.11) was found to be a compatible solute in *A. fulgidus* when the organism encounters both osmotic and heat stress (Lamosa et al, 2006). GIP was also identified as the major osmolyte in the hyperthermophilic bacterium *Aquifex pyrophilus* (Lamosa et al, 2006). The identification of mannosylated DIP in hyperthermophiles was also reported. *T. neapolitana* accumulates di-2-*O*-β-mannosyl-di-myo-inositol phosphate (DMDIP) (Figure 1.11) as well DIP as compatible solutes when growing at supraoptimal temperatures (Martins et al, 1996). DMDIP is also found in *A. pyrophilus* (Lamosa et al, 2006). The monomannosylated DIP (mannosyl-di-myo-inositol phosphate, MDIP)

(Figure 1.11) was also identified as one of the compatible solutes accumulated by *T. maritima* (Rodrigues et al, 2009).

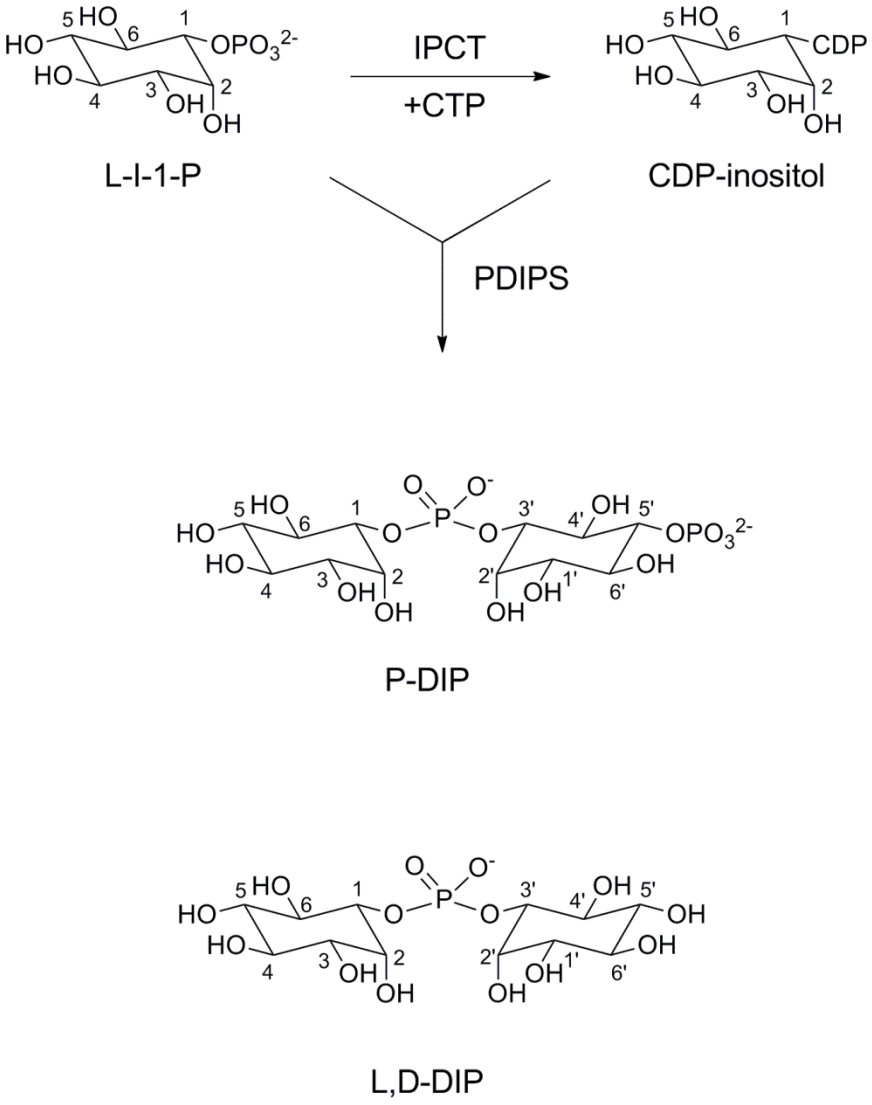

Figure 1.13 Revised DIP biosynthetic pathway (Rodionov et al, 2007; Rodrigues et al, 2007)

1.6 Inositol monophosphatase

Inositol monophosphatase (IMPase, EC 3.1.3.25) catalyzes dephosphorylation of inositol monophosphate to generate inositol. It plays important roles in inositol generation and recycling. Since all inositols, no matter in eukaryotes or prokaryotes, are generated by the same *de novo* synthetic pathway, IMPase and its encoding gene *imp* are found in organisms throughout the three domains of life. However, prokaryotic IMPase proteins, especially those from hyperthermophilic organisms have different properties and structural features compared to their eukaryotic counterparts. The understanding of these differences also contributes to our understanding of how hyperthermophilic proteins are adapted to high temperatures.

From a structural view, hyperthermophilic proteins increase their thermal stability by increasing the intramolecular interactions that hold the native conformations together at high temperature (Razvi & Scholtz, 2006). This can generally be achieved by lowering the volume of cavities or increasing compactness of the protein, increasing the number of ion pairs, increasing secondary structure content with corresponding decrease in irregular regions, truncating solvent-exposed loops, and changing the amino acid composition by increasing prolines and reducing thermally labile amino acids such as Met and Gln (Sterner & Liebl, 2001; Szilagyi & Zavodszky, 2000). However, mechanisms a particular protein uses to adapt to higher temperatures can be very diverse (Feller, 2010).

1.6.1 Eukaryotic IMPase

Several structures of human IMPase and other eukaryotic IMPase with different ligands have been solved by crystallography (Arai et al, 2007; Bone et al, 1994a; Bone et al, 1994b; Bone et al, 1992; Ganzhorn & Rondeau, 1997; Singh et al, 2012). Most

eukaryotic IMPase proteins are dimeric and have a similar core structure with tetrameric fructose-1,6-bisphosphatase (FBPase) (Figure 1.14), although these two proteins have low sequence similarity (Atack et al, 1995; York et al, 1994). The crystal structures of the eukaryotic IMPase show that the proteins contain two or three metal ions. Since this protein is Mg^{2+} dependent and no phospho-enzyme intermediate was found during dephosphorylation, it was suggested that a water molecule instead of protein side chain acts as the nucleophile to dephosphorylate the substrate (Bone et al, 1994b; Bone et al, 1992). Although three metal ions are found in the crystal structures, some studies have suggested a two-metal ion mechanism, in which only two Mg^{2+} are important in catalysis (Pollack et al, 1994; Wang & Hirao, 2013). Two metals at site 1 and 2 can facilitate the deprotonation of water molecule to become nucleophilic and facilitate the release of the product to finish the catalytic cycle (Bone et al, 1994a).

Human IMPase can be inhibited by lithium. The K_i of Li^+ to human IMPase is only 0.3 mM (McAllister et al, 1992). Li^+ inhibits the protein in an uncompetitive fashion (Hallcher & Sherman, 1980), and it is believed that Li^+ occupies the metal binding site 2 to trap the phosphate group from leaving the protein active site and thus inhibits enzyme activity (Atack et al, 1995; Haimovich et al, 2012). IMPase is likely to be the target of Li therapy in the treatment of bipolar disorder, where it is suggested that lithium inhibits IMPase activity to deplete the inositol production, so as to lower the generation of PI and related second messengers to attenuate the response to extracellular stimuli (Atack et al, 1995; Harwood, 2005).

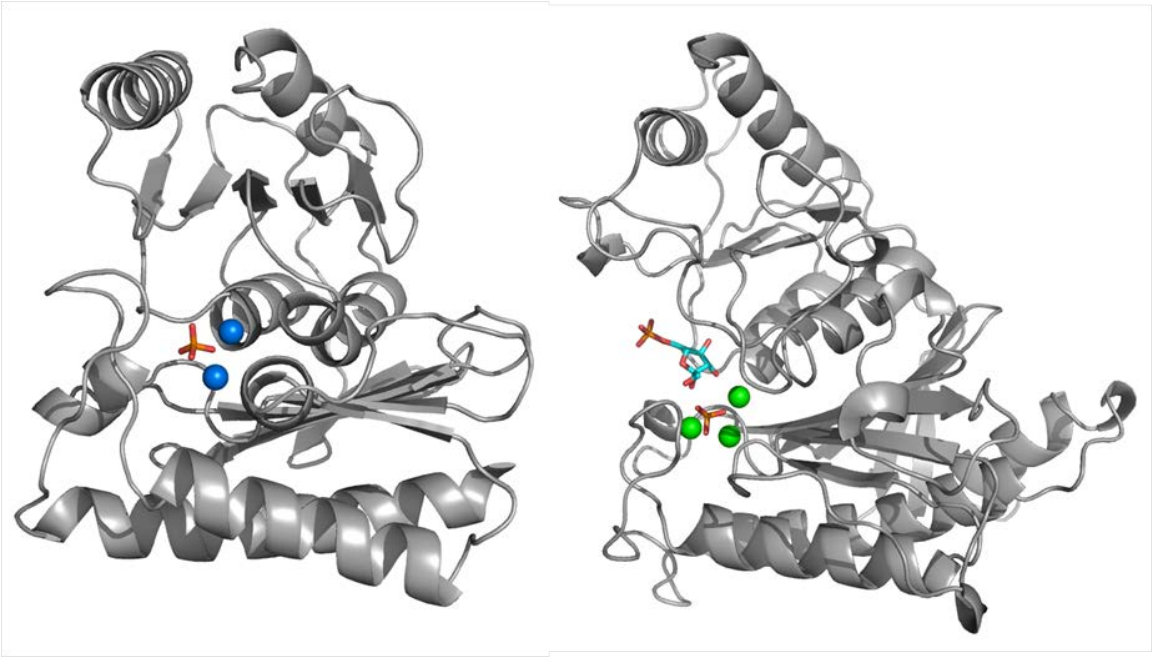

Figure 1.14 Monomer structure of human IMPase (left) with pig kidney FBPase (right). Human IMPase (PDB 1IMC) protein is shown in grey cartoon, 2 Mn^{2+} are shown in blue, 1 PO_4^{3-} ion is shown in orange with oxygen atoms in red. Pig kidney FBPase (PDB 1CNQ) protein is shown in grey carton, 3 Zn^{2+} are shown in green, 1 PO_4^{3-} is shown as in IMPase structure, 1 F6P molecule is shown in cyan, with oxygen atoms in red and phosphorus in orange.

1.6.2 Hyperthermophilic IMPase

Several IMPase enzymes from hyperthermophiles are well characterized with high resolution crystal structures (Johnson et al, 2001; Stieglitz et al, 2002; Stieglitz et al, 2007). Compared to eukaryotic IMPase, there are several striking features of hyperthermophilic IMPase proteins. First, the hyperthermophilic IMPase enzymes are dual-specific phosphatases. They can dephosphorylate fructose-1,6-bisphosphate (FBP) as well as inositol-1-phosphate. This is in contrast to the IMPase enzymes from eukaryotes and other bacteria where dephosphorylation of those two substrates is catalyzed by two separate enzymes, IMPase and FBPase (Stec et al, 2000). Second, they are Li^+ insensitive. Unlike the eukaryotic IMPase which can be inhibited by Li^+ with the

IC_{50} less than 1 mM, the IC_{50} of Li^+ for hyperthermophilic IMPase enzymes is more than 100 mM (Chen & Roberts, 1998; Stieglitz et al, 2002). Third, consistent with their existence in hyperthermophiles, the IMPase protein from these organisms have higher thermal stability. The T_m (mid-point of the thermal denaturation transition) of *A. fulgidus* IMPase (AF2372) is around 88°C (Wang et al, 2006). *Methanocaldococcus jannaschii* IMPase (MJ0109) has higher thermal stability with T_m of 95 °C (Chen & Roberts, 1998) and *T. maritima* IMPase (TM1415) is still active at 100°C (Chen & Roberts, 1999). Last, the dephosphorylation mechanism of the dual-specific hyperthermophilc IMPase is likely to require three-metal ions, similar to FBPase catalysis but not the human IMPase (Johnson et al, 2001) (Figure 1.15). The mobile loop in MJ0109, which is critical for protein activity, is slightly longer (2 residue insertion) than that in human IMPase. It adopts a conformation more similar to the corresponding loop in pig kidney FBPase that would facilitate binding of the third metal ion. Although there is only one residue, Asp38, that has direct contact with the third metal ions (and this metal ion binds relatively weakly at metal binding site 3), the third metal ion together with metal at site 2 provides the right environment for activation of the nucleophilic water molecule and formation and release of products.

The kinetics parameters of IMPase and other related enzyme from different organisms are summarized in Table 1.3, The differences between the dual-specificity IMPase enzymes from hyperthermophiles and the IMPases of other bacteria and eukaryotes are obvious.

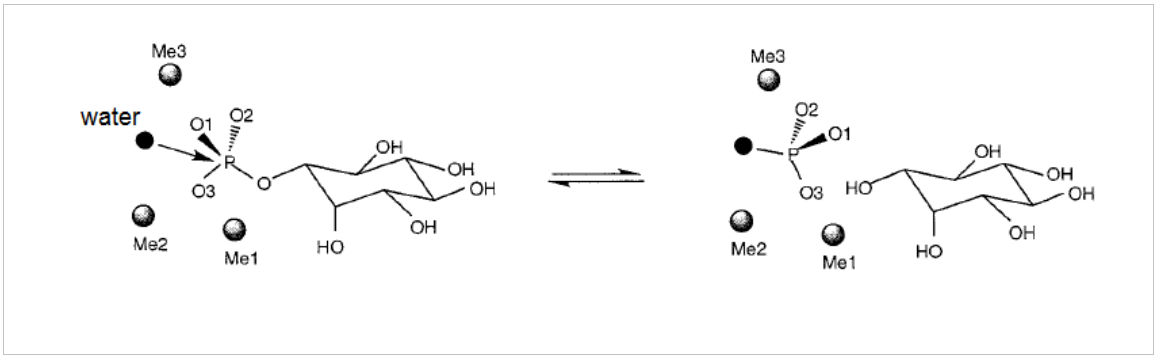

Figure 1.15 Proposed IMPase three-metal ion assisted catalytic mechanism (adapted from Johnson et al, 2001).

Table 1.3 Kinetics parameters for IMPase and FBPase enzymes from different organisms (Chen & Roberts, 1999; Matsuhisa et al, 1995; McAllister et al, 1992; Stec et al, 2000; Stieglitz et al, 2002; Zhang et al, 1996)

Protein	I-1-P		FBP		Li^+ IC_{50} (mM)
	K_m (mM)	k_{cat} (s^{-1})	K_m (mM)	k_{cat} (s^{-1})	
AF2372[a]	0.11	2.5	0.08	2.7	290
MJ0109[a]	0.091	4.2	0.038	7.0	250
TM1415[b]	0.013	207		268	100
E coli SuhB[c]	0.07	6.5		<0.005	0.35
Human IMPase[c]	0.075	17.2			0.3
Pig kidney FBPase[d]		0.02	0.0014	21	1-3[e]

Assays were carried out at (a) 85°C, (b) 95°C, (c) 37°C, (d) 30°C, (e) 24°C.

There is no unique way the hyperthermophilic IMPases have altered structure to adapt to high temperatures. However, a comparison of MJ0109 with human IMPase and pig kidney FBPase does point out some changes (Johnson et al, 2001). The amino acid sequence of MJ0109 has less Met, Ser and no His and Gln, consistent with the above mentioned general change of amino acid content upon adaptation to high temperature. Compared to human IMPase, MJ0109 has a smaller volume and smaller solvent accessible area, indicating the protein has become more compact. Although the pattern of changes in loops is complex in MJ0109 compared to human IMPase, in general the loops

in MJ0109 are shorter. One changed loop (residues 67-76) forms a β-strand rather than the flexible conformation seen for the corresponding loop in human IMPase. The dimer interface of MJ0109 is smaller than that of human IMPase, suggesting dimer stability is not directly linked to the thermal stability of the whole protein. However, there are more charged contacts between the two monomers in the archaeal IMPase interface. All these features are consistent with general observations for thermostable proteins. Again this demonstrates that proteins adopt several strategies instead of a single one to increase their thermal stability (Petsko, 2001).

1.6.3 A. fulgidus IMPase (AF2372)

Like other hyperthermophilic IMPase proteins, AF2372 is also a dual-specific phosphatase. It can dephosphorylate inositol phosphate, both D-I-1-P and L-I-1-P, with similar k_{cat} values. However, the K_m for D-I-1-P is 10-fold lower than that for L-I-1-P, indicating formation of a different hydrogen bond network when these two substrates bind (Morgan et al, 2004). It can also dephosphorylate FBP, but has no activity toward G-6-P or F-6-P (fructose 6-phosphate) (Stieglitz et al, 2002). Along with I-1-P and FBP, AF2372 can also dephosphorylate $NADP^+$ and NADPH with comparable kinetics parameters (Fukuda et al, 2007). Li^+ barely inhibits AF2372 activity. The Li^+ IC_{50} values for enzyme activities toward I-1-P, FBP, NADP and NADPH range from 50 to 300 mM, almost 1000-fold higher than for Li^+ inhibition of the human IMPase (Fukuda et al, 2007; Stieglitz et al, 2002). The activity of AF2372 is dependent on the presence of Mg^{2+}. The apparent K_d for Mg^{2+} or Mn^{2+} is 15-30 mM (depends on substrate concentration since the phosphate esters can bind divalent cations). Ca^{2+} inhibits both the IMPase and FBPase activities (Stieglitz et al, 2002).

Like other IMPase enzymes, AF2372 protein is a homodimer with each monomer consisting of alternating layers of α-β-α-β-α structure (Figure 1.16). The layers of α-helices and β-sheets are connected by loops with variable length (Stieglitz et al, 2002). Compared to the MJ0109 structure, AF2372 has slightly longer N-terminal helices and a deletion of a small helix that is part of the dimer interface in MJ0109. These features cause a looser dimeric organization of AF2372 and may be responsible for the relatively lower thermal stability of AF2372 than MJ0109.

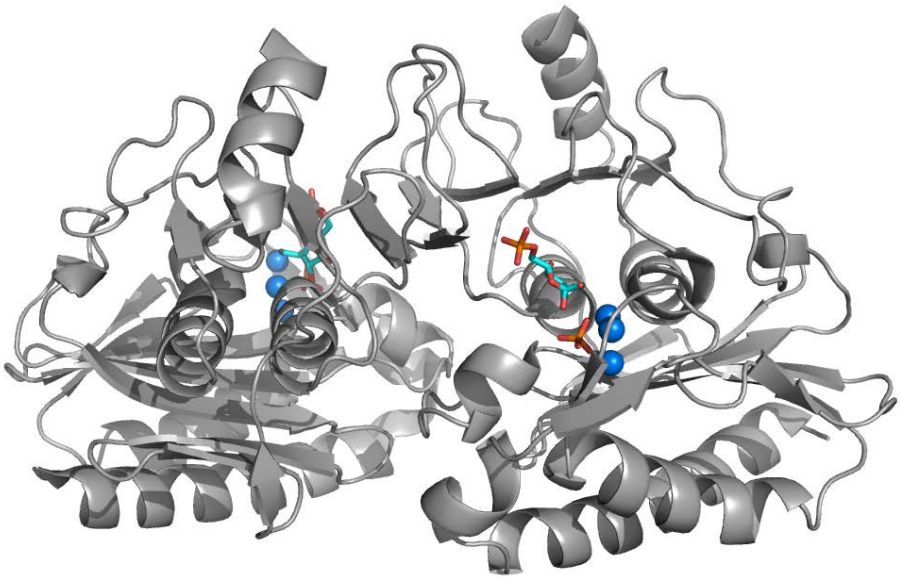

Figure 1.16 Crystal structure of AF2372 (PDB 1LBY). The protein is shown in grey, In each monomers, 3 Mn^{2+} ions are shown in blue; 1 F6P molecule is shown in cyan, with oxygen atoms in red and phosphorus in orange; 1 PO_4^{3-} ions is shown in orange with oxygen in red.

Studies of the conformation of the mobile loop revealed some interesting features in the IMPase superfamily of proteins. The mobile loop in AF2372, MJ0109 and pig kidney FBPase have a similar closed conformation, while human IMPase has the mobile loop with a more open conformation. Similar with what was reported for MJ0109 structures,

this mobile loop in the apo form of AF2372 is unstructured. However, when metal ions and ligands are bound, this loop became ordered and moves toward the metal ions (Figure 1.17). Just like in MJ0109, movement of this mobile loop facilitates metal ion binding and water nucleophile formation. The mobility of the mobile loop is critical for product release to prepare the protein for the next catalytic cycle. The same conformational change of the mobile loop is also observed in FBPase (Choe et al, 1998). The mobility of this critical mobile loop is also related to Li^+ sensitivity. A mutation in the MJ0109 mobile loop, D38A, yielded a protein that was inhibited by Li^+ with an IC_{50} of 12 mM. This mutant protein had significantly lower affinity for Mg^{2+}, indicating the role of that Asp in metal ions binding (Li et al, 2010).

A unique feature of AF2372 is that enzyme activity can be regulated by oxidation (Stieglitz et al, 2003). It was shown that protein activity can be eliminated by oxidation with O_2 for 6 h or incubation with oxidized thioredoxin for 28 h. The oxidation could be reversed by adding a reducing agent, such as DTT. The mutant protein C150S lost the sensitivity to oxidation. The distance between the S atoms of Cys150 and Cys186 in AF2372 is only 4Å, so it is believed that upon oxidation, a disulfide bond could form between these two cysteines. Regulation of IMPase activity by cysteine oxidation and disulfide formation is postulated to be the result of altering the affinity of protein for metal ions.

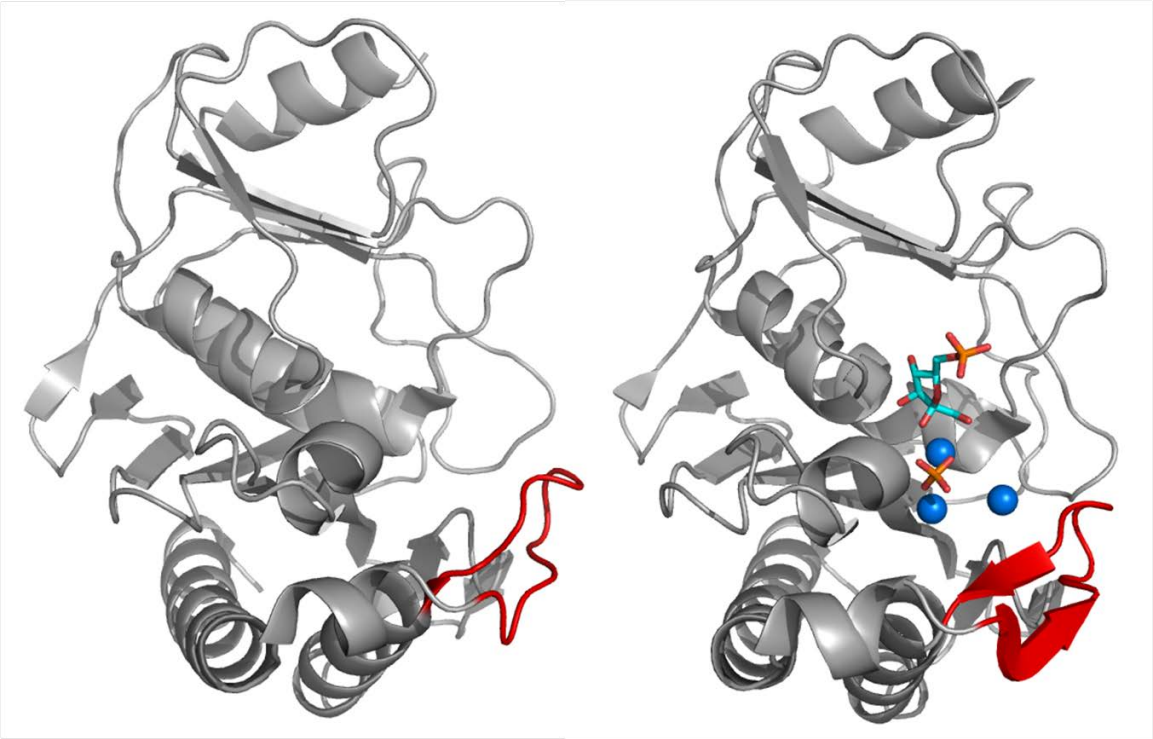

Figure 1.17 Monomer structures of AF2372 apo form (left, PDB 1LBW) and ligand/ metal bound form (right, PDB 1LBY). The mobile loops (residues 32 to 43) in both forms are colored in red. In the ligand/metal bound form, 3 Mn^{2+} ions are colored in blue, 1 F6P molecule is colored in cyan with oxygen in red and phosphorus in orange, 1 PO_4^{3-} ion is colored in orange.

A kinetic study of the temperature dependence of K_m of AF2372 for inositol phosphate revealed the unique regulation of this protein by temperature (Wang et al, 2006). The decrease of K_m for I-1-P from 55°C to 75°C is only 2.5-fold, while the K_m at 85°C decreased 8 to 10-fold compared to that at 75°C. This dramatic decrease of K_m was only observed when using inositol phosphate as the substrate, and it only happened in AF2372 not in MJ0109 or TM1415. A hydrogen bonding network at the active site was suggested to account for this K_m temperature dependence. Higher temperatures might alter the mobility of a loop at the interface which in turn changes this hydrogen bonding network to increase the substrate affinity. The temperature dependence of AF2372 activity toward inositol phosphate also correlates with accumulation of DIP at higher temperatures.

However, when I started my research there was no study of DIP thermoprotection of this particular protein.

1.7 Brief outline of this thesis

The studies addressed in this thesis are focused on two proteins: human PTEN and *A. fulgidus* IMPase (AF2372). Work with PTEN started with a collaboration with Prof. Goran Krilov and his student Qin Wang. They carried out a molecular dynamics simulation of a series of short-chain phosphatidylinositols (and deoxy-PIs) binding to the PTEN phosphatase domain. They identified a hydrophobic site around Arg47 on PTEN that appeared critical for ligand binding to the active site. This model was supported by testing PTEN activity using lipid substrates with different aggregation states. Mutation at Arg47 revealed the importance of this residue in protein activity. The second area of PTEN work centered on studying the interaction of PTEN with lipid molecules using NMR spectroscopy. Different binding modes of activator molecule $PI(4,5)P_2$ and substrate analog lipids were identified by fixed field NMR. Field cycling NMR showed different binding sites for both the activator and substrate analog molecules on the PTEN phosphatase domain that were spatially near each other. This result clearly proves there is a discrete binding site for activator molecules that is separate from the active site, although under some conditions the activator molecule can bind to the protein active site. An NMR study of the PTEN mutant K13E modified the conventional interpretation of this particular mutant by providing evidence for the interaction of K13E with $PI(4,5)P_2$ and other lipid molecules. The last part of the thesis presents a study on the thermoprotection mechanism of DIP as well as other compatible solutes using AF2372 as the model protein. DIP and diglycerophosphate (DGP) showed high thermoprotection of

AF2372 while glutamate ions are less effective. In collaboration with protein crystallographers (Drs. Bog Stec and Rebecca Goldstein), we identified specific binding sites on AF2372 for glutamate anions. Mutation of the glutamate binding sites showed they were not necessary for glutamate thermoprotection. However, the residues of these sites were very important for overall protein thermal stability. A proposed mechanism for compatible solutes protecting AF2372 from thermal denaturation is suggested whereby the compatible solutes bind to either the active site or a specific binding site for glutamate on the protein (that is not detected at low or room temperature and that may be weakly associated) to change the mobility of the active site or the mobile loop, and preserve the protein activity at high temperature.

Chapter 2

Materials and Methods

2.1 Chemicals

2.1.1 Molecular biology reagents

Quikchange site directed mutagenesis kit, *E. coli* XL1-Blue competent cells, and *E. coli* BL21-CondonPlus (DE3)-RIL competent cells were purchased from Stratagene. *E. coli* NovaBlue competent cells and the pET-23b(+) vector were from Novagen. GoTaq PCR Core system kit for cloning was from Promega. The oligonucleotide primers were ordered from Operon. QIAprep spin miniprep kit, QIAquick PCR purification kit and QIAquick gel extraction kit were from Qiagen. NdeI, XhoI, T4 DNA ligase, Antarctic phosphatase and1Kb DNA ladder were from New England Biolabs. Protein standards for SDS-PAGE were from Bio-Rad. LB broth was from Fisher. Lys C endoproteinase was from Wako. PTEN-pET-28a plasmid was the gift of Prof. Wonhwa Cho at University of Illinois, Chicago.

2.1.2 Chemicals

Isopropyl-β-D-thiogalactopyranoside (IPTG), ampicillin, and chloramphenicol are from American Bioanalytical. Sodium dodecyl sulfate (SDS) and 30% acrylamide/bis acrylamide solution were from Bio-Rad. The spin-labeling reagent, 2,2,5,5-tetramethyl-l-oxyl-3-methyl methanethiosulfonate (MTSL), was from Toronto Research Chemicals. D-*myo*-inositol-1-phosphate (D-I-1-P) was from Cayman Chemicals. Kanamycin sulfate, Triton X-100, D_2O, Trizma base, boric acid, EDTA, DTT, β-mercaptoethanol, $MgCl_2$, KCl, NaCl, KH_2PO_4, *p*-nitro-phenyl phosphate (pNPP), fructose-1,6-bisphosphate (FBP), sodium glutamate (Na-Glu), potassium glutamate (K-Glu), sodium aspartate (Na-Asp), potassium aspartate (K-Asp), proline, betaine and other chemicals were from Sigma-Aldrich. Sodium L,L- and D,L-di-myo-inositol-1, 1'-phosphate (DIP) were gifts from Dr.

Christina Longo and Dr. Scott Miller at Yale University. Diglycerol phosphate (DGP) was synthesized by Jessica Chao in our laboratory.

2.1.3 Resins and columns

Ni-NTA agarose resin was from Qiagen. Q sepharose Fast Flow (QFF) ion exchange resin was from GE Health Care Life Science. The micro bio-spin 6 columns were purchased from Bio-rad. The PepClean C-18 spin column was from Thermo Scientific.

2.1.4 Phospholipids

The dioctanoylphosphatidylinositol derivatives (diC_8PI, $diC_8PI(3,4)P_2$, $diC_8PI(4,5)P_2$, $diC_8PI(3)P$) and dipalmitoyl phosphatidylinositol 3-phosphate ($diC_{16}PI(3)P$) were purchased from Echelon. The dihexanoyl phosphatidylinositol compounds (diC_6PI and $diC_6PI(4,5)P_2$) were obtained from Cayman Chemicals. Long-chain phospholipids, including brain phosphatidylinositol-4',5'-bisphosphate ($PI(4,5)P_2$), 1,2-dioleoyl-*sn*-glycero-3-phospho-(1'-myo-inositol-3',4'-bisphosphate) ($DOPI(3,4)P_2$), 1,2-dioleoyl-*sn*-glycero-3-phospho-(1'-myo-inositol-4',5'-bisphosphate) ($DOPI(4,5)P_2$), 1-palmitoyl-2-oleoyl-*sn*-glycero-phosphocholine (POPC) and 1,2-diheptanoyl-*sn*-glycero-3-phosphocholine (diC_7PC), 1,2-dioleoyl-*sn*-glycero-3-phosphoethanolamine-N-(5-dimethylamino-1-naphthalene-sulfonyl) (Dansyl-PE) were obtained from Avanti Polar Lipids. The 3-deoxy-dioctanoylphosphatidylinositol derivatives were gifts of Dr. Yingju Xu and Dr. Scott Miller, Yale University.

2.2 Methods

2.2.1 Mutagenesis

All mutagenesis was done using the QuikChange site-directed mutagenesis kit. This method utilized double strand DNA plasmid as the template. Primers containing the desired mutation (point mutation, insertion or deletion) were extended during PCR amplification by *PfuTurbo* DNA polymerase. This DNA polymerase has high fidelity assuring the replication, but does not change the mutation site. After amplification, the parental plasmid containing methylated adenine was digested by Dpn I endonuclease to leave the newly synthesized mutation containing plasmids present (Nelson & McClelland, 1992). The primer pairs containing the mutation were designed to have 25-45 bases and good annealing to the template plasmid. The CG content should be at least 40% and the melting temperate is optimally above 78°C. Table 2.1and Table 2.2 showed the primers used for generating designated PTEN and *A. fulgidus* IMPase mutants. Typically 50 ng of plasmid was mixed with 125 ng sense and antisense primers in 200 μl PCR tubes with dNTP (deoxyribonucleotide mix) and reaction buffer added following the manufacturer's protocol. 1 μl of *PfuTurbo* DNA polymerase was added. The PCR cycling parameters used heating to 95°C for 30 s for single strand generation, cooling to 55°C for 1 min to allow the DNA and primers to anneal, then heating to 68°C for either 13 min (for PTEN) or 8 min (for *A. fulgidus* IMPase) for elongation. After 16 cycles, the product was cooled to 4°C. Then 1 μl DpnI was added to digest the parental plasmid at 37°C for 1 h. The digested product was transformed into *E. coli* XL1-blue competent cells for plasmid propagation and preparation. All mutants were confirmed by the DNA sequencing (Genewiz, NJ).

Table 2.1 Primers used for PTEN mutagenesis - the nucleotides changed are in bold type and underlined.

Protein mutant	Primers
K13E	5'-GAGATCGTTAGCAGAAAC**G**AAAGGAGATATCAAGAGG-3'
	5'-CCTCTTGATATCTCCTTT**C**GTTTCTGCTAACGATCTC-3'
R47G	5'-GACTTGAAGGCGTATAC**G**GGAACAATATTGATG-3'
	5'-CATCAATATTGTTCC**C**GTATACGCCTTCAAGTC-3'
R47W	5'-GACTTGAAGGCGTATAC**T**GGAACAATATTGATG-3'
	5'-CATCATCAATATTGTTCC**A**GTATACGCCTTCAA-3'
R47K	5'-GACTTGAAGGCGTATACA**A**GAACAATATTGATGATGTAG-3'
	5'-CTACATCATCAATATTGTC**T**TGTATACGCCTTCAAGTC-3'
R47L	5'-GACTTGAAGGCG TATAC**CT**GAACAATATTGATGATGTAG-3'
	5'-CTACATCATCAATATTGTTC**AG**GTATACGCCTTCAAGTC-3'
C124S	5'-GCAGCAATTCAC**A**GTAAAGCTGGAAAG-3'
	5'-CTTTCCAGCTTTAC**T**GTGAATTGCTGC-3'

Table 2.2 Primers used for *A. fulgidus* IMPase mutagenesis - the nucleotides changed are in bold type and underlined.

Protein mutants	Primers
R11A	5'-ATGCGCTGAGAATTTCG**GC**GGAGATTGCAGGAGAGG-3'
	5'-CCTCTCCTGCAATCTCC**GC**CGAAATTCTCAGCGCAT-3'
R18A	5'-GATTGCAGGAGAGGTC**GC**AAAGGCCATTGCGTC-3'
	5'-GACGCAATGGCCTTT**GC**GACCTCTCCTGCAATC-3'
R29A	5'-CAATGCCCTTGAGGGAG**GC**AGTAAAGGACGTGGG-3'
	5'-CCCACGTCCTTTACT**GC**CTCCCTCAAGGGCATTG-3'
R92Q	5'-GGAACCTTCAATGCTACG**CA**AGGGATTCCAGTTTATTC-3'
	5'-GAATAAACTGGAATCCCT**TG**CGTAGCATTGAAGGTTCC-3'
K164E	5'-CAGGAAGTTTCCCTTTGA**GA**GGATGAGGATTTTTG-3'
	5'-CAAAAATCCTCATCC**TC**TCAAAGGGAAACTTCCTG-3'
L57A	5'-CTGCGCTTGAAATT**GC**GAGAAAGGAGAGGGTTACGG-3'
	5'-CCGTAACCCTCTCCTTTCTC**GC**AATTTCAAGCGCAG-3'
V142A	5'-GGAGAGGATTGAGG**C**GAGCGATGCTGAG-3'
	5'-CTCAGCATCGCTC**G**CCTCAATCCTCTCC-3'
L148A	5'-GTGAGCGATGCTGAGGAG**GC**TTACTGCAACGCCATAATC-3'
	5'-GATTATGGCGTTGCAGTAA**GC**CTCCTCAGCATCGCTCAC-3'

2.2.2 Cloning

The *pten* gene was amplified by PCR using the GoTaq PCR Core system kit (Promega). 200 ng PTEN-pET-28a(+) plasmid was used as the template. The sequence of the primers is shown in Table 2.3. 50 pmol of each primer, 2.5 mM $MgCl_2$, DNA template and dNTP (deoxyribonucleotide mix) were mixed in reaction buffer following the manufacturer's protocol. Subsequently, 1.25 μl GoTaq DNA polymerase was added. PCR temperature cycling used 95°C for 2 min for initial production of single-stranded DNA, then 30 cycles of heating at 95°C for 1 min for denaturation, 55°C for 1 min for annealing template DNA with primer, and 72°C for 3 min for chain elongation. After PCR, the mixture was cooled to 4°C. The PCR products were visualized by electrophoresis on a 1% agarose gel with 1 μg/ml ethidium bromide and purified using a gel extraction kit. Purified PCR products and pET-23b(+) vector were doubly digested overnight at 37°C with NdeI and XhoI DNA endonuclease. The digested vectors were treated with Antarctic phosphatase to remove the 5' phosphate to prevent self-ligation, then purified with a gel extraction kit. Digested PCR products were purified using a PCR purification kit. Digested and purified vector and PCR products were mixed at a ratio of 1:6, and 1 μl T4 DNA ligase was added. The ligation reaction was incubated overnight at 16°C. After ligation, the product was transformed into *E. coli* Novablue competent cells for plasmid propagation. Positive cloning plasmid was confirmed by DNA sequencing.

Table 2.3 Primers used for cloning *pten* gene into pET-23b(+) vectors. The NdeI and XhoI restriction sites are underlined.

	Primers
Forward	5'-GCAAGTTCCATATGACAGCCATCATCAAAGAGATCG-3'
Reverse	5'-CTTGATGACTCGAGGACTTTTGTAATTTGTGTATGCTG-3'

2.2.3 Transformation

1 μl of the DpnI digested plasmids obtained from mutagenesis was mixed with 100 or 200 μl *E. coli* XL1-blue competent cells, or 10 μl cloning product were mixed with 100 μl NovaBlue competent cells and incubated on ice for 30 min. After incubation, the cells were heated to 42°C for 45 s for XL1-blue or 30 s for NovaBlue competent cells. After heat shock, the cell mixture was placed on ice for 2 min, and 500 μl LB media were added. The cell mixture was incubated on the rollerdrum for 1 h at 37°C. Then 200 μl cells were spread on LB-agar plates containing appropriate antibiotics. After growing overnight at 37°C, the plates with *E. coli* colonies were stored at 4°C.

2.2.4 Plasmid DNA extraction

A single colony from the plate of transformed XL1-blue competent cells (or NovaBlue competent cells for cloning) was picked and grown overnight in 5 ml LB media with proper antibiotics. DNA plasmid was extracted from the cells using QIAprep spin Miniprep Kit (Qiagen) following the manufacturer's protocol. The final concentration of DNA was measured by the UV absorbance at 260 nm using an extinction coefficient of 0.020 $(\mu g/ml)^{-1}$ cm^{-1}.

2.2.5 Protein overexpression

All the plasmids containing the designated genes are based on pET vectors. In the pET vector expression system, gene expression is controlled by the T7 promoter (Rosenberg et al, 1987; Studier et al, 1990). *E. coli* BL21 competent cells were used for protein overexpression. In the uninduced state, the target gene expression is silent due to the lack of T7 RNA polymerase. Addition of IPTG, which binds to the *lac*UV5 promoter, releases the T7 RNA polymerase for expression. After induction, T7 RNA polymerase initiates

the transcription of the target gene. Since T7 RNA polymerase is more active than RNA polymerase in *E coli*, most of the cells express the target gene, 1 µl plasmid obtained from the miniprep was mixed with 100 µl *E. coli* BL21 condonplus(DE3)-RIL competent cells for transformation. After heat shock at 42°C for 30 s, the cells were incubated for 1 h at 37°C. The cells (200 µl) were spread on LB-Agar plates and grown overnight as single colonies. One of these single colonies was grown overnight in 5 ml LB media with appropriate antibiotics. This 5 ml culture was transferred to a flask containing 2 L LB media and grown at 37°C until the O.D. at 600 nm was between 0.6 and 0.8 (for PTEN the $O.D._{600nm}$ was around 0.9). IPTG at 0.1 mM (for PTEN) or 0.8 mM (for IMPase) was added to induce protein overexpression. After 20 h incubation at 16°C, the cells were harvested by centrifugation and stored at -20°C.

2.2.6 Protein purification

2.2.6.1 PTEN purification

The frozen cells from 2 L culture were resuspended in 45 ml lysis buffer (50 mM Tris, 300 mM NaCl, 10 mM imidazole, 10 mM β-mecaptoethanol, pH 8, stored at 4°C) and incubated on ice for 30 min. The cells were lysed using 15×20 s sonication cycles. After centrifugation at 15,000 rpm for 35 min, the cell debris was removed and the supernatant was loaded at 0.5 ml/min and 4°C onto a column with 7.5 ml Ni-NTA agarose slurry pre-equilibrated with 100 ml lysis buffer. After loading, the column was washed with 150 ml lysis buffer at 1.5 ml/min and 350 ml wash buffer (50 mM Tris, 300 mM NaCl, 20 mM imidazole, 10 mM β-mecaptoethanol, pH 8, pre-cooled to 4°C) at 2 ml/min to remove any contaminating proteins bound on the resin. After the wash step, the protein was eluted with a gradient formed from 75 ml each of 20 and 250 mM imidazole in 50 mM

Tris, 300 mM NaCl and 10 mM β-mecaptoethanol. The purity of the eluted fractions was monitored by SDS-PAGE and fractions >90% pure were pooled and dialyzed overnight at 4^{o}C against 4 L of 50 mM Tris, 1 mM DTT, pH 8. After dialysis, the protein was concentrated to ~4 mg/ml. The protein concentration was measured by UV absorbance at 280 nm with $\varepsilon = 45{,}270\ M^{-1}\ cm^{-1}$. Protein aliquots were flash frozen in liquid nitrogen and stored at -80°C. Once the protein was thawed, it was kept at 4°C and used within 3 days.

For purifying the C-terminal His-Tag PTEN protein, a gel filtration column was used after initial purification with the Ni-NTA affinity column. The protein was eluted in 50 mM Tris pH 8, 100 mM NaCl and 10 mM β-mecaptoethanol buffer. After gel filtration, the fractions containing the protein (monitored by SDS-PAGE) were collected. The protein was dialyzed against 100 mM Tris, 1 mM DTT, pH 8, and stored at -80°C.

2.2.6.2 *Archaeoglobus fulgidus* inositol monophosphatase (IMPase) purification

Cell pellets from 2 L culture were resuspended into 30 ml buffer A (50 mM Tris, 1 mM EDTA), sonicated with 10×30 s pulses, and centrifuged for 30 min at 15,000 rpm to remove insoluble cell debris. After centrifugation, the supernatant was heated (85°C for wild type, 65°C for R11A/R18A and R11A/R18A/R92Q/K164E, and 75°C for other mutants) for 30 min to denature most of the *E. coli* protein. Denatured *E. coli* proteins were removed by centrifugation at 15,000 rpm for 45 min. The supernatant was dialyzed against 4 L buffer A overnight. The dialyzed cell lysates were loaded at 1.5 ml/min onto the QFF resin column (~40ml) equilibrated with 200 ml buffer A. After loading, the column was washed with 40 ml buffer A, and the protein was eluted with a gradient of 0 to 0.6 M KCl in buffer A. The fractions containing >90% pure protein (determined by

SDS-PAGE) were collected and dialyzed twice against 4 L buffer A to remove salts. After dialysis, the protein was concentrated to ~10 mg/ml, and stored at 4°C. The protein concentration was measured by Lowry assay (Lowry et al, 1951).

2.2.7 Large unilamellar vesicles (LUVs) and small unilamerllar vesicles (SUVs) preparation

Desired amounts of lipids in chloroform were mixed together in a 20 ml scintillation glass vial. The organic solvent was removed under a stream of nitrogen and the lipids were dried by lyophilization overnight. The dry lipid film was suspended in 50 mM Tris, pH 8.0, and vortexed. The multilamellar vesicles that formed spontaneously were extruded through a 0.1 μm polycarbonate membrane 25 times to form LUVs (1000 Å average diameter). For SUVs, the resuspended solution of the lipids was put on ice and sonicated with 30 s on and 30 s off cycles until the solution was clear; these have an average diameter 250-300 Å.

2.2.8 Phosphatase assays

Enzyme activities of PTEN and IMPase were determined by measuring the concentration of the inorganic phosphate (Pi) using a colorimetric malachite green assay (Itaya & Ui, 1966). 0.05% (w/v) malachite green oxalate in water was mixed with 4.2% ammonium molybdate in 6 M HCl at a ratio of 3:1 and incubated for 30 min prior to use. KH_2PO_4 was used as the standard: 2, 5, 10, 15 and 20 μl of 1 mM KH_2PO_4 were mixed with 50 or 200 μl 50 mM Tris, pH 8.0. The malachite green reagent (1 ml) was added to each sample, and the absorbance at 660 nm was recorded. Absorbance versus Pi provided a standard curve for calculating the amount of Pi produced by enzyme dephosphorylation of different substrates (Figure 2.1).

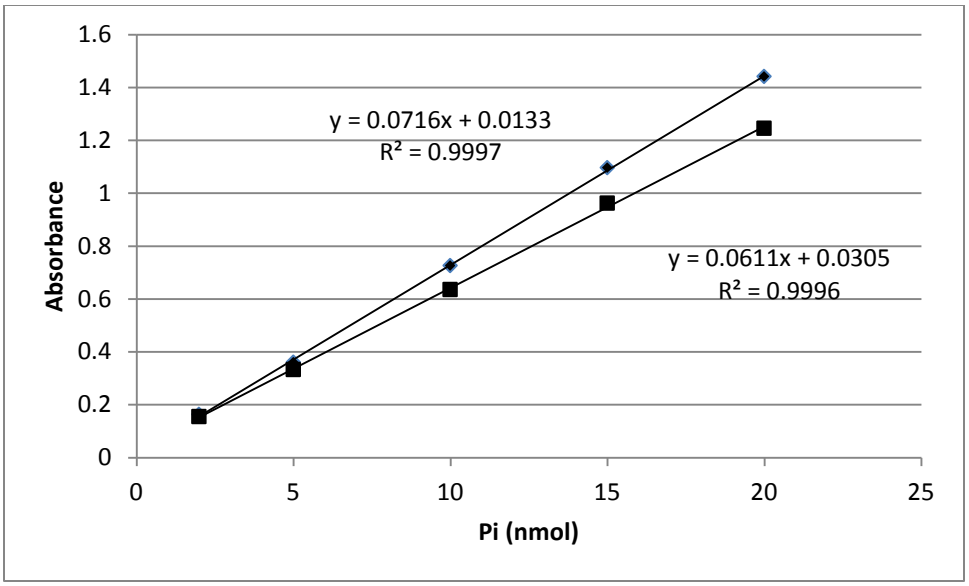

Figure 2.1 Standard curve of phosphatase assay. The absorbance of different amounts of inorganic phosphate (Pi) in total 50 µl (♦) and 200 µl (■) 50mM Tris buffer (pH 8.0) was measured. The data were fitted in a liner equation and the correlation coefficient was shown.

2.2.8.1 PTEN activity

These assays were carried out in 50 mM Tris, pH 8.0, with 2 mM EDTA, 10 mM DTT, and substrates. For each reaction sample, PTEN was incubated with substrate for 20 or 40 min at 37°C, then 1 ml malachite green reagent was added and the absorbance at 660 nm was recorded. The amount of enzyme added to each sample was chosen to obtain 5 to 20% substrate hydrolysis. In a 'monomer' assay system, 0.5 mM diC_8PI(3)P or 0.1 mM diC_8PI(3,4)P_2 was used (the critical micelle concentration, or CMC, for each compound is $\geq$ 0.5 mM). DiC_8PI(4,5)P_2 and diC_7PC concentrations in the assays were one half or equal to that of the substrate. The ratio of Triton X-100 to short chain substrates was 4:1. A mixed micelle system was also used with long-chain phosphoinositides. DOPI(3,4)P_2 with or without DOPI(4,5)P_2 was dissolved in Triton X-100 with a total phospholipid to detergent ratio of 1:4. For assays using vesicles, 5 mM total of DOPI(3,4)P_2/POPC (5:95)

or DOPI(3,4)P_2/DOPI(4,5)P_2/POPC (5:5:90) LUVs were made. Enzyme assays used 1 mM (total phospholipid) LUVs as the substrate.

The effect of deoxy-diC_8PI analogs on PTEN activity was tested using 0.1 mM dipalmitoyl-PI(3)P (D-diC_{16}PI(3)P) as the substrate presented in either Triton X-100 micelles or in LUVs with POPC. For the mixed micelle assay, the substrate was mixed with Triton X-100 at a molar ratio of 1:4 D-diC_{16}PI(3)P/Triton X-100 dissolved in 100 mM Tris-HCl, pH 8.0. For the vesicle system, POPC was mixed with D-diC_{16}PI(3)P at a molar ratio of 9:1 to form LUVs with 1 mM total phospholipid as the substrate. Both types of assays were carried out in 200 μL buffer (100 mM Tris-HCl, pH 8.0, 2 mM EDTA, 10 mM DTT) at 37°C for 20-40 min incubation with the enzyme. Most of the assays were done at least in duplicate. The effect of deoxy-diC_8PI derivatives was measured by mixing the desired concentration of deoxy-diC_8PI derivatives (0.1 mM, 0.5 mM and 1 mM) with the substrates and measuring the amount of Pi produced as described above.

2.2.8.2 *A. fulgidus* IMPase activity and compatible solute thermoprotection effect

The activity of recombinant *A. fulgidus* IMPase was measured at 85°C. Typically, 0.2 μg of protein was added to 0.5 mM D-I-1-P in 50 μl of 50 mM Tris, 1 mM EDTA, 5 mM $MgCl_2$, pH 8.0. The mixture was heated at 85°C for 5 min then placed on ice to cool to room temperature. 1 ml of malachite green reagent was added and the absorbance at 660 nm was measured.

2.2.8.2.1 DIP and compatible solutes thermoprotection at 95°C

Recombinant *A. fulgidus* IMPase, in 50 mM Tris HCl, pH 8.0, was placed in 200 µl PCR tubes to which different compatible solutes (DIP, KCl, NaCl, K^+-glutamate or Na^+-glutamate) were added. The total volume was 50 µl, and the final concentration of protein was 52 µg/ml. Each solution was heated at 95°C in the PCR amplifier (GeneAmp PCR System 9700, PE Applied Biosystems). After 15 min, the samples were removed and placed on ice prior to measuring residual catalytic activity. The activity of the protein after heating with or without the compatible solutes was measured by adding aliquots of the protein from each sample to the substrate buffer. The residual activity was calculated by comparing the specific activity from each assay to what was observed with proteins without heating inactivation in the absence of any thermoprotective agents.

2.2.8.2.2 Compatible solute thermoprotection at 90°C

IMPase (9.6 µg) was mixed with 0, 0.05, 0.1, 0.3 and 0.5 M compatible solutes (KCl, K-Glu, Na-Glu, K-Asp, Na-Asp, proline and betaine) in 50 mM Tris, pH 8.0, and heated at 90°C in the PCR amplifier for 30 min. An aliquot of the heated mixture was removed for measurement of the residual activity compared to untreated enzyme. As another control, the same amount of the each solute was mixed with the untreated enzyme to account for any effect of the solute on enzyme activity. The amount of enzyme added was adjusted to generate 5% to 20% substrate hydrolysis.

The thermoprotection of IMPase by dicarboxylate salts was also tested. IMPase (7.6 µg) was mixed with 0.3 M of tartrate, succinate, methylsuccinate, maleate, fumarate and isocitrate (in sodium form) in 50 mM Tris, pH 8.0, and heated at 90°C for 30 min. The residual activity was measured at 85°C with 0.5 mM D-I-1-P as the substrate.

2.2.8.2.3 DGP thermoprotection of IMPase

In the synthesis of DGP, there is some contaminating Pi that was not completely removed. While irrelevant if DGP is used at mM concentrations, it makes the background in the Pi assay too high to detect signal if high concentrations of DGP are used. Therefore, a different assay and substrate were used. Cleavage of pNPP by IMPase generates PI and *p*-nitrophenol, which has a strong yellow absorbance at 405 nm. Assay mixtures consisted of 2 μg of IMPase and 0.5 mM pNPP in 50 mM Tris, 1 mM EDTA, 5 mM $MgCl_2$, pH 8.0. The reaction was carried out at 85°C for 5 min. The reaction mixture was then placed on ice, and 1 ml of 3 M NaOH was added to quench the reaction. Absorbance at 405 nm was recorded to calculate the amount of *p*-nitrophenol produced using $\varepsilon=1.78x10^4\ M^{-1}\ cm^{-1}$.

For inactivation of the protein, 19.2 μg of IMPase was mixed with 10 or 100 mM DGP in 50 mM Tris, pH 8.0, and heated in PCR tubes at 90°C for 30 min. The residual activity was measured by adding the aliquots of the heated protein into pNPP substrate buffer and measuring the activity as described above. The control protein activity was measured by mixing the same amount of DGP solution with the protein without heating.

2.2.8.2.4 IMPase mutant thermoprotection by compatible solutes

The enzyme activity of specifically mutated proteins and the residual activity after heating these variants were measured as for recombinant IMPase but with minor changes to account for altered thermostability. The activity and extent of thermoprotection of R11A/R18A and the quad-mutant were measured at 55^{o}C with 0.5 mM FBP as the substrate. For thermal denaturation, R11A/R18A was heated for 30 min at 73°C, and the quad-mutant was heated for 30 min at 71°C. The activity and residual activity after

heating of R18A and R29A were measured at 75°C with 0.5 mM D-I-1-P as the substrate. R18A was heated for 26 min at 87°C, while R29A was incubated at 85°C for 30 min. The activities of R92Q and R92Q/K164E were measured at 65°C with 0.5 mM D-I-1-P as the substrate; for thermal denaturation, R92Q was heated at 80°C for 26 min and R92Q/K164E was heated at 77°C for 25 min.

2.2.9 Fixed field ^{31}P NMR spectroscopy

The binding of PTEN to phospholipids was investigated by measuring the phospholipid phosphodiester peak linewidth change in the presence of the PTEN protein. ^{31}P NMR spectra of phospholipids were obtained at 242.7 MHz on a Varian 600 MHz VNMRS system at 25°C. Short-chain phospholipid solutions (diC_8PI, diC_8PIP_x, diC_7PC) in 100 mM Tris, 2 mM EDTA, pH 8.0, were placed in 5 mm Shigemi tubes. PTEN, wild type or mutated protein, was added to the lipid mixture to a final concentration of 0.5 mg/ml (10.1 μM). The peak width at half height ($\Delta\nu_{1/2}$) was measured, and the linewidth difference $\Delta\Delta\nu_{1/2}$ was calculated by subtraction of the linewidth for lipid alone from the linewidth when protein was present ($\Delta\Delta\nu_{1/2} = \Delta\nu_{1/2,\ lipid,\ protein} - \Delta\nu_{1/2,\ lipid}$). ^{31}P spectra were acquired for every lipid concentration at least in duplicate to obtain an average change in linewidth caused by addition of the protein.

2.2.10 High-resolution field cycling NMR

Field cycling NMR was used to study the spin-labeled PTEN protein proximity to bound phospholipid headgroups, and the binding of ^{13}C labeled Glu to spin-labeled IMPase.

2.2.10.1 PTEN ^{31}P field cycling NMR

2.2.10.1.1 Spin-labeling PTEN

Prior to labeling of PTEN cysteine groups, the protein (4 mg/ml protein solution in 100 mM Tris, pH 8.0) was incubated for 30 min with 10 mM DTT to reduce any disulfide bonds that had formed. The protein was then exchanged into 20 mM Tris, pH 7.5, and excess DTT was removed using a micro bio-spin 6 column. MTSL, from a 20 mg/ml stock in acetone, was added to the protein solution at a ratio of protein: MTSL = 1:4 based on the PTEN concentration prior to the spin column (on which about half the protein is typically lost). The incubation time, 1 h for PTEN and 1.5 h for K13E, was chosen so that >90% of the PTEN activity was lost. Unreacted MTSL was removed by two spin columns which also served to exchange the protein back into 100 mM Tris, pH 8.0.

Unmodified cysteine residues were measured using DTNB (Ellman, 1959), by comparing the spin-labeled preparation to unlabeled PTEN. Each protein (10 μg) was incubated with 500 μmol DTNB in 50 mM Tris, pH 8 (total volume 200 μl) for 15 min. The absorbance at 412 nm was used to calculate the free cysteine concentration (ε=13,600 M^{-1} cm^{-1}). The labeling ratio was calculated by $[Cys]_{free,\ PTEN\text{-}SL}$ / $[Cys]_{free,\ PTEN\text{-}WT}$ ×10, since PTEN has a total of 10 Cys residues,

2.2.10.1.2 Mass spectrometry (MS) detection of modification sites of spin-labeled PTEN

MS was used to monitor the extent of MTSL modification of the 10 cysteines on PTEN. The protein (10 μg), before or after spin-labeling, in 50 mM Tris, pH 8.5, was incubated

in 8 M urea for 30 min. The sample was then diluted 8-fold with 50 mM Tris, pH 8.5, and mixed with LysC endoproteinase (Wako) added in a ratio of 1:50 (w/w) LysC / PTEN. After overnight digestion at 37^{o}C, the peptide mixture was desalted on a C18 spin column, dried in a speedvac concentrator (Thermo Scientific) and resuspended in 10 µL Buffer A (95% water, 5% acetonitrile, 0.1% formic acid). LC-MS/MS analysis was performed on an LTQ-Orbitrap Discovery mass spectrometer (Thermo Fisher) coupled to an Agilent 1200 series HPLC system. The LysC digest was pressure loaded onto a 100 µm fused silica column (100 µm fused silica with a 5 µm tip) packed with 10 cm of Aqua C_{18} reverse phase resin (Phenomenex). The peptides were then eluted from the column using a 120 minute gradient of 5–100% buffer B in buffer A (buffer A: 95% water, 5% acetonitrile, 0.1% formic acid; buffer B: 20% water, 80% acetonitrile, 0.1% formic acid), and injected into the mass spectrometer. The flow rate through the column was set to ~0.25 µl/min and the spray voltage was set to 2.75 kV. One full MS scan (FTMS) (400–1,800 MW) was followed by 7 data dependent scans (ITMS) of the n^{th} most intense ions with dynamic exclusion enabled. The tandem MS data were searched using the SEQUEST algorithm (Yates et al, 1995) using a concatenated target/decoy variant of the human International Protein Index database. A differential modification of +185.0874 on cysteine was specified to account for the MTSL modification. SEQUEST output files were filtered using DTASelect 2.0 (Tabb et al, 2002). Discriminant analyses were performed to achieve a peptide false-positive rate below 5%. (Mass spectrometry and peptide identification were kindly done by Prof. Eranthie Weerapana, Boston College).

2.2.10.1.3 High resolution field cycling ^{31}P NMR

^{31}P field-cycling spin-lattice relaxation rate (R_1) measurements were made at 20°C on a Varian Unity^{plus} 500 spectrometer using a standard 10-mm Varian probe in a custom-built device that moves the sample, from the sample probe location to a higher position within, or just above, the magnet, where the magnetic field is between 0.04 and 11.7 T. Lower fields are accessed by shuttling the sample to the middle of a permanent magnet (mounted on the top of the magnet dewar) that can be tuned down to 0.002 T (Roberts & Redfield, 2004a). Concentrations of the phosphorus-containing ligands were usually 3 mM for phosphoinositides, 5 mM for diC_7PC, and 5 mM for inositol phosphates. Spin-labeled protein concentration was usually 0.1 mg/ml (2.0 μM) for diC_8PI samples and 0.25 mg/ml (4.9 μM) for other ligands. The sample buffer was 100 mM Tris, pH 8.0, with 2 mM EDTA. Controls used the same concentration of phospholipids but with 0.1 or 0.25 mg/ml PTEN without spin-labeling. The contribution of unlabeled protein binding to the field dependence of different phospholipids was used to calculate the change in relaxation rate due to the spin-labeled protein: $\Delta R_1 = R_{1,\text{ spin-label}} - R_{1,\text{ control}}$. The data were fit to the following equation:

$$\Delta R_1 = \Delta R_{P\text{-}e}(0) / (1+\omega_p^2\tau_{P\text{-}e}^2) + c$$

where $\Delta R_{P\text{-}e}(0)$ is the low-field limit of ΔR_1. ω_p is the angular frequency of ^{31}P, $\tau_{P\text{-}e}$ is the correlation time of the dipolar relaxation of ^{31}P by nearby nitroxide unpaired electrons. The 'c' term represents a limiting CSA contribution due to the paramagnetic interaction. If the protein contains a single spin-label, the average distance $r_{P\text{-}e}$ between abound phospholipid phosphorus and the unpaired electron of the spin-labeled proteins can be

extracted from the parameters $\Delta R_{P\text{-}e}$ (0) and $\tau_{P\text{-}e}$ along with the concentration of the protein and phospholipid, [PTEN-SL] and [PL]:

$$r_{P\text{-}e}^{6} = ([\text{PTEN-SL}]/[\text{PL}])\,(S^2\,\tau_{P\text{-}e})[0.3\mu^2(h/2\pi)^2\gamma_P^2\,\gamma_e^2]/\,\Delta R_{P\text{-}e}\,(0)$$

However, when more than one cysteine bears a spin-label the relaxation will be an average of the different label positions. Although exact distances are not easy to extract, it is possible to compare the effectiveness of the multiply-labeled protein in relaxing the ^{31}P of different molecules. If the lipids occupy discrete and different sites, then one should see differences in the ratio $(\tau_{P\text{-}e}/\Delta R_{P\text{-}e}(0)) \times [\text{PTEN-SL}]/[\text{PL}]$.

2.2.10.2 *A. fulgidus* IMPase field cycling ^{13}C NMR

2.2.10.2.1 Spin-labeling IMPase

Recombinant IMPase (or R92Q/K164E protein) at 10 mg/ml was incubated with 1 mM DTT for 30 min to reduce any disulfide bonds. Excess DTT was removed and the protein was buffer exchanged into 25 mM Tris, pH 7.5, using a micro bio-spin 6 column (Bio-Rad). The protein was mixed with the 10 mg/ml MTSL stock, at a molar ratio of 1:10 protein/MTSL and incubated at room temperature for 2 h. After incubation, free MTSL was removed by 2 successive spin columns, which also served to exchange the buffer to 50 mM Tris, pH 8.0. The protein concentration after spin-labeling was measured by Lowry assay.

2.2.10.2.2 High resolution field cycling ^{13}C NMR

10 mM or 25 mM ^{13}C-Glu or ^{13}C-Ala (pH 8.0) was mixed with 3 mg/ml of spin labeled IMPase. The ^{13}C field cycling NMR spin-lattice relaxation rate (R_1) measurements were carried out at 25°C and 45°C on a Varian Unity^{plus} 500 spectrometer with the sample

shuttling mechanism and accessible magnetic fields as described above for ^{31}P field cycling. R_1 measurements at high compatible solute concentrations used 25 mM of ^{13}C-Glu with non-isotopically enriched Glu to yield a total solute concentration of 40 and 75 mM; the spin-labeled protein concentration was 3 mg/ml. The contribution of unlabeled protein binding to the field dependence of different salts was measured but was usually minimal, except at the lowest concentration of ^{13}C-Glu used (where binding is very low and the enhancement of the relaxation rate is small). Here, the relaxation rate due to the spin-labeled protein is $\Delta R_1 = R_{1,\text{ spin-label}} - R_{1,\text{ control}}$. The data were fit to the following equation:

$$\Delta R_1 = \Delta R_{C\text{-}e}(0) / (1+\omega_C^2\tau_{C\text{-}e}^2) + a$$

where $\Delta R_{C\text{-}e}(0)$ is the low-field limit of ΔR_1. ω_p is the angular frequency of ^{13}C, $\tau_{C\text{-}e}$ is the correlation time of the dipolar relaxation of ^{13}C by nearby nitroxide unpaired electrons. Again, the 'a' term represents a limiting CSA contribution due to the paramagnetic interaction.

2.2.11 Circular dichroism

CD spectra of proteins were recorded in a 1 cm path length quartz cuvette with 0.04 mg/ml protein in 10 mM borate buffer, pH 8.0, using an Aviv 420 circular dichroism spectrometer (Biomedical Inc.). Protein ellipticity was scanned from 290 to 180 nm with the solution at 25°C. The thermal melting (or denaturation) temperature (T_m) of proteins was monitored by measuring the ellipticity at 222 nm (where only helices contribute to the ellipticity) as the sample temperature was increased from 30°C to 99°C. The T_m is the

temperature at which the derivative of ellipticity with temperature is a maximum (Figure 2.2 provides an example of a denaturation curve for IMPase R92Q/K164E).

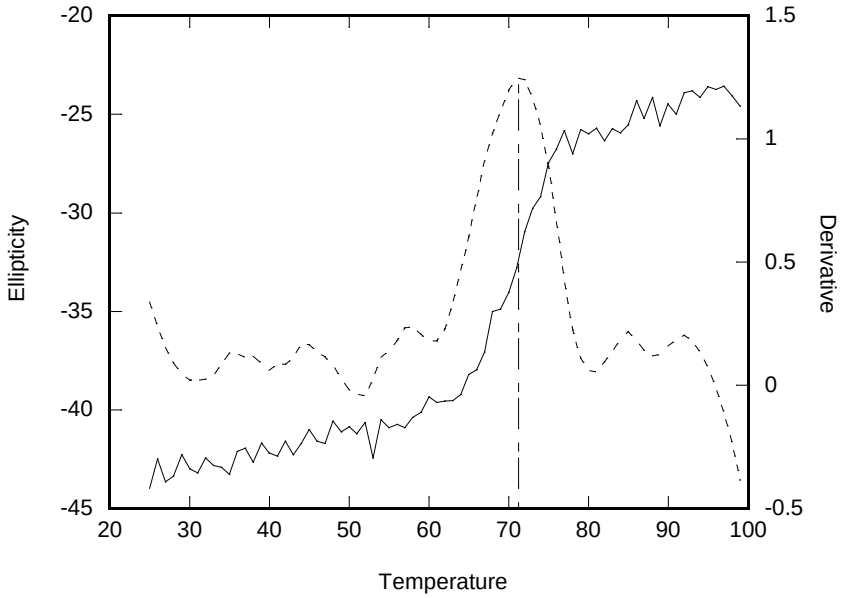

Figure 2.2 0.04 mg/ml *A. fulgidus* IMPase R92Q/K164E ellipticity change (solid line) at 222 nm upon heating measured with circular dichroism (CD) spectrometry. The derivative of ellipticity is calculated (dash line). The temperature at which the derivate is maximal is the T_m.

2.2.12 Fluorescence spectroscopy

Binding of PTEN to the LUVs was measured by Förster resonance energy transfer (FRET) fluorescence spectroscopy. 2% Dansyl-PE containing vesicles were used as the acceptor and Trp residues in PTEN were the donor. The fluorescence spectra of 1.5 or 3 μM PTEN protein in 100 mM Tris, pH 8 containing 2 mM EDTA, 10 mM DTT and 150 mM NaCl were recorded using a Fluorolog R-3 spectrofluorometer. The protein was excited at 290 nm, and the fluorescence spectra were recorded between 300 and 400 nm. A maximum intensity around 340 nm was recorded. Next 2% Dansyl-PE containing vesicles were added into the protein solution to cover the concentration range from 0 to 2

mM total lipid; the total lipid concentration was incremented in 0.2 mM steps. The vesicles used were 88:2:10 POPC/Dansyl-PE/PL (where PL = POPC, DOPS, DOPA, soy PI or brain $PI(4,5)P_2$), 25:2:73 DOPS/Dansyl-PE/ POPC, and 10:5:2:83 DOPS/ $PI(4,5)P_2$/ Dansyl-PE/POPC. The fluorescence intensity change upon the addition of Dansyl-PE containing vesicles was corrected by subtracting the intensity change caused by titrating in vesicles without the fluorophore; a small dilution correction was also used. The apparent dissociation constant (K_d) was calculated by fitting the fluorescence intensity data into the equation: $f_{bound}= c\times[phospholipid]/(K_d + [phospholipid])$ where [phospholipid]is the total concentration of the phospholipids in the vesicles, f_{bound} is the fraction bound. It is calculated from $\Delta I^{corr}/I_0$ where ΔI^{corr} is the corrected intensity change and I_0 is the initial intensity before the lipid added. However, the maximum FRET change in donor fluorescence is not necessarily known so the 'f_{bound}' estimated this way is not a true fraction of protein bound but proportional to it. In the fitting, c is a constant that is proportional to the maximum protein bound.

Chapter 3

Exploring phospholipid binding sites on PTEN

3.1 Introduction

Deoxy-diC_8PI derivatives with one or more hydroxyl groups on the inositol head group removed are analogs of PTEN substrate, diC_8PI(3)P. The structures of these synthetic PI compounds, synthesized by Yingju Xu in the laboratory of Prof Scott Miller when he was at Boston College, are shown in Figure 3.1. The effect of these PI derivatives on PTEN enzymatic activity was tested (Wang et al, 2008); all these deoxy-PI derivatives were inhibitory to PTEN when substrate diC_8PI(3)P was used at 0.5 mM. However, there were some interesting trends in the inhibition effects. Generally, the D-series of deoxy-PI derivatives were more potent than their L-series counterparts, and D-3-deoxy-diC_8PI was the most potent inhibitor. Removing another hydroxyl group from the inositol ring in D-3-deoxy-diC_8PI generated a less potent inhibitor, while this behavior was reversed in L-series compounds. L-3,5-dideoxy-diC_8PI was a considerably more potent PTEN inhibitor than L-3-deoxy-diC_8PI (Wang et al, 2008). All of the deoxy-PI derivatives had similar critical micelle concentration (CMC) values around 0.5 mM. Thus, micelle formation could not explain the specificity of inhibition. The attempt to explain these kinetic results using the known crystal structure of PTEN also failed. The crystal structure of PTEN had a tartrate molecule in the active site (Lee et al, 1999). An I(1,3,4,5)P_4 molecule, the head group of the substrate PI(3,4,5)P_3, could be superimposed on the tartrate molecule. However, the lack of acyl chains (or even the glycerol backbone) made it difficult to understand how the lipid glycerol and acyl chains might interact with the protein. Head group hydrogen bonding to the protein and hydrophobic interaction between the acyl chain(s) and the protein could be the key to explaining how the deoxy-PI derivatives affected PTEN activity so differently.

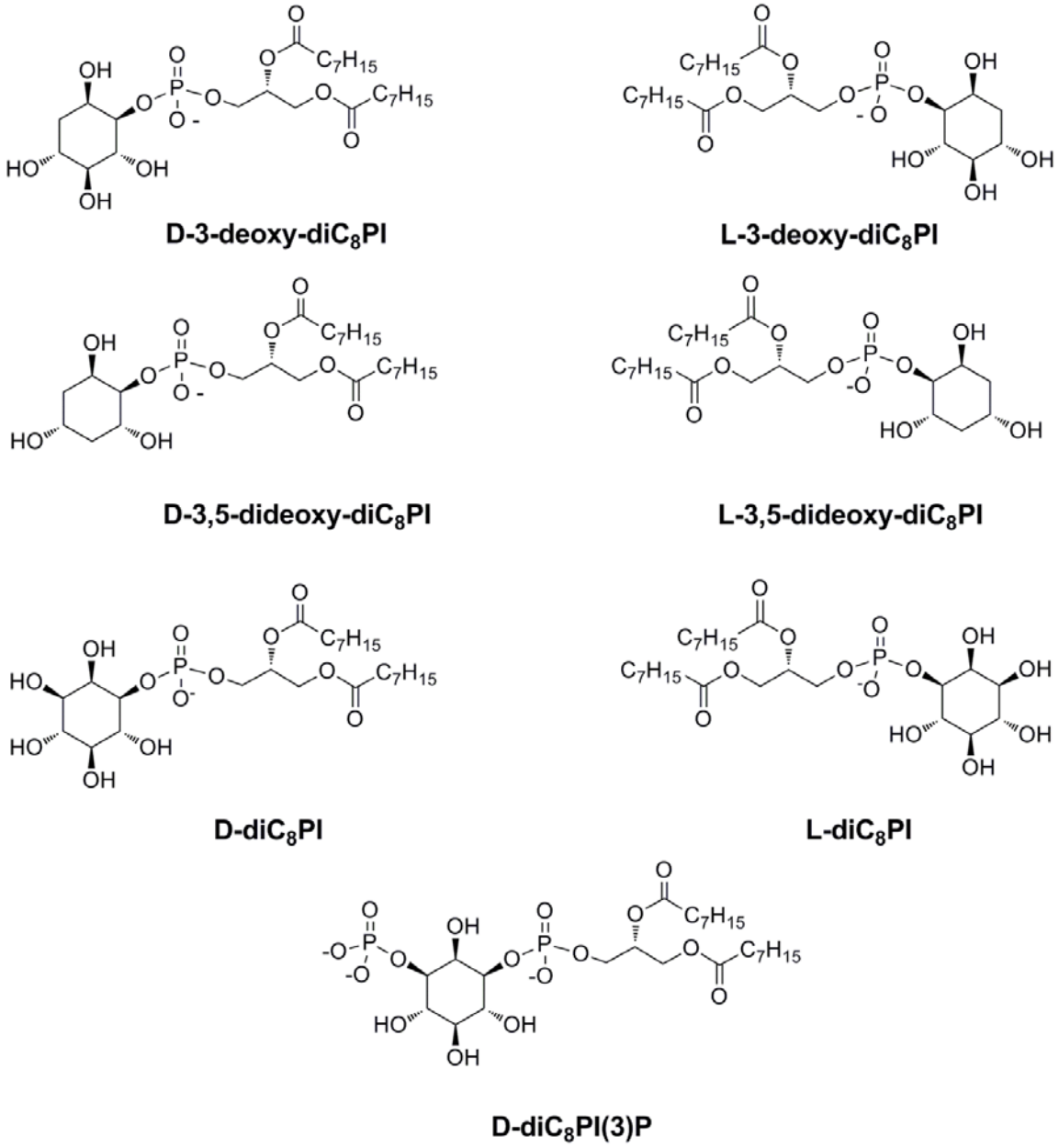

Figure 3.1 The structures of the substrate dioctanoylphosphatidylinositol-3-phosphate (diC$_8$PI(3)P) and the six 3-deoxy-dioctanoylphosphatidylinositol (3-deoxy-diC$_8$PI) inhibitors.

In order to provide an explanation of the inhibitor pattern for the deoxy-PI molecules, molecular dynamics (MD) simulation, quantum mechanical and free energy calculations were used to study the PTEN phosphatase domain interacting with deoxy-diC$_8$PI derivatives and substrate diC$_8$PI(3)P. The simulations and calculations were done by Dr.

Qin Wang in the laboratory of Prof. Goran Krilov (Wang et al, 2010). From the MD simulations, different binding modes were identified between the D- and L- series deoxy-diC_8PI derivatives and PTEN. The head group of all the six deoxy-PI derivatives and the substrate diC_8PI(3)P bound into the active site, forming hydrogen bonds and salt bridge with the protein. Interestingly, the hydrogen bonding decreased as the inhibition potency increased. The poorest inhibitor, L-diC_8PI, actually had the most favorable hydrogen bonding interaction between lipid head group and the protein (Figure 3.2). The most obvious difference was the orientation of the acyl tails of the D- and L- series lipids due to the different inositol chirality (Figure 3.3). In general, the acyl chains of D- series compounds had more contact with PTEN compared to their enantiomer. The one exception was L-3,5-dideoxy-diC_8PI, which had more protein-tail interactions than its D-inositol enantiomer. A hydrophobic cleft formed by the loop pβ_2-α_1 (residues 42-52) on the phosphatase domain was identified; the acyl chain of D-3-deoxy-diC_8PI had the strongest hydrophobic contact with this region of the protein. The interaction between the pβ_2-α_1 loop and the acyl chain was also observed in the energy minimized structure of substrate D-diC_8PI(3)P binding to PTEN. L-3,5-dideoxy-diC_8PI also had a large number of acyl tail-protein contacts, but these contacts were from the residues on the opposite side of the active site instead of the pβ_2-α_1 hydrophobic cleft. L-3,5-dideoxy-diC_8PI was almost as potent an inhibitor as D-3-deoxy-diC_8PI, which had a smaller number of hydrogen bonds of the head group to PTEN. For D-3-deoxy-diC_8PI to be the most potent PTEN inhibitor, the loss in hydrogen bonding interactions was compensated by a greater hydrophobic contact of the acyl chain with the protein.

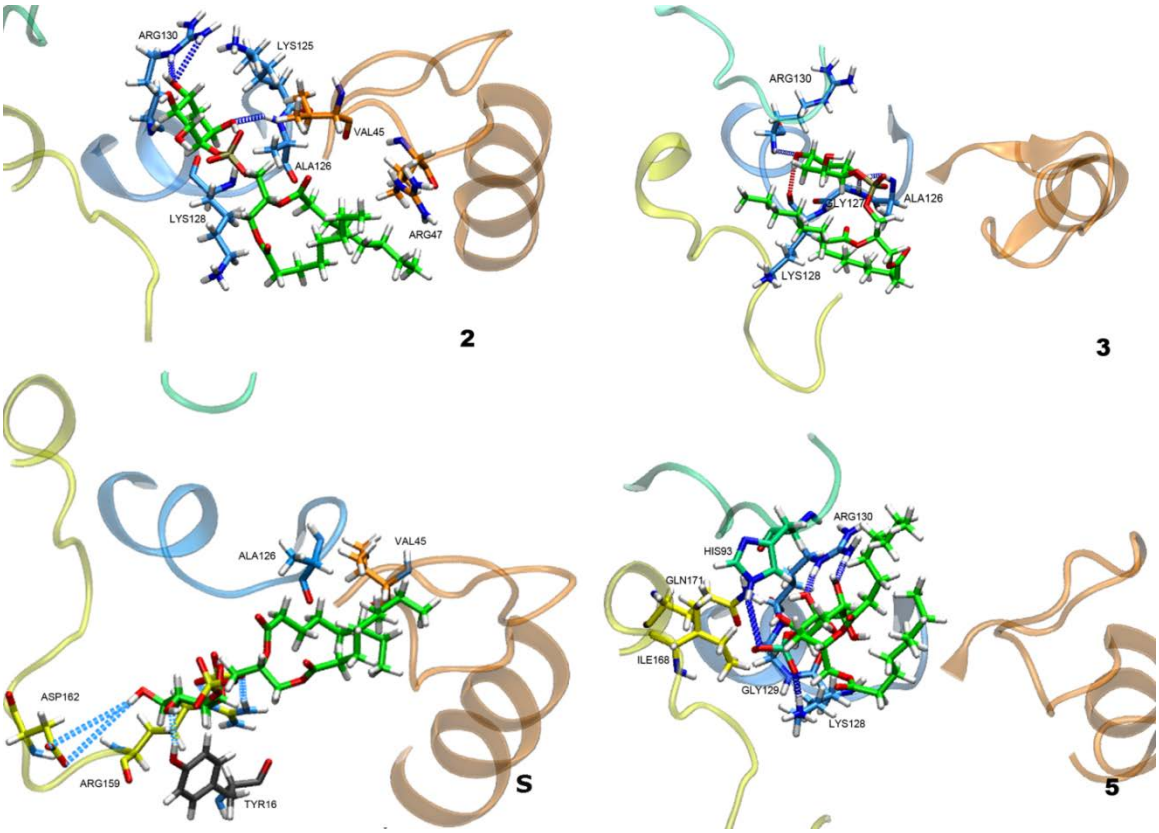

Figure 3.2 Median structures of the PTEN phosphatase domain complexes with compounds 2 (D-3-deoxy-diC_8PI), 3 (L-3,5-dideoxy-diC_8PI) and 5 (L-diC_8PI), and the substrate S (D-diC_8PI(3)P), obtained by clustering configurations collected from a 2 ns MD simulation. The lipids (green) and adjacent protein residues are shown as sticks and the protein backbone as ribbons. Important lipid-protein hydrogen bonds are shown as dark blue dashed lines. Note the difference in tail orientation between the D-series (2 and S) and L-series (3 and 5) PI derivatives (Wang et al, 2010).

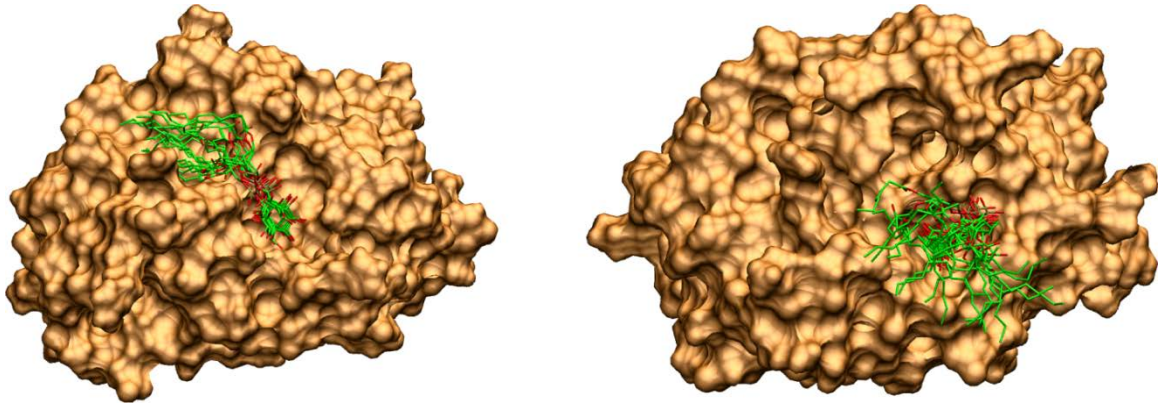

Figure 3.3 Representative snapshots of the conformations of compound 2 (left, D-3-deoxy-diC_8PI) and compound 5 (right, L-3,5-dideoxy-diC_8PI) bound to the active site of the PTEN phosphatase domain from a 2 ns MD simulation. The lipids are shown as sticks, while the accessible protein surface is shown in tan. The difference of the lipid tail flexibility in the two complexes is clearly visible (Wang et al, 2010).

The MD simulations explained the inhibition trend of PTEN by monomeric deoxy-diC_8PI derivatives. A key feature of the simulations was that there is a different balance of hydrophilic and hydrophobic interactions for the different deoxy-PI compounds binding to PTEN. My contribution to this work was to test the importance of the hydrophobic pocket formed by the pβ_2-α_1 loop for interactions with the substrates and soluble dioctanoyl-PI inhibitors. Enzyme kinetics were measured using long chain dipalmitoyl-PI(3)P as the substrate and solubilizing it with the detergent Triton X-100 in mixed micelles or with 1-palmitoyl-2-oleoyl-phosphatidylcholine (POPC) presented in large unilamellar vesicles (LUVs). In both these substrate aggregates, the hydrophobic chains were not, on average, located at the surface, and not likely to be accessible to PTEN. The prediction was that the inhibition potency of the different diC_8PI molecules would vary so that only the interactions of the polar headgroup would dominate PTEN inhibition.

Mutations of key residues in the hydrophobic pocket were also generated in order to investigate the importance of this pocket in processing substrate

3.2 Results

3.2.1 Effect of deoxy-PI derivatives in substrate micelles on PTEN activity

Previously the effect of the deoxy-diC_8PI compounds was assayed with substrate diC_8PI(3)P at 0.5 mM (Wang et al, 2008). At this concentration, substrates existed as mostly monomers with some small micelles. The inhibition efficiency of the deoxy-PI derivatives could change if the substrate was present as mostly micelles, since the substrate acyl chains would not be accessible for interaction with PTEN. In the mixed micelle assay system (0.1 mM dipalmitoyl-PI(3)P and 0.4 mM TX-100), the large excess of detergent may have two effects. It can enhance solubilization of the deoxy-diC_8PI compounds in micelles, particularly as the inhibitor CMC is approached. However, at low concentrations where the inhibitor is likely to exist as a monomer, the detergent molecules (Triton X-100 has a CMC ~0.2 mM) may bind to the protein in the hydrophobic regions suggested by the simulations to harbor the deoxy-PI acyl chains. In either of these cases, the remaining driving force for the short-chain PI derivatives binding to PTEN would be the polar interactions of the inositol ring. As shown in Figure 3.4A, the deoxy-PI compounds tested had little inhibition of PTEN hydrolysis of 0.1 mM dipalmitoyl-PI(3)P, even at concentrations above the CMC of most of the diC_8PI compounds. Only L-diC_8PI appeared to be a significant inhibitor. In the structures obtained in the simulations, L-diC_8PI also appeared to form the strongest hydrogen bonding network with residues in the PTEN active site (Wang et al, 2010). The best inhibitor in assays with monomeric substrate D-diC_8PI(3)P was D-3-deoxy-diC_8PI.

However, this compound had the least interactions of the inositol ring with PTEN. It is not an inhibitor in the mixed micelle assay system, consistent with hydrophobic interactions as the dominant force in the binding of D-3-deoxy-diC_8PI to PTEN.

3.2.2 Effect of deoxy-PI derivatives on PTEN activity towards substrate in vesicles

In contrast to the mixed micelles, PI/PC vesicles are unlikely to present any acyl chain moieties for interaction with PTEN. As long as the diC_8PI compound is below its CMC, it is likely to exist as mostly monomer (Wang et al, 2008). Thus, the most potent inhibitor should be D-3-deoxy-diC_8PI as seen with the original assays using D-diC_8PI(3)P as the substrate (Wang et al, 2008). This is, in fact, what is observed (Figure 3.4). However, at the inhibitor CMC and higher concentrations, all the short-chain compounds will be mixed with the vesicles and all are likely to compete with substrate for binding to PTEN. As observed, at 0.5 mM or higher concentration of diC_8PI compound, all the molecules are inhibitory in this vesicle assay system.

Comparison of the inhibition efficiency of D-3-deoxy-diC_8PI in micelle and vesicle assay systems can provide more information about what binds to PTEN. At 0.1 mM, D-3-deoxy-diC_8PI caused 40% inhibition of PTEN (60% residual activity left) activity in the PI/PC vesicle assay system, but no inhibition by this molecule was detected in the PI/Triton X-100 micelle system. This significant difference in the inhibitory potency of D-3-deoxy-diC_8PI provided evidence that Triton molecules can bind into the novel hydrophobic pocket identified by the simulations. Since potency of D-3-deoxy-diC_8PI depends on binding of its acyl chains to the hydrophobic site, occupation of this site by the detergent (which should have no affinity for the inositol binding site) should reduce inhibition by that deoxy-PI compound. This information was very useful since it provided

a way to investigate the role of the hydrophobic pocket by studying how detergents alter PTEN kinetics with different substrates and inhibitors.

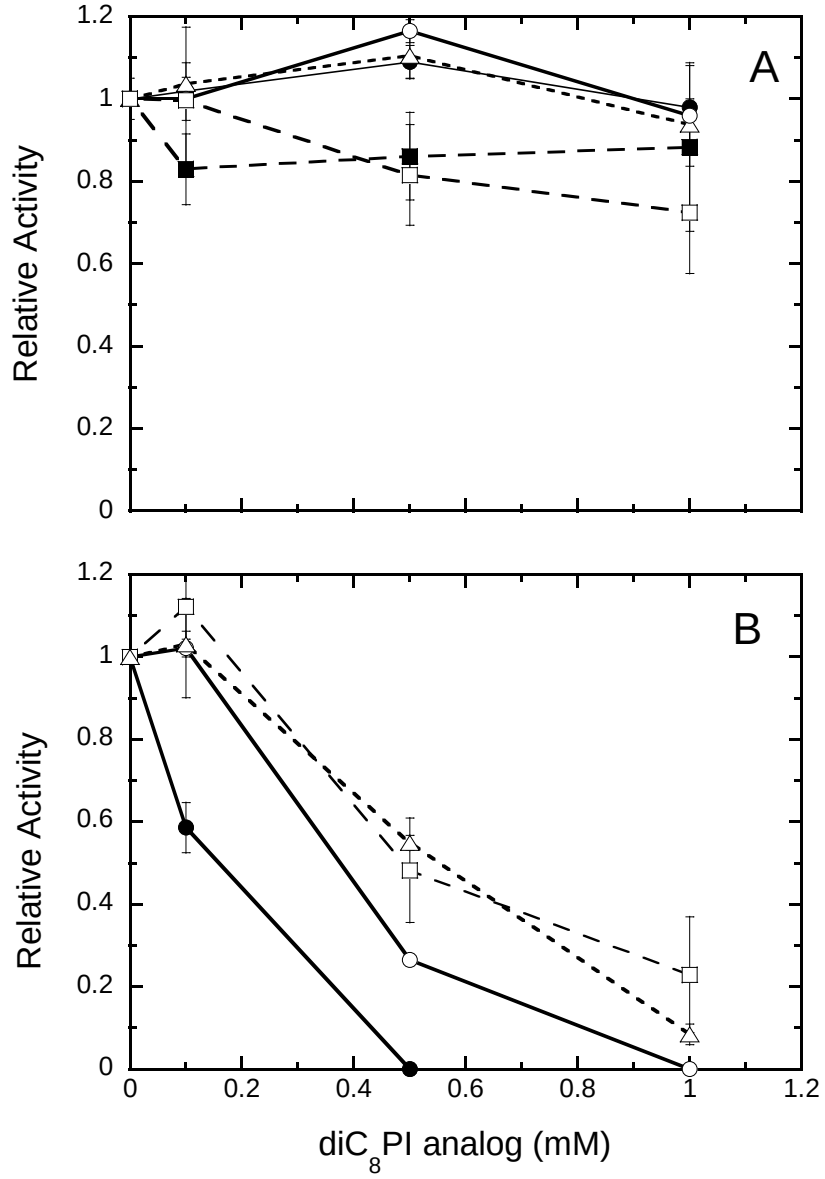

Figure 3.4 Effect of different concentrations of diC$_8$PI compounds on PTEN-catalyzed hydrolysis of 0.1 mM dipalmitoyl-PI(3)P in (A) 0.4 mM Triton X-100 micelles or (B) unilamellar vesicles with 0.9 mM POPC: ●, D-3-deoxy-diC$_8$PI; ○, L-3-deoxy-diC$_8$PI; ■, D-diC$_8$PI; □, L-diC$_8$PI; Δ, L-3,5-dideoxy-diC$_8$PI.

3.2.3 Mutations in hydrophobic site: kinetics of Arg47 mutants

One of the unexpected features of the MD simulations was the hydrophobic site formed by the loop containing Arg47. This region was suggested to be a major part of stabilizing the binding of D-diC_8PI derivatives and not the L-enantiomers. We chose to mutate Arg47 to probe the importance of this residue for enzyme activity. It has two features that may be relevant to PTEN activity: (i) a positive charge, and (ii) a large and hydrophobic side chain, at least until the guanidino group, which appeared to be involved in interacting with the octanoyl- chains of the inhibitors (and the substrate). Characterization of the kinetics of the mutant proteins in different substrate assay systems should reveal the importance of this site for substrate and D-enantiomer ligand binding.

Arg47 was mutated to four different residues: R47G, R47K, R47L and R47W. The proteins expressed moderately well (at least to the extent of wild type PTEN). CD spectra of the mutants as well as the wild type protein were recorded and compared (Figure 3.5). There was no significant difference in the secondary structures of the mutant and wild type proteins. D-diC_8PI(3)P, at 0.5 mM where the molecule alone is mostly monomeric, was first used as the substrate to test the effect of the mutation on protein activity. As shown in Table 3.1, whether Arg47 is replaced with a glycine, a lysine or a hydrophobic residue, the enzyme specific activity towards D-diC_8PI(3)P decreased significantly. R47W was the worst enzyme (3000-fold lower specific activity), presumably because of the bulky and inflexible nature of the tryptophan side chain. The low activity for the R47K enzyme was particularly surprising, since the lysine side chain has both the hydrophobic chain (although now larger) and positive charge of the arginine side chain. There were no differences in the far UV CD spectra indicating that the bulk of the mutant

protein is as folded as normal recombinant PTEN. We cannot easily increase substrate concentration since the aggregation of D-diC_8PI(3)P is likely to complicate kinetics. However, these results clearly showed that the interaction of the side chains from this loop region really do contribute to correct substrate binding and catalysis.

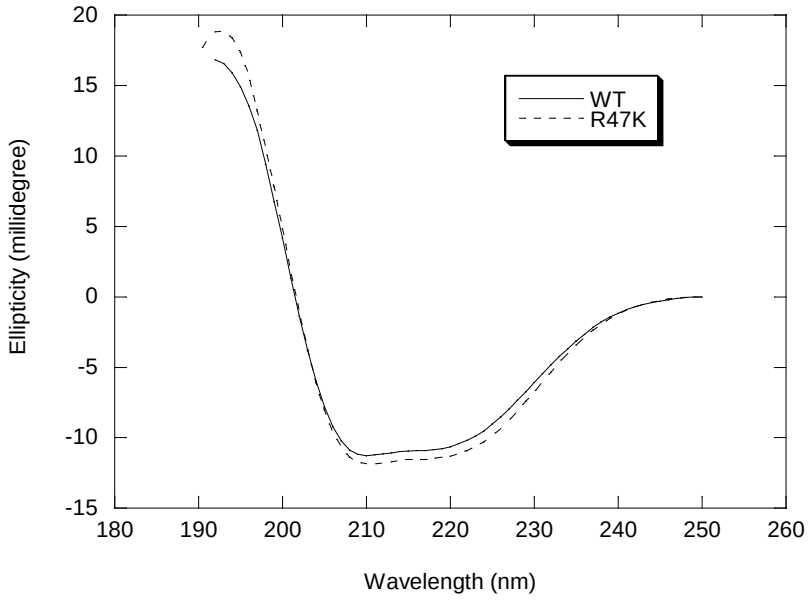

Figure 3.5 CD spectra of 0.04 mg/ml wild type PTEN (solid line) and PTEN R47K (dashed lind) in 1 ml 0.01 M borate, pH8.0.

Table 3.1 Relative activity of Arg47 mutants compared to wild type PTEN

	diC_8PI(3)P 0.5 mM[a]	diC_{16}PI(3)P/ TX100 (1:4)[b]	diC_{16}PI(3)P/ POPC (1:9)[c]	diC_8PI(3,4)P_2 0.1 mM[d]	DOPI(3,4)P_2/ POPC (1:19)[e]
R47G	0.040	0.049	0.063	0.019	0.23
R47W	0.010	0.015	0.052	N.D.	N.D.
R47L	0.014	0.041	0.24	N.D.	N.D.
R47K	0.006	0.018	0.28	0.12	0.29

i) The specific activities of wild type PTEN toward each substrate are (a) 14.2±0.4, (b) 11.5±0.7, (c) 0.27±0.03, (d) 45±4 and (e) 0.59±0.02 nmol/mg/min.
ii) The concentrations of diC_{16}PI(3)P in (b) is 0.1 mM.
iii) The total phospholipid concentrations in (c) and (e) are both 1 mM.
iv) Most of the mutants activities were measured in duplicates with errors less than 20%.

The activities of the Arg47 mutants towards diC_{16}PI(3)P in detergent micelles and diC_{16}PI(3)P in mixed vesicles with POPC vesicles were also measured (Table 3.1). Again, all of the mutants had lower activity than wild type PTEN. R47W always exhibited the lowest activity, consistent with what was observed in the diC_8PI(3)P monomer assay system, suggesting the bulky side chain interferes with proper substrate binding. Interestingly, in the vesicle assay system, R47K and R47L had better activities than the other two mutants (Table 3.1), indicating a middle sized residue with some hydrophobic character is important for occupation of this hydrophobic pocket, possibly by maintaining the local structure of this pocket.

The phosphatase activities of R47G and R47K toward PI(3,4)P_2 were also tested both with monomer diC_8PI(3,4)P_2 and with vesicles of DOPI(3,4)P_2/PC (Table 3.1). Similar to what we observed with diC_8PI(3)P as the substrate, these two mutant PTENs had lower activity than wild type protein towards a multiply phosphorylated substrate. R47K had similar activity to that of R47G towards the PI(3,4)P_2/PC vesicles but had higher activity toward diC_8PI(3,4)P_2 monomers. Given that the head group of PI(3,4)P_2 has two phosphates that would form more hydrogen bonds when binding into the active site, the higher activity of R47K than R47G in diC_8PI(3,4)P_2 monomer assay systems suggested that the lysine side chain at residue 47 also provided some hydrophobic interaction for substrate binding.

As a further test of the relevance of this hydrophobic site to PTEN activity, we examined the potency of L-3,5-dideoxy-diC_8PI as an inhibitor of R47G. In the simulations, this fairly potent L-isomer does not exploit the region around Arg47 for anchoring its acyl chains (Wang et al, 2010). Adding 0.1 mM L-3,5-dideoxy-diC_8PI to substrate diC_8PI(3)P

(0.5 mM) reduced the specific activity of wild type PTEN to 0.73 of the value in the absence of the L-dideoxy-compound, confirming what was observed previously (Wang et al, 2008). The same assay conditions with R47G PTEN led to a more pronounced inhibition – the residual activity of R47G was 0.34±0.04 that in the absence of inhibitor. We can compare this extent of inhibition for R47G PTEN with the published curve for PTEN (Wang et al, 2008), where 0.5 mM L-3,5-dideoxy-diC_8PI was needed to reduce enzyme activity to one third of the value for substrate alone. Thus, as predicted by the molecular dynamics, the L-isomer is a more potent inhibitor of PTEN when interactions of Arg47 with the D-isomer substrate are precluded, presumably because its acyl chains bind to a different site on the protein.

3.3 Discussion

An analysis of MD simulations explained the experimental results for changes in potency of deoxy-PI derivatives inhibiting PTEN and provided evidence for a hydrophobic pocket near (adjacent to) the active site of PTEN. This hydrophobic pocket was shown both by computer calculation and experiment to be important for phospholipid substrate hydrolysis and inhibitor binding. The findings from the MD simulations suggest that the lipophilic tails play a critical role in modulating the activity of the ligands. Kinetic data showing variations in activity across the deoxy-diC_8PI derivatives in assay systems with the substrate presented in detergent micelles or vesicles support this interpretation. The hydrophobically driven tail protein association of the inhibitors would likely be masked by detergent monomers occupying the hydrophobic site on the protein. This explanation was confirmed by the fact that the weakest inhibitor in the monomer assay system (which happened to have the most headgroup interactions in the active site) became most potent

in a PI(3)P/Triton X-100 assay system. In contrast, the binding of the soluble inhibitor molecules to PTEN assayed in a vesicle system should be similar to what is seen with soluble substrates as long as the inhibitor is monomer. However, once it is above the CMC, it will insert into vesicles and directly compete with substrate and at slightly higher concentrations may convert vesicles to mixed micelles. This was observed for all the deoxy-PI derivatives when added to PTEN assays at concentrations above their CMC. The fact that L-series compounds with strong hydrogen bonding interactions are actually poor inhibitors suggested the strongly hydrophobic nature of acyl chain/protein interactions provide a significant contribution to the binding free energy.

Arg47 in the hydrophobic pocket was found to be conserved in PTEN proteins among different species (Figure 3.6A). Also, this residue is conserved in some related human proteins (Figure 3.6B) including tensin, auxilin and PTEN-like proteins, TPTE (transmembrane phosphatase with tensin homolog) (Chen et al, 1999) and TPIP (TPTE and PTEN homologous inositol lipid phosphatase) (Walker et al, 2001). TPIP is a phosphoinositide 3-phosphatase, while TPTE does not dephosphorylate phosphoinositides. However, TPTE was found to be associated with the plasma membrane (Walker et al, 2001). Tensin binds to cytoplasmic tails of integrin via its PTB (phosphotyrosine binding) domain to link actin filaments to integrin (Lo, 2004). The PTEN-like domain in tensin 2 has the active site cysteine (similar to Cys124 in PTEN), and tensin 2 can regulate Akt signaling negatively (Hafizi et al, 2005). Auxilin is the cofactor of Hsc70 (heat shock cognate 70) and mediates the clathrin uncoating in clathrin-mediated endocytosis (Lemmon, 2001). The PTEN-like region in auxilin and its ubiquitous form GAK (cyclin G-associated kinase) binds to phosphoinositides (PI(3)P,

PI(4)P, PI(5)P and PI(3,4)P_2) to recruit the auxilin to the clathrin-coated vesicles (Lee et al, 2006; Massol et al, 2006). So the conservation of R47 reflects the importance of this residue in maintaining the structure of PTEN and PTEN homologues for phosphoinositide binding. The R47G mutation was detected from a patient with Cowden Syndrome (Marsh et al, 2001), also indicating the biological relevance of R47 in PTEN function.

(A)

Human	38	PA-ERLEGVYRNNIDDVVRFLDSKH-KNHYKIYNLCAERHYDTAKFNCR
Mouse	38	PA-ERLEGVYRNNIDDVVRFLDSKH-KNHYKIYNLCAERHYDTAKFNCR
Rat	38	PA-ERLEGVYRNNIDDVVRFLDSKH-KNHYKIYNLCAERHYDTAKFNCR
D. melanogaster	45	PAPDKLEGLFRNRLEDVFKLLEENH-AQHYKIYNLCSERSYDVAKFRGR
X. laevis	38	PA-ERLEGVYRNNIDDVVRFLDSKH-KNHYKIYNLCAERHYDTNKFSCR
D.discoideum	38	PS-EKVEGVFRNPMKDVQRFLDQYH-KDHFKVYNLCSERVYDHSKFYGR
C. elegans	82	PA-TGIEANFRNSKVQTQQFLTRRHGKGNVKVFNLRGGYYYDADNFDGN

(B)

PTEN	38	PA-ERLEGVYRNNIDDVVRFLDSKH-KNHYKIYNLCAERHYDTAKFNCR
TPIP	123	PS-SGRQSFYRNPIEEVVRFLDKKH-RNHYRVYNLCSERAYDPKHFHNR
TPTE	252	PS-SGRQSFYRNPIKEVVRFLDKKH-RNHYRVYNLCSERAYDPKHFHNR
Auxilin	66	PL-DNVDIGFRNQVDDIRSFLDSRH-LDHYTVYNL-SPKSYRTAKFHSR
Tensin 2	146	PA-RPDEQRHRGHLRELAHVLQSKH-RDKYLLFNLSEKRH-DLTRLNPK

Figure 3.6 Protein sequence alignment of human PTEN (NP_000305) with (A) PTEN from mouse (NP_032986), rat (NP_113794), *Drosophila melanogaster* (NP_477423), *Xenopus laevis* (NP_001083831), *Dictyostelium discoideum* (XP_637576) and *Caenorhabditis elegans* (AAD21620.1), and with (B) human PTEN-like protein TPIP (NP_001135440), TPTE (NP_954870), tensin 2 (NP_733610) and auxilin (NP_001243794). The conserved arginine residues are in bold and shadowed. The number of the starting residue is also labeled.

R47G had the highest relative activity toward $PI(3,4)P_2$ vesicles than with other substrates, presumably because in this case hydrogen bonding between the head group and the PTEN active site pocket dominated substrate binding. Two phosphates on the substrate headgroup provide stronger electrostatic contacts with the protein. An interesting observation was that R47K was relatively more active when using vesicles as the substrate. This suggested that the positive charge on the residue at the 47^{th} position may help the protein bind to the membrane, possibly by nonspecific electrostatic interactions with negatively charged phospholipids in the vesicle. Besides providing hydrophobic interactions, Arg47 also contributes electrostatic interactions critical for substrate binding.

To summarize, we demonstrated the existence of a hydrophobic site adjacent to the active site, first identified by MD simulation, that was important for substrate (and inhibitor) binding. This hydrophobic site works synergistically with the active site, presumably to provide correct orientation of the substrate. Mutation at this hydrophobic site impaired substrate binding and thus lowered the protein activity.

Chapter 4

Binding of PI(4,5)P_2 to an allosteric site in PTEN?
NMR studies of PTEN/phospholipids interactions

4.1 Introduction

The first evidence for $PI(4,5)P_2$ activation of PTEN towards its substrates presented in vesicles was reported in 2003 (McConnachie et al, 2003). This research group explained the activation mechanism by postulating that substrate access was enhanced by incorporating the very anionic $PI(4,5)P_2$ into substrate vesicles. This explanation was revised by the observation that $PI(4,5)P_2$ monomers (dioctanoyl chains for the phosphoinositides) could also activate the protein when mixed with substrate monomers (Campbell et al, 2003). The PTEN N-terminus contains the conserved $PI(4,5)P_2$ binding patch (NBP) K/R-X_4-K/R-X-K/R-K/R (Maehama et al, 2001), and $PI(4,5)P_2$ could bind at this site to induce the conformational change that leads to activation of the protein (Campbell et al, 2003). This allosteric mechanism was supported by the reports that mutation or deletion of this NBP eliminated the $PI(4,5)P_2$ activation and caused a loss of PTEN function (Walker et al, 2004; Vazquez et al, 2006; Rahdar etal, 2009).

PTEN can dephosphorylate $PI(3,4,5)P_3$, $PI(4,5)P_2$ and PI(3)P *in vitro* (Maehama et al, 2001), although relative rates decrease with decreasing phosphorylation of the inositol ring. $PI(4,5)P_2$ is the product of $PI(3,4,5)P_3$ dephosphorylation. Previously, we demonstrated that diC_8PI, the product of $diC_8PI(3)P$ hydrolysis, can inhibit the protein with a K_i that was 2-3 fold less than the K_m for $diC_8PI(3)P$ (Wang et al, 2008). Given the similar structure and the same negative charge of $PI(4,5)P_2$ and $PI(3,4)P_2$, we assumed that under some conditions $PI(4,5)P_2$ could also bind in the active site. This raises a question as to whether there is a discrete $PI(4,5)P_2$ binding site other than active site.

In order to demonstrate a distinct $PI(4,5)P_2$ binding site, several methods, including FRET (Redfern et al, 2008) and surface plasma resonance (Das et al, 2003), have been

used to investigate PTEN or its C2 domain binding to phospholipid vesicles. However, these methods are based on the overall partitioning of the protein onto the phospholipid surfaces. Location of an individual lipid on the protein is harder to define and usually relies on mutants that show altered behavior.

Besides using protein kinetics to access the binding behavior of $PI(4,5)P_2$ and other phospholipids to PTEN, we used NMR methods to investigate the PTEN protein binding to phospholipids. In fixed field NMR studies, the NMR linewidth at half height ($\Delta\nu_{1/2}$) is proportional to the spin-spin relaxation rate of the nucleus. When a small phosphorylated molecule, in this case a short-chain phospholipid, forms a larger complex, i.e. binds reversibly to protein, the relaxation rate of the ^{31}P should be the weighted average of the relaxation rate of the small free molecule and the larger relaxation rate of the bound lipid/protein complex. Thus, by measuring changes in the ^{31}P linewidth with protein added, information on the binding process can be obtained. If the relaxation is mainly dipolar, information of potential distances of the ^{31}P to nearby ^{1}H may be obtained. However, for the phosphorus nucleus in phosphate esters, the relaxation mechanism at magnetic fields above 2 T is dominated by chemical shift anisotropy (CSA). CSA reflects electron asymmetry around a nucleus and this mode of relaxation increases with the square of the magnetic field, so at the high magnetic field of conventional NMR spectrometers, any linewidth changes are difficult to interpret. Nonetheless, changes in linewidth at fixed high magnetic field provide an empirical characterization of protein/ligand interactions.

An alternate approach to obtaining and interpreting ^{31}P relaxation is to use high resolution field cycling methods (Roberts & Redfield, 2004a; Roberts & Redfield, 2004b).

This method excites the phosphorus nuclei at the high magnetic field and then shuttles the sample up the bore of the magnet to a defined lower magnetic field for relaxation, in this case spin-lattice relaxation (R_1). After an interaction time the sample is shuttled back down into the probe for read-out of the extent of relaxation. This allows one to measure the relaxation rate of the ^{31}P as a function of magnetic field. The field dependence profile of R_1 can be used to describe the different modes of relaxation mechanisms and the correlation times associated with them (Roberts & Redfield, 2004a). At low magnetic fields (< 2T), ^{31}P relaxation is mainly from dipolar interactions – ^{31}P with nearby ^{1}H – and these can be intra- or intermolecular. If the phosphorylated ligand is exchanging between a free and protein-bound state, R_1 is related to the ratio of the ^{31}P nuclei bound state to free state, and the proximity of ^{31}P to the proton dipoles that relax it (Pu et al, 2009b; Pu et al, 2010). If a much larger dipole, such as an unpaired electron is near ^{31}P, R_1 is further enhanced and overwhelms ^{31}P-^{1}H interactions *if* the ^{31}P and spin-label are within 20 Å. Relaxation theory applied to the field dependence profile then allows one to estimate $r_{P\text{-}e}$, the averaged distance between the ^{31}P and the unpaired electron when the phosphorylated molecule is bound to the protein. This methodology was first used to localize the site for a PC binding to a bacterial PI-specific phospholipase C (Pu et al, 2010).

This methodology has been applied to PTEN to address (i) is there a PI(4,5)P_2 site that is discrete from where substrate binds, and (ii) where is this PIP_2 site with respect to the active site. Cysteines in the protein were labeled with the nitroxide spin label reagent S-(2,2,5,5-tetramethyl-2,5-dihydro-1H-pyrrol-3-yl)methyl methanesulfonothioate (MTSL) and the relaxation enhancement of the ^{31}P nuclei of different short-chain

phosphoinositides was measured. This relaxation enhancement depends on the proximity of the phosphorus to the unpaired electron attached to the protein, thus the extent of the relaxation enhancement is a measure of the distance between the phospholipid and the protein.

4.2 Results

4.2.1 PI(4,5)P_2 effects on recombinant wild type PTEN enzymatic activity

The effect of the PI(4,5)P_2 on PTEN specific activity was assessed using both monomer and vesicle substrate systems. First, as expected, with 0.1 mM diC_8PI(3,4)P_2 as the substrate, 0.05 mM diC_8PI(4,5)P_2 increased recombinant PTEN activity 6-fold (Figure 4.1 A), comparable to what has been reported previously (Campbell et al, 2003). Increasing the diC_8PI(4,5)P_2 to 0.1 mM has little additional effect; the observed activation was 7-fold. In these two conditions, both substrate diC_8PI(3,4)P_2 and activator diC_8PI(4,5)P_2 exist as monomers in solutions, at least in the absence of protein, suggesting that a membrane interface is not necessary for kinetic activation.

DiC_8PI(3)P as a substrate shows somewhat different behavior (Figure 4.1A). The CMC of diC_8PI(3)P was reported as 0.7±0.2 mM (Wang et al, 2008), which means under the assay condition, both substrate and activator would be mostly monomers although perhaps with some micelles, again at least in the absence of protein. With 0.5 mM diC_8PI(3)P as the substrate, 0.25 mM diC_8PI(4,5)P_2 reduced PTEN activity to 70% and 0.5 mM diC_8PI(4,5)P_2 reduced activity to 40% of the rate in the absence of the ‘activating’ lipid. Here diC_8PI(4,5)P_2 is acting as an inhibitor, presumably by binding to the active site. This suggests that the effect of PI(4,5)P_2 depends on the identity and physical state

of the substrate and its ability to bind to the protein. If we assume that the inhibition is because the PIP_2 binds to the active site, we can use the K_m for $diC_8PI(3)P$ to estimate a K_i of 0.1 mM for $diC_8PI(4,5)P_2$.Thus, the $diC_8PI(4,5)P_2$ PTEN product has a considerably higher affinity for the active substrate than the $diC_8PI(3)P$ PTEN substrate.

The dioctanoyl lipids have CMCs around 0.5-1 mM and PTEN could lower the CMC, differently for each lipid. To try and circumvent this potential complication, we also examined the effect of $diC_6PI(4,5)P_2$ on PTEN hydrolysis of $diC_6PI(3,4)P_2$ and $diC_8PI(3,4)P_2$. Resultant activities showed that acyl-chain length is another factor modulating the magnitude of $PI(4,5)P_2$ activation (Figure 4.1B). The shorter molecule, $diC_6PI(4,5)P_2$, was less effective as an activator than $diC_8PI(4,5)P_2$, both for substrates $diC_6PI(3,4)P_2$ and $diC_8PI(3,4)P_2$, indicating the binding of the $PI(4,5)P_2$ to the protein is not just an electrostatic interaction between the anionic charge on the head group of $PI(4,5)P_2$ and cationic charge on protein surface when the monomeric molecules are used. The higher activation observed for systems poised around the CMC suggests that the kinetic activation is enhanced with the formation of an interface.

The effect of inositol-1,4,5-trisphophate ($I(1,4,5)P_3$), the head group of $PI(4,5)P_2$, was also tested for its effect on PTEN activity. No kinetic activation was seen with either $diC_8PI(3,4)P_2$ or $diC_8PI(3)P$, but rather a slight decrease in enzyme activity. PTEN exhibited 80% residual activity when 0.5 mM $I(1,4,5)P_3$ was mixed with 0.5 mM $diC_8PI(3)P$ as the substrate. These results also confirm the interaction between $PI(4,5)P_2$ and protein is stronger when the acyl chains are present and contains more than just electrostatic interactions.

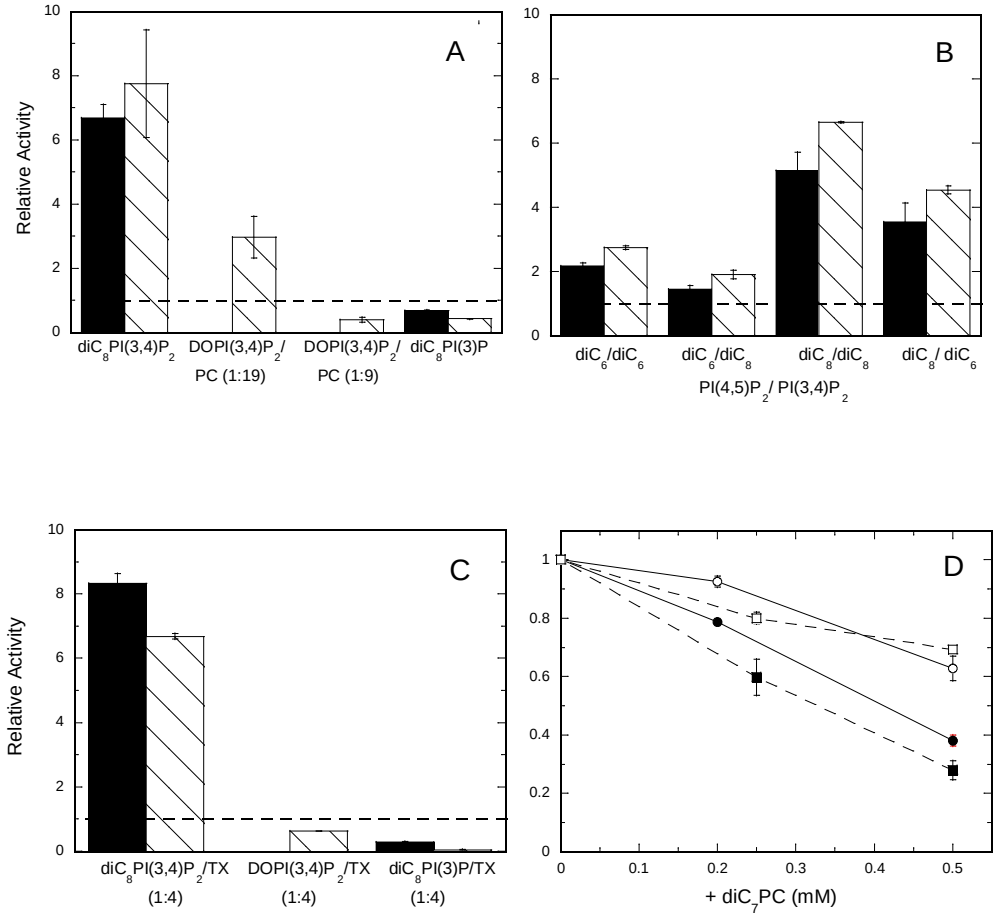

Figure 4.1 (A) Effect of $PI(4,5)P_2$ on PTEN hydrolysis of different substrates. The relative specific activities for PTEN towards 0.1 mM $diC_8PI(3,4)P_2$, $DOPI(3,4)P_2$/ POPC (0.05 mM/0.95 mM) LUVs, $DOPI(3,4)P_2$/POPC (0.1 mM/0.9 mM) LUVs, and 0.5 mM $diC_8PI(3)P$ with $PI(4,5)P_2$ are shown, with substrate:PIP_2 = 0.5 (■) or 1.0 (\\\\). (B) Effect of varying the chain length of substrate and activator. Substrates include 0.1 mM $diC_6PI(3,4)P_2$ or 0.1 mM $diC_8PI(3,4)P_2$ with dihexanoyl- or dioctanoyl-$PI(4,5)P_2$ added, and substrate:PIP_2 = 0.5 (■) or 1.0 (\\\). (C) Effect of PIP_2 and Triton X-100 on PTEN hydrolysis of different substrates. Substrates include $diC_8PI(3,4)P_2$/TX-100 (0.1 mM/0.4 mM), $DOPI(3,4)P_2$/TX-100 (0.1 mM/0.4 mM), and $diC_8PI(3)P$/TX-100 (0.5 mM/2 mM). The PIP_2 concentration was half (■) or the same (\\\) as that of the substrate. (D) DiC_7PC inhibition of PTEN activity toward $diC_8PI(3)P$ (■, □) and $diC_8PI(3,4)P_2$ (●, ○) in the absence (filled symbols) or presence (open symbls) of Triton X-100 present with substrate: TX-100=1:4.

The long chain lipid DOPI(3,4)P_2 was also examined as a substrate (5 or 10 mol % of total lipid) presented in PC large unilamellar vesicles (Figure 4.1A). The addition of brain PI(4,5)P_2 equivalent to the substrate mole fraction in the vesicles could activate the enzyme 3-fold for a sample with 1 mM total lipids and 5 mol % PI(3,4)P_2. However, if the LUVs had a higher percent of DOPI(3,4)P_2 (10 mol% DOPI(3,4)P_2) adding the same amount of brain PI(4,5)P_2 (10 mol% brain PI(4,5)P_2) inhibited the enzyme to 40% residual activity. This indicates that the PIP_2 activator molecule has a higher affinity for a site *not* in the active site but at sufficiently high concentrations in the vesicle, the molecule can bind to the catalytic site as well (again not surprising since it is a product of PI(3,4,5)P_3 hydrolysis).

Along with examining PIP_2 activation of PTEN in PI(3,4)P_2 / PC vesicles, the PI(4,5)P_2 effect was also examined when long chain lipid DOPI(3,4)P_2 and DOPI(4,5)P_2 were solubilized in Triton X-100 micelles. Addition of the same amount of DOPI(4,5)P_2 /TX-100 micelles to substrate DOPI(3,4)P_2/TX-100 micelles (0.1 mM of each lipid) reduced PTEN activity to 63% of that with just substrate DOPI(3,4)P_2/TX-100 micelles (Figure 4.1C). Doubling the DOPI(4,5)P_2/TX-100 concentration increased the inhibition from 63% to 52%. Triton X-100 is a non-ionic detergent that we have shown previously can reduce the inhibition potency of short-chain deoxy-PI derivatives by either binding into a hydrophobic site adjacent to the active site (the ‘adjacent hydrophobic site’ or AHS), or forming micelles that reduce the on/off rates of the PI derivative from accessing PTEN binding sites (Wang et al, 2010). The inhibition observed in the DOPI(3,4)P_2/ DOPI(4,5)P_2/TX-100 micelles indicated at high concentration, the head group of PI(4,5)P_2 had some affinity for the active site, and this molecule could act as an inhibitor.

Along with its effect in long chain phospholipids dispersed in micelles, the effect of TX-100 on PTEN kinetics was also examined with short chain substrate and activator (Figure 4.1C). Adding TX-100 (1:4 = substrate: TX-100) could enhance the inhibition by $diC_8PI(4,5)P_2$ when using $diC_8PI(3)P$ as the substrate. PTEN activity was significantly inhibited to 5% residual activity (i.e., when compared to substrate with Triton X-100 but no $diC_8PI(4,5)P_2$). However, Triton had no effect on the PIP_2 activation in the $diC_8PI(3,4)P_2$/$diC_8PI(4,5)P_2$ assay system, $PI(4,5)P_2$ activation was still observed with Triton X-100 present. It also suggests that the matrix in which $diC_8PI(3)P$ is presented is critical for observing PIP_2 activation as opposed to inhibition. This is another indication that there are two discrete sites for substrate and PIP_2 binding.

PC is often used as the matrix lipid in preparing vesicles. However, in monomer/micelle assay systems, short-chain PC is a very effective inhibitor of PTEN (Figure 4.1D). Comparable concentrations of Triton X-100 have no significant effect on PTEN activity. With 0.5 mM $diC_8PI(3)P$ as the substrate, the addition of 0.25 mM diC_7PC (well below its CMC of 1.5 mM) reduced the enzyme activity to ~60% of the control. For $diC_8PI(3,4)P_2$ (0.1 mM) as well, added diC_7PC reduces PTEN activity but not to the level of what occurs with $diC_8PI(3)P$ (80% residual activity). Interestingly, adding the nonionic detergent Triton X-100 into the mixture reduces the diC_7PC inhibition of PTEN, suggesting the PC molecules may interact with the protein AHS and in so doing alter access to the active site. Triton, in contrast, appears to bind almost exclusively to the AHS; it has little affinity for the active site.

4.2.2 Fixed field ^{31}P NMR study of phospholipids binding to recombinant PTEN

Changes in the ^{31}P linewidths ($\Delta\Delta\nu_{1/2}$) of ligands induced by the presence of the protein were used to characterize lipid binding to PTEN at 14.02 T (Table 4.1). Concentrations of the ligands were 0.25 or 0.5 mM, at or below the CMC of all the phospholipids, and the ratio of phospholipid to protein was usually either 24.7:1 or 49.4:1. The dihexanoylphospholipids exhibited minimal changes in linewidth (<2.5 Hz), consistent with their lack of much kinetic activation of PTEN (and their poor substrate properties). Both diC_6PI and diC_6PI(4,5)P_2 exhibited only a 1-2 Hz increase in linewidth. In contrast, the dioctanoylphosphoinositides showed significantly larger linewidths in the presence of PTEN: (i) D-diC_8PI and L-3,5-dideoxy-diC_8PI, as well as diC_7PC, all of which bind to the active site (Wang et al, 2008; Wang et al, 2010), exhibit a 25-30 Hz increase in linewidth under the experimental conditions used; (ii) non-substrate diC_8PI(4)P and diC_8PI(5)P molecules have intermediate linewidths, 12-17 Hz; and (iii) diC_8PI(4,5)P_2 shows much smaller line broadening in the presence of PTEN (~ 5 Hz increase).

Table 4.1 NMR linewidth changes for the phospholipid phosphodiester resonance upon the addition of recombinant PTEN and variants.. The concentrations of PTEN, spin-labeled PTEN wild type (PTEN-SL), K13E, R47K, and R47G were 10 μM.

$\Delta\Delta\nu_{1/2}$ PDE (Hz)						
PI	(mM)	PTEN	PTEN-SL	K13E	R47K	R47G
diC_6PI	0.25	1.9±0.1				
	0.50	1.2±0.1				
$diC_6PI(4,5)P_2$	0.25	2.3±0.2				
	0.50	1.8±0.1				
diC_8PI	0.25	24.7±1.2	34.8±1.4			
	0.50	38.6±14.4		41.8±7.4	36.9±4.5	32.6±5.3
diC_8PI/TX-100 (2 mM)	0.50	11.5±2.8		6.3±0.5	11.2±3.1	8.8±0.9
$diC_8PI(4)P$	0.25	11.6±0.5				
$diC_8PI(5)P$	0.25	17.3±1.3				
$diC_8PI(4,5)P_2$	0.25	4.7±0.3	6.1±0.4	6.9±0.7	6.7±1.3	6.6±0.9
	0.50	3.8±1.2	3.7±0.3			
L-3,5-dd-diC_8PI	0.50	26.7±0.7	25.3±1.0			
L-3,5-dd-diC_8PI / $diC_8PI(4,5)P_2$	0.25	30.5±0.8	37.8±1.6			
	0.25	5.7±0.2	6.3±1.5			
diC_7PC	1.0	28.3±4.3			37.0±2.0	36.0±7.2
diC_7PC/TX-100 (4 mM)	1.0	3.3±0.2			4.3±0.7	4.5±0.2

Interpreting these linewidth changes is difficult because ^{31}P at this field strength has contributions from CSA as well as dipolar interactions that are also coupled with exchange of molecules onto a protein binding site, and perhaps formation of small micelle aggregates with protein. Interesting, if Triton X-100 is added to the sample with diC_8PI, the linewidth is significantly reduced. Since that nonionic detergent is not an inhibitor (Wang et al, 2008), this suggests that either the diC_8PI/PTEN complex may be large or perhaps that the exchange of ligand on and off the protein is in an intermediate regime and that the Triton, by virtue of providing a micelle reservoir may accelerate such exchange. L-3,5-dideoxy-diC_8PI and diC_7PC, which are also inhibitors of PTEN activity (Wang et al, 2008), also exhibited large line widths in the presence of a small amount of

protein (Table 4.1). This suggests that if a molecule binds to the active site, the change in ligand ^{31}P linewidth will be fairly large. As in the diC_8PI/TX-100 system, adding Triton to diC_7PC samples reduced line broadening to a large extent, from 30-40 Hz change to less than 5 Hz change with that detergent present. This could be explained by competitive binding between diC_7PC and Triton X-100 in the AHS, (although the diC_7PC also binds at least partially in the active site since it is inhibitory) consistent with what was observed in the enzyme kinetics where addition of Triton X-100 reduced the inhibition caused by diC_7PC.

PTEN was also incubated with both diC_8PI(4,5)P_2 and L-3,5-dideoxy-diC_8PI. The phosphodiester peaks of these two lipids have slightly different chemical shifts and linewidth changes in the two can be measured separately. A large increase in linewidth was detected for the deoxy-PI bound in the active site. The 5 Hz increase observed for the diC_8PI(4,5)P_2 phosphodiester is comparable to its behavior in the absence of an active site ligand. Two other phosphoinositides were examined: diC_8PI(4)P and diC_8PI(5)P. Both exhibit linewidths intermediate between diC_8PI and diC_8PI(4,5)P_2 upon the addition of protein. The PTEN-induced increase in linewidth for diC_8PI(4)P was smaller than that for diC_8PI(5)P, suggesting there is a particular orientation for non-substrate phosphoinositides binding to PTEN.

While these fixed field ^{31}P linewidths might perhaps provide a fingerprint for active site (large linewidth change), adjacent hydrophobic site (large change but greatly reduced by the addition of Triton X-100), and activator site binding (small linewidth change), there is no information on where such sites might be and if they are indeed spatially distinct.

4.2.3 Kinetics and fixed field ^{31}P NMR study of PTEN mutants binding to phospholipids

Lys13 has been suggested as a key residue for PIP_2 activation in PTEN (Walker et al, 2004; Redfern et al, 2008). Conversion of this cationic side chain to an anionic one should definitely alter electrostatic interactions of protein and ligand. K13E was less active than wild type PTEN towards $diC_8PI(3)P$ or $diC_8PI(3,4)P$ monomers (less than 10% of wild type PTEN activity), and towards $DOPI(3,4)P_2$ in PC vesicles (25% of the activity of wild type PTEN). K13E could not be activated either by $diC_8PI(4,5)P_2$ or long-chain $DOPI(4,5)P_2$ (Figure 4.2). The enzyme kinetics suggest the activator site has been lost with this mutation. However, they do not address binding. It is possible that the PIP_2 could bind to the protein but communication of that binding with the active site has been altered, hence the loss of kinetic activation.

Arg47 was previously shown to be a key residue in the hydrophobic site adjacent to the active site (Wang et al, 2010). Mutation of Arg47 to replace the cationic side chain with lysine generated an enzyme, R47K, that could still be activated by PIP_2, although the activity was low (5%-30% of wild type depending on the substrate used). When the charge was removed, as for R47G, PIP_2 activation was significantly reduced. $DiC_8PI(4,5)P_2$ monomer activated the protein less than 2-fold with $diC_8PI(3,4)P_2$ as the substrate, while PIP_2 activation was not detected when vesicle substrates were used (Figure 4.2). This kinetic result suggests that the PIP_2 binding site is near the AHS, and the positive charge on Arg47 is important for PIP_2 activation, possibly by interacting with the negatively charged activator molecule. It is also possible that the loop containing Arg47 is involved in the conformational change induced by activator binding, since Gly should alter the flexibility of the loop while Lys is more like the normal Arg.

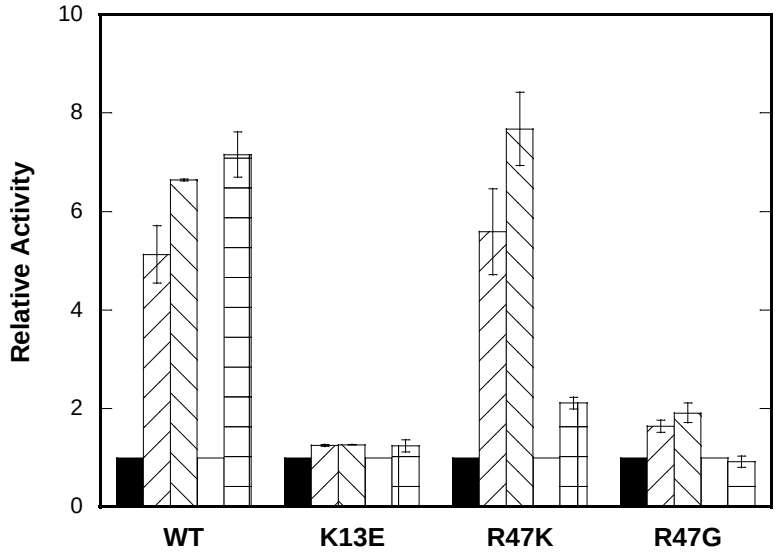

Figure 4.2 Effect of $PI(4,5)P_2$ on the activity of recombinant PTEN and variants K13E, R47K and R47G in monomer and vesicle assay systems. The ratio of the specific activity with PIP_2 added to the activity in its absence is shown for WT and the three mutant proteins. In the monomer substrate mixture $diC_8PI(3,4)P_2/diC_8P(4,5)P_2$ is either 0.1 mM/0mM (■), 0.1 mM/0.05 mM (|///|) or 0.1 mM/0.1 mM (|\\\\|). Vesicles were composed of $DOPI(3,4)P_2$/POPC (0.05 mM/0.95 mM) in the absence (□) or presence (#) of 0.05 mM $DOPI(4,5)P_2$.

Line broadening of ^{31}P resonances in the presence of K13E and R47 mutants was also measured (Table 4.1). DiC_8PI in the presence of these three mutant enzymes still showed a large increase in linewidth with a much smaller linewidth increase (6-7 Hz) for $diC_8PI(4,5)P_2$. DiC_7PC was also broadened in a similar fashion to diC_8PI for the R47G or R47K mutants; when Triton X-100 was added, the increase in linewidth caused by PTEN was reduced, suggesting that Triton X-100 binding to the AHS can still displace the zwitterionic phospholipid for the adjacent hydrophobic site. $DiC_8PI(4,5)P_2$ linewidths in the presence of K13E, R47K or R47G were very similar to the effect of wild type PTEN, again suggesting this lipid binds to the protein, but not at the active site. The loss of

activity and PIP_2 activation for these mutant enzymes does not appear to be caused by a lack of PIP_2 binding to PTEN.

4.2.4 High resolution field cycling ^{31}P NMR study of short chain phospholipids binding to PTEN and its mutants

4.2.4.1 Spin-labeling PTEN

Modifying a protein to introduce a spin-label is a useful method to look for proximity of ligands to discrete places. The large electron dipole can dominate dipolar relaxation of nearby nuclei leading to a paramagnetic relaxation enhancement (PRE) that is distance dependent. PTEN, however, is not an easy target since it has 10 cysteines, 5 on the phosphatase domain, and 5 on the C2 domain. Under our spin-labeling conditions (which used loss of enzyme activity to ensure modification of Cys124), 8 of the 10 cysteines were modified by the spin-label reagent (Figure 4.3). This labeling was confirmed by MS (the result shown in Table 4.2), which showed that 9 out of 10 Cys were labeled, including the active site nucleophile Cys124 and nearby Cys71. The spin-labeled PTEN samples usually had a small amount (<20%) residual activity towards $diC_8PI(3)P$. In the MS analyses of peptides, the peptide containing the unmodified Cys124 could be detected (Table 4.2).

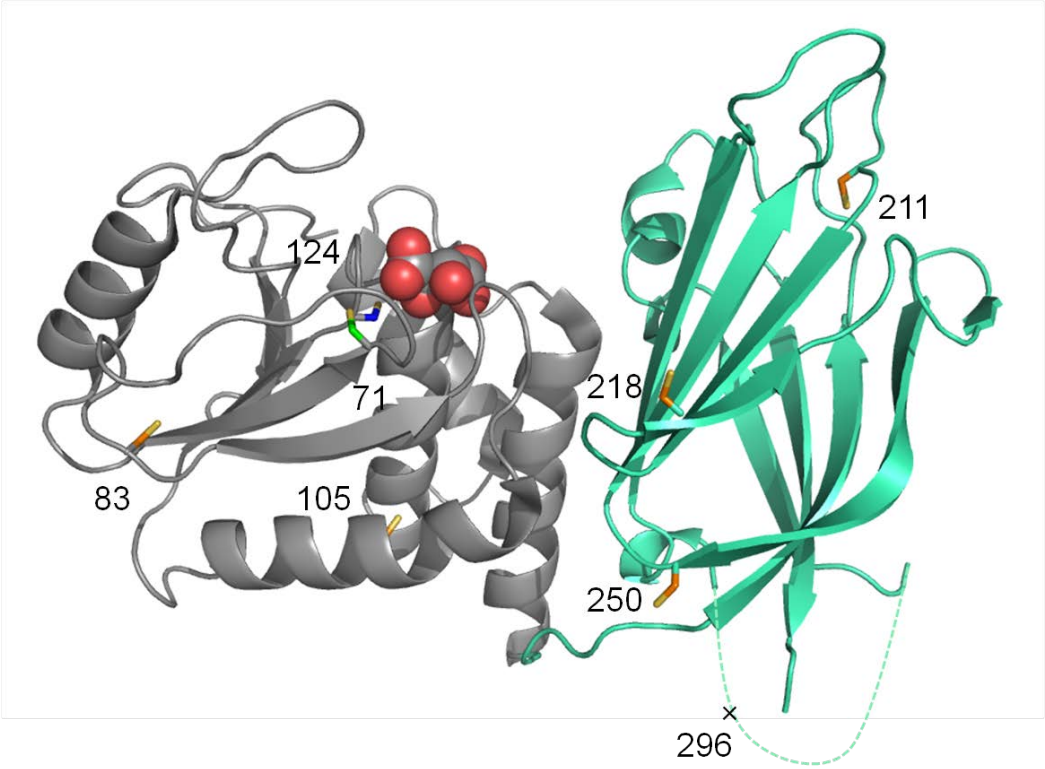

Cysteine	$r_{S–C(1)}$ (Å)	$r_{S–C(4)}$ (Å)
C124	6.0	3.6
C71	10	6.7
C105	18	19
C83	23	20

Figure 4.3 Structure of PTEN showing the thiols of the cysteine residues modified by the spin-labeling reagent as sticks. The phosphatase domain, in grey, has a tartrate molecule in space-filling representation, while the C2 domain is cyan. Cys71 is colored in green, Cys124 in blue and other modified cysteines in orange with S atoms in yellow. The C-terminal loop which is not in the crystal structure is shown in dashed curve. The distances of cysteine S atoms to C(1) and C(4) of tartrate are indicated for the closest Cys in the phosphatase domains.

The phosphoinositide binding sites on PTEN we are examining are all on phosphatase domain. The spin labels on the C2 domain are fairly far from the active site. In the PTEN crystal structure, the distances of the C2 domain cysteine sulfur atoms to tartrate carbons

are > 20 Å. To a first approximation spin-labels on at those sites should not contribute significantly to the relaxation of bound phospholipids. Spin labels attached to Cys83 and Cys105, located in the phosphatase domain, are far from the suggested membrane binding interface (Lee et al, 1999) and protein active site (Figure 4.3) and should be only minor contributors to ^{31}P dipolar relaxation. Thus, the major contributors to relaxation of the phospholipids that dock into the active site should be spin labels on Cys71 and Cys124. Cys71 points into the active site pocket and can form a disulfide bond with the nucleophile Cys124 (Lee et al, 2002). If the site for PIP_2 is near the active site it is likely to be relaxed; if it is further away (but still around the face thought to interact with the membrane interface) relaxation by spin-labeled PTEN will be smaller than for the PI in the active site. Although the large number of modified cysteine residues complicates interpretation of field cycling results, we can still use the method to compare the specific binding environments of different phosphoinositides. In particular, we can confirm a discrete binding site for a PIP_2 molecule on PTEN.

Table 4.2 MS identification of PTEN cysteine modified by the MTSL spin label. The peptides in the tryptic digest containing spin-labeled Cys (C*) and unmodified Cys (C) are indicated. The number of the peptides detected in the sample is also shown.

Peptide	Cys number		Number of digested peptides
IYNLCAERHYDTAK	C71		1
IYNLC*AERHYDTAK			1
FNCRVAQYPFEDHNPPQLELIK	C83		1
FNC*RVAQYPFEDHNPPQLELIK			4
PFC*EDLDQWLSEDDNHVAAIHC*	C105	C124	1
PFC*EDLDQWLSEDDNHVAAIHC*K			7
MMFETIPMFSGGTCNPQFVVCQLK	C211	C218	2
MMFETIPMFSGGTC*NPQFVVC*QLK			6
FMYFEFPQPLPVCGDIK	C250		1
FMYFEFPQPLPVC*GDIK			10
VENGSLCDQEIDSICSIERADNDK	C296	C304	3
VENGSLC*DQEIDSIC*SIERADNDK			3

4.2.4.2 Fixed field NMR study of spin-labeled PTEN binding to phospholipids

The effect of spin-labeled PTEN on different short-chain phosphoinositides was explored first (Table 4.1). Although the contribution of dipolar relaxation to relaxation of ^{31}P at high fields is small, the large dipole of the unpaired electron on the spin-label should enhance relaxation of the phosphorus nuclei in a distance-dependent manner. We can look at monomer concentrations of the phospholipids at fixed high fields so this allows us to gauge proximity. As expected, the spin-labeled PTEN had only small effects on diC_8PI and $diC_8PI(4,5)P_2$ above what is seen with non-labeled PTEN. The increase in the linewidth for 0.25 mM diC_8PI specifically caused by spin-labeled PTEN was 10 Hz; the increase was only 1.5 Hz for 0.25 mM $diC_8PI(4,5)P_2$. This result also confirmed that the field cycling NMR experiment is necessary to detect a substantial paramagnetic relaxation enhancement (PRE).

4.2.4.3 Field cycling of short-chain phospholipids binding to PTEN

PRE can be extremely useful for analyzing the dynamics and proximity of soluble ligands binding to macromolecules with spin-labels (Pu et al, 2009b). However, extracting only the dipolar relaxation becomes more quite difficult in a membranous system, in part because of the dominance of chemical shift anisotropy (CSA) as the main relaxation mechanism at high magnetic fields. High resolution field cycling ^{31}P methods can provide a unique window on phospholipid dynamics and interactions (Roberts & Redfield 2004a; 2004b). In the PTEN case, since more than one cysteine was labeled, we used the low field correlation time ($\tau_{P\text{-}e}$) and extent of relaxation provided by the spin-label extrapolated to zero field ($\Delta R_{P\text{-}e}(0)$) to calculate a parameter proportional to an averaged $r_{P\text{-}e}^{6}$. The effects of all the spin-labels are included, but most of the relaxation is due to the ones closest to the active or activator site. This parameter, which is normalized to the ratio of protein to phospholipid is the following:

$$(\tau_{P\text{-}e}/\Delta R_{P\text{-}e}(0))\times([\text{PTEN-SL}]/[\text{PL}])$$

There are a few key assumptions in the use of this parameter to extract an $r_{P\text{-}e}$.: we assume (i) fast exchange between free and enzyme-bound ligands; (ii) a given site on the enzyme is saturated with 2-5 mM ligand; and (iii) correlation times for the ^{31}P-electron interaction are long enough to characterize a discrete complex. Concentrations of phopholipids were 2-5 mM - the bulk of the diC_8- phospholipids at these concentrations will be micellar, for diC_6- phospholipids, monomers will exist. For protein/micelle complexes, a low field dispersion should reflect overall tumbling of a complex and differences in profiles for PIP_2 versus PI will reflect differences in where the lipids bind.

(1) Monomeric phospholipids

$I(1,4,5)P_3$ is a soluble molecule that mimics the PIP_3 head group and might be expected to bind into the active site or perhaps a discrete PIP_2 site of the protein. However, there was no effect of spin-labeled protein on the ^{31}P resonances of this molecule compared to the unlabeled protein (Figure 4.4). Therefore IP_3 did not bind to the protein, which was consistent with the observation that IP_3 had virtually no inhibitory effect on enzymatic activity. It appears that an acyl or alkyl chain(s) is needed for the ligands to bind to PTEN.

Next, we examined diC_6PI and $diC_6PI(4,5)P_2$. DiC_6PI has a CMC around 10-14 mM (Lewis et al, 1993). The concentration of the diC_6PI and $diC_6PI(4,5)P_2$ used in the field cycling experiment was 3 mM, suggesting the bulk of these two lipids were monomeric in solution. The ratio of PI to PTEN was 555:1 (4.9 μM PTEN and 2.7 mM diC_6PI) in one case and 612:1 in another (same protein concentration and 3 mM diC_6PI). As expected, unlabeled PTEN had no effect on the diC_6PI ^{31}P relaxation behavior at low fields at these ratios of protein to phospholipid. The relaxation enhancement (ΔR_1) induced by the spin-labeled protein at different magnetic fields was calculated by the subtraction of R_1 for the ligand in the presence of unlabeled protein. The field dependence of ΔR_1 is shown in Figure 4.5 (upper graph, the inset has the full field dependence from 0.004 to 11.7 T). There is an enhancement of the ^{31}P R_1 by the presence of spin-labeled protein at fields below 1 T.

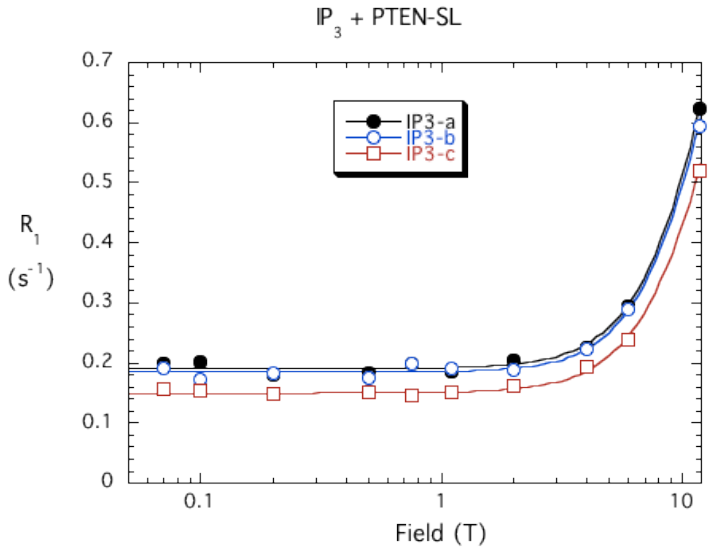

Figure 4.4 The magnetic field dependence of the spin-lattice relaxation rate, R_1, of ^{31}P resonances of I(1,4,5)P_3 (3 mM) in the presence of 4.9μM spin-labeled PTEN: C4 phosphate (a, ●), C1 phosphate (b, ○), and C5 phosphate (c, □). Note that none of the ^{31}P exhibit the low field rise in R_1 indicative of a small molecule/protein complex. This indicates that little of the inositol triphosphate is bound to PTEN.

Several interesting features of the protein-lipid complex were observed. First, $\tau_{P\text{-}e}$ is 172±21 ns, a value significantly larger than expected for a single PTEN molecule. This indicates that presence of the diC_6PI ligand in the active site causes protein/phospholipid aggregates to form, even though by itself the diC_6PI is monomeric. We have observed that the protein loses activity gradually when stored in the absence of substrate, product or analogues at 4 °C for one week. Most of our field cycling experiments were run for 24 hours at room temperature. Since we do not see precipitation of protein at the end of the field cycling experiment, we believe the bulk of the protein is still in an active conformation when the experiment is finished. $([PTEN]/[PIP_x])\times(\tau_{P\text{-}e}/\Delta R_{P\text{-}e}(0))$ is 3.07×10^{-10} s ^{2}, suggesting moderate proximity of the lipid to spin-labels on the protein. However, this is surprising since the diC_6PI is binding at the active and near two spin labels. It is certainly possible that the PTEN active site is not saturated with diC_6PI. A K_m

has not been determined for diC_6PI, but the value for diC_8PI is around 0.1-0.2 mM. If chain length is critical for binding this could be the case.

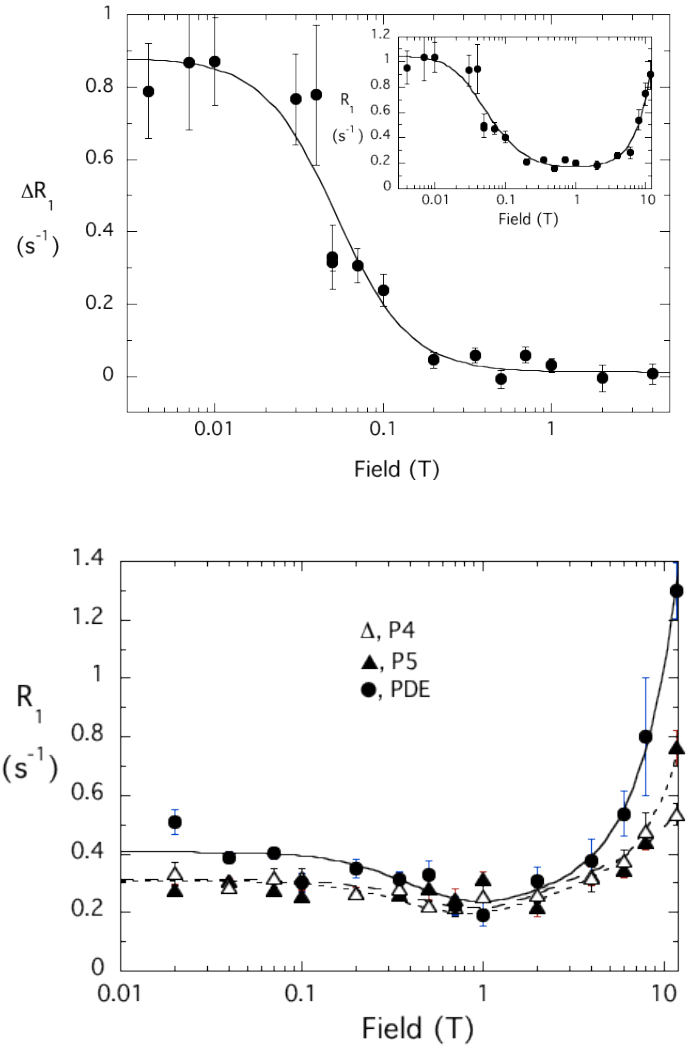

Figure 4.5 *Top*: The relaxation enhancement (ΔR_1) of ^{31}P of diC_6PI (3mM) caused by 4.9 μM spin-labeled PTEN. The inset shows the raw relaxation rates (R_1) of this phosphodiester from 0.004 to 11.7T; ΔR_1 represents the relaxation rate once the data for this lipid with non-spin-labeled protein is subtracted. *Bottom*: The field dependence of R_1 for the ^{31}P resonances of $diC_6PI(4,5)P_2$ (3 mM) in the presence of by 4.9 μM spin-labeled PTEN: phosphodiester, PDE (●), C4 phosphate, P4 (Δ), and C5 phosphate, P5 (▲).

$DiC_6PI(4,5)P_2$ binding to spin-labeled PTEN was also examined. There is little low field effect of the spin-labeled protein on the PIP_2 phosphorus resonances (Figure 4.5, bottom).

This could be explained by a binding site much further from the spin-label sites or by poor binding of this ligand to the protein in the absence of an interface (which did form with submicellar concentration of diC_6PI). The PTEN kinetics indicated that such a short-chain length lipid is a poor activator of similar chain length monomeric substrate. Therefore, it is more likely that the activator molecule has a weaker affinity for the secondary site.

(2) Micellar versus monomeric ligands

The effect of spin-labeled PTEN on diC_8PI and diC_8PI(4,5)P_2, which form micelles at 3 mM, was examined next. By comparing the effects of these dioctanoyl lipids to the results of PTEN binding to diC_6PI and diC_6PI(4,5)P_2, we can assess the effect of the lipid aggregation state, micellar versus monomeric ligands, on the protein/lipid interaction. As shown in fixed field studies, the diC_8PI ^{31}P resonance was significantly broadened in the presence of PTEN (not spin-labeled). The line broadening was larger than expected at high fields (14.1 T) for a protein of the size of PTEN binding a ligand in the fast exchange regime, indicating binding is in the intermediate exchange regime on the NMR time-scale.

The field cycling profile for unlabeled PTEN and diC_8PI showed a low field component significantly greater than for diC_8PI alone and similar to phosphatidylinositol micelles (Wang et al, 2008). This indicated that PTEN interacts with the longer chain PI and forms larger micelles than the PI by itself. The curve for PI with unlabeled protein had both a 4 ns (postulated to represent phospholipid wobbling) and 190 ns (representing particle rotation) dispersion. Field cycling with 3 mM diC_8PI and 0.1 mg/ml spin-labeled PTEN ([PTEN[/[PL] = 7.09×10^{-4}) showed a large enhancement of ^{31}P relaxation (Figure 4.6A).

The relaxation from unlabeled PTEN was subtracted from the one with spin-labeled protein and the resulting ΔR_1 field dependence fit to assess the relaxation due specifically to the spin-labels. As shown in Figure 4.6B, the data could be fit with a single correlation time, $\tau_{P\text{-}e}$, of 33±10 ns; $\tau_{P\text{-}e}/\Delta R_{P\text{-}e}(0) = (1.77\pm0.40)\ x10^{-8}\ s^2$, and normalizing this value to the ratio of PTEN to phospholipid yielded $(1.26\pm0.80) \times 10^{-11}\ s^2$, a value consistent with close proximity of the major spin-label site(s) to the bound diC_8PI.

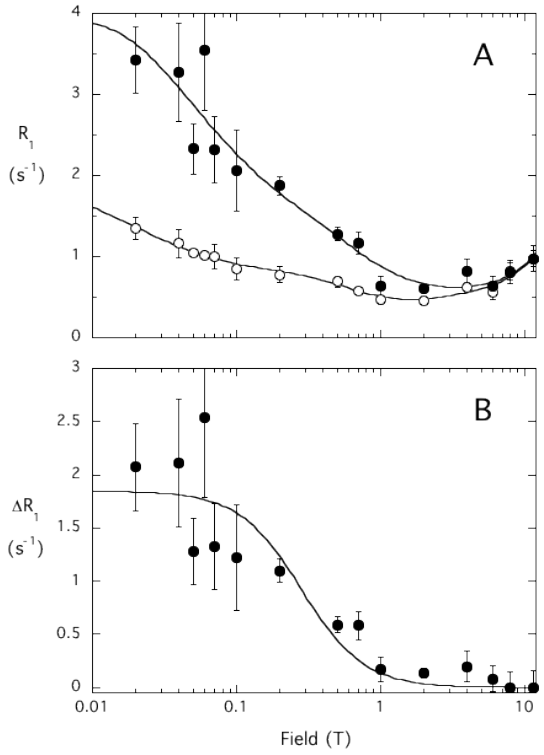

Figure 4.6 Magnetic field dependence of (A) the spin-lattice relaxation rate (R_1) and (B) the paramagnetic relaxation enhancement (ΔR_1) for the ^{31}P of diC_8PI (3.0 mM) caused by 2.0 μM recombinant PTEN (○) and 2.0 μM spin-labeled PTEN (●).

The effect of spin-labeled PTEN (4.9 μM) on 3 mM $diC_8PI(4,5)P_2$ was also examined (Figure 4.7). For these micelles, more spin-labeled protein was needed to get effective relaxation. With this small amount of protein, there was no effect on the $diC_8PI(4,5)P_2$ relaxation in the absence of spin-labeling (the multiply phosphorylated molecule forms

much smaller micelles on its own). The excess relaxation caused by the spin-labeled protein was fit as for diC_8PI. The average correlation time from the three ^{31}P resonances for the phospholipid/protein complex is 119±17 ns. This was significantly larger than what we observed for diC_8PI interacting with the spin-labeled protein. It suggested that binding of this ligand caused formation of a moderately large micellar complex. The $\tau_{P\text{-}e}/\Delta R_{P\text{-}e}(0)$ normalized to the amount of phospholipid and PTEN is $(1.36\pm0.97) \times 10^{-10}$ s^2 for the phosphodiester resonance of diC_8PIP_2 (the ratio for the two phosphomonoesters is a little over twice that). The roughly 10-fold difference in this ratio for diC_8PI and $diC_8PI(4,5)P_2$ indicated that PIP_2 is occupying a different site on the protein, and it is further away from spin label sites. Another feature of $PI(4,5)P_2$ binding is that the phosphomonoester peak attached to C4 of the inositol ring has a higher normalized $\tau_{P\text{-}e}/R_{P\text{-}e}(0)$ value than that attached to C5, indicating the phosphate at C5 is closer to spin labels.

Kinetics with monomers strongly suggested that $diC_8PI(4,5)P_2$ at moderate concentrations was a competitive inhibitor. Some of the relaxation of PIP_2 ^{31}P resonances could be caused by this ligand binding to the active site. To assess this, we examined a sample of 3 mM diC_8PI, 3 mM $diC_8PI(4,5)P_2$ and 0.25 mg/ml protein that was not completely spin-labeled. Under these conditions, phosphodiester resonances for both diC_8PI and diC_8PIP_2 were separable and R_1 values could easily be evaluated for both in the same micelle with protein. If the $PI(4,5)P_2$ relaxation was because it is in the active site, then the presence of the diC_8PI should reduce it substantially. If the two molecules were binding to discrete sites, then the ratio of the $\tau_{P\text{-}e}/\Delta R_{P\text{-}e}(0)$ values for the two phosphodiesters should be the same as when the lipids are mixed separately.

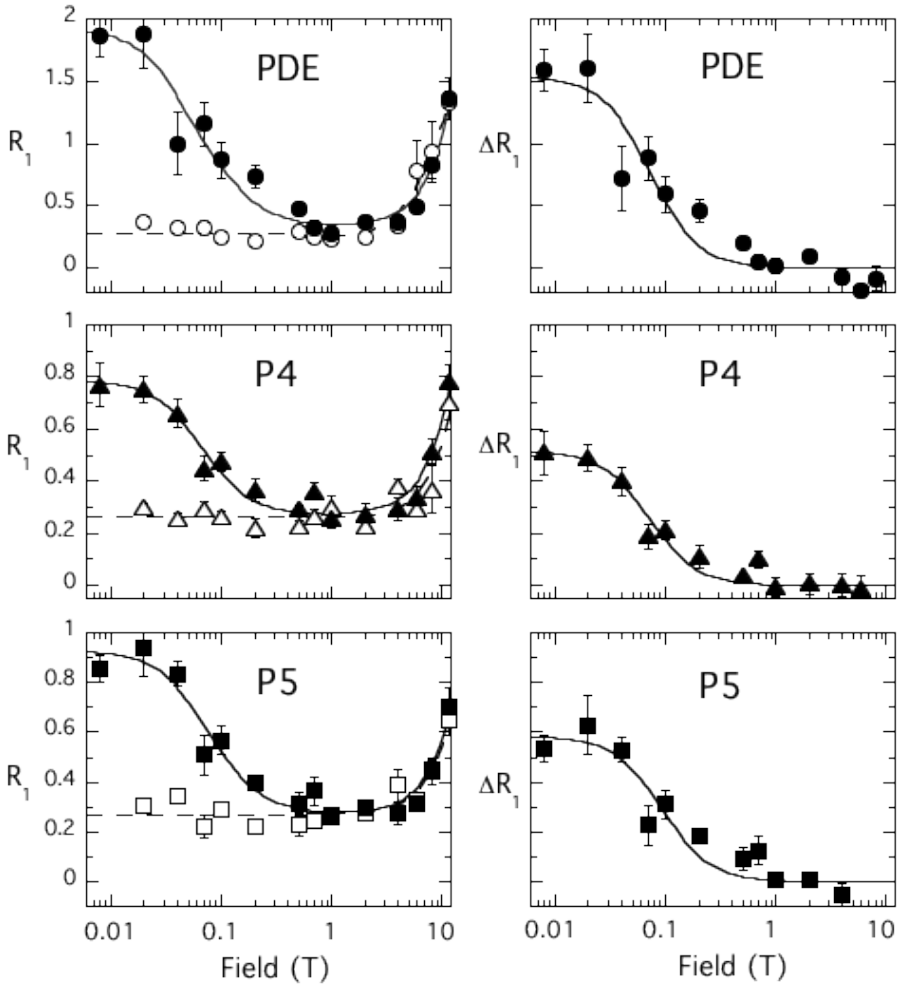

Figure 4.7 The field dependence of (left) R_1 and (right) the relaxation enhancement (ΔR_1) for ^{31}P of $diC_8PI(4,5)P_2$ (3.0 mM) in the presence of 4.9 μM spin-labeled PTEN (solid symbols) and 5.0 μM recombinant PTEN (open symbols): phosphodiester (●), P4 (▲) and P5 (■).

If more completely spin-labeled PTEN is used, it is difficult to obtain a complete enough field dependence profile for the diC_8PI phosphodiester since it relaxes so quickly. Instead, we can use the diC_8PI(4,5)P_2 monophosphates as probes for active site binding. The values of the ration $\tau_{P\text{-}e}/\Delta R_{P\text{-}e}(0)$ for the PI phosphomonoesters are the same in the absence and presence of diC_8PI, indicating that PI(4,5)P_2 is binding to a site spatially distinct from the active site (Figure 4.8).

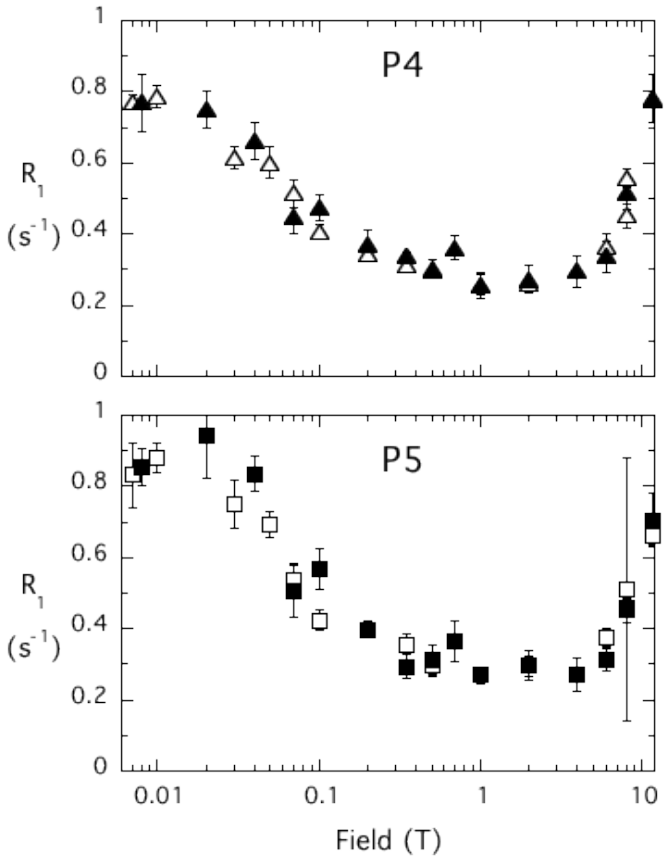

Figure 4.8 The field dependence of R_1 for the phosphomonoesters, P4 and P5, of 3 mM diC_8PI(4,5)P_2 in the absence (open symbol) and presence (filled symbol) of 3 mM diC_8PI and 4.9 μM not fully spin-labeled PTEN.

We can also compare the profiles for other PTEN products that are thought to bind to the active site and not the activator site. The phosphoinositide diC_8PI(4)P could not activate

the enzyme for diC_8PI(3,4)P_2 hydrolysis (Campbell et al, 2003), while placement of the phosphate on the 5-position of the inositol ring generates a lipid that could activate the protein to some degree (Wang et al, 2008). Fixed field studies of diC_8PI(4)P and diC_8PI(5)P indicated an intermediate increase in phosphodiester linewidth when these two monomeric lipid were incubated with PTEN (Table 4.1). Field cycling studies of these two lipids, now presented in a micelle, binding to PTEN showed an increased ΔR_1, especially for phosphodiester peak, at low magnetic fields. However, each sample had 2.5 times the amount of protein used with diC_8PI, so that the comparable values for $\Delta R_{P\text{-}e}(0)$ are really lower. The normalized $\tau_{P\text{-}e}/\Delta R_{P\text{-}e}(0)$ values for the phosphodiesters of diC_8PI(4)P and diC_8PI(5)P were 6.3×10^{-11} and 3.8×10^{-11} s^2 (Table 4.3). This suggests that these PTEN products do not bind in exactly the same way as diC_8PI. Presumably the presence of each phosphomonoester drives the orientation of the inositol ring in the active site. Alternatively they might indicate that the diC_8PI(5)P has some affinity for both sites and so we observed an average reflecting some portion of both sites being occupied. Interestingly, the phosphomonoester P5 was affected more strongly than P4, which was also observed in diC_8PI(4,5)P_2 binding (Table 4.3). From modeling a substrate headgroup into the PTEN crystal structure on top of the tartrate in the active site, it appeared that the P5 was oriented away from the active site and thus should be less affected by a spin-label in Cys124 than P4 (Lee et al, 1999). This inconsistency indicates either the inaccuracy of the modeling or that PI(4)P and PI(5)P bind to the protein with slightly different orientations than the substrate.

Table 4.3 Effect of spin-labeled PTEN on relaxation parameters of short-chain phospholipids as measured by high resolution ^{31}P field cycling

Ligand	[PTEN]/[PL]	$\tau_{P\text{-}e}$ (ns)	$\Delta R_{P\text{-}e}(0)$	([PTEN]/[PL]) $\times\tau_{P\text{-}e}/\Delta R_{P\text{-}e}(0)$	r (Å) [a]
diC_6PI	0.00157	172±21	0.88±0.05	$3.07x10^{-10}$	
	0.00141	107±19	0.45±0.03	$3.35x10^{-10}$	
$diC_6PI(4,5)P_2$	0.00177				
PDE		37±18	0.19±0.04	$3.45x10^{-10}$	
P-4		35±15	0.09±0.01	$6.88x10^{-10}$	
P-5		32±9	0.11±0.01	$5.15x10^{-10}$	
diC_8PI	0.00071	33±10	1.85±0.16	$0.13x10^{-10}$	36±3
$diC_8PI(4,5)P_2$	0.00162				52±4
PDE		128±26	1.53±0.15	$1.36x10^{-10}$	
P-4		131±18	0.52±0.03	$4.08x10^{-10}$	
P-5		99±22	0.58±0.06	$2.76x10^{-10}$	
$diC_8PI/diC_8PI(4,5)P_2$	0.00162				48±3
PDE [b]		103±20	1.47±0.13	$1.14x10^{-10}$	
P-4		169±21	0.45±0.03	$6.08x10^{-10}$	
P-5		153±19	0.53±0.03	$4.68x10^{-10}$	
$diC_8PI(4)P$	0.00177				48±2
PDE		103±15	2.88±0.22	$0.63x10^{-10}$	
P-4		52±11	0.47±0.04	$1.96x10^{-10}$	
$diC_8PI(5)P$	0.00177				36±2
PDE		43±5	2.01±0.10	$0.38x10^{-10}$	
P-5		55±8	0.66±0.04	$1.48x10^{-10}$	
diC_7PC [c]	0.00106	120±15	3.96±0.24	$0.32x10^{-10}$	51±2
diC_7PC/TX-100 [c]	0.00106	118±17	1.68±0.15	$7.44x10^{-10}$	50±2
$diC_7PC/diC_8PI(4,5)P_2$					
PDE/PC [d]	0.00066	110±13	1.79±0.11	$0.41x10^{-10}$	49±2
P-4	0.00177	93±20	0.55±0.03	$2.99x10^{-10}$	
P-5	0.00177	56±15	0.62±0.07	$1.60x10^{-10}$	

[a] This r is an estimate of the average PTEN/micelle complex size obtained by relating $\tau_{P\text{-}e}$ to an isotropic diffusion constant, $\tau_{P\text{-}e} = 1/(6\times D)$ where $D = kT/(8\pi\eta r^3)$ (Shi et al, 2009).

[b] Overlap of the two phosphodiesters occurs. However, with this higher amount of protein, the diC_8PI component is relaxed well before the PIP_2 compound, hence the measured R_1 reflects the $diC_8PI(4,5)P_2$.

[c] The dispersion for diC_7PC was fit with a single $\tau_{P\text{-}e}$.

[d] For the $diC_7PC/diC_8PI(4,5)P_2$ (5 mM: 3 mM) sample, the total phosphodiester concentration is 8 mM and this is used in estimating the ratio PTEN to a particular phospholipid. Both phosphodiesters are used since each compound can bind to the active site.

(3) Other ligands

Kinetics with the synthetic short-chain PIs showed that diC_7PC was very inhibitory while TX-100 had little effect on the observed rate. The Triton X-100 was suggested to bind to a hydrophobic pocket adjacent to (but not in) the active site, the AHS (Wang et al, 2010). The complication with interfacial enzymes is that altering the surface concentration of substrate could have large effects on the rate and lead to surface dilution inhibition (Pu et al, 2009a). Alternatively, reduced activity as a diluent increased could indicate that the molecule was binding to or near the active site and acting as a competitive inhibitor.

With this in mind we explored the effect of spin-labeled PTEN on zwitterionic diC_7PC micelles in the absence and presence of diC_8PI(4,5)P_2, which presumably binds mainly to the activator site. We also examined the effect of spin-labeled PTEN on diC_8PI with a large excess of TX-100 present.

For 5 mM diC_7PC micelles interacting with 5.3 μM spin-labeled PTEN, there was a large effect on the ^{31}P resonance. The value for [PTEN]/[PL])×($\tau_{P\text{-}e}/\Delta R_{P\text{-}e}(0)$)was $3.22\text{x}10^{-11}$ s^2 for this sample (Table 4.3), which was about twice the value for diC_8PI, closed enough to suggest that diC_7PC must be in part of the active site (hence its potent inhibition of PTEN kinetics).

Addition of TX-100 reduced the effectiveness of the spin-labeled protein on diC_7PC. The ([PTEN]/[PL])×($\tau_{P\text{-}e}/\Delta R_{P\text{-}e}(0)$)value was reduced to 7.44×10^{-10} s^2 (Table 4.3). Triton X-100 binding in the AHS reduces diC_7PC binding to the active site, presumably because the PC occupies both the active site and the AHS. This is consistent with the PTEN kinetics that showed that Triton could lessen diC_7PC inhibition of diC_8PI(3)P hydrolysis.

We also examined the effect of Triton X-100 on diC_8PI binding to spin-labeled PTEN (diC_8PI/TX-100 = 3 mM /6 mM). DiC_8PI/TX-100 mixed micelles altered (increased) the average micelle size, and the unlabeled protein control showed a larger contribution of relaxation. Once this was subtracted, the dependence of excess R_1 (due to spin-label) on field was best fit with a correlation time of 68±10 ns; the $([PTEN]/[PIP_x])\times(\tau_{P\text{-}e}/\Delta R_{P\text{-}e}(0))$ ratio was $4.34x10^{-11}$ s^2 (Table 4.3). The surface concentration of diC_8PI had decreased 3-fold with the added TX-100, which was about the same amount as the increase in the ratio of $([PTEN]/[PIP_x])\times(\tau_{P\text{-}e}/\Delta R_{P\text{-}e}(0))$. That most of the strong relaxation was observed indicated there was still a specific interaction of PI with the active site.

After demonstrating that diC_7PC could bind to the active site, we examined the effect of diC_7PC on the PIP_2 interaction with PTEN. The sample had 3 mM $diC_8PI(4,5)P_2$, 5 mM diC_7PC amd 5.3 μM spin-labeled protein. Although the PC phosphodiester dominated the PIP_2 resonance, we could at least examine how the phosphodiester behaved versus the phosphomonoesters of the phosphoinositide. Interestingly, $\tau_{P\text{-}e}$ for the phosphodiester was 85-110 ns and $R_{P\text{-}e}(0)$ decreased when the PIP_2 was present (Table 4.3). In other words, the PIP_2 competed with the diC_7PC. However, the two PIP_2 phosphomonoester peaks actually showed a decrease in $\tau_{P\text{-}e}$ with PC added with little effect on $\Delta R_{P\text{-}e}(0)$. Addition of the zwitterionic PC reduced the $\tau_{P\text{-}e}/\Delta R_{P\text{-}e}(0)$ ratio for the phosphomonoesters. At the very least, these ^{31}P resonances were still well-relaxed by spin-labeled protein regardless of whether diC_7PC was added to dilute the surface. The net result was that diC_7PC did bind to the protein around/in the active site and inhibited the enzyme but the binding did not appear particularly tight and had only minor effects on PIP_2 binding. DiC_7PC also

interacts with the AHS since inclusion of Triton X-100 in the micelles altered its relaxation by the spin-labeled protein.

By using high resolution field cycling NMR, we explored the effect of spin-labeled PTEN binding PI, PI(4,5)P_2 and PC lipids as well as the effect of TX-100 on this phospholipid binding. The head group of PI lipids, I(1,4,5)P_3 does not bind spin-labeled PTEN and shorter chain PIs (diC_6PI and diC_6PI(4,5)P_2) have much weaker interactions, consistent with what were observed in kinetics and fixed field NMR results. DiC_8PI, a product of PI(3)P dephosphorylation and an inhibitor of PTEN, binds in the active site. The fixed field study indicated this lipid binds to the protein in an intermediate exchange regime. If its off-rate is slower, we may not be measuring its relaxation at very low fields. This could explain why the correlation time, $\tau_{P\text{-}e}$, for diC_8PI was usually lower than for diC_8PI(4,5)P_2. Nonetheless, the ^{31}P in this lipid is the closest to the spin-labels in PTEN. A major result of this work is that there is a discrete binding site for PI(4,5)P_2 on PTEN that is near but distinct from the active site.

4.2.4.4 Field cycling NMR study of PTEN mutants

For comparison to the field cycling studies of wild type PTEN, we also examined several mutant proteins, choosing those where PIP_2 activation was affected (Table 4.4). K13E is not activated by PI(4,5)P_2 indicating the activator site was disrupted. C124S is catalytically inactive Since Cys71 is near the active site, it should still be spin-labeled and can be used as an indicator for nearby bound ^{31}P.

Table 4.4 Effect of spin-labeled PTEN K13E (4.9 μM) on relaxation parameters of diC_8PI (3 mM) and/or $diC_8PI(4,5)P_2$ (3 mM) as measured by high resolution ^{31}P field cycling.

Ligand	[K13E]/[PL]	$\tau_{P\text{-}e}$ (ns)	$\Delta R_{P\text{-}e}(0)$ (s^{-1})	([K13E]/[PL]) $\times\tau_{P\text{-}e}/\Delta R_{P\text{-}e}(0)$	r (Å)
diC_8PI	0.00071	144 ±26	3.87±0.40	0.26×10^{-10}	54±3
$diC_8PI(4,5)P_2$	0.00148				
PDE		96±18	0.71±0.07	2.00×10^{-10}	47±3
P-4		58±13	0.23±0.02	3.73×10^{-10}	
P-5		69±18	0.17±0.02	6.01×10^{-10}	
$diC_8PI(4,5)P_2$	0.00141				
PDE		109±14	0.94±0.06	1.64×10^{-10}	49±2
P-4		137±21	0.39±0.03	4.95×10^{-10}	
P-5		127±13	0.33±0.02	5.43×10^{-10}	
$diC_8PI/diC_8PI(4,5)P_2$	0.00141				
PDE		46±10	0.72±0.07	0.90×10^{-10}	37±3
P-4		32±14	0.21±0.04	2.15×10^{-10}	
P-5		46±26	0.13±0.03	4.99×10^{-10}	
PI		87±24	3.81±0.79	0.32×10^{-10}	46±4

[a] r is an estimate of the average PTEN/micelle complex size obtained by relating $\tau_{P\text{-}e}$ to an isotropic diffusion constant, $\tau_{P\text{-}e} = 1/(D\times6)$ where $D = kT/(8\pi\eta r^3)$ (Shi et al, 2009).

The field dependence profile for diC_8PI binding to K13E was similar to that for wild type protein (Table 4.4). The $\tau_{P\text{-}e}$ is large, 144 ±26 ns, for the K13E /diC_8PI complex, a value comparable to what was observed with wild type PTEN binding $diC_8PI(4,5)P_2$. The normalized $([K13E]/[PIP_x])\times(\tau_{P\text{-}e}/\Delta R_{P\text{-}e}(0))$ratio was 2.6×10^{-11} s^2, about double that for the wild type PTEN/PI complex. However, this normalized $\tau_{P\text{-}e}/R_{P\text{-}e}(0)$ is still much lower than that for PTEN binding $diC_8PI(4,5)P_2$. The effect of spin-labeled K13E on $diC_8PI(4,5)P_2$ was also examined. Contrary to the thought that this mutation eliminates $PI(4,5)P_2$ binding, our field cycling results clearly show that $diC_8PI(4,5)P_2$ is still bound to the protein. The average of two separate sample of 0.25 mg/ml K13E plus 3 mM

diC_8PI(4,5)P_2 led to a normalized $\tau_{P\text{-}e}/R_{P\text{-}e}(0)$value for phosphodiester of 1.81×10^{-10} s^2, a value fairly similar to the value of 1.36×10^{-10} s^2 for the wild type protein. The normalized $\tau_{P\text{-}e}/\Delta R_{P\text{-}e}(0)$ values for the two phosphomonoesters were 4.34×10^{-10} s^2 and 5.72×10^{-10} s^2 for P4 and P5, respectively (Table 4.4). These values are larger than the values observed with wild type and with this mutant, P5 is not relaxed as efficiently as P4. These results clearly indicate that K13E still binds diC_8PI(4,5)P_2, but not exactly in the same position as for spin-labeled wild type protein. The larger the normalized $\tau_{P\text{-}e}/R_{P\text{-}e}(0)$, the longer the average distance of the ^{31}P from the nitroxide, so that removal of Lys13 does affect the position of the PIP_2 on the protein. When both 3 mM diC_8PI and 3 mM diC_8PI(4,5)P_2 are incubated with spin-labeled K13E, the field cycling parameters describing the interaction are the same as for the individual lipids. Kinetics studies with K13E indicated this mutant was not activated by this PIP_2, but NMR results, both fixed field and field cycling experiments, still show diC_8PI(4,5)P_2 molecules could interact with the protein. The field cycling shows two discrete changes in lipid binding to this mutant protein. The correlation time of the protein-lipid complex, $\tau_{P\text{-}e}$, is shorter for mutant (41.4±8.5 ns). P5 is now slightly further from the spin-labels compared to P4 – the opposite of what is seen with spin-labeled wild type protein These changes suggest that the K13E mutation may be altering the lifetime of the bound diC_8PI(4,5)P_2 and may also induce small changes in the orientation of that lipid when bound to the protein so that it no longer affects enzyme activity.

Spin-labeling of C124S should still place a nitroxide near the active site, on Cys71. This is likely to be the closest point of spin-label attachment for enhancing PI ^{31}P relaxation. As expected, the PRE is reduced when C124S is bound to diC_8PI and diC_8PI(4,5)P_2,

partially due to the loss of the unpaired electron dipole on spin-labeled Cys124 compared to wild type protein. The $([C124S]/[PIP_x])\times(\tau_{P\text{-}e}/\Delta R_{P\text{-}e}(0))$ value for diC_8PI was 3.05×10^{-11} s^2, around 3 times of what for PTEN wild type bound diC_8PI. If we assumed the $\Delta R_{P\text{-}e}(0)$ difference between C124S and wild type bound diC_8PI is from the single unpaired electron on Cys124, then $\tau_{P\text{-}e} = 5.2\times10^{-8}$ s and $\Delta\Delta R_{P\text{-}e}(0) = 0.623$ s^{-1}. From these parameters, the normalized $\tau_{P\text{-}e}/\Delta R_{P\text{-}e}(0)$ is 5.64×10^{-11} s^2, and this can provide an estimate of the distance between a spin-label attached to Cys124 and the ^{31}P of the bound PI as 9.4 Å. What is actually observed for C124S and PI should mostly reflect the distance between the label on Cys71 and the bound phosphodiester ^{31}P. This value would then be estimated as 8.4 Å.

The PRE effect of spin labeled C124S on $diC_8PI(4,5)P_2$ was also measured. The normalized $\tau_{P\text{-}e}/\Delta R_{P\text{-}e}(0)$ values are considerably larger for both the phosphodiester and phosphomonoester ^{31}P resonances. This stresses that the PIP_2 binding site is indeed near the active site. For the phosphodiester resonance about of half the $\Delta R_{P\text{-}e}(0)$ of the labeled wild type protein is caused by Cys124 labeling. With $\tau_{P\text{-}e}$ ~160 ns and $\Delta\Delta R_{P\text{-}e}(0) = 0.60$ s^{-1}, the normalized $\tau_{P\text{-}e}/\Delta R_{P\text{-}e}(0) = 3.78\times10^{-10}$ s^2. The distance between the spin-label attached to Cys124 and $diC_8PI(4,5)P_2$ is estimated as 12.9 Å. These data clearly show that $diC_8PI(4,5)P_2$ binds to a discrete site on PTEN that is near the active site of the protein.

4.3 Discussion

The major difference between the allosteric and interfacial activation mechanisms proposed to explain $PI(4,5)P_2$ activation of PTEN is that the allosteric mechanism

invokes a specific binding site, other than active site, while the interfacial mechanism proposes alterations in the interface that affect protein binding and accessing its substrate. Here we used kinetics and NMR methods to demonstrate that there is a discrete $PI(4,5)P_2$ binding site on PTEN. In fixed field NMR experiments, the difference in PTEN-induced line broadening of diC_8PI and $diC_8PI(4,5)P_2$ clearly reflected the different binding properties of these two lipids. Mixtures of an active site binding lipid (L-3,5-dideoxy-diC_8PI) and activator lipid $diC_8PI(4,5)P_2$ showed the linewidth changes were the same as when both were examined separately. The different proximity to active site between PI and $PI(4,5)P_2$ in field cycling NMR studies provides independent proof for a discrete activator binding site. By using this method to measure average distances between the spin-label and ^{31}P in molecules bound to the protein, we have shown that the $PI(4,5)P_2$ activator binding site is not very far from the active site. This is consistent with the kinetics for R47G that showed a loss of $diC_8PI(4,5)P_2$ activation, since we know the AHS, to which Arg47 contributes, is close to the active site.

Along with providing evidence for a discrete activator binding site, field cycling studies also indicated what is critical for a phosphoinositide to bind to the PTEN active site. The superimposition of $I(1,3,4,5)P_4$ with tartrate in PTEN crystal structure generated a model of how the phosphoinositides substrates could be bound to the protein (Lee et al, 1999). If this *in silico* extrapolation is correct, it is reasonable for $PI(4,5)P_2$ to bind to the PTEN active site since its head group, $I(1,4,5)P_3$, has only one phosphate group missing from $I(1,3,4,5)P_4$. Our results indeed demonstrated $PI(4,5)P_2$ monomers have an affinity for the PTEN active site. The kinetics show that monomeric $PI(4,5)P_2$ inhibits PTEN activity with PI(3)P as the substrate, although the $PI(4,5)P_2$ effect is substrate and concentration

dependent. In the $diC_8PI(3,4)P_2$ monomer system, $diC_8PI(4,5)P_2$ enhances enzyme activity, and in the long chain $PI(3,4)P_2$/$PI(4,5)P_2$ vesicle system, low concentrations of $PI(4,5)P_2$ activate PTEN while high surface concentrations of $PI(4,5)P_2$ inhibit the enzyme. We believe the different effects of $PI(4,5)P_2$ in different substrate system was due to the different affinity of the substrates. As reported previously (Myers et al, 1998), the specific activity of PTEN towards $PI(3,4)P_2$ is higher than that towards PI(3)P; our kinetic studies agree with this as well. $PI(3,4)P_2$ is likely to have a higher affinity for the protein active site than PI(3)P, a reasonable assumption since the PTEN active site has more lysines than other protein tyrosine phosphatases and prefers highly acidic substrates (Lee et al, 1999; Myers et al, 1997). The addition of the phosphate on the inositol C4 would provide more electrostatic contacts within the PTEN active site. Presumably, the lower affinity of $PI(4,5)P_2$ compared to $PI(3,4)P_2$ for the active site reflects a preferential binding of the phosphate on C3 and perhaps a misalignment with phosphates only at C4 and C5. The lower affinity of $PI(4,5)P_2$ for the active site allows it to bind to the activator site in the presence of $PI(3,4)P_2$. An interfacial activation mechanism for PIP_2 activation of PTEN could not explain the observation that a higher percentage of $PI(4,5)P_2$ in substrate-containing vesicles lowers PTEN specific activity. According to that mechanism, as the $PI(4,5)P_2$ fraction in substrate vesicles increases, interaction of PTEN with the vesicles increases leading to higher enzymatic activity. However in our system, excess $PI(4,5)P_2$ can compete with substrate $PI(3,4)P_2$ in binding to the active site. So more than just driving the enzyme to the interface is involved.

The N-terminal loop was suggested to be the $PI(4,5)P_2$ binding site since this loop has the consensus sequence for protein binding to $PI(4,5)P_2$. This short N-terminal loop was

found to be important for PTEN membrane binding and cellular function. The effect of deleting this binding site or mutation at this site has been widely studied, and proteins with perturbations of this site do not bind to membranes and are dysfunctional in cells (Walker et al, 2004; Vazquez et al, 2006; Rahdar et al, 2009). The mechanism for the loss of PIP_2 activation of PTEN in Lys13 mutants was suggested to be the elimination of this cationic binding (Redfern et al, 2008). Our kinetic results demonstrate the loss of activation of K13E in both substrate monomer and vesicle assay systems. However, similar line broadening of diC_8PIP_2 by K13E and wild type protein in fixed field NMR indicate that the 'activator' molecule can still bind to the enzyme. The field cycling further shows that the $diC_8PI(4,5)P_2$ binds to K13E PTEN, but in a slightly different orientation from what is observed with the wild type protein. The loss of PIP_2 kinetic activation of this mutant cannot be explained by the loss of binding but rather an altered binding site, where the conformation necessary for activation is no longer accessible.

What do we know about this altered bound conformation? In the 'correct' PIP_2 activator binding site, the phosphate at C5 of the inositol headgroup is characterized by a higher PRE effect than the phosphate at C4. Similarly, the monophosphate in $diC_8PI(5)P$ always exhibited a larger linewidth with added PTEN than the monophosphate in $diC_8PI(4)P$. Both these are switched when PTEN K13E binds them.

The acyl chain length of $PI(4,5)P_2$ affects its ability to activate PTEN suggesting either a preference for an interfacial activator or perhaps a direct interaction of one of the acyl chains with PTEN. It was noted (Maehama et al, 2001) that the consensus sequence also contains some hydrophobic residues that could interact with the acyl chains of $PI(4,5)P_2$. A search of the Protein Data Bank for structures containing $diC_8PI(4,5)P_2$ as ligand

introduced seven protein structures containing this molecule, three structures of the K^+ channel Kir 2.2 wild type and its mutants, two structures of the GIRK2 K^+ channel (Kir 3.2), one structure of this ligand bound to the HIV-1 matrix protein, and one structure where the PIP_2 is bound to the CALM N-terminal domain (N-terminal clathrin assembly lymphoid myeloid leukaemia protein). In the Kir 2.2 structure, the specific binding site for P4 and P5 is contained within the conserved consensus sequence, while the P1, glycerol backbone and acyl chains bind nonspecifically in an pocket since they cannot insert into a membrane (Hansen et al, 2011). If $PI(4,5)P_2$ binding to PTEN has similar interactions, especially between the headgroup, the phosphates at inositol C4 and C5, interact with cationic residues in the N-terminal loop with the consensus sequence: Lys6, Lys11 and Lys13 in PTEN are equivalent to Lys183, Arg186 and Lys188 in Kir 2.2 and should bind to the phosphate on inositol C5. Lys 14 in PTEN would be the equivalent of Kir 2.2 Lys189 and should bind to the phosphate on inositol C4. This predicts a stronger interaction of the protein with the C5 phosphate group. Consistent with this, there is always a stronger interaction between P5 and the protein than for P4. This binding mode would also explain the observation that PI(5)P can activate PTEN while PI(4)P does not. There is a binding pocket on Kir 2.2 for interaction with the PIP_2 the acyl chain. This pocket was not identified in PTEN. It is possible that the hydrophobic residues in the N-terminal consensus sequence, Ile8 and Val9, could interact with PIP_2 acyl chains. However, our previous molecular dynamic simulations and the kinetic data in this work suggest the hydrophobic site adjacent to the active site (the AHS) could supply residues for acyl chain interactions.

Indeed, the AHS, which includes residue Arg47 must be involved in PIP_2 activation, since PIP_2 activation is lost in R47G and R47K. Triton X-100, which binds in the hydrophobic site, has no effect toward PIP_2 activation. DiC_7PC, which binds in the hydrophobic site but also partially in the active site (since it is a good inhibitor of PTEN activity), exhibited no alterations in field cycling parameters in the presence of $diC_8PI(4,5)P_2$. This would be consistent with occupation of active and activator / hydrophobic sites at the same time. Another possibility is that the loop with Arg47 might be involved in the conformational change that occurs during PIP_2 activation, rather than directly interact with the activator molecule. If the loop is too flexible (R47G), the structural transition is impaired and no kinetic activation is observed.

Phosphatidylcholine (PC) is one of the most abundant phospholipids in cell membrane. Micellar or monomeric diC_7PC inhibit PTEN by binding in both the active site (the ^{31}P is close to spin-labels at Cys124 or Cys71 similar to what is seen with diC_8PI binding to PTEN) and the AHS (it is displaced by Triton X-100 in NMR experiments as well as in the kinetics). However, the acyl chains of diC_7PC are critical to its binding to PTEN. Without occupation of the AHS (i.e., when excess Triton X-100 is added), the diC_7PC headgroup association and subsequent relaxation are much smaller. This is consistent with the report that PTEN has lower affinity for pure PC vesicles (Redfern et al, 2008) and with plasma membranes of resting cells (Vazquez et al, 2006).

The net result of this work is that there are three functionally distinct but spatially close sites for amphiphiles to bind: (1) the active site, (2) the PIP_2 'allosteric' site, and (3) the AHS (adjacent hydrophobic site). The discrete binding site for $PI(4,5)P_2$ could involve the N-terminal peptide of PTEN (a region not detected in the crystal structure), since

perturbation of Lys13 causes loss of PIP_2 activation. However, this binding site is also near the active site and its adjacent hydrophobic site since mutation of Arg47 in the latter abolishes PIP_2 activation. The interplay / synergism of the three sites provides a variety of ways to regulate PTEN activity. Like many other signaling proteins that cycle on/off the membrane surface, PTEN possess a C2 domain that should transiently anchor it to the membranes via PS interactions. However, the presence of an active site, hydrophobic site, and activator binding site on the phosphatase domain provides novel ways to regulate PTEN activity when it is bound to interfaces.

Chapter 5

Archaeoglobus fulgidus IMPase: thermoprotection by compatible solutes

5.1 Introduction

As the most ancient domain of life, archaea usually reside in extreme environments. Thermophiles and hyperthermophiles thrive only at high temperatures (>60^{o}C). Halophiles live in high salinity (>1 M salt), and methanogens live in anaerobic sites. In these harsh environments, the ability to maintain cellular function and respond to environmental changes is essential. The responses of microorganisms to salt and temperature stress often involve the accumulation of ions or small molecules. Archaea can accumulate a large amount of K^+ to maintain the cell volume during osmotic stress. They also accumulate a group of small organic molecules either by uptake from the external media or de novo synthesis. These small organic molecules are often referred to as osmolytes or compatible solutes, the latter term since although they are accumulated at high concentrations they do not interfere with cell functions (Brown, 1976). The diversity and the functions of archaeal compatible solutes have been the subject of many reviews (Burg & Ferraris, 2008; da Costa et al, 1998; Roberts, 2005; Santos & da Costa, 2002; Santos et al, 2011). Common compatible solutes include polyols, sugars, amino acids and their derivatives. Along with maintaining the turgor pressure of the cells, it has been suggested that compatible solutes can stabilize archaeal proteins. The osmophobic effect was proposed to explain the mechanism of the protein structural stabilization (Bolen & Baskakov, 2001). It postulates that the interaction between protein backbone and the osmolytes is thermodynamically unfavorable. This leads to a more positive free energy for unfolded protein compared to in solution with high concentrations of osmolytes than unfolded protein in solution without those solutes. The osmolytes stabilize proteins by destabilizing the unfolded state. Non-specific interactions with the protein backbone were

shown at the single molecule level using atomic force microscopy (AFM) based single-molecule force spectrometry (Aioanei et al, 2011). These experiments suggest that osmolytes may not play a structural role at the unfolding transition, rather they adjust the solvation quality for the protein chain.

Archaeoglobus fulgidus is a hyperthermophile initially found in thermally heated water around a volcano (Stetter et al, 1987), but also found in marine sediment (Zellner et al, 1989) and oil field water (Beeder et al, 1994). This archaeon can thrive in high temperatures ranging from 70 to 90°C with an optimal growth temperature around 83°C. It normally lives at these temperatures with NaCl equal to or less than 5% w/v in the medium, although a variant surviving higher salt in the growth medium (6.3% w/v NaCl) has been reported (Goncalves et al, 2003). The compatible solute pool of *A. fulgidus* has been studied under different conditions (Martins et al, 1997). Diglycerol-phosphate (DGP) was accumulated upon salt stress, while di-*myo*-inositol-1,1'-phosphate (DIP) was accumulated upon thermal stress (temperature elevation) (Goncalves et al, 2003; Martins et al, 1997). For the organism grown in high salinity (4.5% w/v NaCl) compared to lower salinity (0.9% w/v NaCl), intracellular DGP concentration increased 11-fold. The intracellular DIP concentration was low when the organism grew at 76°C, and after increasing the growth temperature to 87°C, intracellular DIP increased 30-fold. Along with DGP and DIP, other compatible solutes such as glutamate and 1-glyceryl-1-myo-inosityl phosphate (GIP) were identified in these cells (Lamosa et al, 2006). Given the structures of these phosphoesters (which require significant energy for biosynthesis), it is worthwhile to study the roles of these specific compatible solutes in protecting *A. fulgidus* proteins.

A. fulgidus inositol monophosphatase (IMPase) is a dual-specificity phosphatase that can dephosphorylate inositol phosphates and fructose 1,6-bisphosphates (Stieglitz et al, 2002). This enzyme plays a role in the DIP biosynthetic pathway (Rodionov et al, 2007). Compared to IMPase proteins from eukaryotes and bacteria, archaeal IMPase homologues have structures with shorter loops and helices (Johnson et al, 2001; Stec et al, 2000), which may account for their higher thermal stability. However, *A. fulgidus* IMPase is not as stable as the IMPase from M*ethanococcus jannaschii* or *Thermotoga maritima*, possibly due to the smaller dimer interface and increased loop sizes (Stieglitz et al, 2002). *A. fulgidus* IMPase irreversibly denatures a little below 90°C (Wang et al, 2006), a temperature at which the organism can still live. This prompts the question of what stabilizes the IMPase at high temperatures. Previous kinetic studies in our lab of this enzyme showed the K_m of *A. fulgidus* IMPase was reduced 8- to 10-fold when the temperature increased from 75°C to 85°C, facilitating high activity of this enzyme at the high temperatures where DIP is accumulated (Wang et al, 2006). However, the thermoprotection and the stabilization of this model enzyme by compatible solutes were not investigated.

In this project, we tested the thermoprotection effect of DIP, DGP and other small organic molecules on *A. fulgidus* IMPase, to find a possible mechanism of how this particular enzyme was protected from thermal denaturation during this organism's adaptation to increased temperature. Our results showed that: (1) both enantiomers of DIP protected *A. fulgidus* IMPase from thermal denaturation at temperatures well above the unfolding transition; (2) DGP protected *A. fulgidus* IMPase very effectively, most likely by binding in the active site; (3) higher concentrations of aspartate (Asp),

glutamate (Glu) and other dicarboxylates protected the *A. fulgidus* IMPase significantly from thermal unfolding, while monocarboxylates and a tricarboxylate were not very effective. These observations indicate there are differential effects of these small organic molecules, many of them common osmolytes, on the stability of a particular protein. We define these differential effects as the compatible solute specificity, whereby only some compatible solutes provide thermal protection to a particular protein, while others do not, although they may protect other proteins from thermal inactivation; (4) Glu (and Asp) ions bind to *A. fulgidus* IMPase at specific sites, but these specific binding sites on IMPase do not correlate with thermoprotection by Glu. However, these sites where Glu binds have large effects on the protein thermal stability providing insights into what stabilizes this dimer.

5.2 Result

5.2.1 DIP thermoprotection

DIP is accumulated in *A. fulgidus* (Martins et al, 1997) as well as other thermophilic archaea, including *Pyrococcus woesei* (Scholz et al, 1992), *Methanococcus igneus* (Ciulla et al, 1994) and the bacterium *T. maritima* (Ramakrishnan et al, 1997), when the organism is grown above optimal temperature. It is possible that this molecule protects IMPase enzyme at high temperate. DIP is also an odd choice for an osmolyte. When DIP was initially identified it was said to be the chiral L,L-DIP enantiomer (Vanleeuwen et al, 1994). Later studies, based on the biosynthetic pathway suggested that it was not chiral but the L,D-enantiomer (Rodrigues et al, 2007). With this in mind, we thought it would be useful to investigate if both of these enantiomers have similar effects or only one of them is biological relevant in thermoprotection.

Prior to testing the effect of DIP on IMPase thermostability, we examined the effect of KCl, NaCl and the glutamate salts of each cation (Figure 5.1) in protecting the IMPase activity from heating at 95^{o}C for 15 min. This treatment in the absence of compatible solutes nearly inactivated the enzyme; residual enzymatic activity was only 3%. Thermoprotection could be observed with 100 mM added salt, although the effects were much stronger at higher concentrations of the salts. With 500 mM KCl and K^+-glutamate present during heating, protein residual activity was ~50% after heating. Of particular interest was the observation that the sodium salts were virtually ineffective in this concentration range, while KCl and K^+-glutamate were similar and much more effective at protecting IMPase activity.

In order to get a measure of what each stereoisomer of the DIP *anion* might contribute to thermoprotection, we examined the effects of the Na^+-salts of DIP (Figure 5.1, bottom). The two DIP enantiomers were chemically synthesized using a peptide asymmetric catalysis method by Christine Longo in the lab of Prof. Scott Miller at Yale (Longo et al, 2009). We examined 100 mM of each Na^+-DIP on IMPase activity after heating. Interestingly, both Na^+-L,L-DIP and Na^+-L,D-DIP were effective in reducing denaturation (17% and 11% residual activity, respectively). In comparison to the thermoprotection provided by KCl (18% recovery of activity), it is particularly notable that the sodium salts of DIP offer protection while NaCl is completely ineffective, further pointing to the thermoprotective properties of the DIP anions. As a control, 100 mM *myo*-inositol was also examined for any thermoprotection of this enzyme; the inositol (which binds to the active site) alone had no effect. This would suggest that merely occupying the active site with inositol offers little thermoprotection when the protein is heated well

above its T_m. In addition, the Na^+-salt of dimethylphosphate (DMP) offered no thermoprotection, indicating that the DIP anion on its own is unique and has significant thermoprotective effects.

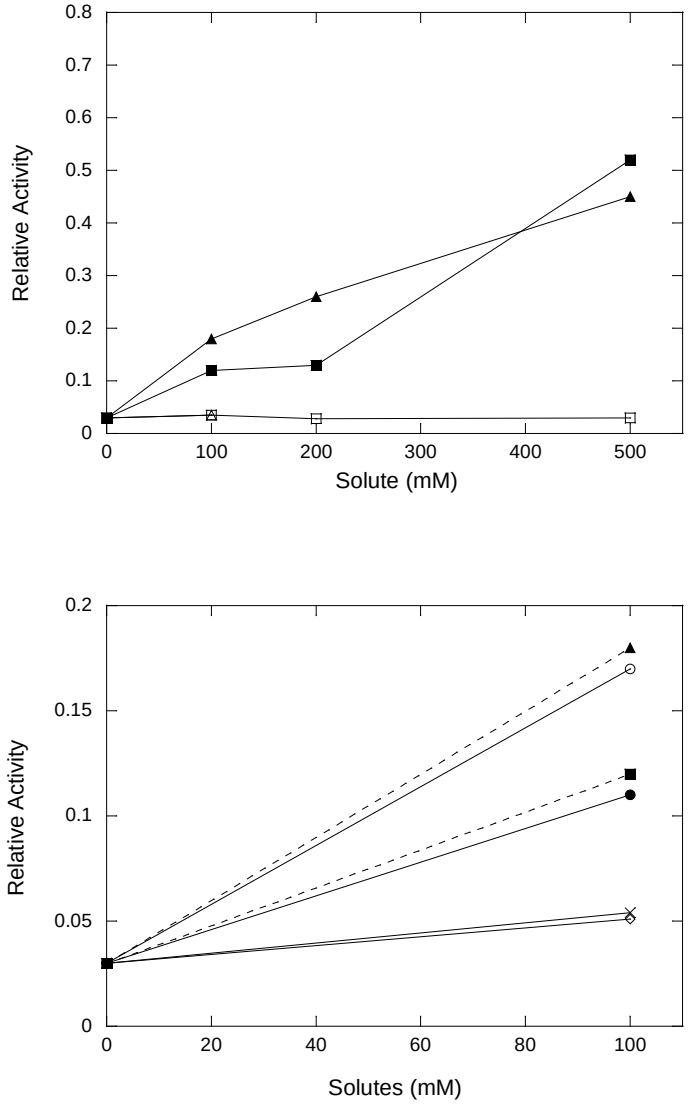

Figure 5.1 Effect of solutes on the residual activity of *A. fulgidus* IMPase, heated to 95 °C for 15 minutes, then cooled and assayed at 85°C: ▲, KCl; Δ, NaCl; ■, K^+-glutamate; □, Na^+-glutamate. The bottom figure shows the effect of the sodium salts of L,L- (○) and L,D- (●) DIP at 100 mm, as well as dimethylphosphate (DMP; ×) and *myo*-inositol (◊) compared to the K^+ salts solutes(dashed lines) shown in the upper figure.

Due to the availability of only small amounts of DIP compounds, we did not measure if high concentration of DIP had any effect to IMPase enzyme activity. However, this IMPase can dephosphorylate P-DIP, the phosphorylated form of DIP *in vitro*, and DIP is the product of this dephosphorylation reaction (Rodionov et al, 2007). Based on this observation, we speculate that DIP might have affinity for the IMPase active site but this affinity should not be very high.

5.2.2 DGP thermoprotectiont

Along with DIP accumulation, *A. fulgidus* also accumulates DGP to balance increased salinity (Martins et al, 1997). Unlike the wide usage of DIP by thermophiles, DGP accumulation appears to only occur in the genus *Archaeoglobus* (Santos et al, 2011). We tested the effect of DGP, synthesized in the laboratory by Jessica Chao, on IMPase activity. However, in this experiment, the protein solution was not heated to 95^{o}C, but to 90^{o}C. Incubation at a temperature a little above the T_m (87-89^{o}C) is a less radical treatment; oxidation of two spatially close cysteine residues in the protein at high temperatures leads to loss of enzymatic activity (Stieglitz et al, 2003). Interestingly, DGP was found to be inhibitory in standard assays of the IMPase enzyme at 85^{o}C. As little as 0.4 mM DGP yielded 70% activity relative to samples with no DGP; with 10 mM DGP present, the enzyme activity was reduced to 5% of the control. Clearly DGP binds to the protein at or in the vicinity of the active site.

To test the thermoprotective ability of DGP, the IMPase was first heated at 90°C for 30 min. The protein in the absence of any solutes had 25% residual activity after heating. DGP was very effective in protecting the IMPase from the heat-induced loss of activity. 10 mM DGP, which must be close to saturating its binding site in or near the active site,

led to 85% residual activity after heating; with 100 mM DGP the residual activity was more than 90% (Figure 5.2).

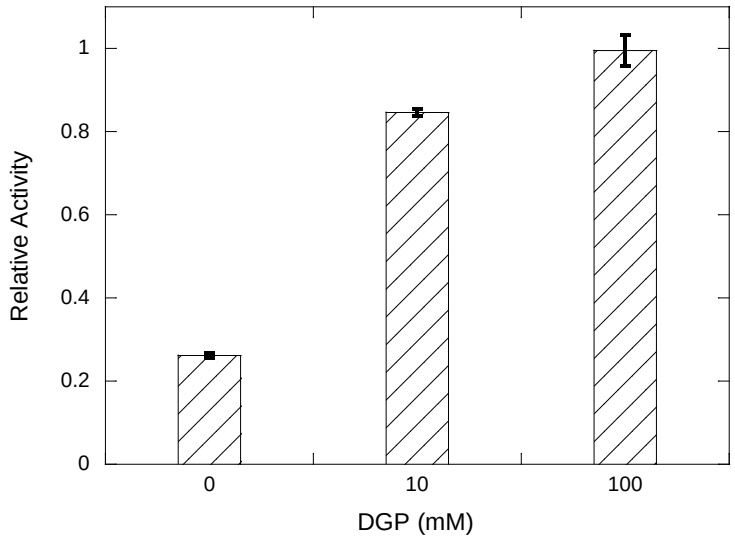

Figure 5.2 Effect of DGP on the residual activity of *A. fulgidus* IMPase that has been heated at 90°C for 30 min, then cooled and assayed at 85°C

The IMPase protein thermal stability in the absence or presence of DGP was also examined by measuring the melting temperature (T_m) of the protein using circular dichroism (CD) spectrometry. With 10 mM DGP (enough DIP to bind in the IMPase active site), the operational T_m of the protein increased from 89°C to above 95°C (Figure 3). This result suggested that by binding in the active site, DGP helps maintain the protein secondary structure when the temperature is increased. The enhanced stability by DIP is very substantial. It should be mentioned that when the IMPase alone was heated to 89°C, about 50% of the secondary structure was lost (Figure 5.3 upper), while heating 30 min at 90°C caused the protein to lose nearly all its enzymatic activity. This finding suggested that specific regions of the tertiary structure, and perhaps quaternary structure (integrity of the dimer), may be critical for the enzyme activity.

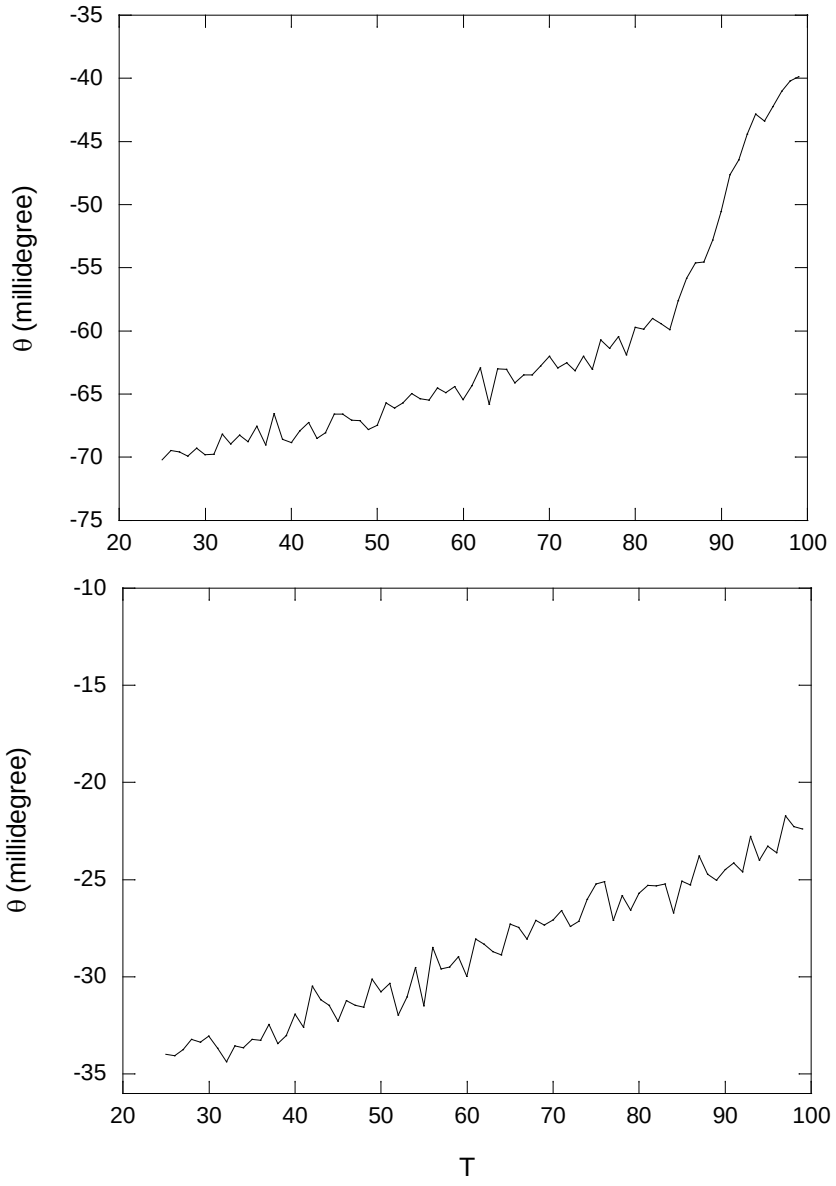

Figure 5.3 Thermal stability of *A. fulgidus* IMPase in the absence (upper panel) and presence (bottom panel) of 10 mM DGP. The protein ellipticity in millidegrees at 222nm was measured by CD spectroscopy as a function of temperature. The protein concentrations in these two experiments are 0.07 mg/ml and 0.04 mg/ml in 1ml 0.01M borate buffer, pH8.0.

5.2.3 Effects of common compatible solutes

Besides DIP and DGP, *A. fulgidus* also accumulates glutamate ions as one of its osmolytes (Martins et al, 1997). Could glutamate as well as other common amino acid compatible solutes have any thermoprotective effects on the IMPase? The results should reflect any specificity in how the compatible solutes protect this particular protein and might be useful in explaining the solute accumulation preferences of this organism. We measured the residual activity of the protein after heating at 90°C for 30 min with or without KCl, proline, glycine betaine, Na^+-glutamate, K^+-glutamate, Na^+-aspartate and K^+-aspartate with concentrations of solutes as high as 0.5 M (Figure 5.4). After heating, the activity of the heated protein was 25% of that of the untreated protein. Proline and glycine betaine offered little thermoprotection. Even at 500 mM, these two solutes could only increase the residual activity from 25 to 50% of the untreated protein. KCl showed a similar extent of protection to proline and betaine at low concentration with 30% residual activity observed with 100 mM KCl present. Better thermoprotection was observed when KCl was 500 mM (65% residual activity). K^+-Glu, Na^+-Glu, K^+-Asp and Na^+-Asp showed similar thermoprotection profiles for the IMPase. Increasing solute concentration from 0.05 M, where residual activity was 30%-40%, to 0.5 M yielded residual activities >90%.

As part of the controls in these experiments, we tested the effects of high concentrations of different solutes in the standard enzyme assay at 85^{o}C. Under these conditions, Glu could inhibit IMPase activity but not strongly. With 20 mM of Glu present, IMPase activity was 80% that of enzyme in the absence of Glu in the assay mixture; 300 mM Glu diminished the enzyme activity to 50%. The Glu inhibition might suggest Glu could also

bind into the protein active site albeit weakly, perhaps achieving thermoprotection by a mechanism similar to that of DGP.

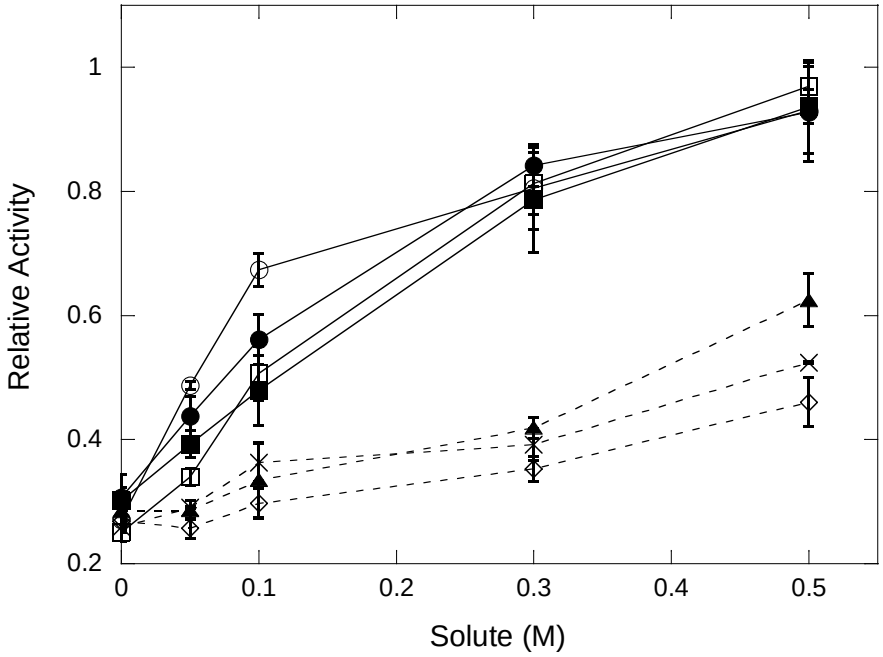

Figure 5.4 Effect of solutes on the residual activity of *A. fulgidus* IMPase, heated to 90 °C for 30 minutes, then cooled and assayed at 85°C: ▲, KCl; Δ, NaCl; ■, K^+-glutamate; □, Na^+-glutamate; ●, K^+-aspartate; ○, Na^+-aspartate; ◊, proline; ×, betaine.

For this enzyme, all the effective thermoprotective solutes are anions – either phosphodiesters or dicarboxylate amino acids. In order to test if the two carboxylates in Asp and Glu were the key features for thermal protection in this class of solutes, we measured the thermoprotective effect on IMPase of a number of other dicarboxylates (tartrate, succinate, methyl-succinate, maleate and fumarate) along with isocitrate, a tricarboxylate. All the dicarboxylate molecules showed very similar thermoprotection patterns. Interestingly, the tricarboxylate isocitrate had no protective effect, and in fact appeared to destabilize the enzyme to heating (Figure 5.5). With 300 mM of these

dicarboxylates present, the protein residual activity after heating was 70 to 90% compared to the 25% without solutes. Isocitrate did not inhibit the enzyme in standard enzyme assays (the enzyme is not heat deactivated), implying it could not bind to / near the active site. In the presence of 130 mM isocitrate, IMPase still had 70% residual activity at 85^{o}C when compared to enzyme in the absence of solutes. For the other dicarboxylates tested, around 20 mM of dicarboxylates present did not change the protein activity very much.

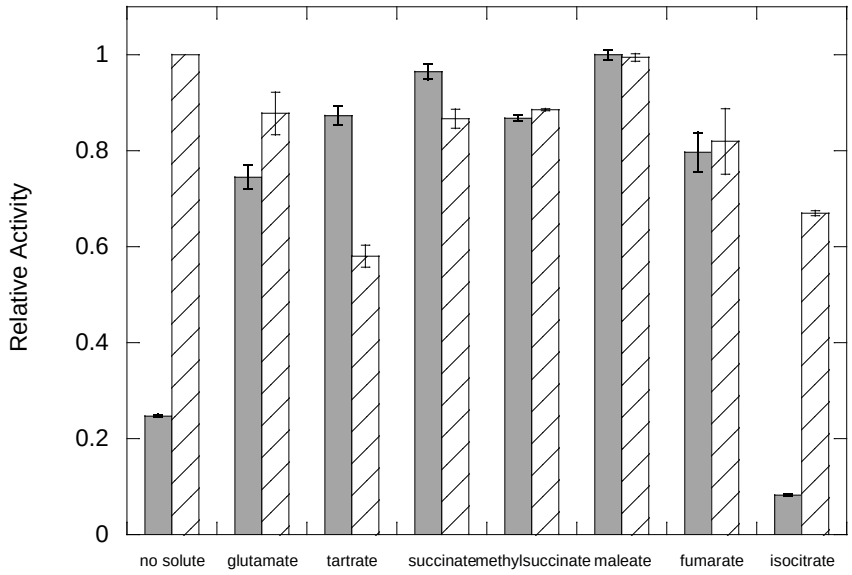

Figure 5.5 Effect of 300 mM dicarboxylates on the residual activity of *A. fulgidus* IMPase heated to 90 °C for 30 minutes, then cooled and assayed at 85°C (solid columns); The relative activities of untreated IMPase in the presence of 24 mM glutamate, 24 mM tartrate, 18 mM succinate, 12 mM methylsuccinate, 12 mM maleate, 18 mM fumarate and 130 mM isocitrate are shown by the hatched columns.

5.2.4 Crystal structures of IMPase with Glu and NMR validation of Glu binding sites

The crystal structures of *A. fulgidus* IMPase with 25 or 400 mM Glu were solved in our laboratory (Goldstein, R. Ph.D. thesis) as an attempt to explore where, if at all, Glu binds to the IMPase. In the structure of the IMPase protein cocrystallized with 400 mM Glu, each monomer of the protein dimer had four glutamate ions bound. As shown in Figure 5.6, two Glu ions (Glu1 and Glu2) are bound in well-defined cationic pockets, one between Arg11 and Arg18, the other interacting with Arg92, Asn151, Arg165 and Lys164. Glutamates occupying these two binding sites were also observed in the crystal structure of the IMPase co-crystallized with 25 mM Glu. Two other Glu anions, only observed in the structure with 400 mM Glu, were bound in the dimer interface region and participated in an extensive hydrogen bonding network in the IMPase structure: Glu3 interacted electrostatically with Arg18 and Glu4 with Arg29. Since Glu3 and Glu4 binding sites were empty in the structure of IMPase with 25 mM Glu, these must be weaker affinity sites. Interestingly, *none* of the Glu anions visualized in the crystal structures were in the active site.

The crystal structures identified specific binding sites for Glu on the IMPase protein, but at low temperature compared to the growth temperature of the organism. Occupation of a binding site in a crystal does not necessarily mean the same site is occupied in solution or at higher temperatures. To demonstrate Glu ions were bound to the protein in solution, we used high resolution ^{13}C field cycling NMR to detect [1-^{13}C]Glu binding. Since the binding is thought to be moderately weak, the sensitivity for detecting interactions was dramatically enhanced by using IMPase spin-labeled on cysteine residues with MTSL. The 1000-fold larger dipole for an unpaired electron compared to a ^{1}H means that it will

dominate the dipolar relaxation of any nearby nuclei. When a ligand is bound to the protein it is relaxed by the spin-label, but when it is free in solution that interaction is lost. What is observed is a weight averaged relaxation rate. The closer the spin-label is to nuclei of the bound ligand, the greater the relaxation. Binding is detected by an increase in R_1 due to the spin-labeled protein. Since dipolar relaxation for ^{13}C-carbonyls is not very effective (the carbonyl carbon of Glu has no directly bonded protons), it is easy to detect a low field rise (where the relaxation is dipolar and not chemical shift anisotropy) if binding occurs (Pu et al, 2009b).

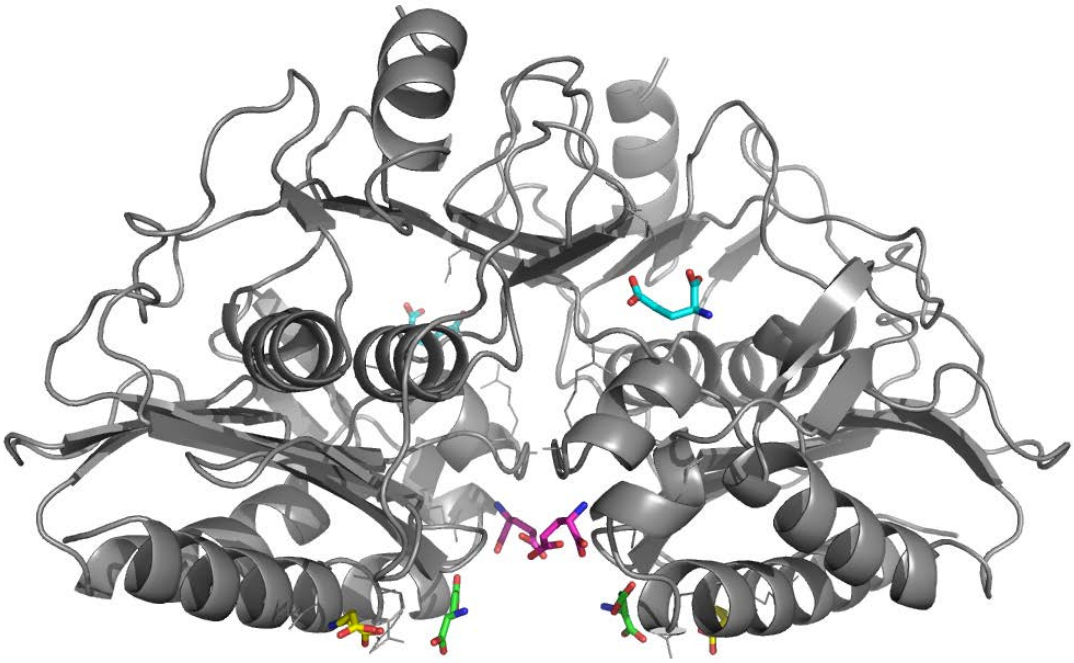

Figure 5.6 Crystal structure of *A. fulgidus* IMPase co-crystallized with 400 mM sodium glutamate. The protein dimer structure is shown in grey; Glu1 is in yellow, Glu2 in cyan, Glu3 in magenta, and Glu4 is shown in green.

Each IMPase monomer contains 4 cysteines (Figure 5.7). As shown before, Cys150 and Cys186, which are in close proximity (S atoms within 4 Å of one another) form a disulfide bond when the protein was oxidized; this abolishes enzyme activity (Stieglitz, 2003). These two cysteines are difficult to chemically modify with sulfhydryl reagents. The other two cysteines, Cys102 and Cys177, are readily accessible to thiol reagents; their modification does not inactivate the enzyme. After treating IMPase with MTSL, each monomer of the dimeric protein should have a nitroxide attached to Cys102 and Cys177. Although the spin-labels on these two Cys are not directly next to any of the potential Glu binding sites, one of them (Cys177) is close enough for the unpaired electron to contribute to the low field dipolar relaxation of Glu ligands that bind to the protein. As shown in Figure 5.7, one of the spin-labels is closest to the Glu3 site (one of the 'weak' sites in the crystal structure), but it is also not that far from Glu2, a tight site occupied in the crystal structure with 'low' (0.025 M) Glu and a bit further from the other sites. Furthermore, the spin-label on one monomer is close to the Glu3 on each monomer, so when this weaker affinity site is occupied, there should be substantial relaxation of the ^{13}C by the spin-label (i.e., at high Glu). Neither spin-label is very close to Glu1 and Glu4 sites, although there may be some effect on relaxation of Glu that bind here. The other labeled Cys is far from all the Glu sites and since R_1 due to the unpaired electron depends on r^{-6}, it will not have much of an effect on Glu occupying any of the binding sites.

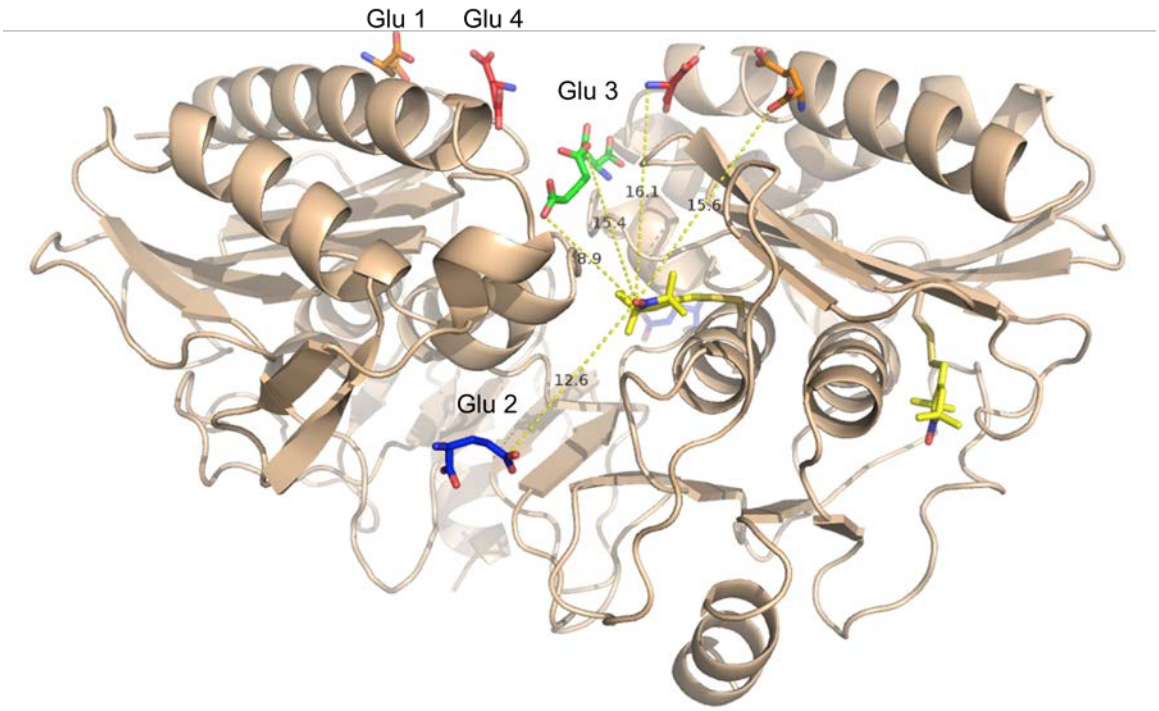

Figure 5.7 *A. fulgidus* IMPase dimer showing the four glutamate binding sites on the protein (where orange, blue, green and red Glus bind) and the two Cys per monomer that are spin-labeled. The two attached nitroxide structures are shown as yellow sticks on one of the monomers (Goldstein, R., Ph.D. thesis)

The ^{13}C-labeled carbonyl carbon of Glu has no directly bonded protons, so its dipolar relaxation is not very effective, and R_1 is quite low (typically 0.02 s^{-1}) at low fields. In the absence of spin-labeled protein, the R_1 field dependence profile of 25 mM α-^{13}C-Glu (Figure 5.8) shows no low field rise, indicative of the small molecule binding to the much larger protein. Even with unlabeled IMPase added, there is no significant effect of the protein on R_1. However, with the spin-labeled protein, there is a detectable rise in R_1 below 4 T that reflects Glu binding to the protein. For the initial experiment, 10 mM Glu was used and 1 mg/ ml (0.036 mM) of the spin-labeled protein (Figure 5.9). The field dependence of the ^{13}C-Glu R_1 was measured at 25°C. With 10 mM Glu, at most Glu will occupy sites 1 and 2 if the Glu sites seen in the crystal structure are also occupied in

solution. As seen in Figure 5.9A, there is a small but measurable increase in R_1 below 4T compared to the sample with either unlabeled protein or no IMPase. Extrapolation to zero-field of R_1 yields a parameter, $\Delta R_{C\text{-}e}(0)$, that reflects how close the spin-label is to the α-carbonyl of any bound Glu. This small effect suggested that a larger amount of ^{13}C-Glu (for better signal-to-noise and also to perhaps increase occupancy of Glu binding sites on the protein) and spin-labeled protein (to make sure a robust PRE was seen) should be used.

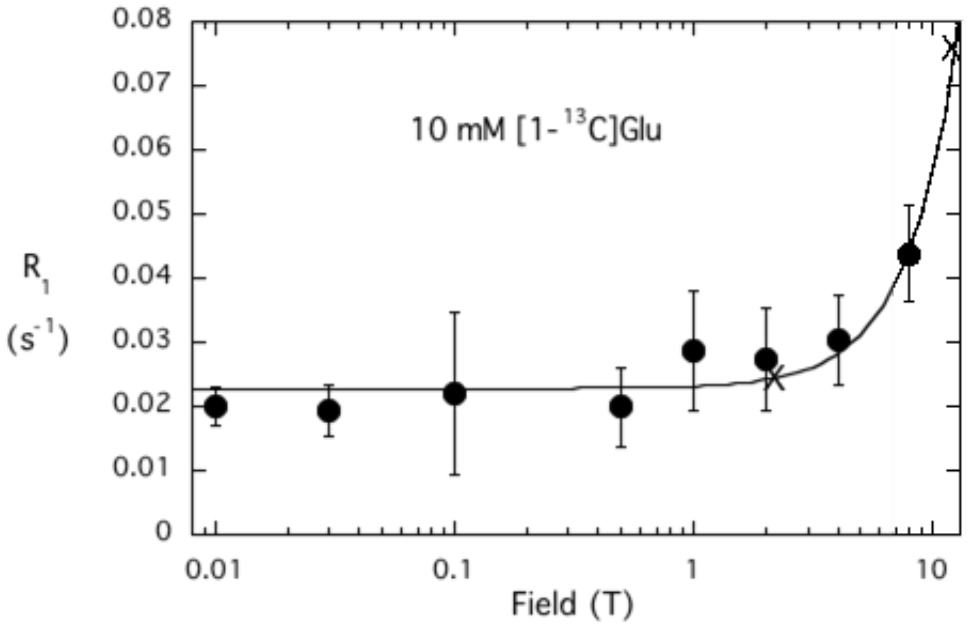

Figure 5.8 Spin-lattice relaxation rate for free α-^{13}C-labeled Glu in the absence (●) and presence (×) of unlabeled IMPase.

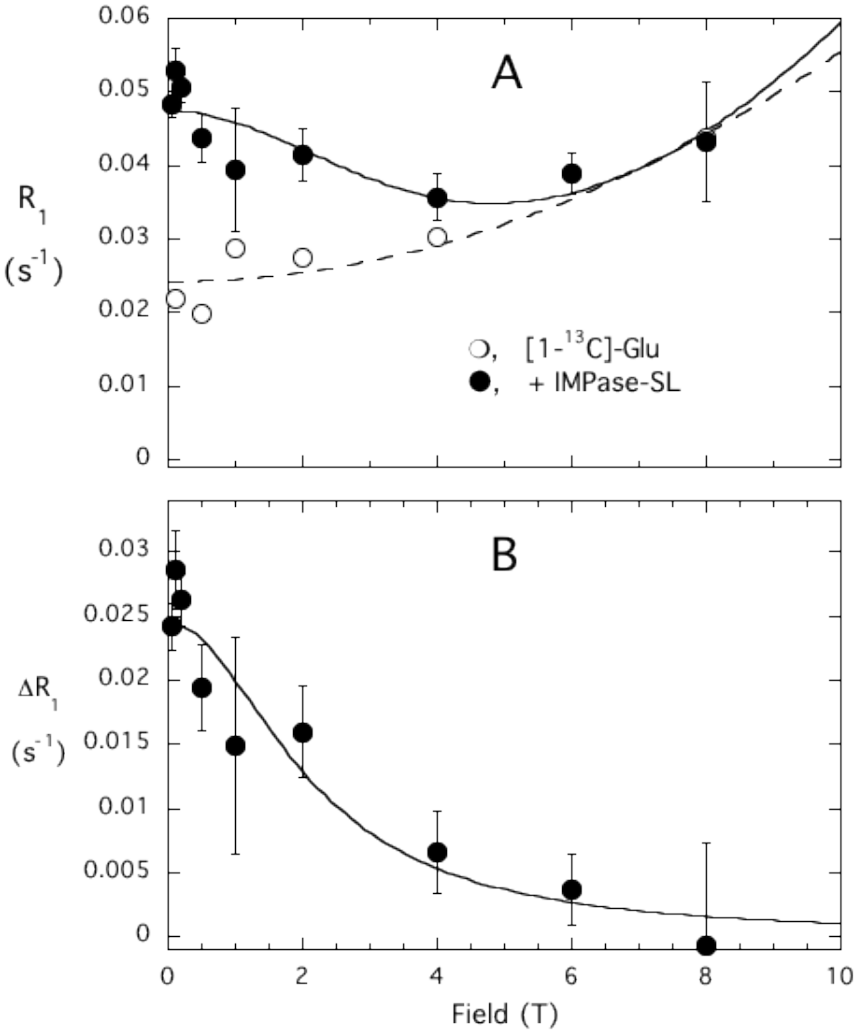

Figure 5.9 (A) Spin-lattice relaxation rate, R_1, for the ^{13}C-labeled α-carboxylate of glutamate as a function of magnetic field in the absence (○) and presence (●) of spin-labeled IMPase (1 mg/ml = 0.036 mM). (B) The relaxation rate, $\Delta R_1 = R_{1(+IMPase\text{-}SL)} - R_{1(-IMPase)}$, specifically attributed to the presence of the spin-labeled protein.

Figure 5.10A shows ΔR_1 as a function of field for 25 mM ^{13}C-Glu in the presence of 3 mg/ml (0.11 mM) spin-labeled IMPase. The profile is shown for two temperatures, 25 and 45^{o}C. Although the correlation times for the interaction have a fair amount of error, the $\Delta R_{C\text{-}e}(0)$ values are clearly different. Increasing the temperature appears to populate more Glu sites on the protein. We can also show that the effect is specific to protein

binding. Alanine is neither an osmolyte nor a ligand for the IMPase. In a sample of 25 mM α-^{13}C-alanine and α-^{13}C-glumatate, the low field rise is significant for the Glu whereas only a very small effect (within the error in measuring the relaxation rates) is seen for Ala (Figure 5.10B).

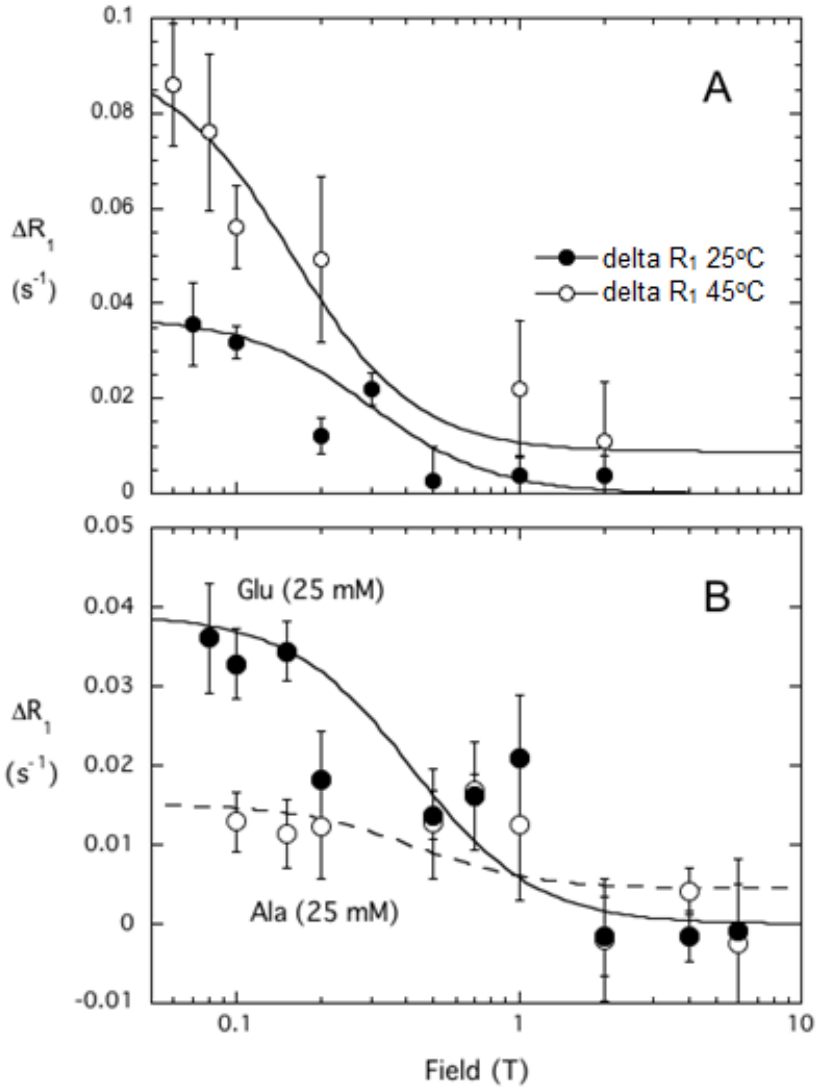

Figure 5.10 (A) Spin-lattice relaxation rate attributed to spin-label, ΔR_1, for the ^{13}C-labeled α-carboxylate of 25 mM glutamate at 25 and 45°C. (B) ΔR_1 for 25 mM glutamate (●) or alanine (○) as a function of magnetic field in the presence spin-labeled IMPase (3 mg/ml = 0.11 mM)

We can get a sense as to average binding affinities of Glu for the IMPase by determining $\Delta R_{C\text{-}e}(0)$ for different concentrations of Glu and normalizing the value to the ratio of Glu to spin-labeled protein. The resultant parameter, $v_{C\text{-}e}$, is a normalized measure of Glu binding (somewhat like the specific activity of an enzyme (Pu et al, 2009b)). If there were a single site, the dependence of this on Glu concentration should saturate.

$$v_{C\text{-}e} = \frac{[\text{Glu}]}{[\text{IMPase-SL}]} \times \Delta R_{C\text{-}e}(0)$$

If there are multiple Glu sites with not only different affinities but different distances from spin-labels the concentration dependence will be much more complex. As shown in Figure 5.11, the plot of $v_{C\text{-}e}$ versus [Glu] is neither hyperbolic (for a single Glu site) or sigmoidal, but rather shows two distinct regimes. Below 30 mM the dependence of $v_{C\text{-}e}$, on glutamate concentration is approximately hyperbolic. At higher concentrations there is a much steeper rise in this parameter that does not look hyperbolic. It likely represents occupation of a weak site that is fairly close to the spin-label, most likely Glu-3. Thus, the field cycling ^{13}C-NMR experiments show that (i) multiple Glu with different affinities bind to the spin-labeled IMPase in solution, and (ii) a weak site is closer to the spin-label (on Cys177) than to either tight Glu site.

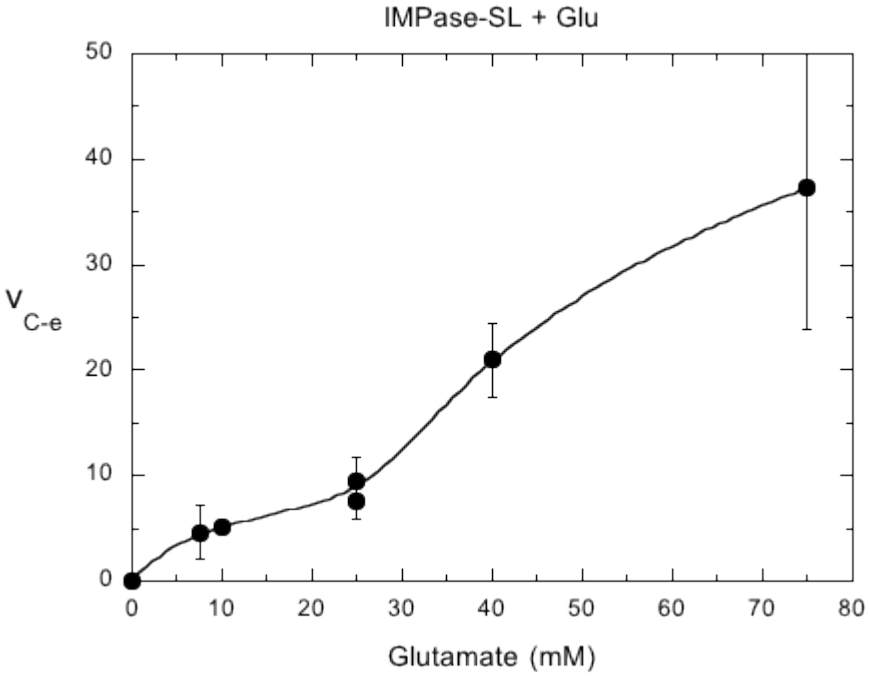

Figure 5.11 Binding of [1-^{13}C]Glu to spin-labeled IMPase (0.1 mM) as a function of glutamate concentration.

5.2.5 Mutation of Glu binding sites and effect on thermoprotection by Glu

In order to see if the specific binding of Glu correlates with its thermoprotection of the IMPase, mutations were constructed to remove each of the specific Glu binding sites. Single mutants, R18A, R29A, R92Q, K164E, double mutant R11A/R18A, R92Q/K164E, and quadruple mutant R11A/R18A/R92Q/K164E were produced. As used with wild type protein, field cycling ^{13}C NMR was also used to detect if the Glu binding was lost by disruption of the interaction between the protein side chains and glutamate ions. The mutant IMPase R92Q/K164E was constructed to remove the 'tight' Glu 2 binding site. This is not the closest Glu to the spin-label sites in the structure, so one would expect that ^{13}C-Glu is still able to bind to some sites and is relaxed. When this mutant protein, which is essentially as active as wild type IMPase, was spin-labeled and then used in an field cycling-C-NMR experiments, there was about a 40% decrease in $\Delta R_{C\text{-}e}(0)$ (Figure 5.12).

This indicates that relaxation of 'tightly' bound Glu 2 contributes significantly to overall ^{13}C-Glu relaxation. The rest of the relaxation has contributions from Glu 1, likely significantly occupied, and perhaps a smaller amount from partially occupied Glu at sites 3 and 4. We could even estimate $r_{C\text{-}e}$, as long as 25 mM Glu saturated site 2.

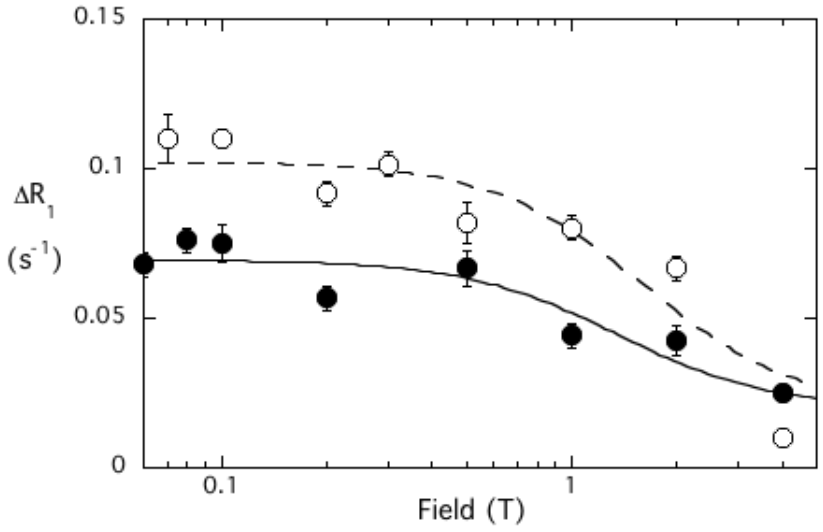

Figure 5.12 R_1 for 25 mM α-^{13}C-Glu as a function of field with 0.1 mM spin-labeled (○) IMPase or (●) R92Q/K164E.

Before we tested the Glu and Asp effect on the mutant proteins, the mutant protein thermal stability in terms of the melting temperature (T_m) was first measured by CD spectrometry. Surprisingly, except for a single variant (K164E) all mutations of the Glu binding sites decreased the protein T_m by 7 to 20°C compared to the protein wild type (Table 5.1), with R11A/R18A and the quadruple mutant having the lowest melting temperature, 69°C, which is 20°C lower than that of protein wild type. This is a striking result since the mostly cationic residues modified are on the surface of the IMPase. K164E had higher T_m, $\geq$ 95°C, which could not be measured accurately. Initially in studying this enzyme, we purposely tried to reduce the T_m by replacing large aliphatic

groups in secondary structure with alanine, an approach thought to reduce overall protein stability (Szilagyi & Zavodszky, 2000). Mutations of internal hydrophobic residues to Ala included L57A, V142A and L148A. These three hydrophobic mutant proteins showed little effect on T_m, at most a 5° drop (Table 5.1).

Table 5.1 Mid-point of the thermal denaturation temperature (T_m) of *A. fulgidus* IMPase wild type and mutants determined from CD measurements at 222 nm as a function of temperature. The denaturation is irreversible so the apparent T_m cannot yield a true thermodynamic parameter but serves as a way to compare mutant protein stability to wild type protein (WT). The Glu binding site(s) thought to be disrupted by the mutation are indicated.

A. fulgidus IMPase	T_m °C	Glu binding site disrupted
WT	89	
R18A	85	Glu3
R29A	82	Glu4
R92Q	75	Glu2
K164E	~95	Glu2
R11A/R18A	69	Glu1
R92Q/K164E	71	Glu2
R11A/R18A/R92Q/K164E	68	All sites
L57A	84	
V142A	89	
L148A	89	

The effect of mutations on the T_m complicated testing for thermoprotection by Glu. In order to test if the loss of Glu binding sites causes the loss of Glu thermoprotection, we first adjusted the heating temperature for every mutant so that all mutants except K164E had 25% residual activity detected after heating for 26-30 min without any Glu or Asp anions. Next we tested the thermoprotective effect of Glu and Asp on all these variants except K164E. The mutant proteins were all still well protected by Na^+-Glu and Na^+-Asp

with the solute concentration dependence similar to the wild type protein. With 100 mM Glu or Asp present, at least 50% residual activity was observed; with 500 mM solutes, the mutant protein activity after heating was completely recovered (Figure 5.12). Since

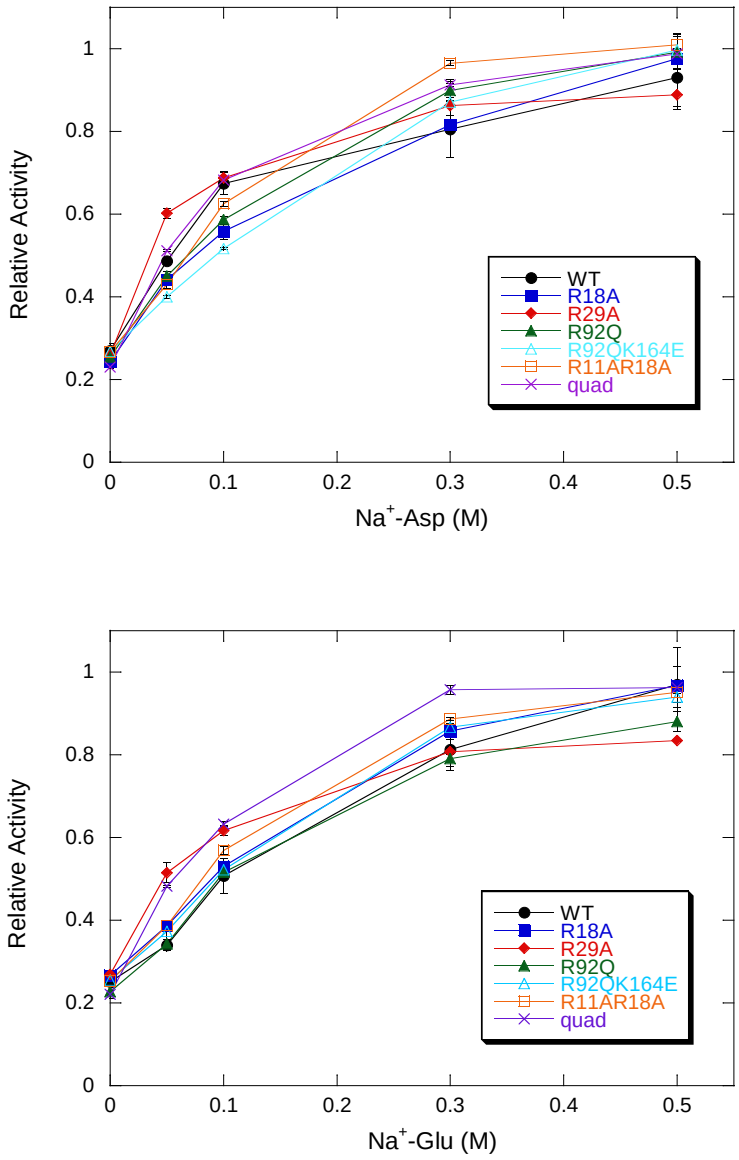

Figure 5.13 Effect of sodium aspartate (upper panel) and sodium glutamate (bottom panel) on the residual activity of *A. fulgidus* IMPase wild type (●), R18A (■), R29A (♦), R92Q (▲), R11A/R18A (□), R92Q/K164E (Δ) and R11A/R18A/R92Q/K164E (×).

the thermal stability of the K164E variant was better than that of the wild type protein (after heating at 95°C for 30 min, 60% residual activity was seen in the absence of solutes), we could not test if Glu and Asp still had any thermoprotective ability.

The experiments with these Glu-site mutants indicated that although Glu ions could bind to IMPase protein at very specific sites, those binding sites could not account for the Glu and Asp thermoprotection. Rather, the residues in these sites were important for maintaining the protein stability. For Glu binding site mutants, Glu still protected the enzymes from thermal denaturation, although the mutants were as not as thermally stable as the protein wild type.

5.3 Discussion

For all three kingdoms of life, it is necessary to adapt to environmental fluctuation, such as changes in temperature, salinity, pH or pressure. Organisms in all three kingdoms (archaea, bacteria and eukaryotes) accumulate compatible solutes as part of the response to these environmental changes (Burg & Ferraris, 2008). There are some compatible solutes that are seen everywhere - glutamate and betaine are accumulated by representative organisms in all domains while other osmolytes are only accumulated by a subset of organism. A good example of the latter is the accumulation of DIP and DGP by thermophiles and hyperthermophiles (Santos & da Costa, 2002). In general, methanogens prefer to accumulate organic anions under high salt stress, and one often sees a switch in the osmolyte composition from zwitterionic and nonionic solutes to anions with increasing salt (Ciulla et al, 1994; Robertson & Roberts, 1991). The reasons for this specificity of osmolytes accumulation are not known, although it has been suggested that evolutionary selection is the origin of this specificity (Santos et al, 2011). Along with

understanding the effects of specific solutes, the study of how compatible solutes stabilize proteins has much practical use. Compatible solutes could help protein folding and suppress protein aggregation, thus they could be used as additives to enhance protein expression *in vitro*, or as potential therapeutic agents for diseases caused by protein folding defects or protein aggregation (Rajan et al, 2011). In this project, we studied compatible solute thermoprotection effects on the model enzyme IMPase from the archaeon *Archaeoglobus fulgidus*.

5.3.1 DIP – a solute generated in response to very high temperatures

First we tested an unusual compatible solute, DIP, restricted to hyperthermophiles. Although L,D-DIP is now generally accepted as the natural product accumulated by hyperthemophiles (Rodionov et al, 2007), our studies of DIP thermoprotection of *A. fulgidus* IMPase showed both the L,D-DIP and L,L-DIP had similar effects. Both of these two enantiomers protected the IMPase enzyme from thermal denaturation. Since both molecules were effective, either the stereochemistry of this compatible solute is not critical or only part of the molecule (perhaps only one of the inositol rings and the phosphate) is important in thermoprotection. The latter could be the case if the DIP interacted with the protein active site which has room for one inositol ring but not two. More generally, the fact that the two DIP enantiomers were more or less equivalent is very intriguing since it suggests that the lack of chirality of the natural product, at least in this case, arises from biological synthetic convenience, not the more conventional thought of evolutionary optimization. Neither *myo*-inositol or dimethylphosphate had any thermprotective effect in the same conditions, an indication that something binding to the active site or a negative charge (in this case another phosphodiester) are the critical

components of DIP thermoprotection, For this system, there is concrete evidence for compatible solute specificity in acting as a thermoprotectant for the *A. fulgidus* IMPase.

DIP thermprotection of other proteins has been reported. For example, 115 mM DIP could enhance the thermal stability of glyceraldehyde-3-phosphate dehydrogenase (Scholz et al, 1992). But it is also surprising that in some cases DIP destabilizes proteins. The study of DIP effects on the model enzyme rabbit muscle lactate dehydrogenase (LDH) showed LDH residual activity after heating with DIP present was much less than that when the protein was heated alone, although they also mentioned that the thermostabilization effect of a compatible solute was dependent on the experimental conditions used in measuring (Borges et al, 2002). So the effect of DIP may depend on individual enzyme. Nonetheless it should be stressed that DIP is specifically accumulated in hyperthermophiles when subjected to supraoptimal temperatures. It is a complex solute to synthesize needing as starting material two glucose-6-phosphate and a CTP molecule. Given that high energy cost, it must be very effective in the organisms that accumulate it, although we do not have details about its mechanism of thermoprotection.

Detailed studies supporting the osmophobic or osmolyte effect have suggested that the hydrogen bonding between the protein backbone and the solvent plays a crucial role in determining if an osmolyte is protective to protein or not (Bolen & Rose, 2008). When transferring the protein from buffer solution to osmolyte solution, the overall transfer free energy is determined by the free energy of transferring protein backbone from aqueous solution to the osmolyte solution, which is in turn controlled by the free energy difference between forming the backbone-solvent hydrogen bonds and the backbone-backbone hydrogen bonds. In aqueous solution, since forming intramolecular hydrogen bonds in

protein is more thermodynamically favorable than forming the hydrogen bonds between the backbone and water, protein is more stable in the folded or native state. The presence of the protecting osmolytes diminishes the water solvent quality that further disfavors the hydrogen bond formation between the protein backbone and solvent, resulting in the stabilization of the protein native state. The ability of an osmolyte to change solvent quality has been confirmed by recent studies, both experimentally (Aioanei et al, 2011) and theoretically (Aioanei et al, 2012). If we apply this theory to our results with DIP, it is possible that increased temperature breaks the hydrogen bonding in proteins to lead to protein denaturation, while DIP enhances intramolecular hydrogen bond formation in the protein thereby stabilizing it in its native state. This enhancement is achieved by lowering the solvent 'quality' of activity. Although the details of this solvent quality change are not known, it is possible that at high temperatures the formation of hydrogen bonds between DIP and water molecules is more favorable than forming hydrogen bonds between water and the protein backbones, which in turn promotes intramolecular bond formation in protein and leads to protein stabilization.

5.3.2 DGP – a very effective thermoprotectant because it binds to the IMPase active site

DGP is the compatible solute accumulated by *A. fulgidus* when the salt concentration in the environment is increased. The intracellular concentration of DGP in *A. fulgidus* grown in high salinity conditions (4.5% NaCl, 76°C) was reported as 1.4 μmol/mg protein, equal to an intracellular concentration of 350 mM (Lamosa et al, 2000). Our DGP studies suggested that this molecule is an excellent thermoprotectant of the IMPase. However, if the intracellular DGP concentration is 100 mM or higher (as suggested from

analyses of osmolyte content in *A. fulgidus*), the enzymatic activity of the IMPase would be extremely low because DGP is such an effective inhibitor of the enzyme. This observation may explain why intracellular DIP concentration does not increase dramatically when the external salt concentration is increased.

The highly protective effect of DGP has been reported for other proteins. 100 to 200 mM DGP minimized the activity lost by rabbit muscle LDH and baker's yeast alcohol dehydrogenase (ADH) upon heating (Lamosa et al, 2000). Similar concentrations of DGP (100 mM) also protected *Desulfovibrio gigas* rubredoxin for thermal denaturation (Lamosa et al, 2000; Lamosa et al, 2003). By using computational methods, researchers suggested DGP protected *D. gigas* rubredoxin by specifically binding to a loop which was important for protein activity and restraining its movement in order to retain the protein activity during heating (Micaelo et al, 2008).

Our kinetic studies provide evidence that DGP can bind into the active site of IMPase. The crystal structure of DGP with IMPase (Goldstein, R., unpublished) had a DGP molecule in the active site in each monomer. The increase in the protein denaturation temperature with DGP present (form 89 to >95^{o}C) indicated that DGP bound at the active site stabilizes the protein secondary structure during heating. These observations provide a likely mechanism for DGP thermoprotection of *A. fulgidus* IMPase. At high temperatures, DGP binds into the protein active site and increases the overall protein stability so that much higher temperatures would be needed for heat denaturation. Relatively little (compared to typical osmolyte concentrations) DGP is needed to stabilize the IMPase. DGP may be critical to the survival of the *A. fulgidus* at 90°C as it starts to divert resources to synthesizing DIP. DGP protection of rubredoxin suggested rigidifying

the protein is the critical event. DGP could have a similar effect on IMPase, possibly by binding in the active site and restricting motion of a mobile loop that contributes a ligand for Mg^{2+} binding (Li et al, 2010).

Glutamate ions could also protect IMPase from thermal denaturation. Since Glu is accumulated by this organism (Martins et al, 1997), this solute also aids in thermal stabilization. In fact, Glu is one of the common ions used in all three domains of life to counteract osmotic and thermal stress. However, Glu was not an effective compatible solute for IMPase once a large amount of loss of secondary structure occurred. When the cells were incubated for 30 min at 95^{o}C, the unfolding transition with a T_m of 89°C, was nearly complete. We showed that when the protein was heated to 95^{o}C, very little enzymatic activity was recovered if the denaturation was done with glutamate. In contrast, heating with DIP served as a much more effective thermoprotectant. Heating the sample to 90^{o}C leads to loss of a little over half the secondary structure and loss of most of the catalytic activity. Under these conditions, the presence of glutamate could stabilize the protein. However, 300 mM Glu was needed to protect the protein to the same extent as 10 mM DGP.

The identification of Glu binding sites on the IMPase by crystallography can provide insight into the specificity of compatible solutes in protecting a particular protein, although the conditions were very different for measuring Glu protection of enzymatic activity and for obtaining a crystal and collecting diffraction data (done in cryo conditions). Glu thermoprotection residual activities were assayed at 85°C, while protein was crystallized with Glu at 20°C. Glu sites in a crystal may not be occupied at high temperatures. ^{13}C field cycling NMR experiments showed two types of sites exist in

solution ant up to 45^{o}C. At the moment that is the safe upper temperature limit for cycling, although current alterations of the machine may allow us to examine data up to 65^{o} and possibly higher. Increasing the temperature often weakens the binding of ligands to a protein, and this could be the case here. Further studies are warranted in exploring this aspect of Glu sites on the *A. fulgidus* IMPase.

One of the surprising outcomes of this work was that the mutation of several of the Glu binding sites dramatically reduced IMPase thermal stability. Normally it is suggested that thermophilic proteins have higher stability by reducing the size of any cavities, the length of surface loops, and increasing the number of salt bridges or hydrophobic contacts (Szilagyi & Zavodszky, 2000). Our results link surface cationic sites to thermal stability of the native protein. The only exception to a decrease in T_m in the series of mutants that we examined was K164E. Its T_m increased compared to normal protein. The reason for this is clear when one examines the crystal structure of this protein. An additional salt bridge can be formed by the new Glu residue at position 164 with Arg165. Adding two salt bridges in the dimer significantly enhances IMPase stability.

According to conventional wisdom, mutation of internal hydrophobic residues (Val, Leu and Ile) to Ala should reduce the hydrophobic contacts in the protein and lead to destabilization. We created several of these mutations to destabilize the IMPase. L57A was the only one with a significantly lower denaturation temperature. However, this mutation only reduced T_m by 5°C. In contrast, mutation at a Glu binding site could reduce T_m by as much as 20°C, which was very surprising. It was reported that mutation of charged surface residues of *Alicyclobacillus acidocaldarius* esterase 2 disrupted the ion network on the protein surface and reduced T_m of the protein (Pezzullo et al, 2013). But

for R11A/R18A mutant, which had the lowest T_m, the sites for Arg11 and Arg18 are on the protein surface and not involved in any salt bridges with other residues. Therefore, using salt bridge disruption to explain what we observed for the IMPase T_m change is not viable. Superimposition of the crystal structure of R11A/R18A with that of wild type protein shows little difference, so the decreased T_m is not caused by structural change of the protein. One possible explanation that cannot be excluded is that an important water network that links the two monomers in the dimer is linked to these Arg on helix A, and once disrupted the protein is less stable. Another possible explanation is that mutation of surface arginines to alanines increases the likelihood of IMPase aggregation as some regions of the protein unfold transiently at high temperatures.

The results of the thermoprotection of the Glu mutants were equally surprising. Crystal structures of the mutants clearly indicated the loss of specific Glu binding sites. In one mutant (R11A/R18A) three of the four Glu sites were abolished (R. Goldstein, Ph.D. thesis). Thus, the Glu sites we see in the crystal do not appear to be directly linked to thermoprotection. However, in the Glu thermoprotection assay controls, we noticed that high concentrations of Glu could inhibit IMPase activity. Furthermore, a crystal structure of IMPase wild type protein with Asp, which also protected protein, showed that an Asp molecule occupied the active site (R. Goldstein, Ph.D. thesis). These results suggested Glu might protect IMPase in the similar way to DGP – it works by binding around or in the active site to stabilize the protein, possibly by restraining the mobile active site loop that provides a ligand for one of the three Mg^{2+}. Since the affinity of Glu for the protein active site, as measured by inhibition of catalytic activity, is weaker than that of DGP, it would be expected to be a less potent thermoprotectant. However, Asp is a more potent

inhibitor of IMPase activity but has the same thermoprotective effect as Glu. This would argue that active site binding is not necessarily the only reason behind thermoprotection.

For the archaeal IMPase proteins that have higher thermal stabilities, it was suggested that it was due to a shorter mobile active site loop (Stieglitz et al, 2002) (Figure 5.14). This mobile loop is important for metal ion binding and protein activity (Li et al, 2010). When protein bound to substrate and metal ions, the mobile loop became less flexible and structured (Stieglitz et al, 2002). Glu (and other solutes) may interact with this loop at higher temperatures to stabilize the protein structure during heating (Figure 5.14 left). It is difficult to demonstrate involvement of the mobile loop in compatible solute thermoprotection, since mutations in this mobile loop will lower the protein activity. Although we did not detect a bound Glu interacting with this mobile loop in the crystal structure, the mobile loop of *A. fulgidus* IMPase contains two lysines at residues 37 and 43, and Lys31 occurs right before the beginning of the mobile loop (Figure 5.14 right). It is possible that at very high temperatures transient interactions between Glu anions and the mobile loop occur.

There is well-defined specificity in what solutes protect this IMPase. Diverse dicarboxylates protected IMPase protein from thermal denaturation, while monocarboxylates (betaine, proline, acetate) or a tricarboxylate (isocitrate) could not. It has been noted that negatively charged compatible solutes provide better protection of proteins from thermophiles than neutral / zwitterionic ones (Borges et al, 2002; Santos et al, 2011). In our experimental conditions, all these carboxylates were negatively charged (heating and residual activity measurement were conducted at pH 8). The isocitrate anions even had three negatively charged carboxylates, so just a net negative charge

could not explain the difference in effectiveness of thermoprotection. It is possible (and in fact probable) that the non-amino acid dicarboxylates could bind to the Glu binding sites on the IMPase. However, binding of Glu at those sites does not correlate with thermoprotection. Perhaps dicarboxylates can interact weakly with the mobile loop and reduce its flexibility, while the isocitrate can chelate Mg^{2+} if it is near the active site and reduce the enzyme activity by depleting the effective concentration of Mg^{2+}, and a monocarboxylate does not had two separate negatively charged groups that appear to be important for thermoprotection.

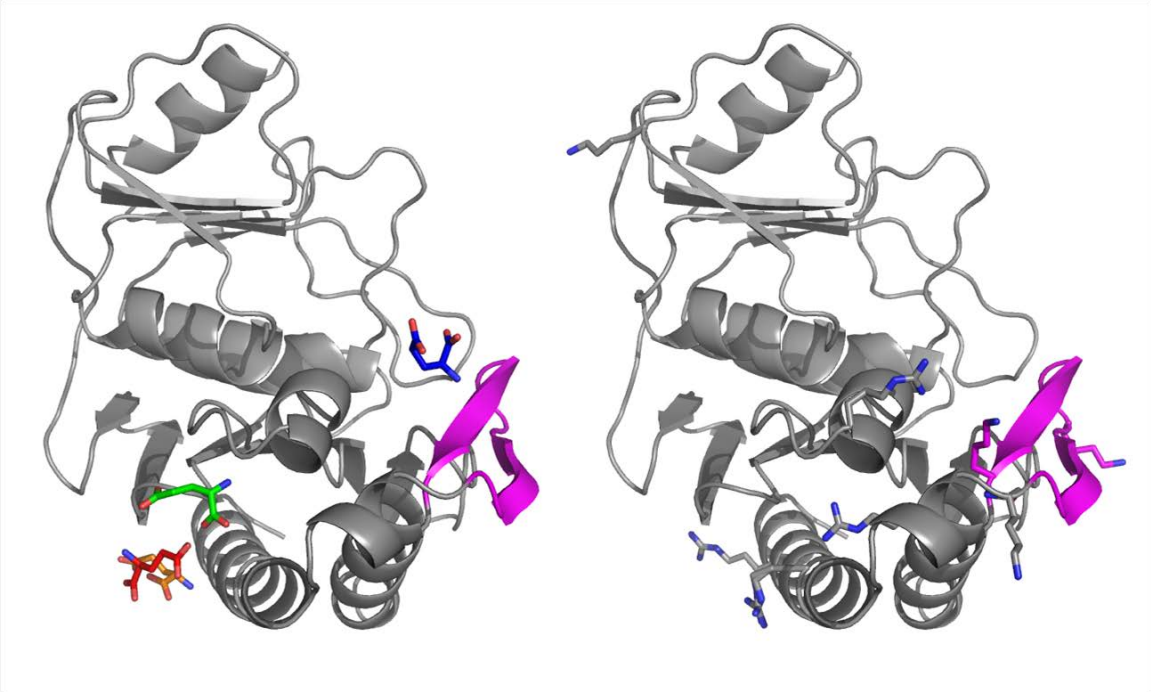

Figure 5.14 Left: IMPase monomer with 4 glutamates (colored orange, blue, green and red) binding. The mobile loop (residue 32-43) is highlighted in magenta. Right: IMPase monomer with mobile loop in magenta. The side chains of Lys37 and Lys43 in the mobile loop as well as Lys 31 before the mobile loop are shown. The side chains of residues Arg11, Arg18, Arg29, Arg92 and Lys164 are also shown with nitrogen atoms colored in blue.

The osmophobic effect theory explains compatible solute thermoprotection in terms of protein folding thermodynamics. The strength of the stabilizing effect of the osmolyte is dependent on the energy difference of the protein backbone interacting with water and with the osmolyte molecules, which was negatively correlated with the fractional polar surface area of an osmolyte. Thermoprotective osmolytes are excluded from the protein surface since their interactions with the protein backbone are less favored than water interacting with backbone (Bolen & Baskakov, 2001; Street et al, 2006). In this study of the thermoprotection effect of compatible solutes on our model protein, *A. fulgidus* IMPase, Asp and Glu have well defined binding sites on the protein. However, these specific sites are not needed for thermoprotection by the osmolytes. While this result appears more consistent with the osmophobic effect, invocation of that nonspecific interaction does not explain the observed specificity in osmolytes. Perhaps, both types of interactions occur in this particular system.

Chapter 6

Future Directions

My thesis work has provided answers to questions in two important (and very different) biological systems. It has also suggested new interesting questions to be answered. In the PTEN hydrophobic site studies, we demonstrated the importance of Arg47 in providing hydrophobic interactions with lipid substrates. Besides Arg47, Asn48 is also well conserved among species (see Figure 3.6). Furthermore, Asn48 mutations (N48I, N48D, and N48K) in patients have also been reported (Liu et al, 2000; Reis et al, 2000; Vega et al, 2003). These results indicated the importance of this particular residue, and this can be revealed by studying the kinetics and lipid binding of Asn48 mutants. Along with Asn48, in the pβ2-α1 loop where Arg47 resides, there are two hydrophobic residues, Val45 and Tyr46 right before Arg47. Do these two residues also contribute to the hydrophobic interaction with acyl chains? The answer, based on the MD simulations of substrate diC_8PI(3)P binding to the PTEN phosphatase domain, is that they probably are important, but this should be demonstrated experimentally. In the simulations, Val45 interacted with short-chain substrate PI(3)P acyl tails (Wang et al, 2010). Studying mutations of these two residues should provide more details about the role of this hydrophobic site in PTEN lipid membrane binding.

In PI(4,5)P_2 activation studies, we used field cycling ^{31}P NMR to provide more evidence for a discrete binding site for PIP_2. However, due to the multiple labeling of PTEN cysteines with MTSL spin-labeling reagents, we could not directly calculate accurate distances between PIP_x and the active site Cys124. It would be ideal if Cys124 or Cys71 were the only site where spin-label is attached. This is hard to achieve, and one possible way is to mutate the other nine cysteines into serines. This method will have high risk since there is no guarantee that after all the mutations the protein will be properly folded

and still active. After an accurate distance between PIP_2 and Cys124 is obtained, computer simulations could help build a model for the PIP_2 site. This information may provide insight into the relative position of the N-terminal loop, the most probable PIP_2 binding site, with the protein active site as the reference.

The conformational change of PTEN induced by binding $PI(4,5)P_2$ is another aspect worth investigating. Preliminary IR results reported by Redfern et al (2008) only provided very rough information about this conformational change. Other methods can also be used. One promising method is hydrogen/deuterium exchange mass spectrometry (HXMS) (Marcsisin & Engen, 2010). This method utilizes mass spectrometry to measure the rate of protein amide protons exchanging with deuterium under different conditions and is very useful to study protein folding, protein-lipid and protein-protein interactions. The incorporation of the deuterium into pepsin digested peptide fragments can be detected by the shift of peptide m/z value, and the H/D exchange rate of a defined region of the protein (characterized by the specific peptic digested peptides) is a measure of the extent of their solvent exposure. The protein conformational change upon activation detected by HXMS has already been reported in many cases, such as Akt (Guo et al, 2009) and PI3K (Burke et al, 2012). Very preliminary data for PTEN HXMS was done when I worked in Prof. Patrick Wintrode's laboratory when he was at Case Western Reserve University. It was shown that about 60% of peptides fragments generated by PTEN peptic digestion could be detected by mass spectrometry (Figure 6.1). This result proved the feasibility of using HXMS method to study PTEN conformational changes upon activation. This could be achieved by comparing the exchange files of PTEN with or

without PI(4,5)P_2 to probe regions where the conformational changes occur upon binding of that phospholipid and subsequent activation.

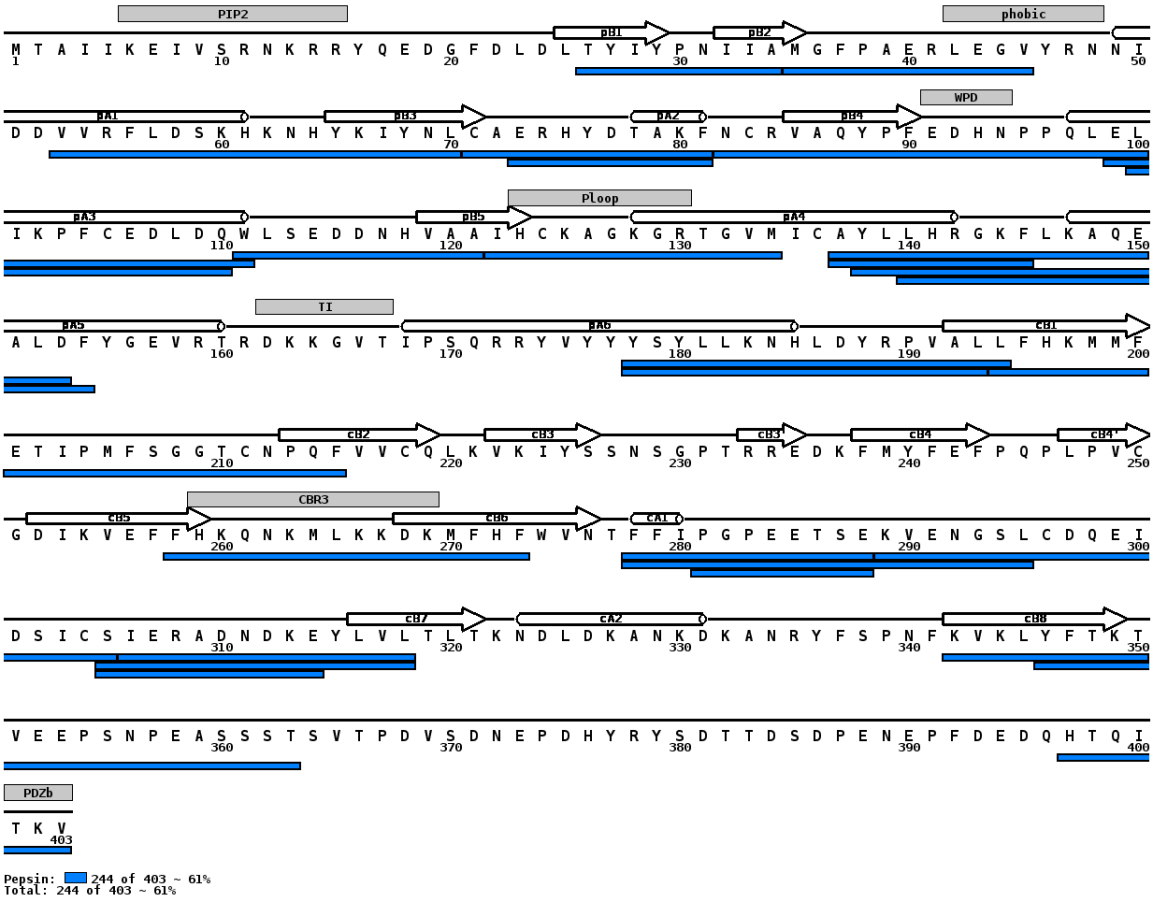

Figure 6.1 Peptide coverage map of PTEN after peptic digestion. 5 µg PTEN was mixed with 200 µl 100mM NaH_2PO_4, pH 2.5. Protein was digested by 5 µg pepsin in 100 mM NaH_2PO_4, pH 2.5, at 0°C for 5 min. The digested sample was injected into a micropeptide trap connected to a C18 HPLC column coupled to a Finnigan LCQ quadrupole ion-trap mass spectrometer. Fragment peptides were eluted using a gradient of acetonitrile in water (2%-45% CH_3CN, 60min) and sequenced by tandem mass spectrometry experiment. The fragments were identified using the search algorithm SEQUEST and manual inspection. Identified peptides are indicated by blue bars under the protein sequence. Helices are shown as cylinders and β-sheets as arrows. Positions of the N-terminal PIP_2 binding motif (PIP_2), the hydrophobic site (phobic), the P loop, WPD loop, TI loop, CBR3 loop and PDZ binding domain (PDZb) are shown in grey boxes.

In searching for mechanisms for the thermoprotection of *A. fulgidus* IMPase, we found evidence that both DGP and DIP likely are very effective because they bind to the active site. However, glutamate has little affinity for the active site. I proposed that one possible protection mechanism for glutamate ions was to stabilize the mobility of the mobile loop. Interactions of glutamates with that mobile feature could occur by their interactions with positively charged residues in the mobile loop. There are three candidate residues in the loop: Lys31, Lys37 and Lys43. It is worth mutating each or all of them and measuring the effect of glutamate on the IMPase thermostability at 90^{o}C. If there is a loss in thermoprotection by the glutamate, then we would imply motions of the mobile loop are a major problem as the temperature is increased. Glutamate and many of the dicarboxylates could transiently interact with this region to keep the loop from unraveling more of the protein. A discretely bound glutamate need not persist. Since the wild type IMPase is still quite stable, these experiments might be best done with one of the Glu-site mutant IMPase proteins. Overall, these results should provide tests of our proposed role for all the dicarboxylate compounds.

References

Agoulnik IU, Hodgson MC, Bowden WA, Ittmann MM (2011) INPP4B: the New Kid on the PI3K Block. *Oncotarget* **2:** 321-328

Agranoff BW (1978) TEXTBOOK ERRORS - CYCLITOL CONFUSION. *Trends in Biochemical Sciences* **3:** N283-N285

Agranoff BW (2009) Turtles All the Way: Reflections on myo-Inositol. *Journal of Biological Chemistry* **284:** 21121-21126

Aioanei D, Brucale M, Tessari I, Bubacco L, Samori B (2012) Worm-Like Ising Model for Protein Mechanical Unfolding under the Effect of Osmolytes. *Biophysical Journal* **102:** 342-350

Aioanei D, Lv S, Tessari I, Rampioni A, Bubacco L, Li H, Samori B, Brucale M (2011) Single-Molecule-Level Evidence for the Osmophobic Effect. *Angewandte Chemie-International Edition* **50:** 4394-4397

Al-Khouri AM, Ma YL, Togo SH, Williams S, Mustelin T (2005) Cooperative phosphorylation of the tumor suppressor phosphatase and tensin homologue (PTEN) by casein kinases and glycogen synthase kinase 3 beta. *Journal of Biological Chemistry* **280:** 35195-35202

Alcazar-Roman AR, Tran EJ, Guo S, Wente SR (2006) Inositol hexakisphosphate and Gle1 activate the DEAD-box protein Dbp5 for nuclear mRNA export. *Nature Cell Biology* **8:** 711-U131

Alcazar-Roman AR, Wente SR (2008) Inositol polyphosphates: a new frontier for regulating gene expression. *Chromosoma* **117:** 1-13

Antonsson B (1997) Phosphatidylinositol synthase from mammalian tissues. *Biochimica Et Biophysica Acta-Lipids and Lipid Metabolism* **1348:** 179-186

Arai R, Ito K, Ohnishi T, Ohba H, Akasaka R, Bessho Y, Hanawa-Suetsugu K, Yoshikawa T, Shirouzu M, Yokoyama S (2007) Crystal structure of human myo-inositol monophosphatase 2, the product of the putative susceptibility gene for bipolar disorder, schizophrenia, and febrile seizures. *Proteins-Structure Function and Bioinformatics* **67:** 732-742

Atack JR, Broughton HB, Pollack SJ (1995) STRUCTURE ACID MECHANISM OF INOSITOL MONOPHOSPHATASE. *Febs Letters* **361:** 1-7

Auger KR, Serunian LA, Soltoff SP, Libby P, Cantley LC (1989) PDGF-DEPENDENT TYROSINE PHOSPHORYLATION STIMULATES PRODUCTION OF NOVEL POLYPHOSPHOINOSITIDES IN INTACT-CELLS. *Cell* **57:** 167-175

Barker CJ, Illies C, Gaboardi GC, Berggren P-O (2009) Inositol pyrophosphates: structure, enzymology and function. *Cellular and Molecular Life Sciences* **66:** 3851-3871

Beeder J, Nilsen RK, Rosnes JT, Torsvik T, Lien T (1994) ARCHAEOGLOBUS-FULGIDUS ISOLATED FROM HOT NORTH-SEA-OIL FIELD WATERS. *Applied and Environmental Microbiology* **60:** 1227-1231

Bennett M, Onnebo SMN, Azevedo C, Saiardi A (2006) Inositol pyrophosphates: metabolism and signaling. *Cellular and Molecular Life Sciences* **63:** 552-564

Berridge MJ (2009) Inositol trisphosphate and calcium signalling mechanisms. *Biochimica Et Biophysica Acta-Molecular Cell Research* **1793:** 933-940

Berridge MJ, Lipp P, Bootman MD (2000) The versatility and universality of calcium signalling. *Nature Reviews Molecular Cell Biology* **1:** 11-21

Bolen DW, Baskakov IV (2001) The osmophobic effect: Natural selection of a thermodynamic force in protein folding. *Journal of Molecular Biology* **310:** 955-963

Bolen DW, Rose GD (2008) Structure and energetics of the hydrogen-bonded backbone in protein folding. *Annual Review of Biochemistry* **77:** 339-362

Bolger TA, Folkmann AW, Tran EJ, Wente SR (2008) The mRNA export factor Gle1 and inositol hexakisphosphate regulate distinct stages of translation. *Cell* **134:** 624-633

Bone R, Frank L, Springer JP, Atack JR (1994a) STRUCTURAL STUDIES OF METAL-BINDING BY INOSITOL MONOPHOSPHATASE - EVIDENCE FOR 2-METAL ION CATALYSIS. *Biochemistry* **33:** 9468-9476

Bone R, Frank L, Springer JP, Pollack SJ, Osborne S, Atack JR, Knowles MR, McAllister G, Ragan CI, Broughton HB, Baker R, Fletcher SR (1994b) STRUCTURAL-ANALYSIS OF INOSITOL MONOPHOSPHATASE COMPLEXES WITH SUBSTRATES. *Biochemistry* **33:** 9460-9467

Bone R, Springer JP, Atack JR (1992) STRUCTURE OF INOSITOL MONOPHOSPHATASE, THE PUTATIVE TARGET OF LITHIUM-THERAPY. *Proceedings of the National Academy of Sciences of the United States of America* **89:** 10031-10035

Borges N, Goncalves LG, Rodrigues MV, Siopa F, Ventura R, Maycock C, Lamosa P, Santos H (2006) Biosynthetic pathways of inositol and glycerol phosphodiesters used by the hyperthermophile Archaeoglobus fulgidus in stress adaptation. *Journal of Bacteriology* **188:** 8128-8135

Borges N, Ramos A, Raven NDH, Sharp RJ, Santos H (2002) Comparative study of the thermostabilizing properties of mannosylglycerate and other compatible solutes on model enzymes. *Extremophiles* **6:** 209-216

Brown AD (1976) MICROBIAL WATER STRESS. *Bacteriological Reviews* **40:** 803-846

Bunney TD, Katan M (2010) Phosphoinositide signalling in cancer: beyond PI3K and PTEN. *Nature Reviews Cancer* **10:** 342-352

Burg MB, Ferraris JD (2008) Intracellular organic osmolytes: Function and regulation. *Journal of Biological Chemistry* **283:** 7309-7313

Burke JE, Perisic O, Masson GR, Vadas O, Williams RL (2012) Oncogenic mutations mimic and enhance dynamic events in the natural activation of phosphoinositide 3-kinase p110 alpha (PIK3CA). *Proceedings of the National Academy of Sciences of the United States of America* **109:** 15259-15264

Burton A, Hu X, Saiardi A (2009) Are Inositol Pyrophosphates Signalling Molecules? *Journal of Cellular Physiology* **220:** 8-15

Campbell RB, Liu FH, Ross AH (2003) Allosteric activation of PTEN phosphatase by phosphatidylinositol 4,5-bisphosphate. *Journal of Biological Chemistry* **278:** 33617-33620

Cao J, Schulte J, Knight A, Leslie NR, Zagozdzon A, Bronson R, Manevich Y, Beeson C, Neumann CA (2009) Prdx1 inhibits tumorigenesis via regulating PTEN/AKT activity. *Embo Journal* **28:** 1505-1517

Chakraborty A, Kim S, Snyder SH (2011) Inositol Pyrophosphates as Mammalian Cell Signals. *Science Signaling* **4**

Chang N, El-Hayek YH, Gomez E, Wan Q (2007) Phosphatase PTEN in neuronal injury and brain disorders. *Trends in Neurosciences* **30:** 581-586

Chen HM, Rossier C, Morris MA, Scott HS, Gos A, Bairoch A, Antonarakis SE (1999) A testis-specific gene, TPTE, encodes a putative transmembrane tyrosine phosphatase and maps to the pericentromeric region of human chromosomes 21 and 13, and to chromosomes 15, 22, and Y. *Human Genetics* **105:** 399-409

Chen LJ, Roberts MF (1998) Cloning and expression of the inositol monophosphatase gene from Methanococcus jannaschii and characterization of the enzyme. *Applied and Environmental Microbiology* **64:** 2609-2615

Chen LJ, Roberts MF (1999) Characterization of a tetrameric inositol monophosphatase from the hyperthermophilic bacterium Thermotoga maritima. *Applied and Environmental Microbiology* **65:** 4559-4567

Chen LJ, Spiliotis ET, Roberts MF (1998) Biosynthesis of di-myo-inositol-1,1 '-phosphate, a novel osmolyte in hyperthermophilic archaea. *Journal of Bacteriology* **180:** 3785-3792

Chen LJ, Zhou C, Yang HY, Roberts MF (2000) Inositol-1-phosphate synthase from Archaeoglobus fulgidus is a class II aldolase. *Biochemistry* **39:** 12415-12423

Choe JY, Poland BW, Fromm HJ, Honzatko RB (1998) Role of a dynamic loop in cation activation and allosteric regulation of recombinant porcine, fructose-1,6-bisphosphatase. *Biochemistry* **37:** 11441-11450

Ciulla RA, Burggraf S, Stetter KO, Roberts MF (1994) OCCURRENCE AND ROLE OF DI-MYO-INOSITOL-1,1'-PHOSPHATE IN METHANOCOCCUS-IGNEUS. *Applied and Environmental Microbiology* **60:** 3660-3664

Clague MJ, Urbe S, de Lartigue J (2009) Phosphoinositides and the endocytic pathway. *Experimental Cell Research* **315:** 1627-1631

Cordier F, Chaffotte A, Terrien E, Prehaud C, Theillet F-X, Delepierre M, Lafon M, Buc H, Wolff N (2012) Ordered Phosphorylation Events in Two Independent Cascades of the PTEN C-tail Revealed by NMR. *Journal of the American Chemical Society* **134:** 20533-20543

D'Angelo G, Vicinanza M, Di Campli A, De Matteis MA (2008) The multiple roles of PtdIns(4)P - not just the precursor of PtdIns(4,5)P(2). *Journal of Cell Science* **121:** 1955-1963

da Costa MS, Santos H, Galinski EA (1998) An overview of the role and diversity of compatible solutes in Bacteria and Archaea. *Advances in biochemical engineering/biotechnology* **61:** 117-153

Das S, Dixon JE, Cho WW (2003) Membrane-binding and activation mechanism of PTEN. *Proceedings of the National Academy of Sciences of the United States of America* **100:** 7491-7496

Davidson L, Maccario H, Perera NM, Yang X, Spinelli L, Tibarewal P, Glancy B, Gray A, Weijer CJ, Downes CP, Leslie NR (2010) Suppression of cellular proliferation and invasion by the concerted lipid and protein phosphatase activities of PTEN. *Oncogene* **29:** 687-697

Di Paolo G, De Camilli P (2006) Phosphoinositides in cell regulation and membrane dynamics. *Nature* **443:** 651-657

Dowler S, Currie RA, Campbell DG, Deak M, Kular G, Downes CP, Alessi DR (2000) Identification of pleckstrin-homology-domain-containing proteins with novel phosphoinositide-binding specificities. *Biochemical Journal* **351:** 19-31

Downes CP, Macphee CH (1990) myo-Inositol metabolites as cellular signals. *Eur J Biochem* **193:** 1-18

Ellman GL (1959) TISSUE SULFHYDRYL GROUPS. *Archives of Biochemistry and Biophysics* **82:** 70-77

Empadinhas N, da Costa MS (2006) Diversity and biosynthesis of compatible solutes in hyper/thermophiles. *International Microbiology* **9:** 199-206

Empadinhas N, Mendes V, Simoes C, Santos MS, Mingote A, Lamosa P, Santos H, da Costa MS (2007) Organic solutes in Rubrobacter xylanophilus: the first example of di-myo-inositol-phosphate in a thermophile. *Extremophiles* **11:** 667-673

Falasca M, Maffucci T (2009) Rethinking phosphatidylinositol 3-monophosphate. *Biochimica Et Biophysica Acta-Molecular Cell Research* **1793:** 1795-1803

Feller G (2010) Protein stability and enzyme activity at extreme biological temperatures. *Journal of Physics-Condensed Matter* **22**

Franke TF (2008) PI3K/Akt: getting it right matters. *Oncogene* **27:** 6473-6488

Franke TF, Kaplan DR, Cantley LC, Toker A (1997) Direct regulation of the Akt proto-oncogene product by phosphatidylinositol-3,4-bisphosphate. *Science* **275:** 665-668

Fratti RA, Chua J, Vergne I, Deretic V (2003) Mycobacterium tuberculosis glycosylated phosphatidylinositol causes phagosome maturation arrest. *Proceedings of the National Academy of Sciences of the United States of America* **100:** 5437-5442

Fukuda C, Kawai S, Murata K (2007) NADP(H) phosphatase activities of archaeal inositol monophosphatase and eubacterial 3'-phosphoadenosine 5-phosphate phosphatase. *Applied and Environmental Microbiology* **73:** 5447-5452

Gamper N, Shapiro MS (2007) Regulation of ion transport proteins by membrane phosphoinositides. *Nature Reviews Neuroscience* **8:** 921-934

Ganzhorn AJ, Rondeau JM (1997) Structure of an enzyme-substrate complex and the catalytic mechanism of human brain myo-inositol monophosphatase. *Protein Engineering* **10:** 61-61

Geijtenbeek TBH, van Vliet SJ, Koppel EA, Sanchez-Hernandez M, Vandenbroucke-Grauls C, Appelmelk B, van Kooyk Y (2003) Mycobacteria target DC-SIGN to suppress dendritic cell function. *Journal of Experimental Medicine* **197:** 7-17

Gericke A, Munson M, Ross AH (2006) Regulation of the PTEN phosphatase. *Gene* **374:** 1-9

Goncalves LG, Huber R, da Costa MS, Santos H (2003) A variant of the hyperthermophile Archaeoglobus fulgidus adapted to grow at high salinity. *Fems Microbiology Letters* **218:** 239-244

Goncalves LG, Lamosa P, Huber R, Santos H (2008) Di-myo-inositol phosphate and novel UDP-sugars accumulate in the extreme hyperthermophile Pyrolobus fumarii. *Extremophiles* **12:** 383-389

Grainger DL, Tavelis C, Ryan AJ, Hinchliffe KA (2012) The emerging role of PtdIns5P: another signalling phosphoinositide takes its place. *Biochemical Society Transactions* **40:** 257-261

Guo MQ, Huang BX, Kim HY (2009) Conformational changes in Akt1 activation probed by amide hydrogen/deuterium exchange and nano-electrospray ionization mass spectrometry. *Rapid Communications in Mass Spectrometry* **23:** 1885-1891

Hafizi S, Ibraimi F, Dahlback B (2005) C1-TEN is a negative regulator of the Akt/PKB signal transduction pathway and inhibits cell survival, proliferation, and migration. *Faseb Journal* **19:** 971-+

Haimovich A, Eliav U, Goldbourt A (2012) Determination of the Lithium Binding Site in Inositol Monophosphatase, the Putative Target for Lithium Therapy, by Magic-Angle-Spinning Solid-State NMR. *Journal of the American Chemical Society* **134:** 5647-5651

Hallcher LM, Sherman WR (1980) THE EFFECTS OF LITHIUM ION AND OTHER AGENTS ON THE ACTIVITY OF MYO-INOSITOL-1-PHOSPHATASE FROM BOVINE BRAIN. *Journal of Biological Chemistry* **255:** 896-901

Hansen SB, Tao X, MacKinnon R (2011) Structural basis of PIP2 activation of the classical inward rectifier K+ channel Kir2.2. *Nature* **477:** 495-U152

Harwood AJ (2005) Lithium and bipolar mood disorder: the inositol-depletion hypothesis revisited. *Molecular Psychiatry* **10:** 117-126

Hatch AJ, York JD (2010) SnapShot: Inositol Phosphates. *Cell* **143:** 1030-U1183

Hawkins PT, Anderson KE, Davidson K, Stephens LR (2006) Signalling through class I PI3Ks in mammalian cells. *Biochemical Society Transactions* **34:** 647-662

Hers I, Vincent EE, Tavare JM (2011) Akt signalling in health and disease. *Cellular Signalling* **23:** 1515-1527

Ho CY, Alghamdi TA, Botelho RJ (2012) Phosphatidylinositol-3,5-Bisphosphate: No Longer the Poor PIP2. *Traffic* **13:** 1-8

Hui STY, Andres AM, Miller AK, Spann NJ, Potter DW, Post NM, Chen AZ, Sachithanantham S, Jung DY, Kim JK, Davis RA (2008) Txnip balances metabolic and growth signaling via PTEN disulfide reduction. *Proceedings of the National Academy of Sciences of the United States of America* **105:** 3921-3926

Iijima M, Devreotes P (2002) Tumor suppressor PTEN mediates sensing of chemoattractant gradients. *Cell* **109:** 599-610

Iijima M, Huang YE, Luo HR, Vazquez F, Devreotes PN (2004) Novel mechanism of PTEN regulation by its phosphatidylinositol 4,5-bisphosphate binding motif is critical for chemotaxis. *Journal of Biological Chemistry* **279:** 16606-16613

Irvine RF, Schell MJ (2001) Back in the water: The return of the inositol phosphates. *Nature Reviews Molecular Cell Biology* **2:** 327-338

Itaya K, Ui M (1966) A NEW MICROMETHOD FOR COLORIMETRIC DETERMINATION OF INORGANIC PHOSPHATE. *Clinica Chimica Acta* **14:** 361-&

Jackson M, Crick DC, Brennan PJ (2000) Phosphatidylinositol is an essential phospholipid of mycobacteria. *Journal of Biological Chemistry* **275:** 30092-30099

Johnson KA, Chen LJ, Yang HY, Roberts MF, Stec B (2001) Crystal structure and catalytic mechanism of the MJ0109 gene product: A bifunctional enzyme with inositol monophosphatase and fructose 1,6-bisphosphatase activities. *Biochemistry* **40:** 618-630

Jones DR, Bultsma Y, Keune W-J, Halstead JR, Elouarrat D, Mohammed S, Heck AJ, D'Santos CS, Divecha N (2006) Nuclear PtdIns5P as a transducer of stress signaling: An in vivo role for PIP4Kbeta. *Molecular Cell* **23:** 685-695

Khan SH, Ahmad N, Ahmad F, Kumar R (2010) Naturally Occurring Organic Osmolytes: From Cell Physiology to Disease Prevention. *Iubmb Life* **62:** 891-895

Koga Y, Morii H (2007) Biosynthesis of ether-type polar lipids in archaea and evolutionary considerations. *Microbiology and Molecular Biology Reviews* **71:** 97-120

Krause M, Leslie JD, Stewart M, Lafuente EM, Valderrama F, Jagannathan R, Strasser GA, Rubinson DA, Liu H, Way M, Yaffe MB, Boussiotis VA, Gertier FB (2004) Lamellipodin, an EnaNASP ligand, is implicated in the regulation of lamellipodial dynamics. *Developmental Cell* **7:** 571-583

Kutateladze TG (2006) Phosphatidylinositol 3-phosphate recognition and membrane docking by the FYVE domain. *Biochimica Et Biophysica Acta-Molecular and Cell Biology of Lipids* **1761:** 868-877

Kutateladze TG (2010) Translation of the phosphoinositide code by PI effectors. *Nature Chemical Biology* **6:** 507-513

Kwon J, Lee SR, Yang KS, Ahn Y, Kim YJ, Stadtman ER, Rhee SG (2004) Reversible oxidation and inactivation of the tumor suppressor PTEN in cells stimulated with peptide growth factors. *Proceedings of the National Academy of Sciences of the United States of America* **101:** 16419-16424

Lamosa P, Burke A, Peist R, Huber R, Liu MY, Silva G, Rodrigues-Pousada C, LeGall J, Maycock C, Santos H (2000) Thermostabilization of proteins by diglycerol phosphate, a new compatible solute from the hyperthermophile Archaeoglobus fulgidus. *Applied and Environmental Microbiology* **66:** 1974-1979

Lamosa P, Goncalves LG, Rodrigues MV, Martins LO, Raven NDH, Santos H (2006) Occurrence of 1-glyceryl-1-myo-inosityl phosphate in hyperthermophiles. *Applied and Environmental Microbiology* **72:** 6169-6173

Lamosa P, Martins LO, Da Costa MS, Santos H (1998) Effects of temperature, salinity, and medium composition on compatible solute accumulation by Thermococcus spp. *Applied and Environmental Microbiology* **64:** 3591-3598

Lamosa P, Turner DL, Ventura R, Maycock C, Santos H (2003) Protein stabilization by compatible solutes - Effect of diglycerol phosphate on the dynamics of Desulfovibrio gigas rubredoxin studied by NMR. *European Journal of Biochemistry* **270:** 4606-4614

Lee DW, Wu XF, Eisenberg E, Greene LE (2006) Recruitment dynamics of GAK and auxilin to clathrin-coated pits during endocytosis. *Journal of Cell Science* **119:** 3502-3512

Lee JO, Yang HJ, Georgescu MM, Di Cristofano A, Maehama T, Shi YG, Dixon JE, Pandolfi P, Pavletich NP (1999) Crystal structure of the PTEN tumor suppressor: Implications for its phosphoinositide phosphatase activity and membrane association. *Cell* **99:** 323-334

Lee SR, Yang KS, Kwon J, Lee C, Jeong W, Rhee SG (2002) Reversible inactivation of the tumor suppressor PTEN by H2O2. *Journal of Biological Chemistry* **277:** 20336-20342

Lemmon MA (2008) Membrane recognition by phospholipid-binding domains. *Nature Reviews Molecular Cell Biology* **9:** 99-111

Lemmon SK (2001) Clathrin uncoating: Auxilin comes to life. *Current Biology* **11:** R49-R52

Leslie NR, Batty IH, Maccario H, Davidson L, Downes CP (2008) Understanding PTEN regulation: PIP(2), polarity and protein stability. *Oncogene* **27:** 5464-5476

Leslie NR, Bennett D, Lindsay YE, Stewart H, Gray A, Downes CP (2003) Redox regulation of PI 3-kinase signalling via inactivation of PTEN. *Embo Journal* **22:** 5501-5510

Leslie NR, Downes CP (2004) PTEN function: how normal cells control it and tumour cells lose it. *Biochemical Journal* **382:** 1-11

Lewis KA, Garigapati VR, Zhou C, Roberts MF (1993) SUBSTRATE REQUIREMENTS OF BACTERIAL PHOSPHATIDYLINOSITOL-SPECIFIC PHOSPHOLIPASE-C. *Biochemistry* **32:** 8836-8841

Li J, Yen C, Liaw D, Podsypanina K, Bose S, Wang SI, Puc J, Miliaresis C, Rodgers L, McCombie R, Bigner SH, Giovanella BC, Ittmann M, Tycko B, Hibshoosh H, Wigler MH, Parsons R (1997) PTEN, a putative protein tyrosine phosphatase gene mutated in human brain, breast, and prostate cancer. *Science* **275:** 1943-1947

Li Z, Stieglitz KA, Shrout AL, Wei Y, Weis RM, Stec B, Roberts MF (2010) Mobile loop mutations in an archaeal inositol monophosphatase: Modulating three-metal ion assisted catalysis and lithium inhibition. *Protein Science* **19:** 309-318

Liu JH, Babaian DC, Liebert M, Steck PA, Kagan J (2000) Inactivation of MMAC1 in bladder transitional-cell carcinoma cell lines and specimens. *Molecular Carcinogenesis* **29:** 143-150

Liu Y, Bankaitis VA (2010) Phosphoinositide phosphatases in cell biology and disease. *Progress in Lipid Research* **49:** 201-217

Lo SH (2004) Tensin. International Journal of Biochemistry & Cell Biology **36:** 31-34

Lombard J, Lopez-Garcia P, Moreira D (2012) The early evolution of lipid membranes and the three domains of life. *Nature Reviews Microbiology* **10:** 507-515

Longo CM, Wei Y, Roberts MF, Miller SJ (2009) Asymmetric Syntheses of L,L- and L,D-Di-myo-inositol-1,1 '-phosphate and their Behavior as Stabilizers of Enzyme Activity at Extreme Temperatures. *Angewandte Chemie-International Edition* **48:** 4158-4161

Lowry OH, Rosebrough NJ, Farr AL, Randall RJ (1951) PROTEIN MEASUREMENT WITH THE FOLIN PHENOL REAGENT. *Journal of Biological Chemistry* **193:** 265-275

Luke KA, Higgins CL, Wittung-Stafshedel P (2007) Thermodynamic stability and folding of proteins from hyperthermophilic organisms. *Febs Journal* **274:** 4023-4033

Ma K, Cheung SM, Marshall AJ, Duronio V (2008) PI(3,4,5)P-3 and PI(3,4)P-2 levels correlate with PKB/akt phosphorylation at Thr308 and Ser473, respectively; PI(3,4)P-2 levels determine PKB activity. *Cellular Signalling* **20:** 684-694

Maccario H, Pereira NM, Davidson L, Downes CP, Leslie NR (2007) PTEN is destabilized by phosphorylation on Thr(366). *Biochemical Journal* **405:** 439-444

Maddika S, Kavela S, Rani N, Palicharla VR, Pokorny JL, Sarkaria JN, Chen J (2011) WWP2 is an E3 ubiquitin ligase for PTEN. *Nature Cell Biology* **13:** 728-U224

Maehama T, Dixon JE (1998) The tumor suppressor, PTEN/MMAC1, dephosphorylates the lipid second messenger, phosphatidylinositol 3,4,5-trisphosphate. *Journal of Biological Chemistry* **273:** 13375-13378

Maehama T, Taylor GS, Dixon JE (2001) PTEN and myotubularin: Novel phosphoinositide phosphatases. *Annual Review of Biochemistry* **70:** 247-279

Manning BD, Cantley LC (2007) AKT/PKB signaling: Navigating downstream. *Cell* **129:** 1261-1274

Marcsisin SR, Engen JR (2010) Hydrogen exchange mass spectrometry: what is it and what can it tell us? *Analytical and Bioanalytical Chemistry* **397:** 967-972

Marsh DJ, Theodosopoulos G, Howell V, Richardson AL, Benn DE, Proos AL, Eng C, Robinson BG (2001) Rapid mutation scanning of genes associated with familial cancer syndromes using denaturing high-performance liquid chromatography. *Neoplasia* **3:** 236-244

Martelli AM, Ognibene A, Buontempo F, Fini M, Bressanin D, Goto K, McCubrey JA, Cocco L, Evangelisti C (2011) Nuclear phosphoinositides and their roles in cell biology and disease. *Critical Reviews in Biochemistry and Molecular Biology* **46:** 436-457

Martins LO, Carreto LS, DaCosta MS, Santos H (1996) New compatible solutes related to di-myo-inositol-phosphate in members of the order Thermotogales. *Journal of Bacteriology* **178:** 5644-5651

Martins LO, Huber R, Huber H, Stetter KO, DaCosta MS, Santos H (1997) Organic solutes in hyperthermophilic Archaea. *Applied and Environmental Microbiology* **63:** 896-902

Martins LO, Santos H (1995) ACCUMULATION OF MANNOSYLGLYCERATE AND DI-MYO-INOSITOL-PHOSPHATE BY PYROCOCCUS-FURIOUS IN RESPONSE TO SALINITY AND TEMPERATURE. *Applied and Environmental Microbiology* **61:** 3299-3303

Massol RH, Boll W, Griffin AM, Kirchhausen T (2006) A burst of auxilin recruitment determines the onset of clathrin-coated vesicle uncoating. *Proceedings of the National Academy of Sciences of the United States of America* **103:** 10265-10270

Matsuhisa A, Suzuki N, Noda T, Shiba K (1995) INOSITOL MONOPHOSPHATASE ACTIVITY FROM THE ESCHERICHIA-COLI SUHB GENE-PRODUCT. *Journal of Bacteriology* **177:** 200-205

Mayinger P (2012) Phosphoinositides and vesicular membrane traffic. *Biochimica Et Biophysica Acta-Molecular and Cell Biology of Lipids* **1821:** 1104-1113

McAllister G, Whiting P, Hammond EA, Knowles MR, Atack JR, Bailey FJ, Maigetter R, Ragan CI (1992) CDNA CLONING OF HUMAN AND RAT-BRAIN MYOINOSITOL MONOPHOSPHATASE - EXPRESSION AND CHARACTERIZATION OF THE HUMAN RECOMBINANT ENZYME. *Biochemical Journal* **284:** 749-754

McConnachie G, Pass I, Walker SM, Downes CP (2003) Interfacial kinetic analysis of the tumour suppressor phosphatase, PTEN: evidence for activation by anionic phospholipids. *Biochemical Journal* **371:** 947-955

Micaelo NM, Victor BL, Soares CM (2008) Protein thermal stabilization by charged compatible solutes: Computational studies in rubredoxin from Desulfovibrio gigas. *Proteins-Structure Function and Bioinformatics* **72:** 580-588

Michell RH (2008) Inositol derivatives: evolution and functions. *Nature Reviews Molecular Cell Biology* **9:** 151-161

Michell RH (2011) Inositol and its derivatives: Their evolution and functions. *Advances in Enzyme Regulation, Vol 51* **51:** 84-90

Miller SJ, Lou DY, Seldin DC, Lane WS, Neel BG (2002) Direct identification of PTEN phosphorylation sites. *Febs Letters* **528:** 145-153

Mitchell J, Wang X, Zhang G, Gentzsch M, Nelson DJ, Shears SB (2008) An Expanded Biological Repertoire for Ins(3,4,5,6)P-4 through its Modulation of CIC-3 Function. *Current Biology* **18:** 1600-1605

Morgan AJ, Wang YK, Roberts MF, Miller SJ (2004) Chemistry and biology of deoxy-myo-inositol phosphates: Stereospecificity of substrate interactions within an archaeal and a bacterial IMPase. *Journal of the American Chemical Society* **126:** 15370-15371

Morii H, Kiyonari S, Ishino Y, Koga Y (2009) A Novel Biosynthetic Pathway of Archaetidyl-myo-inositol via Archaetidyl-myo-inositol Phosphate from CDP-archaeol and D-Glucose 6-Phosphate in Methanoarchaeon Methanothermobacter thermautotrophicus Cells. *Journal of Biological Chemistry* **284:** 30766-30774

Morii H, Ogawa M, Fukuda K, Taniguchi H, Koga Y (2010) A revised biosynthetic pathway for phosphatidylinositol in Mycobacteria. *Journal of Biochemistry* **148:** 593-602

Morita YS, Fukuda T, Sena CBC, Yamaryo-Botte Y, McConville MJ, Kinoshita T (2011) Inositol lipid metabolism in mycobacteria: Biosynthesis and regulatory mechanisms. *Biochimica Et Biophysica Acta-General Subjects* **1810:** 630-641

Morita YS, Yamaryo-Botte Y, Miyanagi K, Callaghan JM, Patterson JH, Crellin PK, Coppel RL, Billman-Jacobe H, Kinoshita T, McConville MJ (2010) Stress-induced Synthesis of Phosphatidylinositol 3-Phosphate in Mycobacteria. *Journal of Biological Chemistry* **285:** 16643-16650

Myers MP, Pass I, Batty IH, Van der Kaay J, Stolarov JP, Hemmings BA, Wigler MH, Downes CP, Tonks NK (1998) The lipid phosphatase activity of PTEN is critical for its tumor suppressor function. *Proceedings of the National Academy of Sciences of the United States of America* **95:** 13513-13518

Myers MP, Stolarov JP, Eng C, Li J, Wang SI, Wigler MH, Parsons R, Tonks NK (1997) P-TEN, the tumor suppressor from human chromosome 10q23, is a dual-specificity phosphatase. *Proceedings of the National Academy of Sciences of the United States of America* **94:** 9052-9057

Nelson M, McClelland M (1992) USE OF DNA METHYLTRANSFERASE ENDONUCLEASE ENZYME COMBINATIONS FOR MEGABASE MAPPING OF CHROMOSOMES. *Methods in Enzymology* **216:** 279-303

Newton GL, Buchmeier N, Fahey RC (2008) Biosynthesis and functions of mycothiol, the unique protective thiol of Actinobacteria. *Microbiology and Molecular Biology Reviews* **72:** 471-+

Newton GL, Ta P, Bzymek KP, Fahey RC (2006) Biochemistry of the initial steps of mycothiol biosynthesis. *Journal of Biological Chemistry* **281:** 33910-33920

Nishizuka Y (1988) THE MOLECULAR HETEROGENEITY OF PROTEIN KINASE-C AND ITS IMPLICATIONS FOR CELLULAR-REGULATION. *Nature* **334:** 661-665

Odriozola L, Singh G, Hoang T, Chan AM (2007) Regulation of PTEN activity by its carboxyl-terminal autoinhibitory domain. *Journal of Biological Chemistry* **282:** 23306-23315

Petsko GA (2001) Structural basis of thermostability in hyperthermophilic proteins, or "there's more than one way to skin a cat". *Hyperthermophilic Enzymes, Pt C* **334:** 469-478

Pezzullo M, Del Vecchio P, Mandrich L, Nucci R, Rossi M, Manco G (2013) Comprehensive analysis of surface charged residues involved in thermal stability in Alicyclobacillus acidocaldarius esterase 2. *Protein Engineering Design & Selection* **26:** 47-58

Pollack SJ, Atack JR, Knowles MR, McAllister G, Ragan CI, Baker R, Fletcher SR, Iversen LL, Broughton HB (1994) MECHANISM OF INOSITOL MONOPHOSPHATASE, THE PUTATIVE TARGET OF LITHIUM-THERAPY. *Proceedings of the National Academy of Sciences of the United States of America* **91:** 5766-5770

Pu MM, Fang XM, Redfield AG, Gershenson A, Roberts MF (2009a) Correlation of Vesicle Binding and Phospholipid Dynamics with Phospholipase C Activity INSIGHTS INTO PHOSPHATIDYLCHOLINE ACTIVATION AND SURFACE DILUTION INHIBITION. *Journal of Biological Chemistry* **284:** 16099-16107

Pu MM, Feng JW, Redfield AG, Roberts MF (2009b) Enzymology with a Spin-Labeled Phospholipase C: Soluble Substrate Binding by P-31 NMR from 0.005 to 11.7 T. *Biochemistry* **48:** 8282-8284

Pu MM, Orr A, Redfield AG, Roberts MF (2010) Defining Specific Lipid Binding Sites for a Peripheral Membrane Protein in Situ Using Subtesla Field-cycling NMR. *Journal of Biological Chemistry* **285:** 26916-26922

Raftopoulou M, Etienne-Manneville S, Self A, Nicholls S, Hall A (2004) Regulation of cell migration by the C2 domain of the tumor suppressor PTEN. *Science* **303:** 1179-1181

Rahdar M, Inoue T, Meyer T, Zhang J, Vazquez F, Devreotes PN (2009) A phosphorylation-dependent intramolecular interaction regulates the membrane association and activity of the tumor suppressor PTEN. *Proceedings of the National Academy of Sciences of the United States of America* **106:** 480-485

Rajan RS, Tsumoto K, Tokunaga M, Tokunaga H, Kita Y, Arakawa T (2011) Chemical and Pharmacological Chaperones: Application for Recombinant Protein Production and Protein Folding Diseases. *Current Medicinal Chemistry* **18:** 1-15

Ramakrishnan V, Verhagen M, Adams MWW (1997) Characterization of di-myo-inositol-1,1'-phosphate in the hyperthermophilic bacterium Thermotoga maritima. *Applied and Environmental Microbiology* **63:** 347-350

Razvi A, Scholtz JM (2006) Lessons in stability from thermophilic proteins. *Protein Science* **15:** 1569-1578

Redfern RE, Redfern D, Furgason MLM, Munson M, Ross AH, Gericke A (2008) PTEN phosphatase selectively binds phosphoinositides and undergoes structural changes. *Biochemistry* **47:** 2162-2171

Reis RM, Konu-Leblebliciogl u D, Lopes JM, Kleihues P, Ohgaki H (2000) Genetic profile of gliosarcomas. *American Journal of Pathology* **156:** 425-432

Roberts MF (2004) Osmoadaptation and osmoregulation in archaea: Update 2004. *Frontiers in Bioscience* **9:** 1999-2019

Roberts MF (2005) Organic compatible solutes of halotolerant and halophilic microorganisms. In *Saline Systems* Vol. 1, p 5. England

Roberts MF, Redfield AG (2004a) High-resolution P-31 field cycling NMR as a probe of phospholipid dynamics. *Journal of the American Chemical Society* **126:** 13765-13777

Roberts MF, Redfield AG (2004b) Phospholipid bilayer surface configuration probed quantitatively by P-31 field-cycling NMR. *Proceedings of the National Academy of Sciences of the United States of America* **101:** 17066-17071

Robertson DE, Roberts MF (1991) ORGANIC OSMOLYTES IN METHANOGENIC ARCHAEBACTERIA. *Biofactors* **3:** 1-9

Rodionov DA, Kurnasov OV, Stec B, Wang Y, Roberts MF, Osterman AL (2007) Genomic identification and in vitro reconstitution of a complete biosynthetic pathway for the osmolyte di-myo-inositol-phosphate. *Proceedings of the National Academy of Sciences of the United States of America* **104:** 4279-4284

Rodrigues MV, Borges N, Almeida CP, Lamosa P, Santos H (2009) A Unique beta-1,2-Mannosyltransferase of Thermotoga maritima That Uses Di-myo-Inositol Phosphate as the Mannosyl Acceptor. *Journal of Bacteriology* **191:** 6105-6115

Rodrigues MV, Borges N, Henriques M, Lamosa P, Ventura R, Fernandes C, Empadinhas N, Maycock C, da Costa MS, Santos H (2007) Bifunctional CTP: Inositol-1-phosphate cytidylyltransferase/CDP-inositol: Inositol-1-phosphate transferase, the key enzyme for di-myo-inositol-phosphate synthesis in several, (hyper)thermophiles. *Journal of Bacteriology* **189:** 5405-5412

Rosenberg AH, Lade BN, Chui DS, Lin SW, Dunn JJ, Studier FW (1987) VECTORS FOR SELECTIVE EXPRESSION OF CLONED DNAS BY T7 RNA-POLYMERASE. *Gene* **56:** 125-135

Ross AH, Gericke A (2009) Phosphorylation keeps PTEN phosphatase closed for business. *Proceedings of the National Academy of Sciences of the United States of America* **106:** 1297-1298

Salman M, Lonsdale JT, Besra GS, Brennan PJ (1999) Phosphatidylinositol synthesis in mycobacteria. *Biochimica Et Biophysica Acta-Molecular and Cell Biology of Lipids* **1436:** 437-450

Salmena L, Carracedo A, Pandolfi PP (2008) Tenets of PTEN tumor suppression. *Cell* **133:** 403-414

Santos H, da Costa MS (2002) Compatible solutes of organisms that live in hot saline environments. *Environmental Microbiology* **4:** 501-509

Santos H, Lamosa P, Borges N, Gonçalves L, Pais T, Rodrigues M (2011) Organic compatible solutes of prokaryotes that thrive in hot environments: the importance of ionic compounds for thermostabilization. In *Extremophiles Handbook, Horikoshi K* (ed), pp 497-520.

Sarkes D, Rameh LE (2010) A novel HPLC-based approach makes possible the spatial characterization of cellular PtdIns5P and other phosphoinositides. *Biochemical Journal* **428:** 375-384

Sasaki J, Kofuji S, Itoh R, Momiyama T, Takayama K, Murakami H, Chida S, Tsuya Y, Takasuga S, Eguchi S, Asanuma K, Horie Y, Miura K, Davies EM, Mitchell C, Yamazaki M, Hirai H, Takenawa T, Suzuki A, Sasaki T (2010) The PtdIns(3,4)P-2 phosphatase INPP4A is a suppressor of excitotoxic neuronal death. *Nature* **465:** 497-U127

Sasaki T, Takasuga S, Sasaki J, Kofuji S, Eguchi S, Yamazaki M, Suzuki A (2009) Mammalian phosphoinositide kinases and phosphatases. *Progress in Lipid Research* **48:** 307-343

Sauer K, Cooke MP (2010) Regulation of immune cell development through soluble inositol-1,3,4,5-tetrakisphosphate. *Nature Reviews Immunology* **10:** 257-271

Scholz S, Sonnenbichler J, Schafer W, Hensel R (1992) DI-MYO-INOSITOL-1,1'-PHOSPHATE - A NEW INOSITOL PHOSPHATE ISOLATED FROM PYROCOCCUS-WOESEI. *Febs Letters* **306:** 239-242

Shi XM, Shao CH, Zhang X, Zambonelli C, Redfield AG, Head JF, Seaton BA, Roberts MF (2009) Modulation of Bacillus thuringiensis Phosphatidylinositol-specific Phospholipase C Activity by Mutations in the Putative Dimerization Interface. *Journal of Biological Chemistry* **284:** 15607-15618

Shi YJ, Paluch BE, Wang XJ, Jiang XJ (2012) PTEN at a glance. *Journal of Cell Science* **125:** 4687-4692

Singh N, Halliday AC, Knight M, Lack NA, Lowe E, Churchill GC (2012) Cloning, expression, purification, crystallization and X-ray analysis of inositol monophosphatase from Mus musculus and Homo sapiens. *Acta Crystallographica Section F-Structural Biology and Crystallization Communications* **68:** 1149-1152

Song MS, Salmena L, Pandolfi PP (2012) The functions and regulation of the PTEN tumour suppressor. *Nature Reviews Molecular Cell Biology* **13:** 283-296

Stambolic V, Suzuki A, de la Pompa JL, Brothers GM, Mirtsos C, Sasaki T, Ruland J, Penninger JM, Siderovski DP, Mak TW (1998) Negative regulation of PKB/Akt-dependent cell survival by the tumor suppressor PTEN. *Cell* **95:** 29-39

Stec B, Yang HY, Johnson KA, Chen LJ, Roberts MF (2000) MJ0109 is an enzyme that is both an inositol monophosphatase and the 'missing' archaeal fructose1,6-bisphosphatase. *Nature Structural Biology* **7:** 1046-1050

Steck PA, Pershouse MA, Jasser SA, Yung WKA, Lin H, Ligon AH, Langford LA, Baumgard ML, Hattier T, Davis T, Frye C, Hu R, Swedlund B, Teng DHF, Tavtigian SV (1997) Identification of a candidate tumour suppressor gene, MMAC1, at chromosome 10q23.3 that is mutated in multiple advanced cancers. *Nature Genetics* **15:** 356-362

Sterner R, Liebl W (2001) Thermophilic adaptation of proteins. *Critical Reviews in Biochemistry and Molecular Biology* **36:** 39-106

Stetter KO, Lauerer G, Thomm M, Neuner A (1987) ISOLATION OF EXTREMELY THERMOPHILIC SULFATE REDUCERS - EVIDENCE FOR A NOVEL BRANCH OF ARCHAEBACTERIA. *Science* **236:** 822-824

Stieglitz KA, Johnson KA, Yang HY, Roberts MF, Seaton BA, Head JF, Stec B (2002) Crystal structure of a dual activity IMPase/FBPase (AF2372) from Archaeoglobus fulgidus - The story of a mobile loop. *Journal of Biological Chemistry* **277:** 22863-22874

Stieglitz KA, Roberts MF, Li WZ, Stec B (2007) Crystal structure of the tetrameric inositol 1-phosphate phosphatase (TM1415) from the hyperthermophile, Thermotoga maritima. *Febs Journal* **274:** 2461-2469

Stieglitz KA, Seaton BA, Head JF, Stec B, Roberts MF (2003) Unexpected similarity in regulation between an archaeal inositol monophosphatase/fructose bisphosphatase and chloroplast fructose bisphosphatase. *Protein Science* **12:** 760-767

Streb H, Irvine RF, Berridge MJ, Schulz I (1983) RELEASE OF CA-2+ FROM A NONMITOCHONDRIAL INTRACELLULAR STORE IN PANCREATIC ACINAR-CELLS BY INOSITOL-1,4,5-TRISPHOSPHATE. *Nature* **306:** 67-69

Street TO, Bolen DW, Rose GD (2006) A molecular mechanism for osmolyte-induced protein stability. *Proceedings of the National Academy of Sciences of the United States of America* **103:** 13997-14002

Studier FW, Rosenberg AH, Dunn JJ, Dubendorff JW (1990) USE OF T7 RNA-POLYMERASE TO DIRECT EXPRESSION OF CLONED GENES. *Methods in Enzymology* **185:** 60-89

Szilagyi A, Zavodszky P (2000) Structural differences between mesophilic, moderately thermophilic and extremely thermophilic protein subunits: results of a comprehensive survey. *Structure* **8:** 493-504

Tabb DL, McDonald WH, Yates JR (2002) DTASelect and contrast: Tools for assembling and comparing protein identifications from shotgun proteomics. *Journal of Proteome Research* **1:** 21-26

Takahashi Y, Morales FC, Kreimann EL, Georgescu MM (2006) PTEN tumor suppressor associates with NHERF proteins to attenuate PDGF receptor signaling. *Embo Journal* **25:** 910-920

Tamura M, Gu JG, Takino T, Yamada KM (1999) Tumor suppressor PTEN inhibition of cell invasion, migration, and growth: Differential involvement of focal adhesion kinase and p130(Cas). *Cancer Research* **59:** 442-449

Torres J, Pulido R (2001) The tumor suppressor PTEN is phosphorylated by the protein kinase CK2 at its C terminus - Implications for PTEN stability to proteasome-mediated degradation. *Journal of Biological Chemistry* **276:** 993-998

Traynorkaplan AE, Harris AL, Thompson BL, Taylor P, Sklar LA (1988) AN INOSITOL TETRAKISPHOSPHATE-CONTAINING PHOSPHOLIPID IN ACTIVATED NEUTROPHILS. *Nature* **334:** 353-356

Trotman LC, Wang X, Alimonti A, Chen Z, Teruya-Feldstein J, Yang H, Pavletich NP, Carver BS, Cordon-Cardo C, Erdjument-Bromage H, Tempst P, Chi S-G, Kim H-J, Misteli T, Jiang X, Pandolfi PP (2007) Ubiquitination regulates PTEN nuclear import and tumor suppression. *Cell* **128:** 141-156

Tsui MM, York JD (2010) Roles of inositol phosphates and inositol pyrophosphates in development, cell signaling and nuclear processes. *Advances in Enzyme Regulation, Vol 50* **50:** 324-337

Van Themsche C, Leblanc V, Parent S, Asselin E (2009) X-linked Inhibitor of Apoptosis Protein (XIAP) Regulates PTEN Ubiquitination, Content, and Compartmentalization. *Journal of Biological Chemistry* **284:** 20462-20466

Vanhaesebroeck B, Guillermet-Guibert J, Graupera M, Bilanges B (2010) The emerging mechanisms of isoform-specific PI3K signalling. *Nature Reviews Molecular Cell Biology* **11:** 329-341

Vanhaesebroeck B, Stephens L, Hawkins P (2012) PI3K signalling: the path to discovery and understanding. *Nature Reviews Molecular Cell Biology* **13:** 195-203

Vanleeuwen SH, Vandermarel GA, Hensel R, Vanboom JH (1994) SYNTHESIS OF LL-DI-MYO-INOSITOL-1,1'-PHOSPHATE - A NOVEL INOSITOL PHOSPHATE FROM PYROCOCCUS-WOESEI. *Recueil Des Travaux Chimiques Des Pays-Bas-Journal of the Royal Netherlands Chemical Society* **113:** 335-336

Vazquez F, Grossman SR, Takahashi Y, Rokas MV, Nakamura N, Sellers WR (2001) Phosphorylation of the PTEN tail acts as an inhibitory switch by preventing its recruitment into a protein complex. *Journal of Biological Chemistry* **276:** 48627-48630

Vazquez F, Matsuoka S, Sellers WR, Yanagida T, Ueda M, Devreotes PN (2006) Tumor suppressor PTEN acts through dynamic interaction with the plasma membrane. *Proceedings of the National Academy of Sciences of the United States of America* **103:** 3633-3638

Vazquez F, Ramaswamy S, Nakamura N, Sellers WR (2000) Phosphorylation of the PTEN tail regulates protein stability and function. *Molecular and Cellular Biology* **20:** 5010-5018

Vega A, Torres J, Torres M, Cameselle-Teijeiro J, Macia M, Carracedo A, Pulido R (2003) A novel loss-of-function mutation (N48K) in the PTEN gene in a Spanish patient with Cowden disease. *Journal of Investigative Dermatology* **121:** 1356-1359

Walker SM, Downes CP, Leslie NR (2001) TPIP: a novel phosphoinositide 3-phosphatase. *Biochemical Journal* **360:** 277-283

Walker SM, Leslie NR, Perera NM, Batty IH, Downes CP (2004) The tumour-suppressor function of PTEN requires an N-terminal lipid-binding motif. *Biochemical Journal* **379:** 301-307

Wang Q, Wei Y, Mottamal M, Roberts MF, Krilov G (2010) Understanding the stereospecific interactions of 3-deoxyphosphatidylinositol derivatives with the PTEN phosphatase domain. *Journal of Molecular Graphics & Modelling* **29:** 102-114

Wang X, Trotman LC, Koppie T, Alimonti A, Chen Z, Gao Z, Wang J, Erdjument-Bromage H, Tempst P, Cordon-Cardo C, Pandolfi PP, Jiang X (2007) NEDD4-1 is a proto-oncogenic ubiquitin ligase for PTEN. *Cell* **128:** 129-139

Wang XQ, Hirao H (2013) ONIOM (DFT:MM) Study of the Catalytic Mechanism of myo-Inositol Monophosphatase: Essential Role of Water in Enzyme Catalysis in the Two-Metal Mechanism. *Journal of Physical Chemistry B* **117:** 833-842

Wang YK, Chen W, Blair D, Pu M, Xu Y, Miller SJ, Redfield AG, Chiles TC, Roberts MF (2008) Insights into the Structural Specificity of the Cytotoxicity of 3-Deoxyphosphatidylinositols. *J Am Chem Soc* **130:** 7746-7755

Wang YLK, Morgan A, Stieglitz K, Stec B, Thompson B, Miller SJ, Roberts MF (2006) The temperature dependence of the inositol monophosphatase K-m correlates with accumulation of di-myo-inositol 1,1 '-phosphate in Archaeoglobus fulgidus. *Biochemistry* **45:** 3307-3314

Whitman M, Downes CP, Keeler M, Keller T, Cantley L (1988) TYPE-I PHOSPHATIDYLINOSITOL KINASE MAKES A NOVEL INOSITOL PHOSPHOLIPID, PHOSPHATIDYLINOSITOL-3-PHOSPHATE. *Nature* **332:** 644-646

Wu XY, Hepner K, Castelino-Prabhu S, Do D, Kaye MB, Yuan XJ, Wood J, Ross C, Sawyers CL, Whang YE (2000) Evidence for regulation of the PTEN tumor suppressor by a membrane-localized multi-PDZ domain containing scaffold protein MAGI-2. *Proceedings of the National Academy of Sciences of the United States of America* **97:** 4233-4238

Xu D, Yao Y, Jiang X, Lu L, Dai W (2010) Regulation of PTEN Stability and Activity by Plk3. *Journal of Biological Chemistry* **285:** 39935-39942

Yancey PH (2005) Organic osmolytes as compatible, metabolic and counteracting cytoprotectants in high osmolarity and other stresses. *Journal of Experimental Biology* **208:** 2819-2830

Yates JR, Eng JK, McCormack AL, Schieltz D (1995) METHOD TO CORRELATE TANDEM MASS-SPECTRA OF MODIFIED PEPTIDES TO AMINO-ACID-SEQUENCES IN THE PROTEIN DATABASE. *Analytical Chemistry* **67:** 1426-1436

York JD, Odom AR, Murphy R, Ives EB, Wente SR (1999) A phospholipase C-dependent inositol polyphosphate kinase pathway required for efficient messenger RNA export. *Science* **285:** 96-100

York JD, Ponder JW, Chen ZW, Mathews FS, Majerus PW (1994) CRYSTAL-STRUCTURE OF INOSITOL POLYPHOSPHATE 1-PHOSPHATASE AT 2.3-ANGSTROM RESOLUTION. *Biochemistry* **33:** 13164-13171

Zellner G, Stackebrandt E, Kneifel H, Messner P, Sleytr UB, Demacario EC, Zabel HP, Stetter KO, Winter J (1989) ISOLATION AND CHARACTERIZATION OF A THERMOPHILIC, SULFATE REDUCING ARCHAEBACTERIUM, ARCHAEOGLOBUS-FULGIDUS STRAIN-Z. *Systematic and Applied Microbiology* **11:** 151-160

Zhang RL, Villeret V, Lipscomb WN, Fromm HJ (1996) Kinetics and mechanisms of activation and inhibition of porcine liver fructose-1,6-bisphosphatase by monovalent cations. *Biochemistry* **35:** 3038-3043

Zhang XC, Piccini A, Myers MP, Van Aelst L, Tonks NK (2012) Functional analysis of the protein phosphatase activity of PTEN. *Biochemical Journal* **444:** 457-464

AppendixI

Study of PTEN binding to phospholipid vesicles by fluorescence spectroscopy

1. Introduction

In the PI3K/Akt signaling pathway, PTEN is the gatekeeper, requiring it to bind to lipid membranes to dephosphorylate PI(3)P molecules thus preventing generation of PIP_3. In resting cells, most PTEN protein is in the cytosol. Clearly an important question is how PTEN binds to the membrane. To test PTEN membrane binding, we used lipid vesicles as the membrane model, and used fluorescence energy transfer spectroscopy (FRET) to detect the interactions between the PTEN protein and the membrane vesicles. Tryptophan residues in PTEN, excited at 285 nm, would be expected to transfer that excitation energy to an appropriate fluorophore in vesicles if the distance between the protein and the vesicles is within the effective distance of FRET (usually within 30 Å). If FRET is observed when mixing PTEN and fluorophore-containing vesicles together, the protein has bound to the vesicles. Different kinds of phospholipids were mixed with POPC, which served as the matrix, to assess their necessity for protein binding.

2. Results

(1) Effect of vesicles composition to PTEN binding

As a control, only matrix POPC vesicles were used for PTEN binding studies. After adding 2 mol% of PE with a dansyl group on the amino group (dansyl-PE) into POPC vesicles, emission of Trp fluorescence at 340 nm was decreased and emission of the dansyl fluorophore at 520 nm was observed, indicating energy transfer from Trp to the dansyl group. The energy transfer was measured by the decrease in Trp emission. As more dansyl-labeled vesicles were added, Trp emission continued to decrease. Binding of PTEN to the POPC vesicles was weak with no saturation of the curve showing the loss of intensity via FRET. A problem with such weak binding is that LUVs scatter light and this

alters the fluorescence signal as the LUV concentration increases. For weak binding, it is extremely difficult to estimate a meaningful apparent dissociation constant (K_d) (Figure Apx 1).

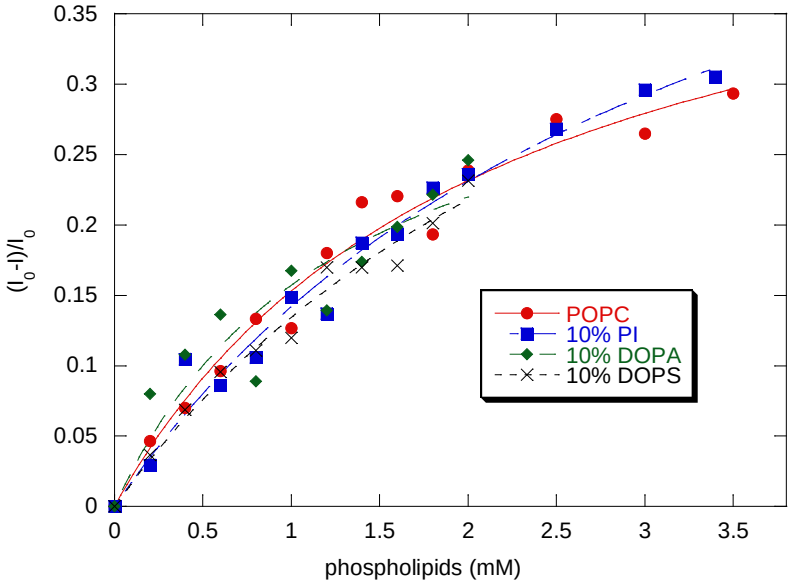

Figure Apx 1 The fluorescence energy transfer from PTEN to 2 mol% Dansyl-PE containing vesicles. 0-3 mM LUVs of 98 mol% POPC LUVs (●) and 10 mol% soy PI/88 mol% POPC (■), 0-2 mM LUVs of 10 mol% DOPA/88 mol%POPC (♦) and 10 mol% DOPS/88 mol%POPC (×) were titrated into 1.5 μM PTEN, and the fraction of Trp emission decrease (I_0-I) to the initial emission ((I_0-I)/I_0) was calculated. The data were fitted with a simple hyperbolic expression.

Different anionic phospholipids were added to the POPC matrix to test the effect of charge on protein binding. These vesicles contained 10 mol% PI, PA or PS. Compared to the zwitterionic PC molecules, PI, PA and PS have a net negative charge, and PTEN could bind to these lipid containing vesicles by electrostatic interaction since the protein has many positively charged residues on surface (Das et al, 2003). However, the FRET for the protein binding to these anionic lipid containing vesicles showed a similar pattern compared to PTEN binding to POPC alone (Figure Apx 1). This result indicated that

mere electrostatic interactions were not the main source for protein binding to vesicles (at least with only 10 mol% of anionic lipids in the LUVs). We then tested PTEN binding to 25 mol% PS containing vesicles (Figure Apx 2). Compared with 10 mol% PS/PC vesicles, increasing the negatively charged component did not enhance protein binding, confirming that electrostatic interactions could not provide enough driving force for PTEN binding to the membranes.

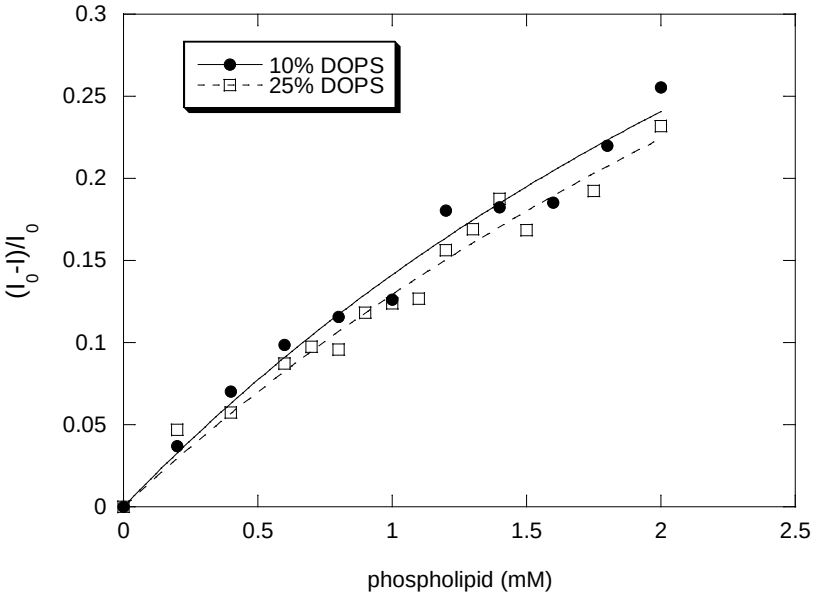

FigureApx 2 Binding of PTEN to 2 mol% Dansyl-PE containing 10 mol%DOPS /POPC (●) and 25 mol% DOPS/POPC (□) LUVs.

PTEN can be activated by $PI(4,5)P_2$, and the activation was possibly induced by conformational change upon binding to $PI(4,5)P_2$ (Campbell et al, 2003). This fact raises the possibility that adding $PI(4,5)P_2$ into vesicles may enhance PTEN binding. So 5 mol% brain $PI(4,5)P_2$ was incorporated into 10 mol% PS/POPC mixtures and the protein binding was measured. Compared to PS/POPC vesicles, adding $PI(4,5)P_2$ enhanced the extent of the FRET (Figure Apx 3). At the same concentration of total vesicles, the

protein bound fraction was larger when PI(4,5)P_2 was present. This result provided the hint that adding PI(4,5)P_2 may enhance protein binding to the vesicles. However, the change in fluorescence due to the FRET did not level off at higher vesicle concentrations (again possibly due to increased light scattering), making extraction of a binding constant difficult.

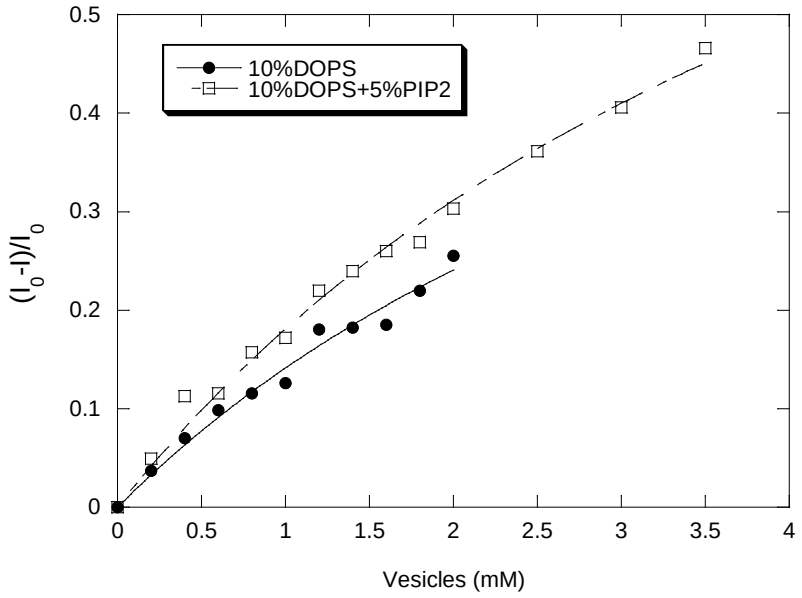

Figure Apx 3 PTEN binding to 2 mol% Dansyl-PE containing 10 mol% DOPS/POPC (●) and 10 mol% DOPS/5 mol% brain PI(4,5)P_2/POPC (□) LUVs.

(2) Effect of membrane curvature to PTEN binding: LUVs vs. SUVs

Most of the binding studies of PTEN have been done using lipid LUVs, which are relatively large (100 nm diameter) and less curved. In order to test if the curvature of the vesicles affects the protein binding, SUVs of 10 mol% PS/PC were used. SUVs have a smaller size (average 30 nm diameter) and large curvature. Compared to PTEN binding to PS/PC LUVs, introducing more curvature only induced very small changes (Figure Apx 4). Light scattering is much less of a problem with SUVs. There is a sense that the

binding curve would eventually saturate with the PS/PC SUVs, but the apparent K_d would be rather high.

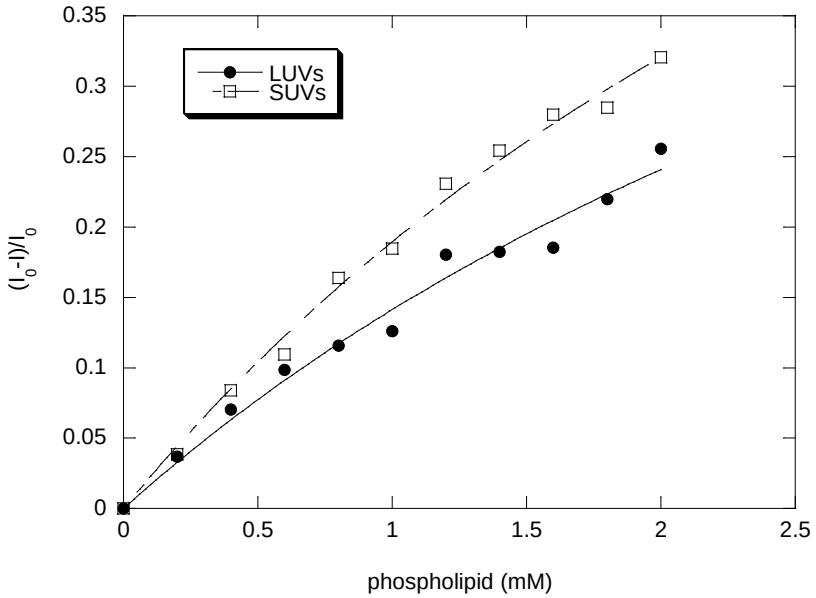

Figure Apx 4 PTEN binding to 10 mol% DOPS/2 mol% Dansyl-PE/88 mol% POPC LUVs (●) and SUVs (□).

(3) Effect of binding conditions: pH and salts concentration

The measurement of the PTEN protein binding to vesicles so far has been done at pH 8.0 with 150 mM NaCl present. The effect of pH was first tested by measuring the binding at pH 8.0 and pH 7.0. The theoretical pI of PTEN is 6.3, so changing pH from 8 to 7 should not influence the binding very much. As expected, PTEN binding to 10 mol% PS/PC LUVs was very similar at both pH values (Figure Apx 5, upper pannel). Binding was weak in both these two conditions. The higher ionic strength in physiological conditions serves to disrupt nonspecific or weak electrostatic interactions and amplify hydrophobic interactions. Therefore, we examined PTEN binding to LUVs in the absence or presence of NaCl equivalent to physiological conditions For 10 mol% PS/PC there was little

change with NaCl. For LUVs of 10 mol% PS/5 mol% PI(4,5)P_2/PC, the FRET was greater with NaCl added (Figure Apx 5, bottom). However, the light scattering still made it extremely difficult to measure PTEN partitioning with any accuracy.

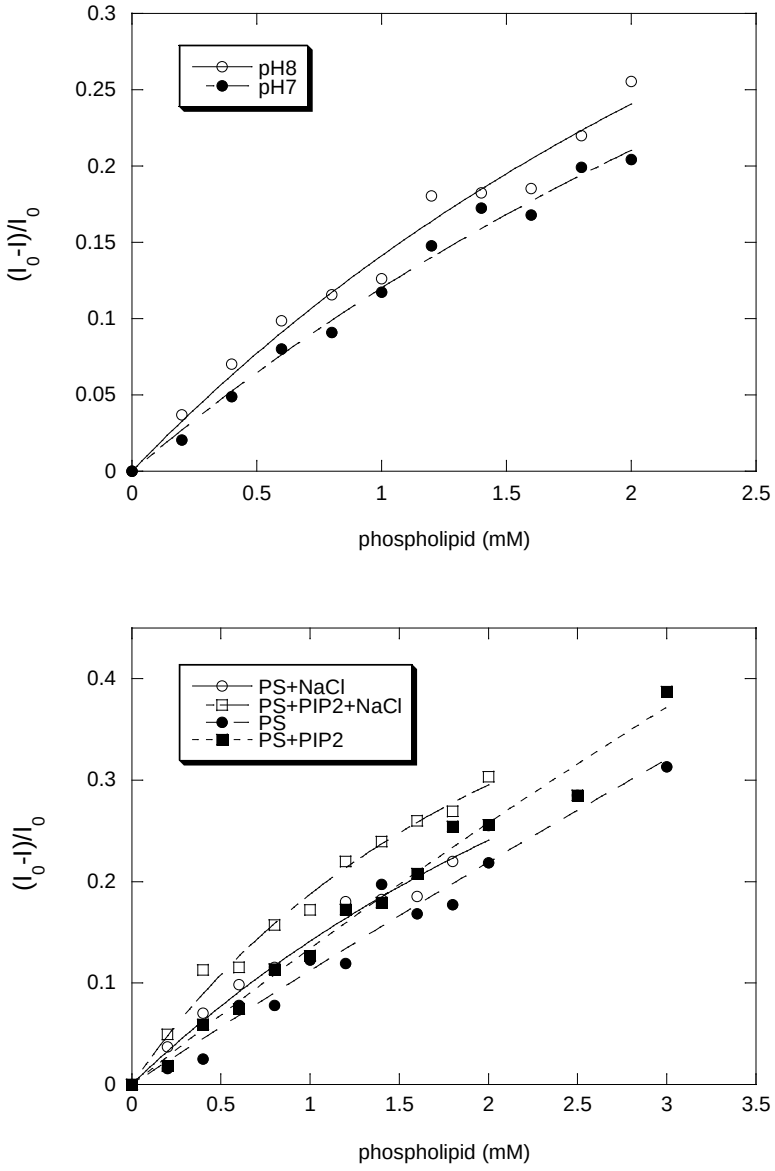

Figure Apx 5 PTEN binding to 10 mol% PS LUVs at pH 7.0 (●) and pH 8.0 (○) (upper), and binding to 10 mol% PS (circles) and 10 mol% PS/5mol% PI(4,5)P_2 (squares) in the presence (empty symbols) and absence (solid symbols) of 150 mM NaCl (bottom).

(4) Effect of florophore: dansyl-PE vs. pyrene-PE

Pyrene-PE as well as dansyl-PE were used as the FRET accepter. Both of the fluorophores are attached to the PE head group and should sense PTEN binding. The size of the pyrene group is bigger than that of dansyl group but if the pyrene-PE diffuses around the vesicle it should be as effective as the dansyl-PE in serving as a FRET acceptor with PTEN. 2 mol% pyrene-PE was incorporated into 10 mol% PS/POPC, or 10 mol% PS/5 mol% PI(4,5)P_2/PC LUVs, and PTEN binding to these vesicles was measured (Figure Apx 5). Compared to dansyl-PE containing vesicles, protein binding to pyrene-PE containing vesicles appeared tighter, with a change in the apparent K_d from greater than 3 mM to less than 1 mM. This result indicated that the disposition of the pyrene group in the membrane is a better sensor of PTEN binding to the LUV. However, the binding was still not particularly tight so we opted to forgo further vesicle binding studies with PTEN.

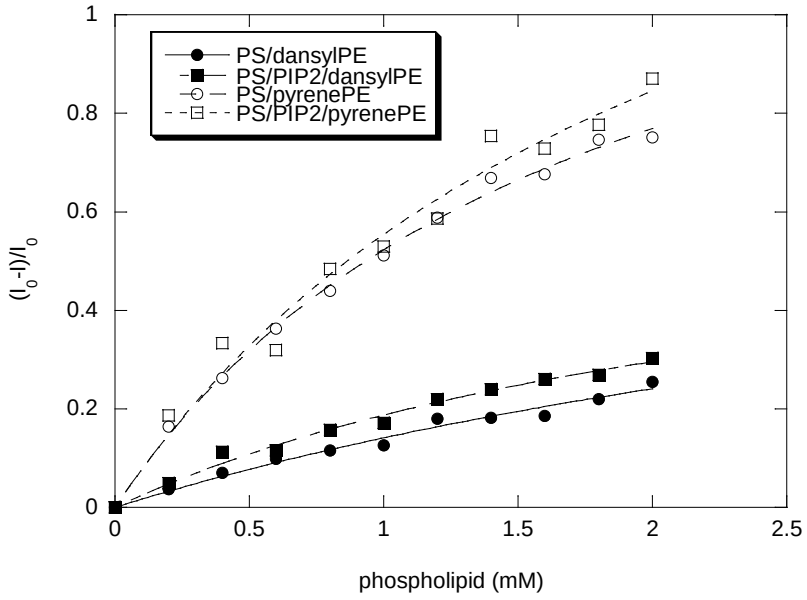

Figure Apx 6 PTEN binding to 2 mol% dansyl-PE containing (solid symbols) or 2 mol% pyrene-PE containing (empty symbols) 10 mol% DOPS (circles) and 10 mol% DOPS/5mol% PI(4,5)P_2 (squares) LUVs.

(5) Effect of the position of His tag on PTEN to vesicle binding

The PTEN protein used in the fluorescence experiments has a hexa-His tag at the N-terminus of the protein. Since we did not observe significant PI(4,5)P_2 enhanced protein binding to vesicles (labeled with the dansyl-group), and PI(4,5)P_2 was suggested to bind at the N-terminal loop, it is possible that the inability of PI(4,5)P_2 induced binding enhancement was caused by His-tag interference with PI(4,5)P_2 binding. In order to exclude this factor, PTEN with the His-tag on the C-terminus was produced, and binding of this protein to 5 mol% PI(4,5)P_2/10 mol% PS/2 mol% pyrene-PE/83 mol% PC vesicles was measured by FRET. Compared to N-terminal His-tagged PTEN, this C-terminal His-tagged PTEN protein had similar activities toward 0.5 mM diC_8PI(3)P. However, changing the His-tag attachment did not affect PTEN binding to PI(4,5)P_2 containing vesicles (Figure Apx 7). The apparent K_d values for these two proteins were very similar.

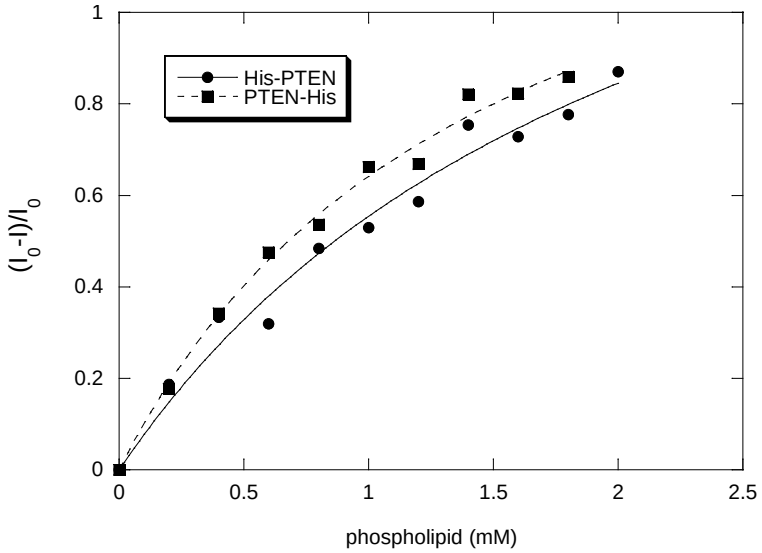

Figure Apx 7 The effect of His-tag place to PTEN binding. The binding of PTEN protein with His-tag on N-terminus (●) or C-terminus (■) to 5 mol% PI(4,5)P_2/10 mol% PS/2 mol% pyrene-PE/83mol % POPC LUVs monitored by measuring the FRET from the protein to pyrene-PE in the LUVs.

3. Discussion

In this study, PTEN protein binding to phospholipid vesicles with different components under different conditions was measured by fluorescence spectroscopy. In all the measurements shown above, PTEN had very weak binding to dansyl-PE containing phospholipid LUVs, but significantly stronger (although still not very tight) binding to LUVs incorporating a pyrene-PE as the FRET acceptor. Assessing PTEN binding to vesicles with fluorescence has been reported previously (Redfern et al, 2008). In that study, pyrene-PE was used as the fluorophore. Combined with our findings, it is hard to determine whether the pyrene group in the lipid vesicles enhanced PTEN binding, the presence of dansyl group reduced protein affinity to vesicles, or the orientation and position of the fluorophore on the membrane was very different for the dansyl group and the pyrene and this alters FRET efficiency. My results also suggested that using FRET to measure PTEN binding to fluorophore labeled lipids vesicles is problematic. These early studies were one of the reasons that we utilized NMR to study PTEN/lipid interaction (and chose a short-chain PI system).

We also found that incorporation of $PI(4,5)P_2$ did not dramatically enhance PTEN binding to phospholipids, which appears controversial to what was reported (Redfern et al, 2008). However, we noticed that except for the original paper and subsequent reports from that group, the importance of $PI(4,5)P_2$ in PTEN membrane association was demonstrated based on the fact that deletion or mutation of N-terminal loop or depletion of $PI(4,5)P_2$ in plasma membrane eliminates PTEN binding. There is no concrete evidence that PIP_2 is needed for PTEN binding. To our knowledge, there is no other report, especially *in vivo* studies, showing that increasing $PI(4,5)P_2$ content in the plasma

membrane enhanced PTEN binding. Clearly, a thorough understanding of PTEN has a long way to go.

4. Reference

Campbell RB, Liu FH, Ross AH (2003) Allosteric activation of PTEN phosphatase by phosphatidylinositol 4,5-bisphosphate. *Journal of Biological Chemistry* **278:** 33617-33620

Das S, Dixon JE, Cho WW (2003) Membrane-binding and activation mechanism of PTEN. *Proceedings of the National Academy of Sciences of the United States of America* **100:** 7491-7496

Redfern RE, Redfern D, Furgason MLM, Munson M, Ross AH, Gericke A (2008) PTEN phosphatase selectively binds phosphoinositides and undergoes structural changes. *Biochemistry* **47:** 2162-2171